whereas the one step of NR was due to the random chain scission of isoprene units in NR. When a small amount of NR (5 pph) was added in PP, the one stage of degradation retained. The initial degradation temperature (T_{id}) of PP/NR at blend ratio of 95/5 was at an intermediate value (440 ^{o}C). The peak degradation temperature shifted to a higher value as compared to the neat PP. This result indicated the compatibility between NR and PP phases, and was possibly due to the presence of a PP-g-MAH compatibilizer. By further adding the NR phase, i.e. 50 pph NR, the thermal degradation of TPE became two stages, corresponding to the degradation of NR and PP parts, respectively. In case of TPEs prepared from PP/ENR, similar situations were observed. However, the incorporation of ENR, instead of NR, improved the thermal stability of TPEs. The addition of 5 pph ENR increased the T_{id} of TPEs from 440 to 443 ^{o}C and T_p from 474 to 478 ^{o}C. With further addition of 50% pph ENR, T_{id} and T_p of the first and the second stages shifted to much higher degradation temperatures as compared to the neat PP. The thermal degradation of polymer blend depended on morphology and extent of interaction between phases [8]. The improved thermal stability of the blends at 50/50 blend ratio was possibly due to the co-continuous phase of rubber (NR or ENR) formed along with PP.

Table 2: Thermal properties of TPEs at various blend ratios.

composition	1^{o} stage (^{o}C)		2^{o} stage(^{o}C)	
	T_{id}	T_p	T_{id}	T_p
PP	452	472		-
NR	330	356	-	-
PP/NR: 95/5	440	474		-
PP/ENR: 95/5	443	478		-
PP/NR: 50/50	367	392	459	477
PP/ENR: 50/50	403	435	468	481

4. Conclusions

In this study, TPEs were successfully prepared from the blends of PP/NR and from PP/ENR in the presence of a PP-g-MAH compatibilizer without dynamic vulcanization. The incorporation of rubber phase in PP improved the toughness, but scarified with the reduction in Young's modulus and tensile strength. The modulus and tensile strength of TPEs prepared from the PP/ENR blends were found to be higher than those of TPEs prepared from the PP/NR, but an opposite situation was found in case of the impact resistance. The changes in mechanical properties could be explained by the reduction in % crystallinity as compared to the neat PP. The dependence of rubber loadings on the decrease in % crystallinity was found up to 15 pph of rubber contents, but then slightly increased and remained with further additions. The compatibility between PP and rubber was found the in the blends of PP/NR and PP/ENR at small rubber content (5 pph). Thermal stability of TPEs prepared from PP/ENR blends was higher than that of TPEs prepared from PP/NR.

Acknowledgements

Author would like to gratefully thank the Department of Chemistry, KMUTT for financial support throughout this work, and Mettler Teledo, Ltd, Thailand for TGA measurements. Acknowledgements are also given to the Nation University project held at KMUTT.

References

[1] P. Sae-Oui, C. Sirisinha, P.Sa-nguanthammarong and P. Thaptong, *Polym Test.* **29** (2010) 346-351.

[2] Y.-W. Chang, J. K. Mishra, S.-K. Kim and D.-K. Kim, *Mater. Lett.* **60** (2006) 3118-3121.

[3] C. Nakason, S. Saiwari and A. Kaesaman, *Polym. Test*, **25** (2006) 413-423.

[4] H. Ismail and Suryadiansyah, *Polym. Test.* **21** (2002) 389-395.

[5] G.M. Shashidhara and S.H. Kameshwari Devi, *Indian J. Eng. Mater. Sci.* **18** (2011) 69-78.

[6] E.G. Bajsić, A. Pustak, I. Šmit and M. Leskovac, *J. Appl. Polym. Sci.* **177** (2010) 1378-1384.

[7] S.Mahapram and S. Poompradub, *Polym. Test.* **30** (2011) 716-725.

[8] S. George, K.T. Varuhese and S.Thomas, *Polymer* **41** (2000) 5485-5503.

STYRENE AND DIVINYLBENZENE-ASSISTED MELT GRAFTING OF GLYCIDYL METHACRYLATE ONTO LOW DENSITY POLYETHYLENE

Chavakorn Samthong, Anongnat Somwangthanaroj*

Department of Chemical Engineering, Faculty of Engineering, Chulalongkorn University, Phayathai Road, Bangkok 10330, Thailand

* E-Mail: Anongnat.s@chula.ac.th, Tel. +66 818184542

Abstract: We have focused on functionalization of low density polyethylene (LDPE) with glycidyl methacrylate (GMA), an unsaturated monomer having reactive epoxy ring, and investigating the effects of reaction condition and comonomer on grafting degree and grafting efficiency. The melt grafting was operated in an internal mixer using benzoyl peroxide (BPO) and dicumyl peroxide (DCP) as radical initiators, and using styrene (St) and divinylbenzene (DVB) as assisting comonomers. FTIR spectrum of graft product displayed stretching carbonyl group of GMA at 1730 cm^{-1}, while ^{1}H NMR data exhibited a peak at chemical shift of 4.32 ppm, representing a methylene proton of GMA. Therefore, these results evidenced that GMA was actually attached onto LDPE backbone. In comparison with DCP, adding BPO gave a higher grafting degree at the same content because BPO has shorter half-life at the operating temperature leading to greater concentration of radical and, in turn, better grafting degree. Moreover, the grafting degree was found to increased, as expected, as a function of GMA content. Besides, it was also found that incorporation of comonomer can enhance grafting degree significantly. Furthermore, the Molau test was carried out as a preliminary test for checking the reactivity of epoxy group of LDPE-*g*-GMA and endgroups of poly(lactic acid), PLA. The system with LDPE-*g*-GMA showed the colloidal suspension solution after a long period of time, which is attributed to the emulsifying effect of graft copolymer formed during the melt blending. This result implied that LDPE-*g*-GMA is a potential reactive compatibilizer in PLA/LDPE blends.

1. Introduction

Low density polyethylene (LDPE) is one of the most well known commodity thermoplastics that has been widely used such as household goods and industrial products. However, its application is limited because it is inert and possesses low polarity. Therefore, modification of polymer backbone with reactive group is of great importance to widen its utilization. There are many methods to functionalize polymer, e.g., UV photografting, plasma, solution grafting [1], but free radical melt grafting is a post-polymerization method available due to its advantages including easy scaling-up, cheap and no solvent required [2-4]. The peroxide used as initiator is thermally cleaved into primary free radical that attacks a hydrogen atom along the polymer backbone, forming macroradicals. These macroradicals further react with reactive monomer, generating targeted graft product.

Glycidyl methacrylate (GMA) is an unsaturated monomer with epoxy ring that has been grafted onto polyolefin for using as reactive compatibilizer because it is very reactive towards many functional groups including hydroxyl (-OH), carboxylic (-COOH) and amine ($-NH_2$). Wei et al. [5] blended polyamide 6 (PA6) with LDPE-*g*-GMA and they found the enhancement of phase dispersion and interfacial adhesion. In comparison with poly(ethylene terephthalate) (PET)/polypropylene (PP) blends, incorporating PP-*g*-GMA instead of PP present the uniformly finer PP domain size and improved physical-mechanical properties [6].

Unfortunately, the side reactions can be happened during the melt grafting. The macroradical can react themselves producing a crosslinking product. Additionally, the homopolymerized GMA is yielded resulting in poor grafting efficiency. To avoid this, a comonomer is added into the system in order to not only increase the degree of grafting, but also reduce the undesired products. In principle, comonomer is more reactive towards macroradical than GMA creating a more stable macroradical, which will couple with GMA further. Styrene is a commercially used comonomer due to its highly stable aromatic ring [7-9]; however, divinylbenzene is an interesting alternative comonomer that has been investigated little [10].

The aim of this work is to prepare LDPE-*g*-GMA with high grafting degree and high grafting efficiency. The effects of styrene and divinylbenzene as comonomer were also investigated. The standard tests were conducted to characterize the chemical structure and content of grafted GMA. Finally, Molau test was done to confirm the *in situ* compatibilization between PLA and LDPE-*g*-GMA.

2. Materials and Methods

2.1 Materials

LDPE (LD1905F) was an available product from SCG Chemicals, Thailand [MFI = 4.9 g/10 min (at 190 ^{o}C/2.16 kg); specific gravity = 0.92]. Poly(lactic acid) (PLA) was purchased from Natureworks LLC, USA [MFI = 6 g/10 min (at 210 ^{o}C/2.16 kg)]. Dicumyl peroxide (DCP; 98%), benzoyl peroxide (BPO; 75%), glycidyl methacrylate (GMA; 97%), styrene (St; 99%), divinylbenzene (DVB; 80%) as shown in Figure 1 were bought from Aldrich. BPO was recrystallized two times using $CHCl_3$ and ethanol (1:1 v/v) mixture. All solvents were used as received without further purification.

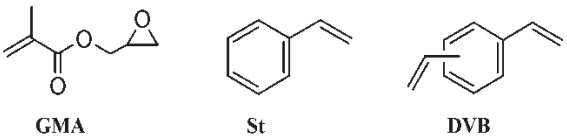

Figure 1. Chemical structures of GMA, St and DVB.

2.2 Preparation of LDPE-*g*-GMA

LDPE was vacuum dried at 80 ^{o}C overnight before use. The specified amounts of LDPE, initiator and monomer were mixed manually in a glass container to let the liquid monomer absorbed onto LDPE pellet. The premixed blend was fed into a chamber of internal mixer (58 cm^3 volume of chamber, MX105-D40L50, Chareon Tut Co., Ltd, Thailand) preheated at 180 ^{o}C. The volume of material was fixed at 70% of the chamber capacity. The rotors were rotated at a constant speed of 60 rpm for 10 min. The sample was cut into small pieces and cooled down to room temperature.

2.3 Purification

About 3 g of crude sample was dissolved in 100 ml toluene at 100-110 ^{o}C until the clear solution was obtained. After that, the solution was poured into 200 ml cold acetone, stirred for 10 min and filtered. The unreacted GMA is soluble in acetone and transferred into the filtrate. The residue was washed with excess amount of fresh acetone several times before drying in vacuum oven at 80 ^{o}C for 24 h.

2.4 Instruments

Fourier transform infrared spectroscopy (FTIR) and proton nuclear magnetic resonance (^{1}H NMR) were used to analyze the chemical structure of product. The purified products were compressed at 170 ^{o}C under 40 bar for 2 min into a thin film (100 μm thick) before FTIR measurement. FTIR spectra were collected in the ATR mode on a FTIR spectrometer (FTIR spectrum GX, PerkinElmer) in a wavenumber range from 4000-650 cm^{-1} at a resolution of ±4 cm^{-1} and number of scan of 128. ^{1}H NMR (Varian INOVA 400 MHz spectrometer) analyze was performed in a deuterated benzene (C_6D_6, δ_H 7.2 ppm) as solvent and tetramethylsilane (TMS, 0.0 ppm) as an internal reference.

2.5 Gel measurement

The small amount of crude product (0.4-0.6 g) was carefully packed into a 120-mesh stainless steel cage followed by extracted with toluene at reflux condition for 24 h. Then, a cage was washed with hot toluene to remove the dissolved LDPE that attached onto surface of cage. The sample and cage were dried in vacuum oven at 80 ^{o}C till the weight was constant. Gel-like crosslinked product was a part that cannot be dissolved through a mesh. Gel content is a percentage of remaining sample weight after extraction divided by initial sample weight.

2.6 Molau test

The Molau test was carried out to check the reaction between epoxy groups of LDPE-*g*-GMA and hydroxyl and carboxylic endgroups of PLA, as reference. PLA, LDPE and LDPE-*g*-GMA were blended in a co-rotating twin screw extruder (L/D = 40, D = 20 mm, LTE 20-40, Labtech Engineering, Thailand). The barrel temperatures were held at 190 ^{o}C except at die, which is 165 ^{o}C. The screw speed was 60 rpm. About 1 g of compound was shook vigorously in vial contained 20 ml chloroform for 2 h. Chloroform is a solvent for PLA but non-solvent for LDPE. The mixture was decanted for 2 weeks and observed by taking pictures by digital camera.

3. Results and Discussion

FTIR and ^{1}H NMR techniques were performed to confirm the grafting of GMA onto LDPE. As shown in Figure 2, peaks at 1462 cm^{-1} and 1368 cm^{-1} are CH_2 and CH_3 bending of LDPE backbone, respectively. A new absorption peak at 1730 cm^{-1} was presence in case of LDPE-*g*-GMA, which is attributed to the attached carbonyl group of GMA. Furthermore, the ^{1}H NMR data in Figure 3 displays a peak at δ 4.32 ppm, corresponding to the methylene proton of GMA. Therefore, these results confirmed that GMA was really grafted onto LDPE backbone.

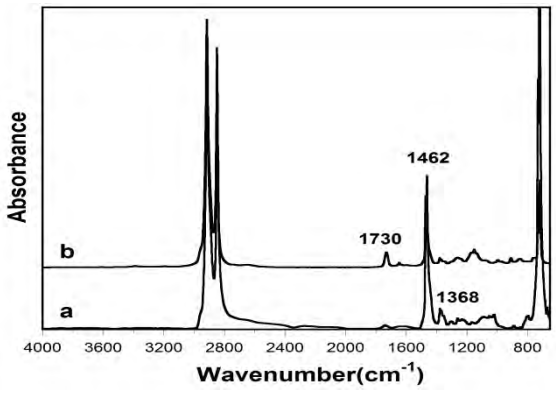

Figure 2. FTIR spectra of a) LDPE; b) LDPE-*g*-GMA.

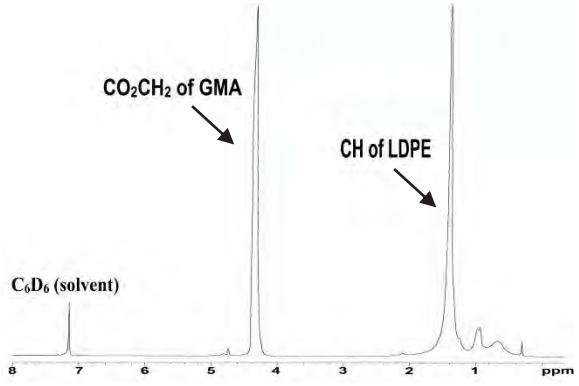

Figure 3. ^{1}H NMR spectrum of LDPE-*g*-GMA.

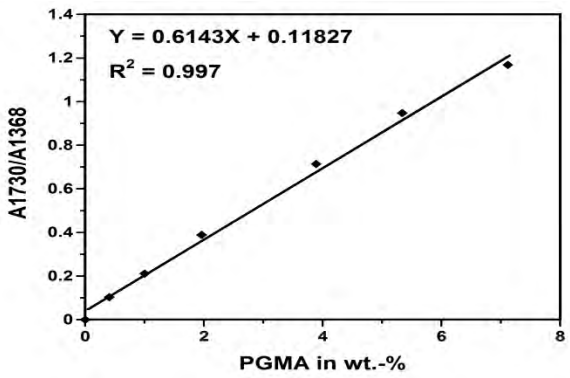

Figure 4. Calibration curve for calculating grafting degree of GMA by FTIR.

In order to calculate the amount of grafted GMA of graft product, poly(glycidyl methacrylate) (PGMA) as standard [11] was synthesized via free radical solution polymerization in ethyl acetate using BPO as initiator at 80 ^{o}C for 8 h [12]. Then, PGMA was blended with virgin LDPE at different compositions in an internal mixer at 180 ^{o}C for 5 min, followed by compression into a thin film before ATR-FTIR measurement. The absorbance at 1730 cm^{-1} and 1368 cm^{-1} were collected as references of carbonyl group of GMA and CH_3 bending of LDPE, respectively. Hence, the calibration curve can be constructed by this method as depicted in Figure 4. The calibration curve is a straight line as a function of PGMA concentration, suggesting that it followed the Beer-Lambert law. There are 2 important parameters; grafting degree (GD) and grafting efficiency (GE), which define as the amount of grafted GMA with respect to weights of purified LDPE-*g*-GMA and initial GMA (W) as listed below. GD was calculated using equation shown in Figure 4.

$$GD = \left(\left[\frac{A_{1730}}{A_{1368}}\right] - 0.1187\right)/0.6143$$

$$GE = \frac{GD}{W}$$

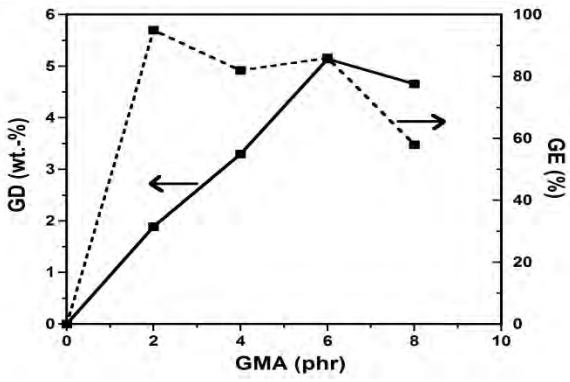

Figure 5. Effect of GMA monomer concentration on GD and GE. $[BPO]_i$ = 1.0 phr.

We would like to mention that in all cases the gel formed during the grafting was not noticed. The effect of GMA content on GD and GE was shown in Figure 5. It reveals that GD increased from 1.89 to 5.14 wt.-% as a content of GMA in feed increased from 2 to 6 phr, as expected, because the possibility for GMA to react with LDPE macroradicals at high GMA concentration was elevated. However, GD slightly decreased to 4.66 wt.-% when GMA content was 8 phr, which might be due to the fact that GMA can possibly form undesired PGMA or loss during the premixing before feeding into a chamber. Moreover, this result is in agreed with a significant drop of GE, which decreased from 86 to 58% as GMA content of 6 and 8 phr, respectively.

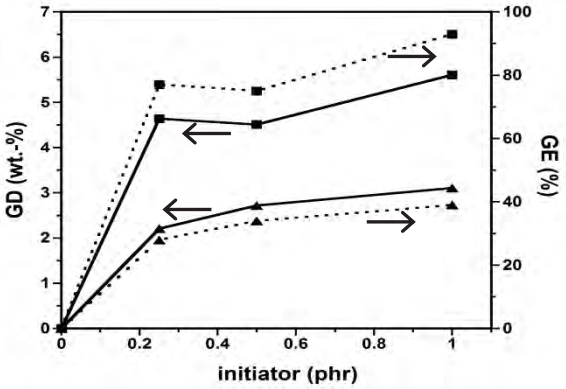

Figure 6. Effect of initiator on GD and GE: (▬■▬) GD and (▪■▪) GE of LDPE/GMA/BPO system, $[GMA]_i$ = 6.0 phr; (▬▲▬) GD and (▪▲▪) GE of LDPE/GMA/DCP system, $[GMA]_i$ = 8 phr.

Figure 6 demonstrates the influences of type and concentration of initiator on GD and GE. GD increased as a function of initiator concentration. This can be explained by the increase of amount of free radicals, which will react with LDPE and, in turn, the increase of macroradicals as well. In addition, using BPO as initiator can improve GD higher than DCP at the same content, which can be described by half-life of the initiator. Half-life is a time that the weight of material reduces by a half at a certain condition. At the operating temperature (180 ^{o}C), BPO and DCP have half-life of 1.2 s and 29 s, respectively [2]; thus, BPO decomposed faster and generated higher concentration of free radical in the system during grafting resulting in enhanced degree of grafting [1].

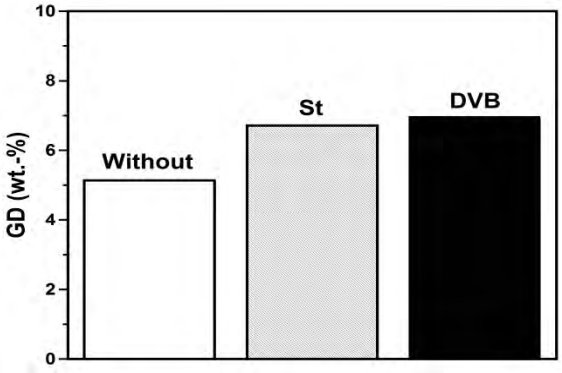

Figure 7. The effect of comonomer on GD.

Besides, it was also found that the presence of St and DVB as assisting comonomer can improve GD. Addition of St and DVB increased GD from 5.14 to 6.72 and 6.92 wt.-%, respectively. The mechanism of free radical melt grafting and effect of comonomer are explained as follows. First, the organic peroxide was thermally decomposed into primary radicals, which readily attack hydrogen atoms of LDPE forming macroradicals. Nonetheless, these macroradicals were unstable and prompt to react with themselves, yielding crosslinking product, while GMA radicals can undergo homopolymerization, producing undesired PGMA. So, comonomer plays a key role in hindering these side reactions. For instance, styrene is very reactive towards macroradical than GMA leading to stable macroradicals as a result of resonance of aromatic ring of styrene. These highly stable styryl macroradicals were then coupled with GMA producing LDPE-*g*-(GMA-*co*-St) [7]. From this reason, GD tended to increase considerably because GMA and LDPE macroradicals were more preferred in grafting instead of crosslinking reaction or homopolymerization.

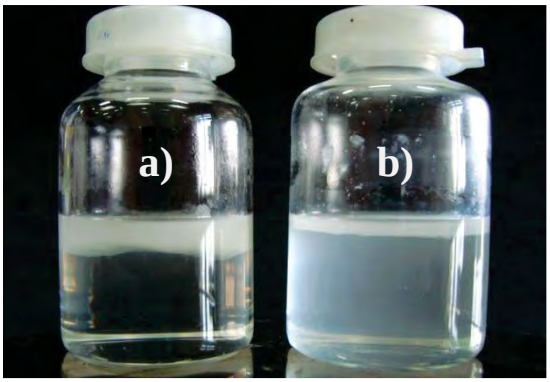

Figure 8. The Molau test solutions in $CHCl_3$ of the PLA/LDPE/LDPE-*g*-GMA blends with composition: (a) 90/10/0; b) 90/2/8 wt.-%.

Here, the formation of *in situ* copolymer from the reaction between PLA and LDPE-*g*-GMA was explored by Molau test. Figure 8 illustrates the stability of PLA/LDPE with and without adding LDPE-*g*-GMA in chloroform. In case of PLA/LDPE, PLA was totally dissolved in chloroform whereas LDPE was separated as supernatant layer. Nevertheless, adding LDPE-*g*-GMA at 8 wt.-% exhibited a milky and colloidal suspension solution after decanting more than 2 weeks. This stability is due to the emulsifying effect, which proved the formation of (LDPE-*g*-GMA)-*g*-PLA copolymer formed *in situ* during melt blending and acted as surfactant in the PLA solution [13, 14].

4. Conclusions

It was summarized that GMA was successfully grafted onto LDPE backbone in an internal mixer using peroxide as initiator and using St and DVB as assisting comonomer to improve the degree of grafting. FTIR and ^{1}H NMR were conducted to characterize the chemical structures of graft products. By adjusting the reaction condition, the optimal GD and GE of 5.14 wt.-% and 86% was achieved at GMA and BPO content of 6 and 1 phr, respectively. Additionally, incorporating St and DVB gave GD of 6.72 and 6.92%, respectively. This outcome can be explained by the fact that the highly stable styryl macroradicals were very reactive in copolymerization towards GMA. Lastly, the reaction between epoxy group of LDPE-*g*-GMA and hydroxyl/carboxylic endgroups of PLA was confirmed by Molau test. The stable milky colloidal solution was seen indicating the emulsifying effect as a result of (LDPE-*g*-GMA)-*g*-PLA, acting as surfactant in PLA solution. It is worth noting that this preliminary test indicates the potential of prepared LDPE-*g*-GMA as reactive compatibilizer in PLA/LDPE system.

Acknowledgements

We would like to express our sincere gratitude to the Royal Golden Jubilee Ph.D. Program under the Thailand Research Fund for financial support.

References

[1] K. Y. Cho, J. Y. Eom, C. H. Kim and J. K. Park, *J. Appl. Polym. Sci.* **108** (2008) 1093-1099.
[2] G. Moad, *Prog. Polym. Sci.* **24** (1999) 81-142.
[3] S. Al-Malaika and W. Kong, *J. Appl. Polym. Sci.* **79** (2001) 1401-1415.
[4] E. Passaglia, S. Coiai and S. Augier, *Prog. Polym. Sci.* **34** (2009) 911-947.
[5] Q. Wei, D. Chionna, E. Galoppini and M. Pracella, *Macromol. Chem. Phys.* **204** (2003) 1123-1133.
[6] M. Pracella and D. Chionna, *Macromol. Symp.* **198** (2003) 161-171.
[7] H. Cartier and G. Hu, *J. Appl. Polym. Sci.* **36** (1998) 2763-2774.
[8] E. Burton, M. Woodhead, P. Coates and T. Gough, *J. Appl. Polym. Sci.* **117** (2010) 2707-2714.
[9] Y. Zhou, Y. Zhao, W. Yao and B. Huang, *Polym Eng. Sci*. **51** (2011) 1669-1674.
[10] S. Al-Malaika and E. Eddiyanto, *Polym. Degrad. Stab*. **95** (2010) 353-362.
[11] N. Torres, J. J. Robin and B. Boutevin, *J. Appl. Polym. Sci.* **81** (2001) 581-590.
[12] M. H. Espinosa, P. J. O. del Toro and D. Z. Silva *Polymer* **42** (2001) 3393-3397.
[13] G. E. Molau, *J. Polym. Sci., Part A: Polym. Chem.* **4** (1965) 1267-1278.
[14] P. Ma, D. G. Hristova-Bogaerds, P. Schmit, J. G. P. Goossens and P. J. Lemstra, *Polym. Int*. **61** (2012) 1284-1293.

MODIFICATION OF HIGHLY CONDUCTIVE POLYMER PEDOT:PSS WITH GRAPHENE

Chutimar Deetuam and Anongnat Somwangthanaroj*

Department of Chemical Engineering, Faculty of Engineering, Chulalongkorn University, Phayathai Road, Patumwan, Bangkok, 10330 Thailand

* E-Mail: Anongnat.s@chula.ac.th, Tel. +66818184542

Abstract: Graphene is one of the most interesting materials because it is the thinnest conducting material which has potential for electronics and sensor applications. One of the simple methods to synthesize graphene is chemical oxidation of graphite flakes followed by chemical reduction. Because of its high electrical conductivity, graphene was filled into PEDOT:PSS solution at varied weight fractions for improving the electrical conductivity. However, the dispersion of unmodified graphene in organic solvents and in polymer matrix was poor. Thus, the interaction between graphene sheet and PEDOT:PSS was improved by covalent modification. In this research, the surface of graphene sheet was functionalized via amidation with alkyne group (C≡C), while PEDOT:PSS with azide group (N≡N) was also prepared. Then, these two reactive functional groups were coupled via click chemistry in a mild condition. The chemical structures were examined and their properties were also investigated.

1. Introduction

Nowadays, the electronics packaging becomes smaller, thinner as well as lighter than that in the past. For achieving these purposes, the conductive polymer has been attracted much attention in electronics fields because of their excellent properties including the good film forming, leading to ease to be coated and printed on the flexible substrates such as PI and PET. Polyethylenedioxythiophene:polysulfonic acid (PEDOT:PSS) which has the outstanding properties in high electrical mobility, high stability in air and moisture than those of other conductive polymers was selected to be used as the matrix in this research. However, its electrical conductivity is still not high enough to optimize their application performance and it is the crucial limitation. Then, many previous researches have attempted to improve the electrical conductivity with different methodologies including secondary dopant doping [1,2] and incorporation of the excellent electrical conductive filler in polymer matrix [3]. Carbon based filler was investigated because it has superior properties in thermal strength as well as electrical conductivity [4].

Graphene, a two-dimensional single layer sheet of carbon atoms arranged in hexagonal lattice, is an interesting material owing to its thinnest conducting material in which it has potential for development in electronics and sensors [5-7]. Graphene can be synthesized from natural graphite via chemical oxidation [8] followed by chemical reduction [9]. This chemical method can produce large amount of graphene and can be applied in this work. According to the previous researches, it was found that the synthesized graphene oxide (GO) had many functional groups at the edges and both of basal plane, e.g., epoxide, carboxyl and hydroxyl groups leading well-dispersion in water [10]. After chemical reduction, a loss of epoxide and hydroxyl groups of GO [11] results in graphene with hydrophobic nature that may agglomerate irreversibly; thus, it is difficult to re-disperse in water or organic solvents making it difficult to process further.

The composite of PEDOT:PSS and graphene prepared by mechanical stirring showed the agglomeration of graphene which was the defect in coated films on substrate and the expected properties was not achieved as well. Therefore, the surface modification of graphene should be investigated for increasing the dispersability of graphene. The previous works preferred to modify surface of graphene with small molecules, polymer chains, surfactant, as well as charges during the chemical reduction. Actually, the surface modification can be classified into covalent and non-covalent modification. The covalent modification is the most promising method for applying in this case. Click chemistry was conducted to form a covalent linkage between functionalized graphene and PEDOT:PSS as depicted in Figure 1.

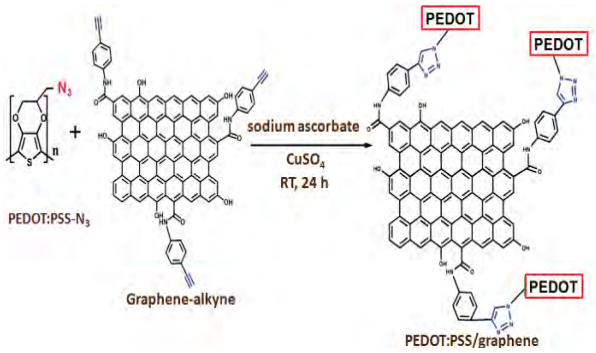

Figure 1. Schematic diagram of click reaction of PEDOT:PSS and graphene.

To confirm the chemical structures of products, Fourier transform infrared spectroscopy (FTIR), X-ray photoelectron spectroscopy (XPS), and thermogravimetric analysis (TGA) were employed. The surface morphology as well as chemical and physical characteristics of PEDOT:PSS-graphene at different graphene loadings were monitored by scanning electron microscopy (SEM). Also, the electrical conductivity was measured using four-point probe.

2. Materials and Methods

2.1 Materials

In case of synthesis of graphene, high purity graphite powder (99.99%, particle size ≤ 45 μm), hydrazine hydrate (5.51 wt%), 4-ethynyl aniline and N,N'-dicyclohexylcarbodiimide (DCC) were purchased from Sigma-Aldrich. Sulfuric acid, sodium nitrate powder, potassium permanganate powder, hydrogen peroxide (30% v/v) and hydrochloric acid were bought from Merck. In case of synthesis of azide-modified PEDOT:PSS, 3,4-dimethoxythiophene, 3-bromo-1,2-propanediol, *p*-toluenesulfonic acid (98%), sodium azide, iron (III) *p*-toluene sulfonate hexahydrate, sodium peroxodisulfates and polystyrene sulfonic acid (PSSA, 18 wt% in H_2O) were obtained from Sigma-Aldrich. Copper sulfate and sodium ascorbate were also bought from Sigma-Aldrich for click reaction. Other solvents were analytical grade and used as received without further purification.

2.2 Graphene-alkyne synthesis

Graphite powder (2 g) was added into a mixture of H_2SO_4 (50 ml) and $NaNO_3$ (1 g) and stirred in an ice bath at temperature below 20 ^oC for a few minutes followed by dropping $KMnO_4$ (6 g) slowly. The mixture was then stirred at room temperature for 2 hours. After that, 100 ml of DI water was added into the solution. When the temperature of the mixture was decreased to 60 ^oC, H_2O_2 was added gently until a colour changed to a yellow brown indicating the complete reaction. Next, the diluted HCl in DI water (1:20 v/v) was added into the oxidized suspension. The mixture was washed and filtrated several times with DI water until pH was neutral. The crude product was dried by freeze-drying process achieving a fine dark brown GO powder.

Thirty milligram of GO was re-dispersed in 130 ml of DMF. The solution of 87 mg of 4-ethynylaniline in 20 ml of DMF was added into GO solution followed by 4.1 g of DCC. The mixture was then heated to 90 ^oC and stirred under N_2 for 2 hours. The mixture was filtered through PTFE membrane and washed with ethanol. The crude product was re-suspended in 30 ml of DI water, and then 0.37 ml of hydrazine hydrate was added. The reaction was operated at 95 ^oC for 10 hours. The synthesized graphene-alkyne was washed with DI water and filtered to remove excess hydrazine hydrate. Then, graphene-alkyne slurry was dried by freeze-drying process.

2.3 PEDOT:PSS-N_3 synthesis

0.41 mg of 3,4-dimethoxythiophene, 1.11 g of 3-bromo-1,2-pro-panediol and 0.08 g of *p*-toluenesulfonic acid were poured into a 30 ml of toluene. The mixture was stirred at 100 °C for 48 hours. After cooling, toluene was removed under vacuum and the product was dissolved in CH_2Cl_2, and extracted with Na_2CO_3 solution. The organic phase was dried with anhydrous $NaSO_4$ and concentrated in rotary evaporator. The collected product was purified by column chromatography to separate EDOT-Br.

0.22 g of EDOT-Br and 0.08 g of NaN_3 were dissolved in 10 ml of DMF and then stirred at room temperature for 24 hours. DI water was added extracted with diethyl ether. The combined organic phases were dried with $NaSO_4$. The collected product, EDOT-N_3, was concentrated using rotary evaporator.

20 mg of EDOT-N_3 and 278 mg of 18 wt% PSSA aqueous solution were dissolved in 5 ml of DI water and stirred for 1 hour. Then, 41.8 mg of iron (III) *p*-toluene sulfonate and 33.4 mg of $Na_2S_2O_4$ were filled and stirred at room temperature for 24 hours, yielding a dark blue homogeneous solution.

2.4 Click reaction of PEDOT:PSS/graphene

5 mg of graphene-alkyne sheet was re-dispersed in 5 ml of aqueous solution of PEDOT:PSS-N_3. $CuSO_4$ (10 μL, 0.1 M, 1 μmol) and sodium ascorbate (20 μL, 0.1 M, 2 μmol) were mixed by stirring at room temperature for 48 hours.

3. Results and Discussion

As shown in Figure 2a, FTIR spectrum exhibited the broad absorption band at 3434 cm^{-1}, which is attributed to the existence of hydroxyl groups (-OH) and adsorbed water molecules. The skeleton vibration of graphene sheet appeared at 1627 cm^{-1}. The terminal alkyne (-C≡C-) absorption band appeared at the center of peak at 2150 cm^{-1}. However, its intensity is weak due to its very high symmetry resulting in difficulty to detect [12]. The amidation between the graphene sheets and terminal alkyne molecules was evidenced by carbonyl (-C=O) stretching at 1565cm^{-1}, representing the formation of amide-carbonyl (-NHCO-) [13].

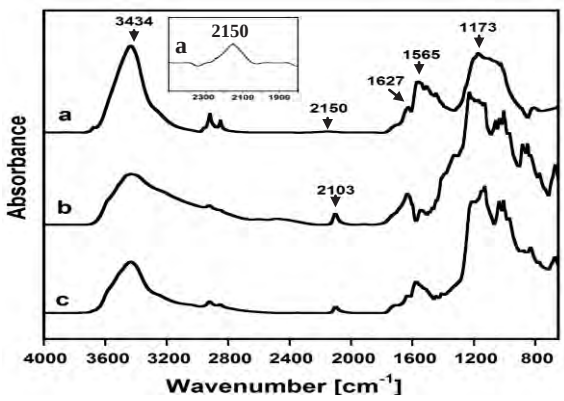

Figure 2. FTIR spectra of a) graphene-alkyne, b) PEDOT:PSS-N_3, and c) PEDOT:PSS/graphene.

Besides, the absorption peak at 2103 cm^{-1} of PEDOT:PSS-N_3 (Figure 2b) was assigned to azide stretching. After click reaction with modified graphene (Figure 2c), this band was reduced indicating that most of azide functional groups of PEDOT:PSS-N_3 were reacted with alkyne of graphene, implying that the click reaction was occurred.

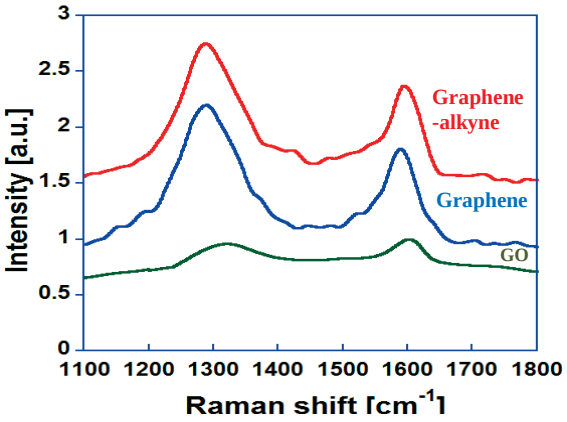

Figure 3. Raman spectra of GO, graphene, graphene alkyne.

The chemical reduction of graphene was also observed by Raman spectroscopy. Dispersive Raman spectrum of graphene oxide shown in Figure 3. displayed a G-band that observed for sp^2 domains around 1603 cm^{-1} and a broad D-band that described to edge of basal sheet and disordered structures [14] around 1321 cm^{-1} with I_D/I_G ratio of 0.97. Upon hydrazine treatment, The D-band of Raman shift moved to 1589 cm^{-1} and G-band also moved to 1289cm^{-1} and I_D/I_G ratio also changed to 1.32, which is significantly higher than those of graphene oxide. The increasing I_D/I_G ratio of graphene was attributed to a decrease in size of the in-plane sp^2 domains and an increase in degree of disorder and edge planes of synthesized graphene [9, 15]. In comparison to synthesized graphene, G-band of alkyne functionalized graphene slightly shifted to 1595 cm^{-1} indicating the better exfoliation of functionalized graphene sheets. The carboxylic group as functional group from acid treatment was reacted react with amine of terminal alkyne substance and I_D/I_G ratio was 1.33 [16].

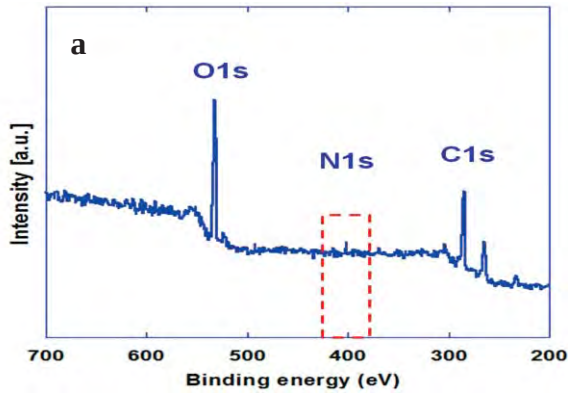

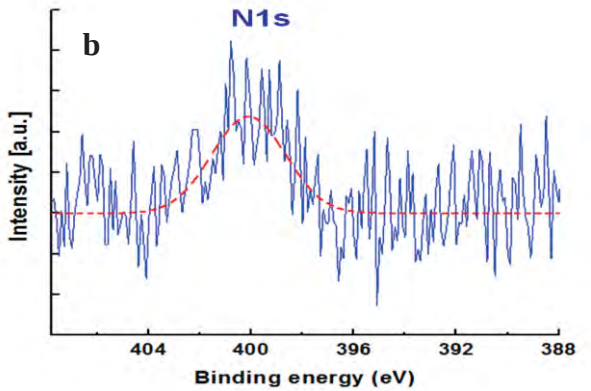

Figure 4. a) XPS spectra of PEDOT:PSS/graphene b) N1s core-level peak.

The C1s, O1s and N1s spectra of PEDOT:PSS/graphene are displayed in Figure 4a. N1s spectrum as shown in Figure 4b consists of C-N peak at 399.8 eV resulting from triazoles generated from the click reaction between alkyne and azide.

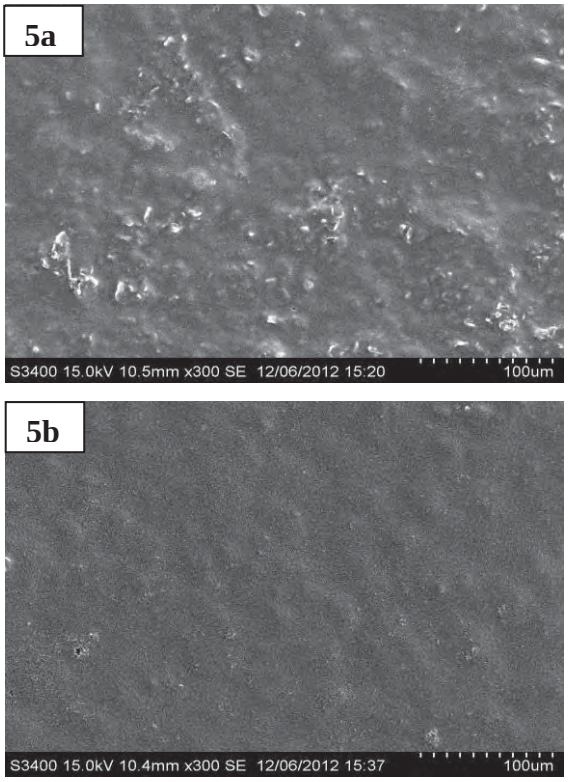

Figure 5. SEM images a) un-click polymer composite and b) click polymer composite.

Morphological characterization was carried out on coated PEDOT:PSS-graphene composite films on the silicon wafer. The composite with 1 wt % loading of graphene in aqueous PEDOT:PSS was dried under room temperature. The morphological differences were depicted in Figure 5. The un-modified composite surface showed poorer dispersion than the modified one resulting in high roughness surface. The agglomeration of hydrophilic graphene was the cause of the film defect as showed in Figure 4a. However, the modification via click chemistry with the covalent

linkage between graphene and PEDOT:PSS took place showing more compatible, good dispersion of graphene in PEDOT:PSS solution and smoother thin films as demonstrated in Figure 5b.

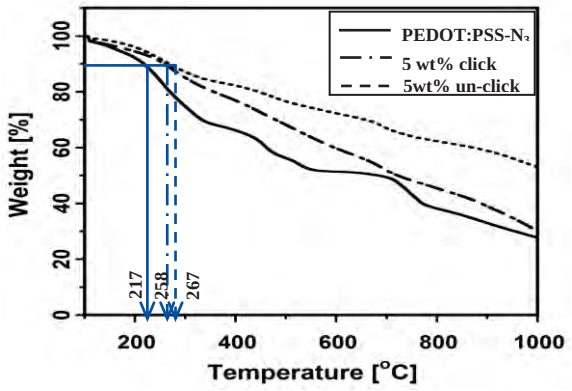

Figure 6. TGA curves of PEDOT:PSS-N_3, 5 wt% click composite, 5 wt% un-click composite.

TGA measurements as a function of temperature for three samples were performed to determine the mass loss of composites. Thermal stability of dried composite was obtained from TGA curves operating in a temperature range between 100-1000 ^{o}C at 10 ^{o}C/min under N_2 atmosphere. Focusing on 10% weight loss, PEDOT:PSS-N_3 (at 217^{o}C) showed lower thermal stable than that of 5 wt% click (at 258^{o}C) and 5 wt% un-click (at 267^{o}C), respectively. Graphene is a very thermally stable material; therefore, thermal stabilities of polymer composites with 5 wt% graphene loading were improved and also gave the same results at other loadings. On the other hand, the click reaction formed the amide linkages and had much functionality leading to greater mass loss.

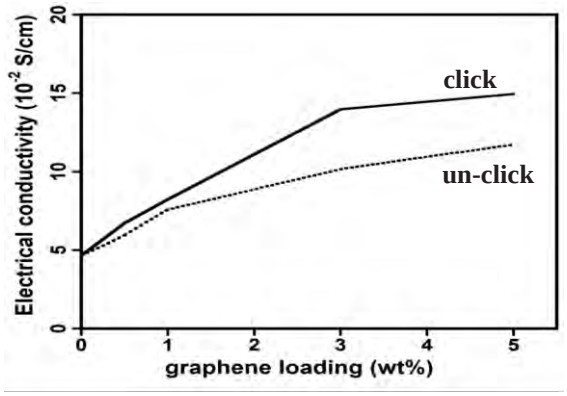

Figure 7. Electrical conductivity of composites at varied weight percentages of graphene.

The electrical conductivity of casted PEDOT:PSS/graphene on glass slide was monitored by 4-point probe as illustrated in Figure 7. The electrical conductivity dramatically increased at the graphene loading lower than 3 wt% and then slightly increased. According to the SEM image from Figure 5a, the poor dispersion of un-click graphene in PEDOT:PSS showed the agglomeration resulting to lower electrical conductivity. On the contrary, click reaction formed the thiazole linkage between graphene and PEDOT:PSS caused the well dispersion and higher electrical conductivity.

4. Conclusions

The chemical modification of PEDOT:PSS-graphene composite was done and characterized by standard tests. The occurrence of click reaction can be proved by deconvoluted N1s spectra from XPS data. The good dispersion of graphene in PEDOT:PSS solution can be achieved via click coupling as evidenced by SEM micrographs. The modified PEDOT:PSS/graphene at 5 wt% of graphene loading exhibited the significantly increased electrical conductivity in comparison with the unmodified PEDOT:PSS.

Acknowledgements

We gratefully thank the Royal Golden Jubilee Ph.D Program under the Thailand Research Fund for financial support.

References

[1] A. Onorato, M. A. Invernale, I. D. Berghorn, C. Pavlik, G. A. Sotzing and M. B. Smith, *Synth. Met.* **160** (2010) 2284–2289.
[2] J. Ouyang, Q. Xu, C. Chu, Y. Yang, G. Li and J. Shinar *Polymer* **45** (2004) 8443–8450.
[3] T. T.Tung, J. H. Yeon, T. Y. Kim and K. S. Suh, *Synth. Met.* **160** (2010) 1266–1272.
[4] A. A. Balandin, S. Ghosh, W. Bao, I. Calizo, D. Teweldebrhan, F. Miao and C. N. Lau, *Nano Lett*. **8** (2008) 902-907.
[5] S. Sodano, A. Mahmood and E. Dujardin, *Carbon* **48** (2010) 2117-2150.
[6] S. R. Dhakate, N. hauhan, S. Sharma, J. Tawale, S. Singh, P. D. Sahare and R. B. Mathur, *Carbon* **49** (2011) 1946-1954.
[7] Y. Shao, J. Wang, H. Wu, J. Liu, I. A. Aksay and Y. Lin, *Electroanal*. **22** (2010) 1027-1036.
[8] G. Wang, J. Yang , J. Parki, X. Gou, B. Wang, H. Liu and J. Yao, *J. Phys.* Chem. *C* **112** (2008) 8192-8195.
[9] S. Stankovich, D. A. Dikin, R. D. Piner, K. A. Kohlhaas, A. Kleinhammes, Y. Jia, Y. Wu, S. T. Nguyen and R. S. Ruoff, *Carbon* **45** (2007) 1558-1565.
[10] S. Stankovich, R. D. Piner, S. T. Nguyen and R. S. Ruoff, *Carbon* **44** (2006) 3342-3347.
[11] Y. Geng, S. J. Wang and J. K. Kim, *J. Colloid Interface Sci.* **336** (2009) 592-598.
[12] M. Castelain, G. Martinez, P. Merino, J. A. Martin-Gago, J. L. Segura, G. Ellis and H. J. Salavagione, *Chem. Eur. J* **18** (2012) 4965-4973.
[13] T. Kuila, P. Khanra, A. K. Mishra, N. H. Kim and J. H. Lee, *Polym. Test.* **31** (2012) 282-289.
[14] P. Lian, X. Zhu, S. Liang, Z. Li, W. Yang, H. Wang, *Electrochim. Acta* **55** (2010) 3909-3914.
[15] T. N. Lambert, C. C. Luhrs, C. A. Chavez, S. Wakeland, M. T. Brumback, T. M. Alam, *Carbon* **48** (2010) 4081-4089.
[16] E. Y. Choi, T. H. Han, J. Hong, J. E. Kim, S. H. Lee, H. W. Kim, S. O. Kim, *J. Mat. Chem.* **20** (2010) 1907-1912

EFFECT OF DRY NATURAL RUBBER AND NATURAL RUBBER LATEX ON PROPERTIES OF BLENDED POLY(LACTIC ACID) BLOWN FILMS

Pidsawat Numpiboonmarn, Parima Tantipiriyakij, Peerut Suwanpimolkul, Uraiwan Ketwattha and Anongnat Somwangthanaroj*

Department of Chemical Engineering, Faculty of Engineering, Chulalongkorn University, Bangkok, Thailand

* Author for correspondence; *E-mail:* anongnat.s@chula.ac.th, Tel. +66 22186864, Fax. +66 22186877

Abstract: Packaging film derived from biodegradable polymer has recently been attracted many interests. Poly(lactic acid) (PLA) is one of the most interesting biodegradable polymers derived from renewable resources such as corn and cassava. Owing to its good physical and mechanical properties, PLA has been widely studied as an alternative to petroleum-based materials. However, PLA is stiff and brittle at room temperature which limits its use in several applications. The aim of this research is to improve toughness and gas permeability of PLA blown film by adding 5-15 wt% of natural rubber (NR). The effect of dry natural rubber (dryNR) and natural rubber latex (NRL) was also compared. Elongation at break and tensile toughness of PLA/dryNR and PLA/NRL films dramatically increased at 5 wt% dryNR and 10 wt% NRL of rubber content, respectively and then gradually dropped due to large domain size of rubber. Besides, the oxygen permeation (OP) and water vapor permeation (WVP) of PLA/dryNR films increased as a function of rubber content; on the other side, OP and WVP of PLA/NRL films did not significantly changed. It can be concluded that the final properties of blended PLA blown films can be controlled by adjusting type of rubber and rubber loading.

1. Introduction

Polymers derived from natural resources recently attracted many interests as an alternative to petroleum-based materials as well as a solution to waste problems. Thus, the development of such materials is a crucial issue in order to reduce an environmental impact of plastic production and waste.

PLA is one of the most interesting biodegradable thermoplastics derived from renewable resources such as corn and cassava. It exhibits high strength and modulus that is comparable to other plastics. However, PLA is stiff and brittle at room temperature which limits its use in several applications [1-3]. Therefore, rubber is incorporated to improve toughness of brittle PLA because it has high elasticity and flexibility. Many researchers reported the blending of poly(lactic acid) with natural and synthetic rubbers such as poly(ether)urethane elastomer (PU elastomer) [4], acrylonitrile–butadiene rubber (NBR), isoprene rubber (IR), ethylene-propylene copolymer (EPM) and ethylene-acrylic rubber (AEM) [5]. NR is good choice for toughening PLA because of its biodegradability, good impact properties and flexibility. Dry natural rubber (dryNR) can be prepared from natural rubber latex (NRL) by adding acid to coagulate NRL suspension in an aqueous medium, yielding dryNR. Generally, acid carries positive charges and eliminates negative charges of rubber particles resulting in a decrease of repulsion between particles and coagulation. In addition, the advantage of direct blending NRL into polymer without coagulation process is short time consumption and low cost.

Gas permeability is one of the most important factors in food packaging especially oxygen permeation (OP) and water vapor permeation (WVP). Suitable gas permeability of film in food packaging (high OP and WVP) can maintain the quality and extend shelf life of food products [6-13]. In this work, mechanical and thermal properties of blended films were considered. Herein, the effect of dryNR and NRL on properties of blended PLA blown films was comparatively investigated in our research.

2. Materials and Methods

2.1 Materials

Poly(lactic acid) (PLA) grade 2003D pellets were purchased from Nature Works. Dry sheet of commercial natural rubber (air-dried sheet (ADS)) was purchased from Hi Yangpara, Rayong, Thailand. High ammonia concentrated natural rubber latex (NRL) with 60% dry rubber content was purchased from Rubber Research Institute of Thailand, Kasetsart University and used as received.

2.2 Blending and blowing films

PLA/dryNR and PLA/NRL blends were obtained by twin-screw extruder (co-rotating, L/D = 40, D = 20 mm, Labtech Engineering, Thailand) at screw speed of 60 rpm. In case of NRL, the blend composition is calculated based on dry rubber content in NRL excluding water weight (60% dry rubber content). The compositions of PLA/dryNR and PLA/NRL blend (temperature range between 190-200 °C) are shown in Table 1. Moisture was eliminated from pellets at 80°C in an oven overnight. Blown film process was performed by using single screw extruder attached to blown film die (L/D = 25, D =20 mm, Collin, Germany) at screw speed of 80 rpm. Operating temperature was varied along the barrel from 170-220 °C. The morphology of neat PLA, PLA/dryNR and PLA/NRL blown films in machine direction (MD) were investigated with scanning electron microscope (SEM: JEOL, JSM 5800LV,

Japan) at an acceleration voltage of 10 kV. The samples were immersed in liquid nitrogen and cut. Thermal properties were investigated by differential scanning calorimeter (DSC: TA Instruments 2910, USA). 5-10 mg of samples was heated from 30 to 200 ^{o}C at heating rate of 10 ^{o}C/min under nitrogen atmosphere. Tensile properties of blown film samples were performed according to ASTM D 882 by universal testing machine (Instron: model 5567, USA). Crosshead speed of this tensile testing was 12.5 mm/min at 1 kN of load cell. Oxygen permeation (OP) of blown film samples was measured according to ASTM D 3985 by Mocon OX-TRAN model 2/21 with an oxygen flow rate of 40 cm^3/min at 0 %RH and 23 °C. The area of specimens was 100 cm^2. Water vapor permeation (WVP) of the blown film samples was measured according to ASTM F 1249 by Mocon PERMATRAN-W model 398.ll measurements were tested under nitrogen flow rate of 250 cm^3/min at 90 %RH and 37.8 °C.

Table 1. compositions of PLA/dryNR and PLA/NRL blends

Symbols	PLA (wt%)	dryNR (wt%)	NRL (wt%)
5 wt% dryNR	95	5	-
10 wt% dryNR	90	10	-
15 wt% dryNR	85	15	-
5 wt% NRL	95	-	5
10 wt% NRL	90	-	10
15 wt% NRL	85	-	15

3. Results and Discussion

3.1 Morphology

Figure 1 shows SEM micrographs of fractured PLA/dryNR and PLA/NRL films in MD. SEM micrograph of neat PLA shows smooth fractured surface (Figure 1(b)). When dryNR and NRL were added, domain sizes of rubber increased with increasing rubber content owing to coalescence of rubber particles. However, it was found that domain sizes of rubber in PLA/dryNR were larger than those in PLA/NRL films.

To make dryNR, acid is added into natural rubber latex, coagulation of rubber particles which are suspended in aqueous medium, occurs and sheet of rubber was obtained. Before melt mixing dryNR with PLA, dryNR sheet was cut into small pieces (around 4 mm). Small pieces of dryNR were put through hopper into extruder. Shear force, temperature and mixing time in an extruder would break and disperse rubber domains through PLA matrix. Even though there is shear force acting on dryNR particles, it is quite difficult to break up dryNR particles to be as small as rubber domain from rubber latex.

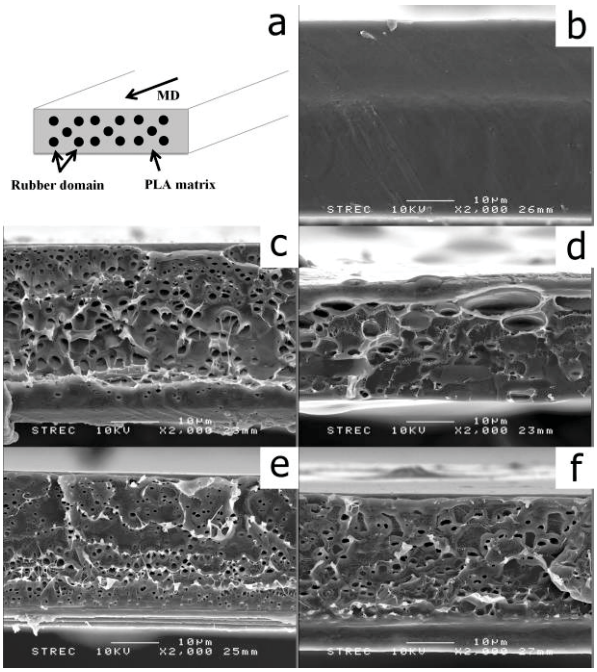

Figure 1. SEM micrographs of cross-sectional fractured surfaces of blown films in MD: (a) schematic drawings of dispersed rubber domain in PLA matrix (b) neat PLA, (c) 5 wt% dryNR, (d) 15 wt% dryNR, (e) 5 wt% NRL, (f) 15 wt% NRL

3.2 Thermal properties

Thermal properties of neat PLA, dryNR, PLA/dryNR and PLA/NRL blown films at 5, 10 and 15 wt% rubber content from the first scan of DSC thermograms are shown in Table 2. Although glass transition temperatures (Tg) of dryNR and NRL were -72.2 °C, Tg of all blends were nearby that of neat PLA film (about 60 ^{o}C) because the addition of NR did not affect chain mobility of PLA, indicating the immiscibility between PLA and NR. The degree of crystallinity (X_c) was calculated in Equation 1. The degree of crystallinity slightly increased with increasing rubber content because rubber could act as nucleating agent for PLA.

$$X_c = \frac{\left(\Delta H_m - \Delta H_{cc}\right)}{\left(\Delta H_o \times \Phi\right)} x100 \qquad \text{Equation 1}$$

Where, ΔH_m and ΔH_{cc} are enthalpies of melting and cold crystallization of PLA blends, ΔH_o (93 J/g) is the melting enthalpy of 100% crystalline PLA and Φ is weight fraction of PLA in blend.

Table 2. Thermal properties of neat PLA, dryNR, PLA/dryNR and PLA/NRL blown films at various rubber contents from the first scan of DSC thermograms

Sample	T_g (°C)	T_{cc} (°C)	T_{m1} (°C)	T_{m2} (°C)	ΔHc (J/g)	ΔHm (J/g)	X_c (%)
NeatPLA	60.1	123.1	-	151.7	11.92	13.33	1.51
dryNR	-72.2	-	-	-	-	-	-
PLA/5 wt% dryNR	59.9	102.2	146.2	155.6	20.53	23.75	3.64
PLA/10 wt% dryNR	59.7	99.1	144.5	154.6	20.52	24.08	4.25
PLA/15 wt% dryNR	59.0	97.7	144.8	155.3	16.01	19.80	4.79
PLA/5 wt% NRL	61.4	105.8	146.4	155.12	20.07	29.27	1.28
PLA/10 wt% NRL	61.3	104.4	145.6	154.8	23.41	24.71	1.55
PLA/15 wt% NRL	61.4	103.7	145.6	155.6	23.12	26.40	4.15

3.3 Tensile properties

Figure 2 shows elongation at break and tensile toughness of neat PLA, PLA/dryNR, and PLA/NRL blown films. PLA/dryNR and PLA/NRL blown films shows higher elongation at break and tensile toughness than those of neat PLA film. The maximum elongation at break and tensile toughness were achieved when PLA was incorporated with dryNR and NRL at 5 and 10 wt%, respectively. The increases in these properties can be explained by toughness mechanism such as crack-craze or the formation of micro voids in polymer matrix [4,5]. Then, these properties gradually dropped due to large domain size of rubber, resulting from coalescence. The elongation at break and tensile toughness of PLA/dryNR films were lower than those of PLA/NRL films because domain sizes of dryNR in polymer matrix films were larger than NRL in PLA. The degree of crystallinity in PLA/dryNR and PLA/NRL slightly increased with an increase of natural rubber content. It was found that large domain size of rubber was the major effect for tensile properties of PLA/dryNR blown film; thus, the decrease in both elongation at break and tensile toughness at high rubber content were observed.

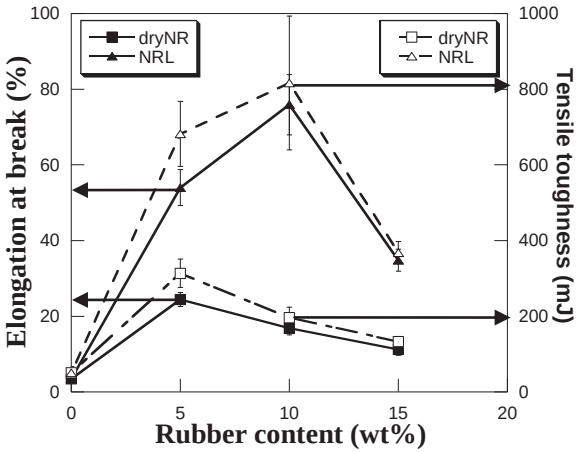

Figure 2. Tensile properties of PLA/dryNR and PLA/NRL blown films in MD

3.4 Gas permeability properties

Addition of natural rubber into PLA matrix resulted in increased oxygen permeability (OP) and water vapor permeability (WVP) as shown in Figure 3. PLA film with dryNR showed higher OP and WVP than those of neat PLA film because gas or vapor molecules can pass through gaps and free volume in amorphous rubber. Therefore, agglomeration of NR enhanced OP and WVP in PLA/dryNR blown films [14-16]. In case of NRL, OP and WVP did not significantly changed as rubber content increased due to small domain size of rubber in PLA/NRL blown films.

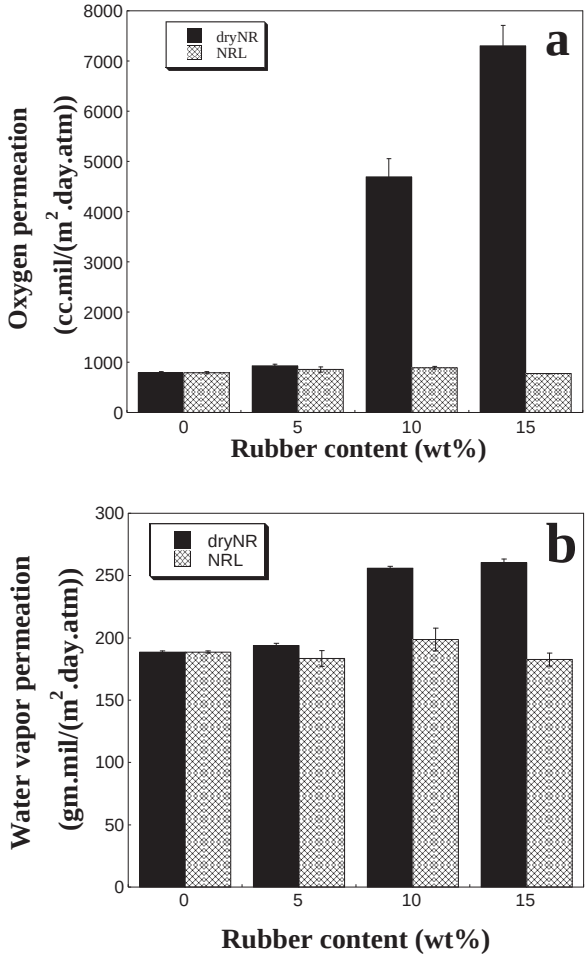

Figure 3. Gas permeability of PLA/dryNR and PLA/NRL blown films: (a) OP, (b) WVP

4. Conclusions

Adding dryNR and NRL into PLA could improved elongation at break, tensile toughness as well as gas permeability of neat PLA film. PLA/dryNR films showed higher gas permeability than PLA/NRL films as can be described by size of rubber domain. On the other hands, PLA/NRL films showed higher elongation at break and tensile toughness than PLA/dryNR films. It can be concluded that suitable properties of PLA films for Food packaging can be adjusted by varying type and content of rubber.

Acknowledgements

The authors would like to acknowledge Stimulus Package 2 (SP2) of Ministry of Education under the theme of Green Engineering for Green Society, and CU.GRADUATE SCHOOL THESIS GRANT from Graduate School of Chulalongkorn University for financial support.

References

[1] R. Auras, B. Harte, S. Selke, *Macromolecular Bioscience*. 4 (2004) 835-864.
[2] R. Auras, L.T. Lim, S.E.M. Selke, H. Tsuji, *Poly(lactic acid): Synthesis, Structures, Properties, Processing, and Applications*, Wiley, New Jersey, 2010.
[3] M.N. Belgacem, A. Gandini, *Monomers, polymers and composites from renewable resources*, Elservier, Amsterdam, 2008.
[4] Y.J. Li, H. Shimizu, *Macromolecular Bioscience*. 7 (2007) 921-928.
[5] S. Ishida, R. Nagasaki, K. Chino, T. Dong, Y. Inoue, *Journal of Applied Polymer Science*. 113 (2009) 558-566.
[6] I. Arvanitoyannis, C.G. Biliaderis, H. Ogawa, N. Kawasaki, *Carbohydrate Polymers*. 36 (1998) 89-104.
[7] I. Arvanitoyannis, E. Psomiadou, C.G. Biliaderis, H. Ogawa, N. Kawasaki, A. Nakayama, *Starch - Stärke*. 49 (1997) 306-322.
[8] G. Bang, S.W. Kim, *Journal of Industrial and Engineering Chemistry*. 18 (2012) 1063-1068.
[9] P. Monprasit, C. Ritvirulh, T. Sooknoi, S. Rukchonlatee, A. Fuongfuchat, D. Sirikittikul, *Polymer Engineering & Science*. 51 (2011) 1264-1272.
[10] B. Raj, K. Udayasankar, Siddaramaiah, *Advances in Polymer Technology*. 23 (2004) 32-45.
[11] Siddaramaiah, T. Jeevananda, K.S. Jagadeesh, H. Somashekarappa, R. Somashekar, *Journal of Applied Polymer Science*. 90 (2003) 2938-2944.
[12] R. Stephen, C. Ranganathaiah, S. Varghese, K. Joseph, S. Thomas, *Polymer*. 47 (2006) 858-870.
[13] S.A. Stern, J.R. Fried, *Permeability of Polymers to Gases and Vapors Physical Properties of Polymers Handbook*, Springer, New York, 2007.
[14] H. Cong, M. Radosz, B.F. Towler, Y. Shen, *Separation and Purification Technology*. 55 (2007) 281-291.
[15] T.C. Merkel, B.D. Freeman, R.J. Spontak, Z. He, I. Pinnau, P. Meakin, A.J. Hill, *Chemistry of Materials* 15 (2002) 109-123.
[16] G. Choudalakis, A.D. Gotsis, *Current Opinion in Colloid & Interface Science*. 17 (2012) 132-140.

CONTROLLED MOLECULAR WEIGHT POLYCARBONATE SYNTHESIS FROM MELT TRANSESTERIFICATION OF BISPHENOL-A AND DIPHENYL CARBONATE

Sunanta Klayposri[1], Suchada Tragoonwichian[2], Sarawut Rimdusit[1*]

[1] Department of Chemical Engineering, Faculty of Engineering , Chulalongkron University, Phayathai Road.Pathumwan, Bangkok, 10330 Thailand
[2] Innovation and Technology Department, PTT Phenol Company Limited, Chatuchak, Bangkok, 10900 Thailand.
*E-mail: sarawut.r@chula.ac.th, Tel. +66 22 186878, Fax. +66 22 186877

Abstract: Melt transesterification was carried out to produce polycarbonate (PC) in order to utilize the environmental friendly aspect of the process without the use of hazardous phosgene reactant. In this work, PC from aromatic dihydroxy compound i.e. bisphenol-A (BPA) and a diaryl carbonate i.e. diphenyl carbonate (DPC), was polymerized via melt transesterification reaction. The polycarbonate prepolymer with a critical molecular weight (Mc) of about 5,000 was prepared as a precursor for branched PC synthesis. The conditions for the prepolymer preparation were investigated and properties of the as-synthesized PC prepolymer were characterized. The reaction could be performed at relatively low temperature, using no catalyst, and by varying mole ratios of DPC/BPA reactants. In the latter case, the initial mole ratios of DPC/BPA were varied at 1.05:1.00 and 1.26:1.00. The initial mole ratio of DPC/BPA at 1.05:1.00 yielded higher PC molecular weight than that at 1.26:1.00 mole ratio comparing to the same synthesis conditions. The mole ratio of the functional end groups of the two reactants tended to be almost unity during the course of the polymerization when the initial DPC/BPA of 1.05:1.00 was used due to the slight loss of DPC from the reaction. Finally, the PC prepolymer prepared using the initial DPC/BPA mole ratio of 1.26:1.00 was found to be appropriate for the preparation of the PC precursor to provide a molecular weight in a range that suitable for branched PC production.

1. Introduction

Polycarbonate is one of engineering thermoplastics possessing favorable properties such as very high impact resistance, outstanding optical clarity, and high dimensional stability [1]. The structure of polycarbonate is linear in most commercial grade. It is widely used in data storage devices, structural materials for electrical and electronic applications, automobiles, and constructions [2]. However, in processes and applications such as blow molding or extrusion of sheet products, it is more desirable to use branched polycarbonate due to its higher melt strengths and melt elasticity [3].

Polycarbonate is synthesized industrially either by an interfacial phosgenation process or by a melt transesterification process. In a typical melt transesterification process, diphenyl carbonate (DPC) and bisphenol-A (BPA) are polymerized in the presence of a catalyst to yield sufficiently high molecular weight of the resulting PC. During this polymerization process, a partial loss of diphenyl carbonate may occur as the reaction by-product, phenol, is removed from the reactor. To obtain a high molecular weight polymer under high temperature and low pressure conditions, a stoichiometric mole ratio of the two reactive end groups needs to be maintained during the polymerization [4]. Therefore slightly excess amount of DPC is needed to compensate the evaporation loss above.

In this work, polycarbonate prepolymer from diphenyl carbonate (DPC) and bisphenol-A (BPA) will be prepared via transesterification reaction. The polycarbonate prepolymer was synthesized to be used as a precursor for branched PC production. The critical entanglement molecular weight (Mc) of polycarbonate was 5,000 as reported by Z.Dobkowski [5]. This molecular weight is a critical value for the PC precursor preparation in order to synthesize branched PC with long chain branching characteristics and to provide desirable rheological behaviors. This level of branch molecular weight could improve melt strength of the polycarbonate which makes it particularly suitable for such types of polymer processing procedures as blow molding of large, hollow containers, corrugate sheet and the extrusion of complex profile as discussed by Hoeks et al.[6]. The suitable conditions for the branched PC prepolymer preparation will be investigated in this study.

2. Experimental

2.1 Materials

Bisphenol-A was supplied by PTT Phenol Co., Ltd. Purity of BPA is 99.97% with melting temperature of 159^{o}C. Diphenyl carbonate as a co-monomer was purchased from Aldrich. Purity of the DPC is 99.9% with melting temperature of 81^{o}C. Tetrahydrofuran (THF, HPLC grade) and chloroform (AR grade) were purchased from RCI Labscan. A linear PC with molecular weight of 49,171, used as a reference, was supplied by Chi Mei Corp.

2.2 Synthesis of Polycarbonate Prepolymer

Batch melt transesterification experiments were carried out using a 250 ml round-bottomed four-necked flask as a reactor equipped with a mechanical stirrer. The reaction of diphenyl carbonate (DPC) and

bisphenol-A (BPA) was carried out by varying initial DPC/BPA mole ratios under nitrogen atmosphere. The reactor was then heated to the desired reaction temperature with constant pressure of 760 mmHg under mechanical stirring and a rotation speed of 200 rpm. After 90 min, the pressure was immediately reduced to 100 mmHg. The generated vapour from the polymerization process was trapped by passing the outgassing products through an ice-cooled vacuum trap.

2.3 Sample Characterizations

Weight average molecular weight (Mw) of as-synthesized PC precursor was determined by gel permeation chromatography (GPC). The GPC system consisted of a Waters 600 E chromatographer, Waters 410 refractometer and three Waters Styragel columns (HR-4, HR-3 and HR-2). The mobile phase i.e. tetrahydrofuran (THF), was maintained at 40°C and at a flow rate of 1.0 ml/min. The GPC was calibrated with narrow polydispersity polystyrene standards, and molecular weights of the obtained products were reported as polystyrene equivalents.

Chemical structures of polycarbonate were studied by FT-IR spectroscopic technique. The FTIR spectra were recorded on a Spectrum GX FTIR spectrometer from Perkin Elmer at a resolution of 4 cm^{-1} in transmittance mode with the frequency range from 4000 to 400 cm^{-1}. The analysis was performed on thin film, obtained from $CHCl_3$ solution casting onto a potassium bromide (KBr) plate. Evaporation of the solvent was done at room temperature.

Glass transition temperature (Tg) of polycarbonate was determined by a differential scanning calorimeter (DSC) model 2910 from TA Instruments. Each specimen with a mass in a range of 3-5 mg was sealed in an aluminum pan with lid. The specimen was heated from room temperature to 300°C using a heating rate of 10°C/min under nitrogen atmosphere. The purge nitrogen gas flow rate was maintained at 50 ml/min.

Rheological properties of synthesized PC were examined using a Rheometer (Haake Rheo Stress 600, Thermo Electron Cooperation) equipped with 25 mm parallel plate geometry. The measuring gap was set at 1 mm. For dynamic frequency sweep mode, the dynamic viscoelastic properties were determined with frequencies ranging from 0.01 to 100 Hz at fixed temperature of 260°C.

3. Results and Discussion

3.1 Synthesis Condition of Polycarbonate Precursor

The polycarbonate precursor was synthesized from diphenyl carbonate and bisphenol-A via melt transesterification reaction as seen in Scheme 1.

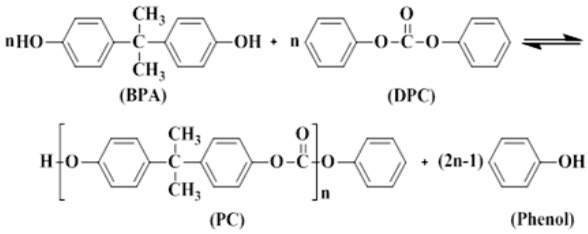

Scheme 1. Transesterification of BPA and DPC.

One measure to drive the reaction forward is thus by a removal of the phenol by-product. This was done by the application of relatively high vacuum. In this work, the evacuated pressure of 100 mmHg was found to be sufficient for this purpose.

The synthesis condition of PC is shown in Figure 1. It is desirable to minimize the loss of DPC at the beginning of the reaction by maintaining the polycondensation at a relatively low temperature of 180°C for 60 min. At this stage, the monomers will be converted to less volatile or higher molecular weight oligomers thus suppressing the loss of the reactant above. After that, the reactor was operated at reduced pressure and increased temperature up to 200°C in order to facilitate a removal of the condensation by-product (phenol) and to reduce melt viscosity due to the increasing in molecular weight of the reaction mixture as a function of reaction time.

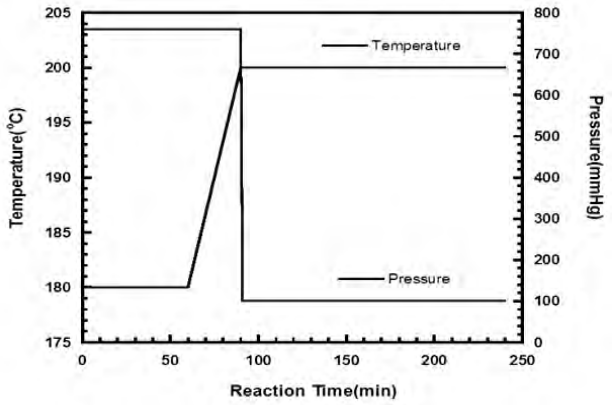

Figure 1. Synthesis condition of polycarbonate precursor in this study.

In this work, the synthesis condition of polycarbonate perpolymer have been studied experimentally in a batch reactor. Number-average (Mn) and weight-average (Mw) molecular weights of the synthesized PC during the course of the synthesis were measured by GPC. From the results, when the molar ratios of DPC/BPA used were 1.05/1.0 and 1.26/1.0, the synthesis of polycarbonate prepolymer with a molecular weight of above its critical molecular weight (Mc) of 5,000 was achieved at temperature of 200°C and at a pressure of 100 mmHg without a catalyst addition. In addition, it is found that a base catalyst which is normally required in the transesterification reaction was not needed in our polymerization process. This is due to the fact that the BPA used in this work which was supplied by PTT Phenol Co. contains some trace amount of NaOH. The chemical was used to stabilize BPA in the production

process as reported by the company. Consequently, no additional base catalyst was needed in our PC precursor preparation.

3.2 FTIR Investigation of As-synthesized PC

FTIR spectra of the synthesized PC precursor and commercial PC (Chimei) are compared in Figure 2. The CH_3 absorption bands at 2970 cm^{-1} and 2874 cm^{-1} corresponded to asymmetric and symmetric CH_3 stretching vibrations, and the bands at 1465, 1387 and 1365 cm^{-1} corresponded to asymmetric and symmetric CH_3 deformation vibrations. The carbonate absorption band at 1773 cm^{-1} was assigned to the free carbonyl stretching vibration, whereas the bands at 1235 cm^{-1}, 1194 cm^{-1}, 1164 cm^{-1} were assigned to C-O stretching vibration. The bands at 1081 cm^{-1}, 1015 cm^{-1}, and 831 cm^{-1} were assigned to C-H deformation vibration of ring hydrogen, while the bands at 1602 cm^{-1} and 1506 cm^{-1} were from C-C stretching vibration. In addition, the bands at 1387 cm^{-1} and 1365 cm^{-1} were assigned to $C(CH_3)_2$ asymmetric bending vibration of substituted phenyl, and the weak band at 757 cm^{-1} was assigned to ring deformation vibration. The obtained FTIR spectra of the commercial linear polycarbonate and the as-synthesized polycarbonate are closely similar. These assignments are in good agreement with those of linear PC as reported by Delpech et al. [7].

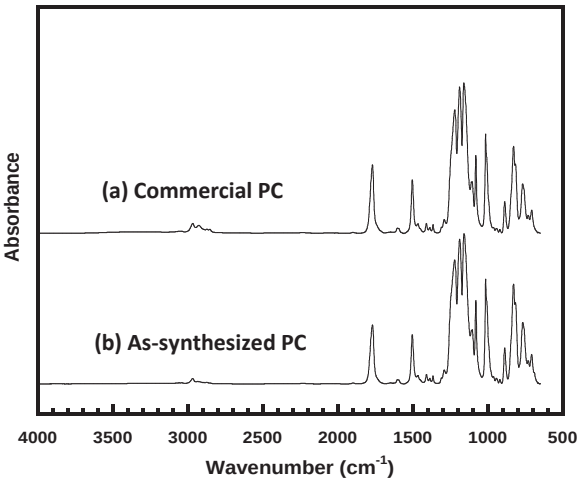

Figure 2. FTIR spectra of (a) Commercial PC, and (b) As-synthesized PC.

3.3 Effect of DPC/BPA Mole Ratio on Molecular Weight of Synthesized Polycarbonate

In principle, the synthesis of PC precursor can be performed in a more slowly and controllable manner by decreasing reaction temperature, using no catalyst, and by varying mole ratio of DPC/BPA. In this work, we had varied the initial mole ratios of DPC/BPA at 1.05:1.00 and 1.26:1.00 and the development of the PC molecular weight as a function of time was examined by GPC. From Figure 3, it was observed that the polymer molecular weights at various reaction time were significantly different when the initial mole ratio of the two reactants were varied. It was also found that the higher molecular weight was obtained when the initial mole ratio of DPC/BPA was 1.05:1.00. Theoretically, the highest molecular weight of the condensation polymerization product is obtained when the concentrations of the two functional end groups are equal as also can be seen in the results reported by Woo et al [4]. The observed phenomenon might be due to the small loss of the DPC comonomer during the synthesis. The small loss of DPC occurs as the reaction by-product phenol is removed from the reactor by high vacuum.

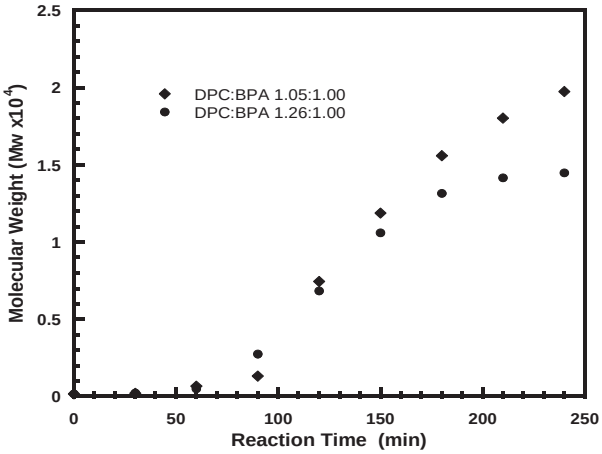

Figure 3. Molecular weight profiles of synthesized polycarbonate at mole ratios of DPC/BPA = 1.05:1.00 and 1.26:1.00.

In the case of DPC/BPA of 1.05/1.0, the obtained molecular weight at the reaction time of 240 min was found to be about 20,000 whereas lower molecular weight value of about 14,000 was obtained when the mole ratio of DPC/BPA was fixed at 1.26/1.0. At the latter mole ratio of the two reactants, the observed molecular weight of the end product tended to reach a relatively constant value. This molecular is sufficient for the preparation of long chain branching PC in the next part of our work. Therefore, the PC prepolymer at the initial DPC/BPA mole ratio of 1.26:1.00 was used in our following investigation.

3.4 Effect of Molecular Weight on Glass Transition Temperature of Synthesized Polycarbonate

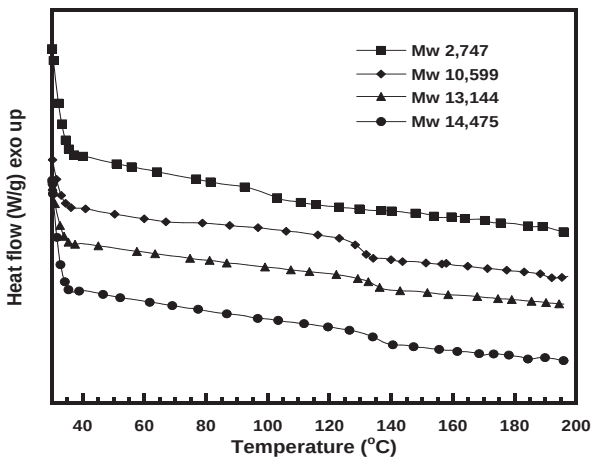

Figure 4. DSC thermograms of as-synthesized PC at different molecular weights; (■) Mw 2,747, (◆) Mw 10,599, (▲) Mw 13,144, and (●) Mw 14,471.

Figure 4.exhibits DSC thermograms of as-synthesized PC precursor at different molecular weights ranging from 2,747 to 14,475. The Tg values at the corresponding molecular weight determined from the step change of the thermograms were 101^{o}C, 130^{o}C, 133^{o}C and 136^{o}C, respectively. The results suggested that as the molecular weight of PC increased, the Tg significantly shifted to higher values. In theory, the Tg of polymer increases with a decrease in free volume due to increasing molecular weight. The higher the molecular weight, the lower free volume contribution from the terminal ends of the polymer [8]. The molecular weight of the PC of our prepolymer is lower than the reported PC molecular weight of approximately 150^{o}C of the commercial grade is obviously due to the lower molecular weight values of the prepolymer compared to that of the commercial grade.

4. Conclusions

Polycarbonate prepolymer with a molecular weight above its critical molecular weight value of 5,000 was successfully synthesized to be used as PC precursor for further branched PC preparation. The reaction could be performed at low temperature, and by varying mole ratios of DPC/BPA reactants. The development of the molecular weight of the PC product was followed by GPC technique. The initial mole ratios of DPC/BPA were varied at 1.05:1.00 and 1.26:1.00. The PC prepolymer prepared using the initial DPC/BPA mole ratio of 1.26:1.00 was found to be appropriate for the preparation of the PC precursor to provide a molecular weight in a range that suitable for branched PC production with long chain branching characteristics. The obtained FTIR absorption bands suggested the formation of PC by condensation of BPA with DPC. The Tg significantly increased with increasing molecular weight of the synthesized PC.

Acknowledgements

This work is supported by Innovation and Technology Department PTT Phenol Company Limited and the Higher Education Research Promotion and National Research University Project of Thailand office of the Higher Education Commission (AM1076A).

References

[1] S. P. Kim, J.S. Lee, S.H. Kim, B.H. Lee, S. H. Kim, and W.G.Kim, Ind. Eng. Chem. Res., 5, 268-273 (1999).
[2] B. G. Woo, K. Y. Choi and K. H. Song, Ind. Eng. Chem. Res., 40, 3459-3466 (2001).
[3] D. Karlik, H. P. Brack, H. Verhoogt, J. P. Lemmon, J. H. Kamps, W. L. Sederel, J.M.D. Goossens, U.S. Patent 6,504,002 B1 (2003).
[4] B.G. Woo, K.Y. Choi, K.H. Song, and S.H. Lee, J. Appl. Polym. Sci., 80, 1253-1266 (2001).
[5] Z. Dobkowski, Rheolo. Acta, 34, 578-585 (1995).
[6] T. L. Hoeks, A. M. Kusters, Y.G. Lin, P. J. MeCloskey, R. Mestanza,P.P. Wu, U.S. Patent 6,087,468 (2000).
[7] M.C. Delpech, F.M.B. Coutinho, M.E.S. Habibe, Polym. Test., 21, 155-161 (2002).
[8] L.H. Sperling. Introduction to Physical Polymer Science. New York : John Wiley & Sons, Inc., 2006.

EFFECT OF BLEND COMPOSITIONS ON PROCESSING AND MECHANICAL PROPERTIES OF POLYCARBONATE / ACRYLONITRILE-STYRENE-ACRYLATE BLENDS

Sirisak Laopetcharat[1], Ruksapong Kunanuruksapong[2], Sarawut Rimdusit[1*]

[1]Department of Chemical Engineering, Faculty of Engineering, Chulalongkorn University, Pathumwan, Bangkok, 10330 Thailand.
[2]Innovation and Technology Department, PTT Phenol Company Limited, Chatuchak,
Bangkok, 10900 Thailand.
*E-mail: sarawut.r@chula.ac.th, Tel. +66 22 186878, Fax. +66 22 186877

Abstract: PC/ASA blends are increasingly used commercially because these materials provide products with outstanding balance of properties such as good processability, low notch sensitivity and, in particular, good weatherability. This research aims to study processing behaviors, impact strength and dynamic mechanical properties of PC/ASA blends as a function of their compositions. PC/ASA mixtures at the mass ratios between 100/0 to 50/50 were blended by melt mixing in a twin screw extruder at temperature ranging from 210-240°C. The test specimens were fabricated by injection molding at various temperatures to obtain highest impact strength of each blend ratio. The experimental results revealed that storage modulus (E′) at room temperature of the PC/ASA blends systematically increased with increasing PC amount in the blends. Furthermore, the glass transition temperatures (T_g) of both PC and ASA phases in the blends were found shifted towards each other with increasing PC fraction. In addition, processing temperature showed substantial effect on impact strength of the blends. The optimal processing temperature tended to increase with an increase of PC mass fraction. Moreover, the impact strength of PC/ASA blends was found to increase steadily with an increase of PC content which obeys the rule of mixtures.

1. Introduction

Polycarbonate (PC) is a widely used engineering thermoplastic because it possesses several distinct properties such as transparency, high heat distortion temperature, toughness and excellent electrical resistance [1]. However, some deficiency of properties of PC deters its specific use such as thickness dependence of the notched impact strength and the poor radiation, solvent, or hydrolysis resistance. To solve these shortcomings, efforts have been made through development of polymer blends and alloys of PC.

ASA resins are widely used in industrial applications, for example, coating, adhesives, and paints. Furthermore, ASA can also be blended with many polymers to make alloys and compounds in order to utilize ASA's weather and impact resistance [2]. ASA was prepared by grafting copolymerization of styrene and acrylonitrile monomers onto acrylic rubber particles. The copolymer has been used for PC modification due to improvement on weatherability, notch-sensititvity and flow properties [3].

In this research, we aim to study effects of ASA contents on major properties of the resulting blends with PC including processing behaviors, notched Izod impact strength and dynamic mechanical properties.

2. Materials and Methods

2.1 Materials

Polycarbonate (PC) used as one of components of the blends is injection grade and another component of the blends, acrylonitrile-styrene-acrylate graft copolymer (ASA) is extrusion grade.

2.2 Preparation of Polymer Blends

Blends of PC and ASA were prepared by melt mixing in a twin-screw extruder. Temperatures of the ten zones of the extruder were set at 210°C - 240°C from die side. PC and ASA were dried at 110°C and 90°C, respectively, for 4 hours in a vacuum oven in order to remove moisture. The PC/ASA blends were prepared at different weight ratios, which were varied between 100/0 and 50/50 in a twin-screw extruder. The test specimens were obtained by an injection molding machine.

2.3 Characterization Methods

Dynamic mechanical properties i.e. storage modulus (E′) and loss tangent (tanδ) data were measured with dynamic mechanical testing apparatus (model DMA 242C, Netzsch). The dimension of the specimens was rectangular with 50 mm in length, 10 mm in width, and 2 mm in thickness. The three point bending mode of deformation was used under a test temperature range of 30 °C to 180 °C with a heating rate of 2 °C/min. The test was performed in a temperature sweep mode with a constant frequency of 1 Hz.

Notched Izod impact strength was measured by an impact tester from Yasuda Seiki Seisakusho Ltd. (Japan) according to ASTM D256. The impact bar specimen had a length of 63 mm, a width of 12.7 mm, and a thickness of 3 mm. A notch at one side centered in the direction along the length with a depth of 2 mm was made for each specimen.

3. Results and Discussion

3.1 Dynamic mechanical properties of PC/ASA blends

Storage modulus (E′) and loss tangent (Tan δ) obtained from DMA tests were utilized to characterize the neat PC and ASA and all of their blends to get information about dynamic mechanical properties. The DMA thermograms of all blend samples are shown in Figure 1-2. Figure 1 exhibits storage modulus (E′) as a function of temperature of the PC/ASA blends. From this figure, storage modulus at room temperature of PC was determined to be 2.9 GPa while that of ASA was about 1.3 GPa.

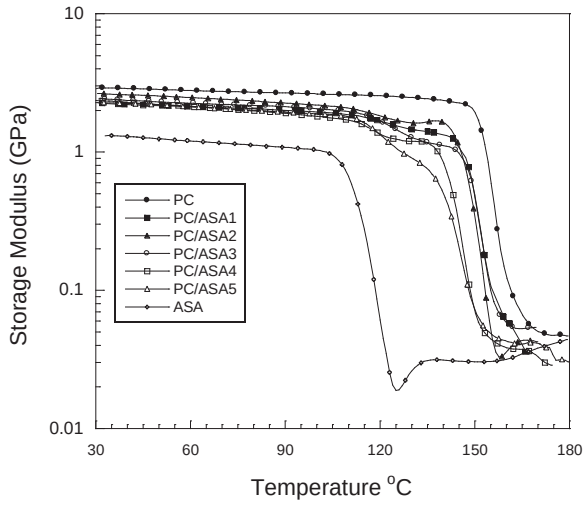

Figure 1. Storage modulus versus temperature (°C) of PC/ASA blends at various blend ratios: (●)PC, (■)PC/ASA1, (◆)PC/ASA2 , (▲)PC/ASA3**,** (□)PC/ASA4, (△)PC/ASA5, (◇)ASA.

Furthermore, storage modulus at room temperature was observed to increase with increasing the amount of PC in the blends since PC was inherently more rigid than ASA. Moreover the blends exhibited two step decreases in the modulus values corresponded to the positions of glass transition temperature (T_g) of the PC and ASA phases. From the figure, the positions of T_g's of both PC and ASA phases in the blends were slightly shifted towards each other with increasing the fraction of PC. This observation suggested the partially miscible nature of these polymer blends.

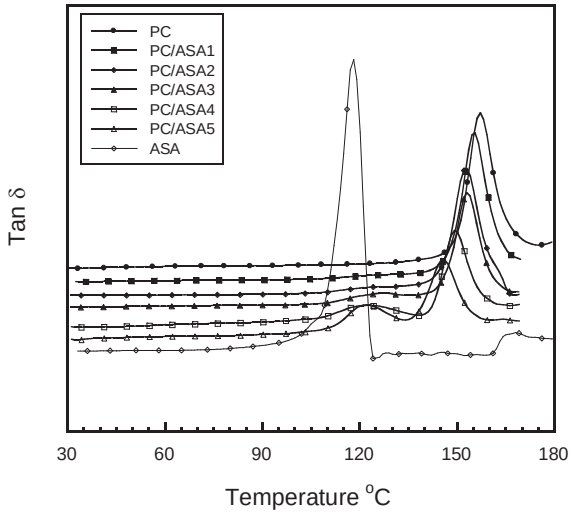

Figure 2. Loss tangent versus temperature (°C) of PC/ASA blends at various blend ratios: (●)PC, (■)PC/ASA1, (◆)PC/ASA2, (▲)PC/ASA3**,** (□)PC/ASA4, (△)PC/ASA5, (◇)ASA.

Glass transition temperatures of PC/ASA blends were more clearly observed in the DMA thermograms based on the α-relaxation peaks of tanδ. Figure 2 illustrates the tanδ curves of PC/ASA blends at various compositions. The T_g's from the peak of tanδ of the neat ASA and the neat PC were found to be 118°C and 157°C respectively. For the PC/ASA blends, one dominant peak was observed when ASA content reached the optimum level. However, when the ASA content was greater than that point, two clearly separated peaks of the ASA-rich phase and of the PC-rich phase were observed. From the figure, the position of T_g of the ASA phase increased with increasing the fraction of PC in the blends. On the other hand, T_g of PC was slightly shifted to lower temperature with increasing the fraction of ASA in the blends as T_g of PC is higher than that of ASA.

3.2 Notched Izod impact strength of PC/ASA blends

The effect of PC content on the toughness of the two blending systems was investigated based on the impact energy measured from the notched Izod impact tests. Figure 3, shows the notched Izod impact strength as a function of the blend ratios of PC/ASA. The greater the PC component, the higher the impact strength of the PC/ASA blends which the values shown in Figure 3. The impact strength of the blends increased from 384 J/m of pure ASA to the value 835 J/m of pure PC due to the fact that of impact value of PC is higher than that of the ASA [4]. It was found that the notched Izod impact strength of PC/ASA increased steadily with an increasing PC content which obeys the rule of mixture.

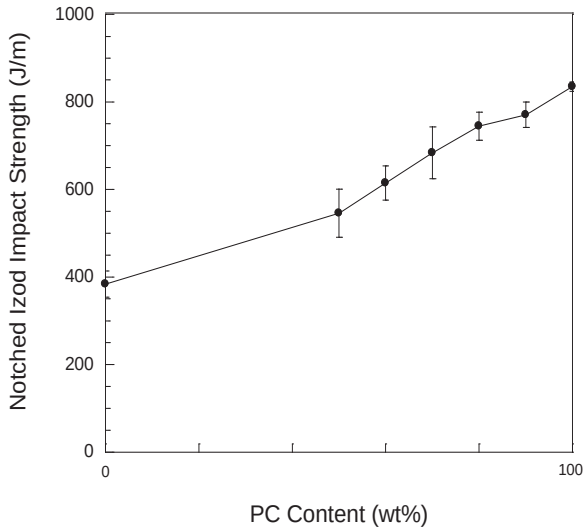

Figure 3. Notched Izod impact strength versus blend ratios of PC/ASA.

3.3 Effect of processing temperature on impact properties of PC/ASA blends

The impact behavior as a function of processing temperature of PC/ASA blends was studied and illustrated in Figure 4. The notched Izod impact was observed to show a maximum value with an increasing processing temperature. This may be due to phase separation in a lower critical solution type of the PC/ASA blends at high temperature. It was suggested that the processing temperature had a significant effect on the impact strength. In ASA/poly(butylene terephthalate)(PBT) blend system[5,6], the similar optimal processing temperature to yield maximum mechanical properties of the blends was found to be in a range of 230 ^{o}C. The same range of processing temperature of ASA/PBT system was also found to be appropriate for ASA/PET blend i.e. 210-220 ^{o}C. The rather low impact strength at low processing temperature in our study was likely due to poor flow ability of the blend.

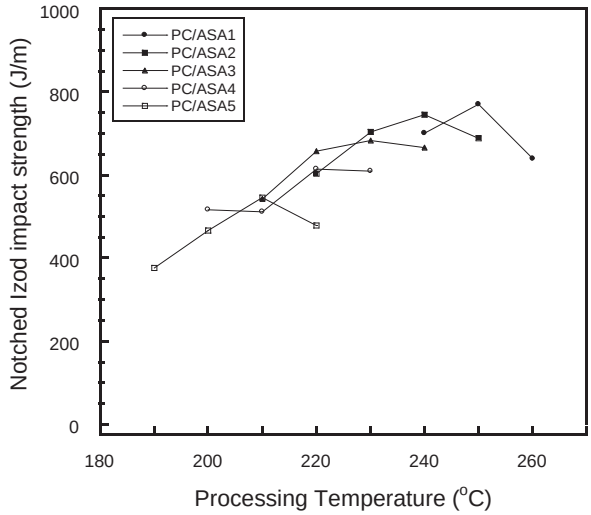

Figure 4. Notched Izod impact strength versus processing temperature of PC/ASA blends at various blend ratios: (●)PC/ASA1, (■)PC/ASA2, (▲)PC/ASA3**,** (▲)PC/ASA4, (□)PC/ASA5.

4. Conclusions

The effects of PC contents in PC/ASA blends on their dynamic mechanical and impact properties were investigated. As PC content increased, the storage modulus at room temperature and notched Izod impact strength of the PC/ASA blends were found to increase steadily. According to the loss tangent curves, the PC/ASA blends exhibited two separated T_g's that represented the T_g of the PC and ASA rich phases. T_g's of ASA and PC phases were also found to shift towards each other with increasing amount of PC suggesting the partially miscible nature of the PC/ASA blends. The processing temperature showed substantial effect on impact strength of the blends. The optimal processing temperature tended to increase with the PC mass fraction in the blends.

Acknowledgements

This work is supported by Innovation and Technology Department PTT Phenol Company Limited and the Higher Education Research Promotion and National Research University Project of Thailand, Office of the Higher Education Commission (AM1076A).

References

[1] D. Freitag, U. Grigo, P.R. Muller and W. Nouvertne, Polycarbonates, *Encyclopedia of Polymer Science and Engineering*, **11** (1988) 648-718.

[2] S. Tolue, M.R. Moghbeli and S.M. Ghafelebashi., *Preparation of ASA (Acrylonitrile-Styrene-Acrylate) Structural Latexs via Seeded Emulsion Polymerization*, Eur Polym J., **45** (2009) 714-720.

[3] G. Works, *Acrylonitrile-acrylic-styrene elastomer terpolymer*, Polymeric Materials Encyclopedia, C.S. Joseph, ed., **1** (1996) 78.

[4] H. Schirmer et al., *Thermoplastic molding compositions of a polycarbonate and a graft copolymer of styrene and acrylonitrile on an acrylic acid ester polymer*, U.S. Pat. 3,891,719 (1975)

[5] F.L. Italian and J. Sciarra, *Composition of a Weatherproof Roofing Material*, U.S. Pat. 4,737,532 (2000)

[6] L.E. Nielsen and R.F. Landel, *Mechanical Properties of Polymers and Composites*, 2nd ed. The United State of America, Marcel Dekker, (1994).

EFFECT OF ZINC ON ANTI-CORROSION OF STEEL SHEETS COATED WITH EPOXY POLYESTER POWDER CONTAINING POLYANILINE

Sureerat Tipoo[1], Supawan Tantayanon[2,3*]

[1] Program in Petrochemistry and Polymer Science, Faculty of Science, Bangkok 10330, Thailand
[2] Green Chemistry Research Laboratory, Department of Chemistry, Faculty of Science, Chulalongkorn University, Bangkok 10330, Thailand
[3] Center of Petroleum and Advanced Material, Chulalongkorn University, Bangkok 10330, Thailand

[*] E-Mail: supawan.t@chula.ac.th, Tel. +662 218 7641, Fax. +662 218 7641

Abstract: Normally the epoxy resins are used to coat the steel sheets for corrosion protection. In this study, the epoxy polyester powder was employed. In addition, zinc dust and zinc flake were added to the epoxy polyester powder containing polyaniline (PANI) for steel sheet coating. PANI was synthesized by chemical oxidative polymerization method using ammonium peroxydisulfate as oxidant. The resulting polymer was characterized by FT-IR spectroscopy and had conductivity in the range of 3 to 4 x 10^{-2}S/cm, measured by a four-point probe meter. The content of zinc dust and zinc flake at the ratio of 4:1 was varied, 25-50 phr, while the amount of PANI was kept constant at 5 phr. Each of eight epoxy polyester powder formulations was deposited on a steel sheet by electrostatic spray coating. The anti-corrosion test of these coated steel sheets was performed using the salt spray technique according to ASTM B-117 and evaluating with ASTM D-1654. When the amount of zinc increased, size and frequency of blistering appeared to be smaller. It was observed that the formulation with zinc 50 phr showed better anti-corrosion than the others. It indicated that the presence of zinc was necessary as the zinc corroded and blocked further corrosion attack. The physical and mechanical properties of all the coated steel sheets, such as adhesion to substrate, impact resistance and gloss, had also been evaluated. The steel sheet coated with epoxy polyester powder containing zinc 50 phr and PANI 5 phr had the satisfactory anti-corrosion as well as physical and mechanical properties.

1. Introduction

Protection of metals against corrosion by using coatings is an area of great interest. The development of new paint based coatings attempts to improve the corrosion resistance. Powder coatings offer several advantages including little or no volatile organic compound (VOC), high utilization rates and elimination of hazardous waste [1]. Normally the anti-corrosion powder coatings are often formulated from epoxy. Epoxies do provide excellent protection but have other limitations, primarily their poor resistance to sunlight or other ultraviolet radiation, they "chalk". Epoxy polyester can be considered part of the epoxy family except that the high percentage of polyester utilized, these coatings are more closely like to epoxies than polyester. A major advantage of the polyester component is a higher resistance to over-bake yellowing in the cure oven. These systems begin to chalk almost as fast as an epoxy, but the deterioration is slower and discoloration less severe. Zinc, one of the most effective anti-corrosion pigment was used in order to protect steel from corrosion, well performed by high loadings that must maintain zinc particle to zinc particle contact within its continuum and contact between zinc and substrate to ensure electrical conductivity within the coating layer and across the interface [2]. Indeed, above a concentration of about 70% by weight of zinc particles, manufacturers of powder coatings encounter problems of powder homogeneity. This means that that zinc, binder and other additives are not well distributed in each powder particle after extrusion and before application. When the coating is cured, this fact finally allows zinc-rich and zinc-poor areas inside the coating. In order to resolve these technological restrictions, zinc flake are introduced, in combination with spherical zinc dust [3]. Conducting polymers have recently been studied as a new class of materials for the corrosion protection of metals [4-12]. The most popular among conducting polymers is polyaniline (PANI) due to its acceptable chemical stability together with a relatively high electrical conductivity and ease to synthesis [13]. In this study, we studied the influence of polyaniline and zinc content on the anti-corrosion of epoxy polyester powder. PANI is added in order to improve electrical contact between zinc particles themselves and the steel substrate.

2. Materials and Methods

2.1 Synthesis of PANI

The conductive form of polyaniline (PANI-CL: emeraldine salt) is produced by the oxidative polymerization of hydrochloride aniline (97% pur. from Aldrich) by ammonium peroxydisulfate (98% pur. from Aldrich) in hydrochloric acid (37% pur. from Merck). The preparation of PANI-Cl followed the method which was reported by Stejskal and Gilbert [14]. Very fine and uniform PANI powder was obtained (140 mesh size) after crushing. The PANI powder was characterised by SHIMADZU IR Prestige-21 FTIR spectrophotometer in KBr medium at room temperature in the region of 2000-500 cm^{-1}.

2.2 Preparation of epoxy polyester powder

Coatings were prepared by using materials as follow:

(a) Polyester resin (Synthese, Thailand)
(b) Epoxy resin (Aditya-Birla, Thailand)
(c) Levelling agent (Cytec industries, USA)
(d) Degassing agent (Jingjiang hongtai, China)
(e) Zinc dust, mean diameter 4 μm (Umicore, Malaysia)
(f) Zinc flake, mean length 20 μm (Eckart, Germany)

For powder coating, the following compositions have been used: epoxy resin (30%), polyester resin (70%), levelling agent (1 phr), degassing agent (0.3 phr) while the amount of PANI was kept constant at 5 phr [6] and the content of zinc dust and zinc flake at the ratio of 4:1 was varied.

Table 1: Zinc content in epoxy polyester containing polyaniline

No.	Zinc dust (phr)	Zinc flake (phr)	Total (phr)
1	40.00	10.00	50.00
2	35.00	8.75	43.75
3	30.00	7.50	37.50
4	25.00	6.25	31.25
5	20.00	5.00	25.00

All ingredients were homogenously mixed in high speed mixer and extruded by lab model single screw extruder (BUSS PCS30-7D, Switzerland) at 110-115 ˚C followed by cooling, grinding and sieving for obtaining the final powder for coating. Steel substrates (7 cm x 15 cm x 0.8 mm) which were polished with fine emery paper and cleaned with xylene were used for coating. Electrostatic spray gun used for deposition of powder coating which was held at 80 kV potential with respect to the substrate (grounded). After obtaining uniform coverage of powder, the coated steel sheets were placed in oven for curing at 180 ˚C for 15 min. The coated plates were then cooled in air. The coating thickness was in the range of 40-60 μm.

2.3 Physical and mechanical properties of the coatings layer

Because free coating films are difficult to prepare, the properties of the coatings were measured directly on metal bases in accordance with standardized test.

2.3.1 Gloss

The gloss was measured by BYK-Gardner Tri-angle gloss meter (20˚, 60˚, 85˚).

2.3.2 Adhesion (ASTM D 3359)

A lattice pattern with eleven cuts in each direction is made in the film to the substrate, pressure-sensitive tape is applied over the lattice and then removed, and adhesion is evaluated by comparison with descriptions and illustrations.

2.3.3 Impact resistance (ASTM D 2794)

The test revealed the height of the free fall of weight (1,800 g) at which the paint film still resists damage. The test was performed on the coated side of the panel.

2.4 Differential scaning calorimetry (DSC)

The thermal behaviors of coating were performing by Differential scaning calorimetry (DSC). A few milligrams of uncured powder were placed in aluminium pan. Thermograms of coating formulation were recorded in after second heating cycles, First heating was carried out up to 280 ˚C at rated 10 ˚C/min. The cured sample was then cooled and heating route was repeated at a rate of 10˚C/min and recorded the heating curve until all transitions have been completed. Tg of cured powder were determined.

2.5 Corrosion test

The coated samples were intentionally marked to create a scribe mark. These were tested for corrosion resistance using salt spray technique following ASTM B-117. Edges of the panels were properly sealed using the tape. Both edge sealing and rear side painting of the panel was to avoid corrosion of unprotected part of the substrate during in salt fog chamber. The evaluation of corrosion processes was carried out in accordance with ASTM D 1654.

3. Results and Discussion

3.1 Characterization of PANI

The conductivity of PANI was measured by the four probe method using a Keithley current source and the room temperature electrical conductivity was found in range of 3 to 4 x 10^{-2} S/cm which suggests that it is moderately doped as against the highly dope PANI obtained in acidic media [6].

The IR spectrum (Fig. 1) of the synthesized PANI-Cl is in a good agreement with previously reported results [15-17]. The main peaks at 1570 cm^{-1} and 1490 cm^{-1} in the spectrum of PANI-HCL correspond to quinoid ring and benzenoid ring stretching deformation. The band at 1300 cm^{-1} corresponds to π-electron delocalization induced in the polymer by protonation. The band characteristic of the conducting protonated form is observed at 1246 cm^{-1} and interpreted as a C-N^+ stretching vibration in the polaron structure [18]. The 1136 cm^{-1} band is assigned to a vibration mode of the –NH^+= structure, which is formed during protonation [19].

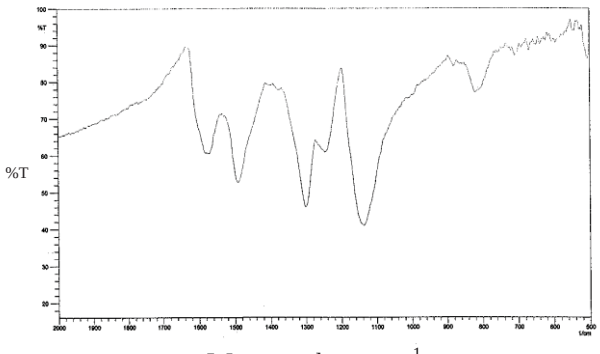

Figure 1. Infrared spectrum of PANI

3.2 Physical and mechanical properties of coating layer

The zinc and PANI affect the gloss of the coating. The film gloss is not an important property from the anti-corrosion coating, but on the basis of differences between zinc content, optimum zinc particle packing in the coating can be evaluated. The results of the mechanical test are given in Table 2. Compared to the zinc or PANI alone, a synergic effect to improve mechanical properties of the coating layer was provided.

Table 2: Results of mechanical tests

No.	Gloss (%)		Adhesion	Impact (Kg.cm.)
	20°	60°		
No zinc No PANI	99	108	5B	180
No zinc PANI 5 phr	81	95	3B	10
Zinc 50 phr No PANI	32	79	5B	170
1	30	75	5B	180
2	27	73	5B	180
3	25	71	5B	180
4	29	75	5B	50
5	24	68	5B	30

3.3 DSC study

The values of Tg derived from DSC thermogrames are compiled in Table 3.

Table 3: DSC result with Tg

No.	Tg (°C)		
	Onset	Mid point	End point
No zinc No PANI	70.99	75.79	78.75
No zinc PANI 5 phr	66.78	72.74	75.24
Zinc 50 phr No PANI	75.28	79.44	81.57
1	82.95	84.58	89.66
2	78.09	82.72	86.54
3	83.73	84.12	87.59
4	79.34	80.62	84.24
5	77.66	79.80	83.92

There is considerable increase of Tg in epoxy polyester containing PANI and varied zinc as compared with pure epoxy polyester which indicates higher crosslink density. The shift of Tg is related to crosslink density through following equation [20]:

$$\Delta Tg = Tg - Tg(0) = \frac{5}{(M_c/M) \times N_{rot}}$$

Where Tg(0) is the glass transition for uncrosslinked sample, M_c is the molecular weight between crosslink, M is molecular weight of the whole linear chain and N_{rot} is degree of freedom for rotation of the group between crosslink. Combination of PANI and zinc effected to Tg according to rigid characteristic of zinc content and higher crosslink of epoxy with amine terminal group in polyaniline [6]. The corrosion resistance of organic coating depends on its barrier properties. The higher crosslink density, the permeability of water and ions through the coating film becomes less and it leads to more resistance to corrosion including [21] effect of zinc content.

3.4 Corrosion test

The steel sheets coated with each of eight epoxy polyester after exposure to salt spray 240 hours are displayed in Fig. 2. As expected, the incorporation of PANI and zinc improves the resistance against corrosion and when the amount of zinc increased, size and frequency of blistering appeared to be smaller. It indicated that the presence of zinc was necessary as the zinc corroded and blocked further corrosion attack.

Figure 2. Coated sheets after exposure to salt spray

According to ASTM standard method D 1654, the progress of rust indicates the loss of adherence near to the scribe mark. Fig. 3 shows the coated steel sheets that were scrapped after 240 hours of corrosion assays. It is evident that the loss of adherence was significantly higher for the epoxy polyester coating without zinc and PANI, which indicate that PANI combination with zinc promote the adherence between the coating and the substrate and offer protection in the scribed areas. This is also reflected by the evolution of the area corroded under the coating layer.

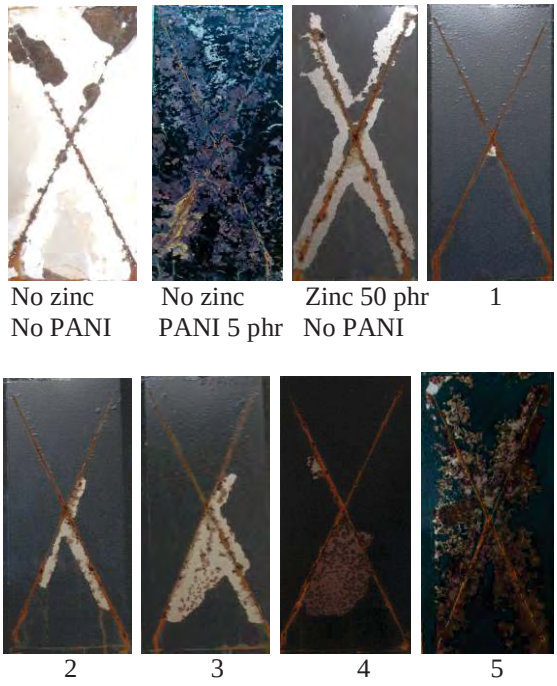

Figure 3. Scrapped coated sheets after exposure to salt spray

4. Conclusions

The conductive form of polyaniline PANI (emeraldine salt) was synthesized and added to epoxy polyester powder. The synergic effect of PANI and zinc was proved with varied zinc content to their anti-corrosion efficiency. The incorporation of PANI and zinc was provided better anti-corrosion and mechanical properties when compared with epoxy polyester containing zinc or PANI alone and increased with increasing of zinc content.

Acknowledgements

This work was supported by Program in Petrochemistry and Polymer Science, Faculty of Science, Chulalongkorn University.

References

[1] David A.Bate, *The Sciences of Powder Coatings*, **Vol.1**, Selective Industrial Training Associates Limited, London (1990), pp. 3-19
[2] John D. Keane, *Good Painting Practice*, **Vol.1**, Steel Structures Painting Council, Pittsburgh (1982), pp. 1-18.
[3] H. Marchebois, S. Touzain, S. Joiret, J. Bernard and C. Savall, *Prog. Org. Coat.* **45** (2002) 415-421.
[4] B. Wessling and J. Posdorfer, *Synth. Met.* **102** (1999) 1400.
[5] M.G. Hosseini, M. Sabouri and T. Shahrabi, *Mat. Corr.* **57** (2006) 407.
[6] S. Radhakrishnan, N. Sonawane and C.R. Siju, *Prog. Org. Coat.* **64** (2009) 383–386.
[7] A. Meroufel, C. Deslouis and S. Touzain, *Electrochim. Acta.* **53** (2008) 2331-2338.
[8] E. Armelin, A. Meneguzzi, C.A. Ferreira and C. Alemán, *Surf. Coat. Technol.* **53** (2008) 2331-2338.
[9] A. Kalendová, D. Veselỳ and J. Stejskal, *Prog. Org. Coat.* **62** (2008) 105-116.
[10] E. Akbarinezhad, M. Ebrahimi and H.R. Faridi, *Prog. Org. Coat.* **64** (2009) 361-364.
[11] I.L. José, C. Franciseco and L.M. Franciseco, *Prog. Org. Coat.* **52** (2005) 151-160.
[12] S. Sathiyanarayanan, K. Maruthan, S. Muthukrishnan and G. Venkatachari, *Prog. Org. Coat.* **66** (2009) 113-117.
[13] J. Cao, P. Smith and A.J. Heeger, *Synth. Met.* **57** (1993) 715-719.
[14] J. Stejskal, R.G. Gilbert, *Pur. Appl. Chem.* **5** (2002) 857–867.
[15] M. Trchova, I. Sapurina, J. Prokes and J. Stejkal, *Synth. Met.* **135/136** (2003) 305.
[16] M. Trchová, I. Sedenková, E. Tobolková and J. Stejkal, *Polym. Degrad. Stab.* **86** (2004) 179–185.
[17] Z. Yingjun, S. Yawei, Z. Tao, M. Guozhe and W. Fuhui, *Corr. Sci.* **53** (2011) 3747–3755.
[18] S. Quillard, G. Louarn, J. Buisson, M. Boyer, M. Lapkowski, A. Pron, et al. *Synth Met* **84** (1997) 805–806.
[19] J. Chiang, A. MacDiarmid, *Synth Met* **13** (1986) 193–205.
[20] J.P. Pascault, R.J.J Williams, *Polym.Phys.* **28** (1990) 85.
[21] R. Mafi, S.M. Mirabedini, R. Naderi and M.M. Attar, *Corros .Sci.* **50** (2008) 3280-3286.

BENZOXAZINE-MODIFIED ASPHALTS FOR PAVEMENT APPLICATION

Anchalee Oumpancharoen[1], Sarawut Rimdusit[1*]
[1] Department of Chemical Engineering,Faculty of Engineering,
Chulalongkorn University, Payathai Road. Pathumwan, Bangkok, 10330, THAILAND.

[*] E-mail: sarawut.r@chula.ac.th, Tel. +66 22 180006, Fax. +66 22 186877

Abstract: The use of polymers for modification of asphalt is an attempt to prolong the service life and improve the performance of asphalt particularly for road pavement applications. This research aims to study thermal and mechanical properties of asphalt modification by bisphenol A based benzoxazine resin. The 60/70 penetration grade asphalts were modified by varying the amount of benzoxazine modifier at 1wt%, 3wt%, 5wt%, 7wt% and 9wt%. The suitable mixing condition was achieved by mechanical mixing for 1 hr. at 80°C and a mixing speed of 500 rpm with a stirrer and followed by curing for 1 hr. at 190°C. The effects of the benzoxazine modifier on the resulting asphalts were examined by dynamic mechanical analysis (DMA), penetration test, softening point measurement and optical microscope. The results revealed that glass transition temperature, storage modulus and softening point of the benzoxazine-modified asphalt increased with increasing the benzoxazine resin contents while the penetration depth decreased when the benzoxazine ratio increased. Appreciable decrease in formation of rutting, bleeding and cracking are thus expected to be achieved by the use of the benzoxazine-modified asphalts.

1. Introduction

Majority of road material is bitumen because of its low cost, inherent cohesive nature, rheological properties and thermal resistance. It is the refinery product from petrochemical process. Bitumen is a viscoelastic material that is flexible and flowable at high temperature, brittle at low temperature and exhibits permanent deformation at high loading [1]. Because of, increased number of vehicles, increased axle load and increased tire pressure, asphalt road becomes rutting, cracking and stripping [2]. To improve the temperature sensitivity and permanent deformation, asphalts are modified by widely used polymers. Polymer modifiers for asphalt could be classified into four main groups: thermoplastics, rubbers, thermosets and block copolymers. The purpose of using e.g. styrene-butadiene copolymer is to improve low-temperature cracking but does not show any clear improvement in high-temperature condition. [3].Furthermore, Modified bitumen with epoxy resin was reported to exhibit improved brittleness at low temperature, good flexibility at high temperature and mechanical properties with relatively low amount on epoxy resin used. However, epoxy was rather incompatible with asphalt maleic anhydride and adipic acid were used as curing agents to improve incompatibility with the asphalt [4]. Polybenzoxazine is a thermosetting polymer that is relatively easy to synthesize, low price, no volatile by-product, low viscosity, high thermal stability and good adhesion.

The objective of the study is to investigate effects of benzoxazine resin contents on properties of the resulting modified asphalt. Its characteristics will be examined using dynamic mechanical analysis, penetration and softening point measurement and optical microscope.

2. Materials and Methods

2.1 Materials

The 60/70 penetration grade asphalt used was obtained from IRPC Co., Ltd. Properties of asphalt used in all experiment are given in Table 1.Benzoxazine resin (BA-a) is based on bisphenol-A, aniline, and formaldehyde. Thai Polycarbonate Co., Ltd. (TPCC) supplied the bisphenol-A (polycarbonate grade). Paraformaldehyde (AR grade) was purchased from Merck Company and aniline (AR grade) was obtained from Panreac Quimica SA Company.

2.2 Methods

Asphalt was heated at 80±5°C. Then benzoxazine resin was added to the hot asphalt at varying ratios of 1wt%, 3wt%, 5wt%, 7wt% and 9wt% and stired mechanically at 500 rpm. for 1 hr. These asphalt samples were cured at 190±5°C in an air-circulated oven for 1 hr. to crosslink the benzoxazine. The dynamic mechanical analyzer (DMA) model DMA242 from Netzsch Instrument was used to investigate dynamic mechanical properties of the specimens.The test was performed under the constant frequency of 1 Hz. The testing temperature was varied from -70°C to 40°C at a heating rate 1°C/min. Morphological properties were measured by optical microscope (model Nikon ECL1PSE E600 POL). Conventional tests for pavement application are penetration test (ASTM D5) and softening points measurement (ASTM D36) for pavement application.

Table 1: Chemical and physical properties of asphalt grade 60/70 penetration.

Property	Data
Penetration, 25°C	71
Softening point (°C)	47
Ductility (cm.)	100
Viscosity, 135°C (Pa s)	0.5

3. Results and Discussion

Fig.1 shows phase morphology of benzoxazine resin (BA-a) and asphalt blends. The light phase in the picture represents the benzoxazine resin, and the dark phase is the asphalt. Benzoxazine fraction was found to disperse as small particles in asphalt and the light region increased when benzoxazine resin content increased.

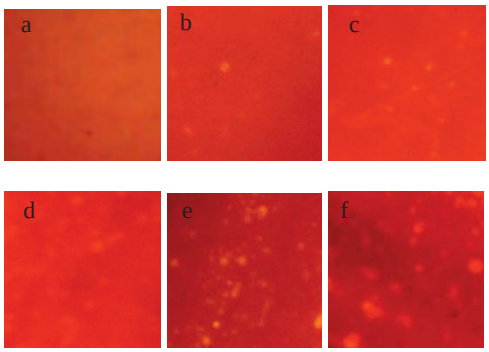

Figure 1: Optical photomicrographs of benzoxazine-modified asphalts of : (a) Neat asphalt; (b) 1%BA-a; (c) 3%BA-a; (d) 5%BA-a; (e) 7%BA-a; (f) 9%BA-a.

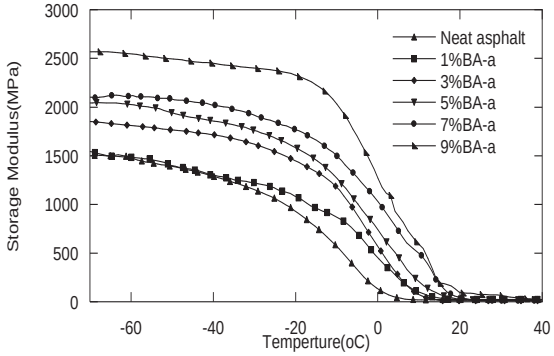

Figure 2: Storage modulus of benzoxazine modified asphalts.

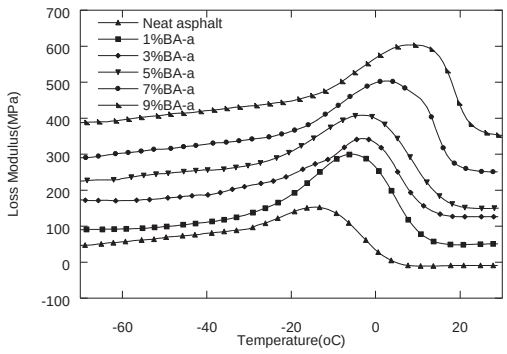

Figure: 3 Loss modulus of benzoxazine modified asphalts.

Figures 2 and 3 show the temperature dependency of storage modulus (E´) and loss modulus (E´´) for each binder in temperature ranging from -70°C to 40°C. The results indicated that benzoxazine-asphalt binder showed an increase in the storage modulus compared to that of the original asphalt and the values increased when benzoxazine content increased. The glass transition temperature (Tg) of original asphalt was determined to be -14.5°C and those values of the modified asphalts increased to 4.6°C in 9% benzoxazine modified asphalt. The results also suggested that the benzoxazine-modified asphalts were stiffer than the original asphalt and exhibited improved performance at high temperature [5].

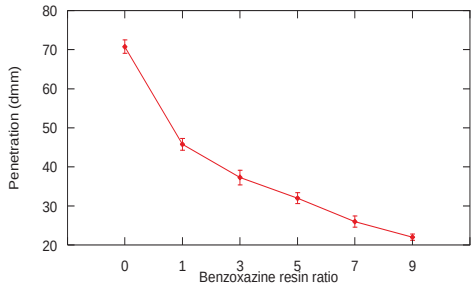

Figure 4: Penetration of benzoxazine-modified asphalts.

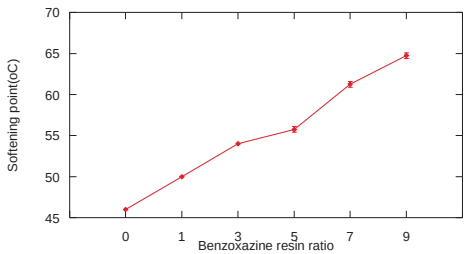

Figure 5: Softening point of benzoxazine-modified asphalts.

Figures 4 and 5 show the penetration values and softening points of the benzoxazine-modified asphalts. Penetration and softening point tests were applied to the original and the benzoxazine-modified asphalts. The addition of the benzoxazine modifier was found to decrease the penetration values of the asphalt from 71 to 22 at 9wt% of the BA-a content whereas the softening points increased from 47°C to 64.5°C. As a consequence, the benzoxazine modification caused the hardening of the asphalt and substantially improved the road pavement properties [6].

4. Conclusions

Morphological study of benzoxazine-modified asphalts revealed the immiscible nature between the benzoxazine resin and the asphalt. The storage modulus, glass transition temperature (Tg) and penetration were increased while the softening points

was decreased when benzoxazine content increased. Therefore, benzoxazine-modified asphalts can improve the road pavement properties required in hot and humid region as well as highly heavy traffic loads to help prevent rutting, bleeding and cracking deformation of the pavement.

Acknowledgements

This work is supported by the Higher Education Research Promotion and National Research University Project of Thailand, Office of the Higher Education Commission (AM1076A).

References

[1] Andreja Zupancic and Miha Zumer, Rheogical examination of temperature dependence of conventional and polymer-modified road bitumens, *The chemical journal of chemical engineering*, Volume80 (2002).
[2] A.A. Cuadri, P. Partal ⇑, F.J. Navarro, M. Garca-Morales, C. Gallegos, Bitumen chemical modification by thiourea dioxide, *Fuel* 90 (2011) 2294–2300.
[3] Nadkarni VM, Shenoy AV, Mathew J. Thermomechanical behavior of modified asphalts. *Ind Eng Chem Prod* Res Dev 1985;24:478.
[4] Yang Kang, Zhiming Chen, Rubber-Like Reaction of asphalt and maleic anhydride : Kinetics and mechanism, *Chemical engineering journal* 164(2010)230-237.
[5] A.H. Fawcett, T.McNally, Blends of bitumen with various polyolefins, Northern Ireland, UK, *Polymer* 41 (2000) 5315-5326.
[6] Meltem Cubuk a, Metin Gurua *, M. Kurs_at Cubuk b a Gazi ,Improvement of bitumen performance with epoxy resin, *Fuel*88 (2009) 1324-1328

SYNTHESIS OF POLY(METHYL METHACRYLATE-*co*-2-VINYLPYRIDINE) VIA ATOM TRANSFER RADICAL POLYMERIZATION

Piyaporn Deacha, Samitthichai Seeyangnok*

Department of Industrial Chemistry, Faculty of Applied Science,
King Mongkut's University of Technology North Bangkok, Bangkok, 10800 Thailand

* Author for correspondence; E-mail: samitthichais@kmutnb.ac.th, Tel. +66 2 555 2000 Ext. 4806, Fax. +66 2 587 8251

Abstract: Poly(methyl methacrylate-*co*-2-vinylpyridine) consists of Lewis base contained repeating unit which help to improve its conductivity in electro-chemical applications. To synthesize Methyl methacrylate-2-vinyl pyridine copolymer, Atom Transfer Radical Polymerization (ATRP) technique is emphasized due to the controlled living polymerization mechanism. The suitable conditions for polymerization process is investigated by vary parameters such as time, temperature and catalyst system (initiators, metal halides, and ligands). Result to the appropriate condition is the polymerization of MMA at 100 ºC for 24 h. however; the reaction time is extended to 72 h for copolymer caused by 2VP monomer. Moreover, effect of molar ratios on starting materials (MMA:BzBr:Cu(I)Br:en) are examined and the molar ratio at 100:1:1:2 with 78% conversion of monomer. Successively, this condition is applied to synthesize random and block copolymers using 50:50:1:1:2 molar ratio of 2VP:MMA:BzBr:Cu(I)Br:en for 72 h with 99% and 79% conversions of monomer, respectively. All polymer products are characterized by FT-IR and ^{1}H-NMR techniques for their chemical structure and DSC analysis for their thermal properties.

1. Introduction

Polymer Electrolyte Membrane Fuel Cell (PEM FC) is very popular **for the use** as energy source interms of portability, low investment of production and environment friendly [1-5]. PEM is one of the most important parts for transfering proton from anode side to cathode side. **Recently**, Dupont is represent the polymer electrolyte membrane, Nafion®, sulfonic tetrafluoropolyethylene based polymer which is suitable for PEMFC. However, Nafion® is not stable at temperature over 85 ^{o}C, the sulfonic part is decomposed and lost their proton exchange property and also cost of Nafion® is very expensive [6]. Above-mentioned, many kind of new polymer electrolyte are developed for improving properties of materials such as more heat stability and more proton transfer. This research is focused on the appropriate condition to synthesize polymer electrolyte for using in PEMFC via Atom Transfer Radical Polymerization (ATRP). ATRP is a technique used to control stability of free radical species, as a result the molecular weight and polydispersity index of polymer cab be controlled.

Initially, the metal complex (catalyst) reacts alkyl bromide via single electron transfer mechanism which transfers electron from metal to alkyl bromide (initiator) to generate alkyl free radical. Then this free radical reacts with vinyl monomer to form monomer free radical species as shown in Figure 1 [7,8].

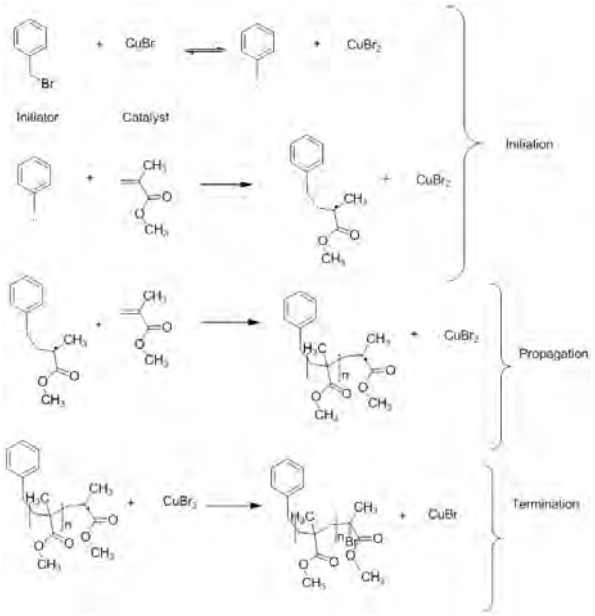

Figure 1 Reaction mechanism for ATRP of poly(methyl methacrylate)

2. Materials and Methods

2.1 Chemicals

Methyl methacrylate ($C_3H_8O_2$) was purchased from Sigma-Aldrich Co.Ltd. Copper(I)bromide (Cu(I)Br) and Benzyl bromide (C_7H_7Br) from Sigma-Aldrich Co.Ltd. were used as received. Tetrahydrofuran (THF) (C_4H_8O) was purchased from QRec Co.Ltd. Ethylenediamine (en) ($C_2H_8N_2$) and 2-Vinylpyridine were purchased from Merck-Schuchardt Co.Ltd. Anhydrous sodium sulfate (anh. Na_2SO_4) was purchased from Univar Co.Ltd.

2.2 ATRP of PMMA in bulk polymerization technique.

The Oxygen gas in the system was replaced by nitrogen gas then MMA 375 mmol, Cu(I)Br 3.75 mmol, en 7.5 mmol and BzBr 3.75 mmol were added

into the three-neck round bottom flask. The reactor was refluxed at 60 ºC for 24 h and the polymer products were collected at ½, 1, 2, 4, 8 and 24 h, respectively. After the reactor cooled down to ambient temperature, the solution mixture was filtrated under reduced pressure and solvent was removed to obtain a greenish blue solid product. This product was purified by column chromatography over silica gel with THF eluent. After THF solvent was removed, the colorless solid was obtained.

The condition parameters that influence the synthesis of PMMA via ATRP are investigated in terms of concentration of ligands**,** reaction temperature and reaction time.

2.3 ATRP of PMMA P2VP random copolymer in bulk polymerization.

The Oxygen gas in the system was replaced by nitrogen gas then MMA 187.5 mmol, 2VP 187.5 mmol, Cu(I)Br 3.75 mmol, en 7.5 mmol and BzBr 3.75 mmol were added into the three-neck round bottom flask. The reactor was refluxed at 100 ºC for 72 h and the greenish blue color **products** were obtained. **These products were** purified by column chromatography over silica gel with THF eluent. After THF solvent was removed, the colorless solid was obtained.

2.4 ATRP of PMMA P2VP block copolymer in bulk polymerization.

The oxygen gas in the system was replaced by nitrogen gas then MMA 187.5 mmol, Cu(I)Br 3.75 mmol, en 7.5 mmol and BzBr 3.75 mmol were added into the three-neck round bottom. The reactor was refluxed at 100 ºC for 1 h then 2VP 187.5 mmol was introduced into the solution mixture by using dropping funnel and the reaction was still refluxed for 70 h. The greenish blue color products were obtained. **These products were** purified by column chromatography over silica gel with THF eluent. After THF solvent was removed, the colorless solid was obtained.

2.5 Analysis and characterization of Poly(methyl methacrylate) and Poly(methyl methacrylate-*co*-2-vinylpyridine)

All various kinds of **p**oly(methyl methacrylate) and **p**oly(methyl methacrylate-*co*-2-vinylpyridine) were characterized by FT-IR and ^{1}H-NMR techniques for chemical structure and DSC analysis for their thermal properties.

3. Results and Discussion

3.1 The effect of reaction temperature and reaction time on ATRP of poly(methyl methacrylate).

To investigate the effects of reaction time and reaction temperature on the polymerization process, reactions were carried out at 60, 80 and 100 ºC for 24 h and in the meanwhile the polymer products were collected during 30 min, 1, 2, 4, 8 and 24 h. The sampling polymers were used to determine %conversion of monomer at the time. From figure 2, the correlation of %conversion and reaction time showed that increasing reaction temperature resulted in an increasing rate of polymerization.

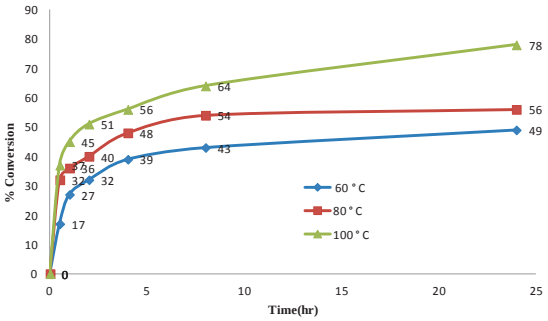

Figure 2 Correlation between %conversion of monomer and reaction time in various reaction temperatures.

These results indicate that the reaction temperature at 100 ºC is appropriate for synthesis of poly(methyl methacrylate) due to the highest polymerization rate.

3.2 The effect of ATRP condition on synthesis of poly(methyl methacrylate-*co*-2-vinylpyridine)

In this research, the ATRP of copolymer were [was?] carried out under the appropriate condition with indicated molar ratios on table 1.

Table 1: Polymerization conditions for synthesis of copolymers and %conversion of monomer.

Copolymer	[2VP]:[MMA]:[I]:[CuBr]:[L]	%Conversion
Random Copolymer	50:50:1:1:2	99
Block Copolymer	50:50:1:1:2	79

The ATRP of random copolymer was carried out by introducing methyl methacrylate and 2-vinyl pyridine into the reaction flask. After the completion of reaction, polymer product of 99%yiled was obtained. In the same way, this condition was used to synthesize block copolymer with 79% yield.

3.3 Characterization of polymer products.

FT-IR spectrum of PMMA showed C-O functional group at wavenumber 1080-1300 cm^{-1}, C=O functional group at wavenumber 1690–1760 cm^{-1} and C–H functional group at wavenumber 2850–2960 cm^{-1}. FT-IR spectra of both poly(methyl methacrylate-*co*-2-vinylpyridine) copolymers showed C=O group function at wavenumber 1732 cm^{-1}, C–H aromatic at wavenumber 2946 cm^{-1} and pyridine group function is C–H stretching vibration at wavenumber 1435 cm^{-1}.

Chemical structure analysis of PMMA was examined by ^{1}H-NMR Spectroscopy, as shown in Figure 5. The methyl proton resonance (A) of methyl of methyl methacrylate present at 1.0 ppm and the proton resonance of methyl of methoxy group (C) present at 3.5 ppm and the proton resonance of methylene group at 2.1 ppm.

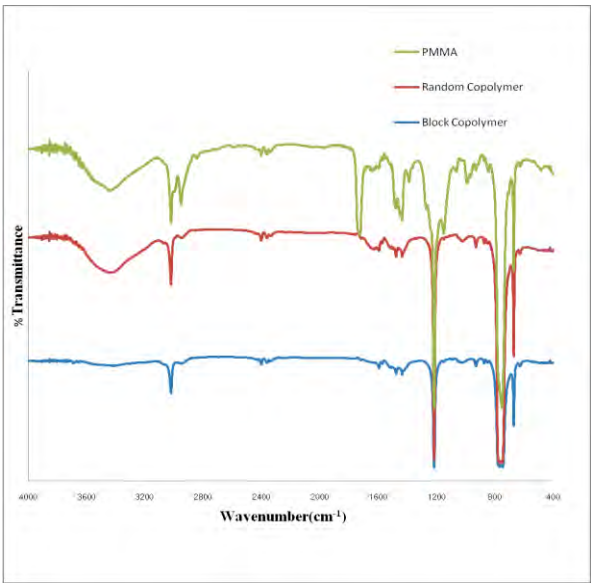

Figure 3 Correlation of Infrared spectra data of poly(methyl methacrylate) and poly(methyl methacrylate-*co*-2-vinylpyridine)

The glass-transition temperature of poly(methyl methacrylate), poly(2-vinylpyridine), random copolymer and block copolymer of Poly(methyl methacrylate-*co*-2-vinylpyridine) are showed at about 112 °C, 99 °C, 114 °C and 115°C respectively. The glass-transition temperature of copolymers are increased which may cause from the crystal structure of copolymers.

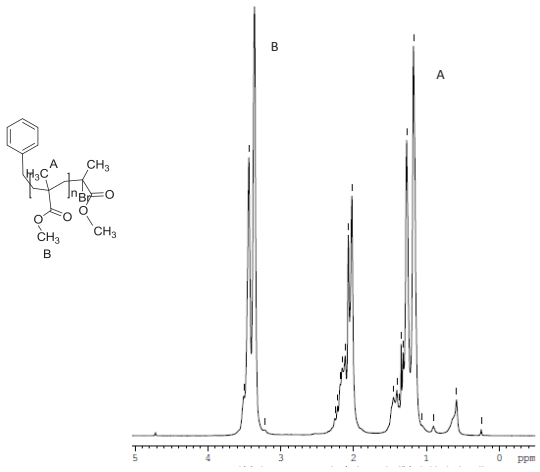

Figure 4 Proton NMR spectrum of poly(methyl methacrylate)

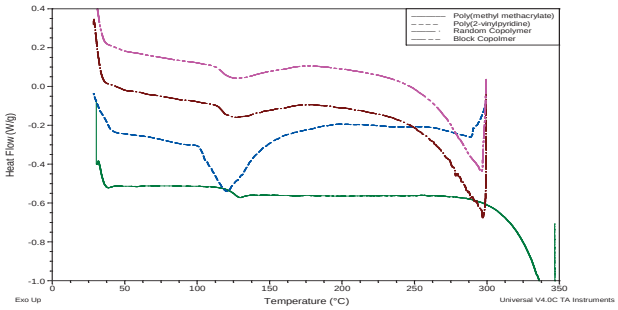

Figure 5 DSC thermogram of poly(methyl methacrylate), poly(2-vinylpyridine), random copolymer and block copolymer of poly(methyl methacrylate-*co*-2-vinylpyridine)

4. Conclusions

The appropriate condition to synthesize poly(methyl methacrylate-*co*-2-vinylpyridine) via ATRP using the molar ratio of 50:50:1:1:2 (2VP:MMA:BzBr:Cu(I)Br: en)at 100 ºC for 72 h. However, the %conversion of monomer is not optimized due to the difference of polarity. The further study will be focused on solution polymerization technique.

Reference

[1] J. Jiang, X. Lu, and Y. Lu, *Polymer*. **49** (2008) 1770-1776.
[2] M.F. Hordeski, *Alternative fuels : the future of hydrogen, second edition*, The Fairmont Press, Boca Raton (2008).
[3] S. Matar and L.F. Hatch, *Chemistry of petrochemical processes*, Gulf Publishing Company, Houston (2000).
[4] S.J. Paddison and K.S. Promislow, *Device and Materials Modeling in PEM Fuel Cells*, Springer, New York (2008).
[5] F.J. Barclay, *Fuel Cells : Engines and Hydrogen*, John Wiley & Sons Ltd, West Sussex (2006).
[6] L.O. Vasquez, *Fuel cell Research Trends*, Nova Science, New York (2007).
[7] C. Janvanitch, *Basic polymer chemistry*, Odian Store, Bangkok (1984).
[8] J. Brandrup, E.H. Immergut and E.A. Grulke, Polymer Handbook, John Wiley & Sons, Inc, New York (1999

MODIFICATION OF CASSAVA STARCH AS FILLER FOR POLYPROPYLENE COMPOUND

Nuchanart Charoennit[1,2], Thirawudh Pongprayoon[1,2*]

[1]Department of Chemical Engineering, Faculty of Engineering, King Mongkut's University of Technology North Bangkok, Bangkok, 10800 Thailand
[2]Center of Eco-materials and Cleaner Technology, King Mongkut's University of Technology North Bangkok, Bangkok, 10800 Thailand
*E-mail: tpongprayoon@yahoo.com

Abstract: Cassava starch was modified by admicellar polymerization for using as a filler of polypropylene (PP) compound. The starch modified was coated by ultra-thin film of polyisoprene that was characterized by Fourier Transform infrared Spectroscopy (FT-IR), Zeta potential analyzer (Zeta), Ultraviolet Spectroscopy (UV), Particle size Analyzer and Scanning Electron Microscopy (SEM). The modified starch/PP compound samples were prepared by two-roll mill and compression molding. The mechanical properties of the modified starch/PP compound were examined and compared with the unmodified starch/PP compound. The results showed that the modified starch was coated by polyisoprene film and the character or its surface changed from hydrophilicity to be hydrophobicity. The compound can be prepared when the starch content was less than 30%. When higher starch content was incorporated, the compounds were brittle and difficult to produce the samples for testing. The mechanical properties such as tensile properties, flexural properties, impact strength, % moisture absorption and biodegradability of modified starch/PP compound were better than those of the unmodified starch/PP compound.

1. Introduction

Cassava or tapioca is an economically important crop in Thailand and the cheapest raw material of starch production [1]. Starch has been used as a reinforcement for rubber and polymer because of its relatively high specific strength and modulus [1]. However, it has high level of moisture absorption, poor compatibility and poor wettability by non-polar plastics. For this reason, it was modified by admicellar polymerization for improving the compatibility between the interface of starch and polypropylene in this work.

Admicellar polymerization consists of four main steps [2,3,4]. The first step is called admicelle formation, involing the adsorption of a surfactant bilayer onto the surface of starch. In the second step (called adsolubilization), the monomer using isoprene was solubilized into the admicelle. In the third step, isoprene monomers were polymerized. The low temperature initiator [5] was needed to use in this work. In the last step, the polymer film is exposed by washing out the outer layer of surfactant.

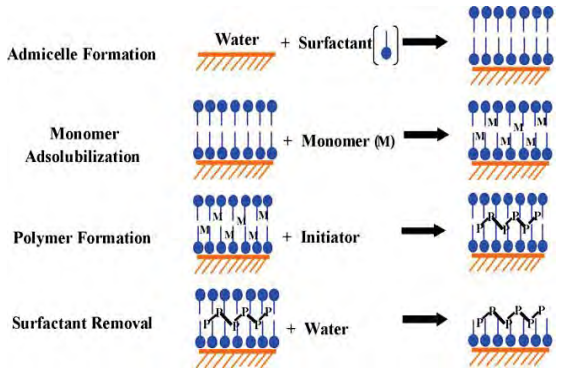

Figure 1. Four steps of admicellar polymerization

Polypropylene (PP) is used in many different settings, both in industry and in consumer goods. The properties of polypropylene is low specific gravity, high melting point, good stiffness, excellent chemical resistant and low cost. Many researchers studied the effect of corn and cassava starch blends on the mechanical properties and biodegradability of polymers [6,7,8]. The results showed that increasing starch loading diminished the tensile strength of the polypropylene to about the same degree. The tensile strength of the polymer decreased and the biodegradability of 10% starch filled polymer composite within 30 days incubation was enhanced by more than 70% [7].

2. Materials and Methods

2.1 Meterials

The cassava starch powder was supplied by Universal Starch Public Co., Ltd. (Thailand). Cetyltrimethylammoniumbromide (CTAB) in high pure grade was purchased from Amresco, USA. Isoprene (98%) and Ammonium persulfate (APS 98%) were purchased from Thermo Fisher Sciencetific, (USA). Ethyl alcohol was purchased from ITALMAR Co., Ltd. (Thailand).

2.2 Adsorption isoterm

Adsorption experiments of CTAB on the starch were conducted in vials. 1-g starch was mixed into 40 ml of CTAB surfactant solution by varying concentration from 500 μM to 100000 μM and stirring for 24 hr. The equilibrium concentration of surfactant remaining in the aqueous phase was analyzed by UV

spectroscopy at 200 nm that is the maximum wavelength of CTAB. The adsorption of CTAB on starch was calculated.

$$CTAB_{absorp} = \frac{([CTAB]_I - [CTAB]_E)//1000 \times V_{sol}}{W_{starch}} \quad (1)$$

$CTAB_{adsorp}$ = Adsorption of CTAB (μmol/g)
$[CTAB]_I$ = Initial concentration of CTAB solution (μM)
$[CTAB]_E$ = Equilibrium concentration of CTAB (μM)
V_{sol} = Volume of solution (ml)
W_{starch} = Weight of starch (g)

2.3 Admicellar polymerization

Admicellar polymerization of the starch was carried out using 7500 μM CTAB solution at slightly below CMC point. The ratio of isoprene monomer to initiator was selected at 12:1.2. 1 g. Cassava starch was added into 40 ml vial containing the CTAB solution. The system was left for 24 hr to reach the equilibrium for admicelle formation on the starch surface. Then ethanol and isoprene monomer were added to the mixture at room temperature and the system was left for 24 hr. Next, ammonium persulfate was added to the system. The polymerization was carried out for 2 hr at room temperature. Finally, the treated starch was washed with distilled water so that the surfactant foam was completely removed. Then the treated starch was dried in an oven at 80°C for 24 hr.

2.4 Preparation of starch/PP blends

Modified starch was mixed with polypropylene at varying contents (0-30%) by a two roll mill at 180°C for 10 min.

The compounds were warmed for 5 min in the compression mold setting at 180°C and then compressed for 5 min. Lastly, the molded was cooled down at room temperature.

2.5 FT-IR and SEM

Fourier transform infrared spectrometer (FTIR), Perkin Elmer Model 2000, was applied to identify polyisoprene film on starch surface by the KBr disc technique. The morphology of the unmodified and modified cassava starch was investigated by a scanning electron microscopy (SEM), Jeol SEM model JSM 5800LV.

2.6 Mechanical properties and biodegradability properties

The specimens of modified starch/PP composite were prepared for mechanical properties examination, by a universal testing machine, LLOYD Instruments LR 10 K. The moisture absorption of starch/PP composite was measured by weight loss. Biodegradability was tested by keeping the samples in the soil box under the surface at 5 cm. for 2 weeks at room temperature and then the weight loss was measured.

3. Results and Discussion

3.1 Zeta potential of starch

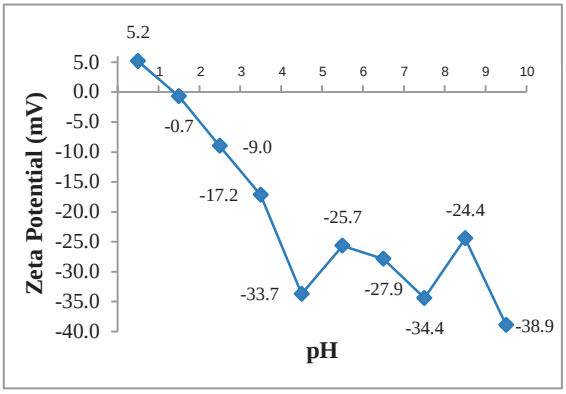

Figure 2. Zeta potential of starch as a function of pH.

The isoelectric point of starch was found to be at the pH of 1.4. The results showed that starch had a negative charged when pH was higher than 1.4. These show that the suitable cationic surfactant should be used in this work. Cetyltrimethylammoniumbromide (CTAB) was selected as the cationic surfactant for this study.

3.2 Adsorption isotherm of CTAB

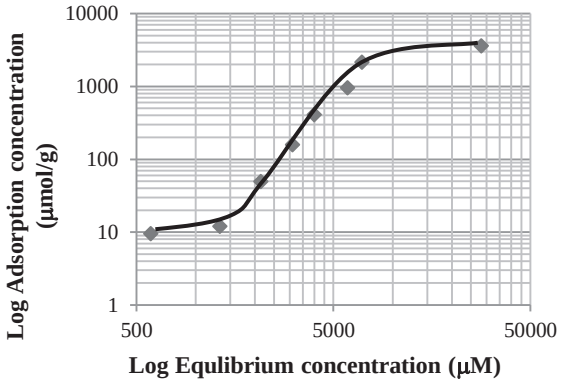

Figure 3. Adsorption isotherm of CTAB on cassava starch

Figure 3 shows adsorption isotherm of CTAB on the starch surface. At low concentrations (500-1000 μM) adsorption occurs through ion exchange [3] and the adsorbed amounts were small due to the low surface charge density of cassava starch under the used conditions. At the higher concentrations (1000-5000 μM) above the CMC (Critical Micelle Concentration), the adsorption increases well above the ion exchange capacity and surface aggregates were formed. At concentrations above CMC (> 10000 μM) the adsorbed amount finally reaches a plateau value independent of surfactant concentration. In this work, the CTAB concentration should be used below the CMC of CTAB, approximately 7500 μM.

3.3 FT-IR characterization

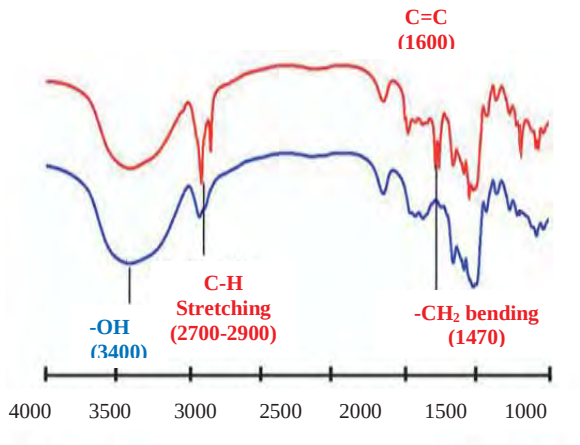

Figure 4. FT-IR spectra of unmodified cassava starch and modified cassava starch.

The FT-IR spectra of unmodified starch exhibit the characteristic broad peak at 3700-3200 cm^{-1} of O-H stretching. The C-H bending for CH_3 appears at peak 1345 cm^{-1} shown.

In addition, FT-IR spectra of modified starch show a peak corresponding to polyisoprene formed by admicellar polymerization at 2700-2900 cm^{-1} of C-H stretching. The C-H bending for CH_2 appears at peak 1470 cm^{-1}. The C=C stretching appears at peak 1600 cm^{-1}.

3.4 SEM surface images

The morphology micrographs of the unmodified cassava starch and modified cassava starch were performed by scanning electron microscopy (SEM) shown in Figure 5. The SEM images of the unmodified and modified cassava starch were obviously different. Figure 5 (b) showed a thin film coated on the starch surface. This confirmed the presence of polyisoprene coated on the surface of starch.

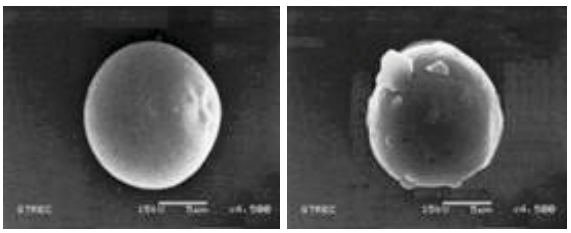

(a) (b)

Figure 5. SEM micrographs of (a) unmodified cassava starch and (b) modified cassava starch.

3.5 Mechanical Properties

Mechanical Properties of starch/PP blends including tensile strength, flexural strength and impact strength are shown in Figures 6, 7 and 8, respectively.

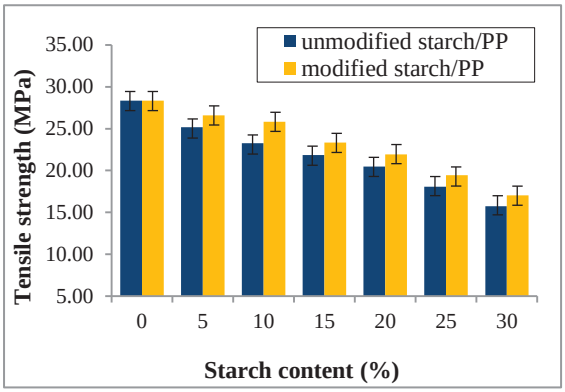

Figure 6. Tensile strength of starch/PP blends.

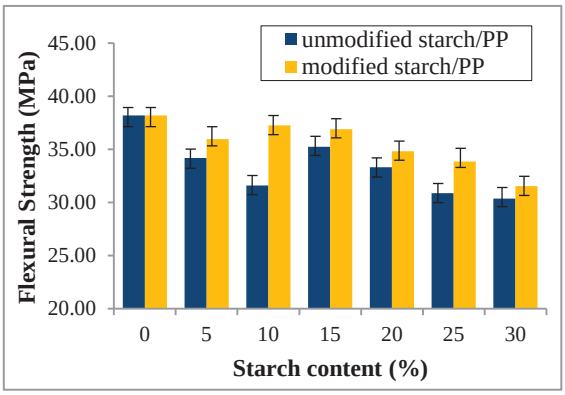

Figure 7. Flexural strength of starch/PP blends.

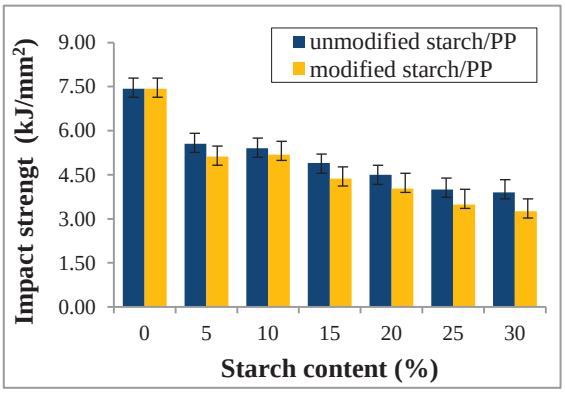

Figure 8. Impact strength of starch/PP blends.

The results obtained from Figures 6-8 show the same tendency. The mechanical properties decreased with increasing starch content. This observation suggests that both, modified and unmodified starchs were non-reinforcing. However modified starch/PP blends exhibited higher tensile and flexural strengths than those of the unmodified starch/PP blends, whereas the impact strength of modified starch/PP blends was lower than that of ummodified starch/PP blends. The reason is that starch itself is hard and brittle so the starch does not help absorbing the impact load.

3.6 Moisture absorption

Moisture absorption of starch/PP blends is shown in Figure 9.

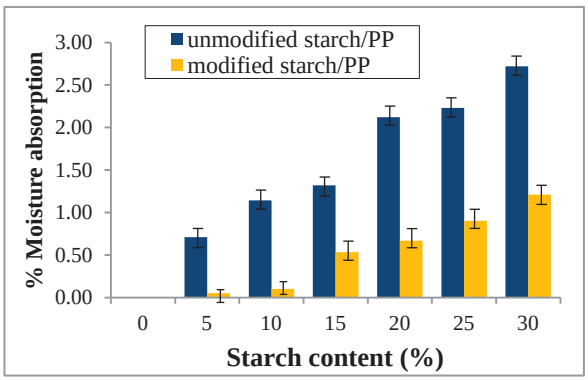

Figure 9. % Moisture absorption of starch/PP blends.

Moisture absorption of unmodified starch/PP and modified starch/PP blends increased with increasing amount of starch. Moisture absorption of modified starch blends was less than that of the modified samples due to the polymer film formation on the starch surface.

3.7 Biodegradability

The results of biodegradability are in good agreement with those of moisture absorption. Biodegradability of unmodified starch/PP blends increased with increasing amount of starch as shown in Figure 10.

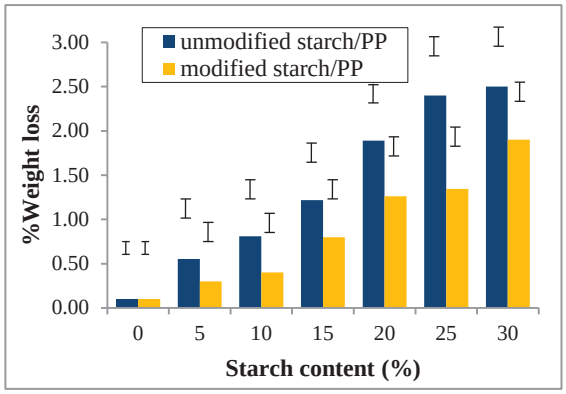

Figure 10. Biodegradability of starch/PP blends.

Biodegradability of unmodified starch blends was higher than that of the modified samples because of modified starch/PP blends are highly hydrophobic and do not well absorb water for breaking down plastic by microorganisms.

4. Conclusions

The mechanical properties including tensile properties and flexural properties of modifed starch/PP compound were better than those of the unmodified starch/PP compound. % Moisture absorption of modified starch/PP was significantly less than unmodified starch/PP while the biodegradability was slightly lower than that of unmodified starch/PP compound.

Acknowledgements

The authors would like to thank the Office of Higher Education Commission for financial support, Universal Starch Public Co., Ltd. (Thailand) for supplying cassava starch and the Institute of Technological Development Industry, King Mongkut's University of Technology North Bangkok, for polymer testing support.

References

[1] K. Sriroth, K. Piyachomwan, K. Sangseethong, C. Oates, *Paperpresented at X International Starch Convention*, Poland (2002) 11-14.

[2] T. Pongprayoon, N. Yanumet, O'Rear, E. A., *J. Colloid and Interface Science*. **249** (2002) 227-234.

[3] S. Boufi, A. Gandini, *J. Cellulose*. (2002) 1-10.

[4] S. Sangthong, T. Pongprayoon, N. Yanumet, *Composites Part A: Applied Science and Manufacturing*, **40** (2009) 687-694.

[5] H. Castano, O'Rear, E. A, Peter S. McFetridge, Vassilios I. Sikavitsas, *J. Macromol. Biosci.* **4** (2004) 785–794.

[6] S. Kiatkamjornwong, P. Thakeow, M. Sonsuk, *Polym. Degrad. Stabil.*,**73** (2001) 363–375.

[7] A.O. Ogah and J.N. Afiukwa, *Continental J. Biological Sciences*. **5(1)** (2012) 20 – 25.

[8] P. Rungruang, B.P. Grady, P. Supaphol, *Colloids and Surfaces A: Physicochem. Eng. Aspects*, **275**(2006) 114-125.

[9] V. Pimpan, K. Ratanarat, M. Pongchawanakul, *J. Sci. Res. Chula. Univ*. **26** (2001).

EFFECT OF ENR ON CURE CHARACTERISTIC AND MECHANICAL PROPERTIES OF NR/NBR BLENDS

Nantika Sangampai[1], Nittada Jeungsawad[1], Patchara Sukwanichwichai[1], Rattiya Rodsanthia[1] and Chanchai Thongpin[1]*

Materials Science and Engineering Department, Faculty of Engineering and Industrial Technology, Silpakorn University, Sanamchandra Palace Campus, Nakornpathom, 73000, Thailand.

* Author for correspondence; E-mail address: chanchai@su.ac.th, cmaterials@hotmail.com

Abstract:

NR blended with polar synthetic polymer has been an interesting rubber preparation for oil resistant rubber. Using NR as the main phase would gain the excellent mechanical properties whereas using synthetic polar rubber would enhance solvent resistance of the rubber vulcanizate. NR/NBR blend has been one of an interesting blend system as having NR as main rubber phase. As both rubbers are totally incompatible, the obtained blended elastomer shall show their drawback in both cure characteristic and mechanical properties. This research was aimed to improve their blend compatibility including mechanical properties. It was found that the incorporation of NBR into the NR would suffer curing reaction and undoubtedly mechanical properties. We, therefore, improved their compatibility using epoxidized natural rubber (ENR). In this part of the work, the content of ENR is maintained at 10 %wt. of the rubber where the rubber formulation; NR/ENR/NBR, is varied as follow:100/0/0, 80/10/10, 70/10/20, 60/10/30, 50/10/40, 40/10/50 compare to the rubber blend system of NR/NBR: 100/10, 90/10, 80/20, 70/30, 60/40 and 50/50. From this work, it could be concluded that the addition of ENR into NR/NBR blends cure characteristic properties of the blend could be improved. Moreover the tensile property of the blend was also improved. The vulcanizates possess high tensile strength as well as NR vulcanizate.

1. Introduction

Rubber is class of polymer materials, which is expected to show elasticity when in use. Natural rubber is in use for its versatility as an elastomeric material. Synthetic rubbers, which appeared much later than natural rubber, now are commonly used, especially for pneumatic tires, after blending with other rubber and carbon black as a reinforcing agent [1].

Nitrile rubber (NBR) is a copolymer of acrylonitrile and butadiene. It is the acrylonitrile component which makes NBR an oil-resisting rubber; the higher its proportion then greater the oil resistance. The blending together of natural rubber (NR) and NBR is intended to produce vulcanizate with the best properties from each component, i.e. NBR's high resistance to swelling by oils and NR's good strength properties. In practice the result is often disappointing in terms of properties and service life. Cause includes a distribution of crosslinks which results in an over-crosslinked phase and poorly crosslinked phase. For bends of two rubbers differing in polarity, such as NR and NBR, distribution of crosslinks can arise through preferential solubility of the curatives and vulcanization intermediates.

The extent of crosslinking across the interface between NR and NBR is another problem. The difference in polarity of the rubbers results in high interfacial tension, which is detrimental. It will severely limit mixing at interface, and hence the opportunity for crosslinking between the rubbers. This can cause poor phase morphology, which characterize by large phase sizes. The immiscibility [2] between NR and NBR also cause phase separation blending. To solve this problem, epoxidized natural rubber (ENR) [3] is considered as potential compatibilizer for this blend system. ENR has epoxide groups along the double bond of the NR molecular chain This will impart excellent oil resistance, gas barrier, good wet grip, and high damping characteristics, while including high polarity and promoting miscibility with polymers.

This research is aim to prepare rubber blend between NR and NBR and to improve the compatibility of this two rubber by using ENR which contains 50 % epoxidation. The content of ENR was fixed at 10 %

2. Materials and Methods

Preparation of rubber compound: The rubber formulation of NR:NBR were varied as 0:100, 20:80, 30:70, 40:60, 50:50, 60:40, 70:30, 80:20 and 100:0. The rubbers were kneaded on a two roll mill at 35 °C for 15 minutes or until it form banding. The curing additives which are ZnO 2.5phr, stearic acid 1.5 phr, TBBS 0.6 phr, TMTD 0.4 phr and sulfur 2.5 phr were added stepwise and mixed thoroughly. The mixing time on the two roll mill should not exceed 30 minutes. The rubber formulation of NR/ENR/NBR of 10/10/80, 20/10/70, 30/10/60, 40/10/50, 50/10/40, 60/10/30 and 70/10/20 were also prepared in the same manner.

Cure Characteristic Properties determination: The rubber compound was then characterized for their scorch and cure time, and minimum and maximum torques using moving die rheometor (GOTECH, Thaiwan) at 160 °C.

Specimen Preparation: The rubber compound were then compressed in a compression molding at 160 °C follow cure time obtained from MDR and under pressure of 1200 psi.

Mechanical Properties: The dumbbell specimens were cut from the slab and performed tension test, according to ASTM D638, using Instron machine model 5969 tensile tester with a crosshead speed of 500 mm/min.

3. Result and discussion

Cure Characteristic Properties:

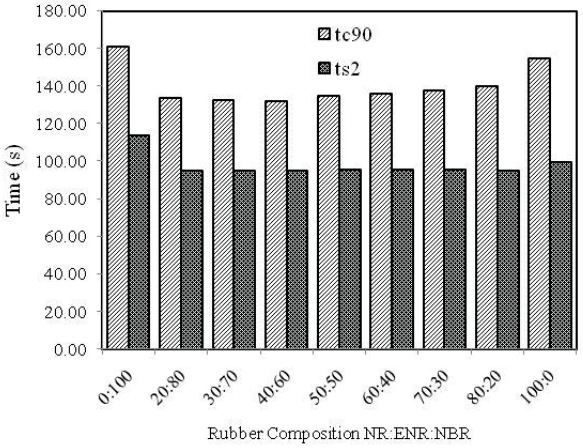

Figure 1 Scorch time and cure time of NR/NBR blend

It was found from the **Figure 1** that scorch time of the blends seems to be lower than that of the neat rubber. In the case of NBR, curing using sulfur system always performs slow reaction. On the other hand, sulfur curing system for NR will be considerately fast compared to NBR. Nonetheless, the incorporation of NBR into NR result in decreased of scorch time. This could be by the formation of Zn stearate complex that can be form very fast in NR phase, as NR and NBR are not compatible, and thus induced the reaction to occur. In term of cure time, it was found that the curing of rubber blend seem to be faster with high content of NBR.

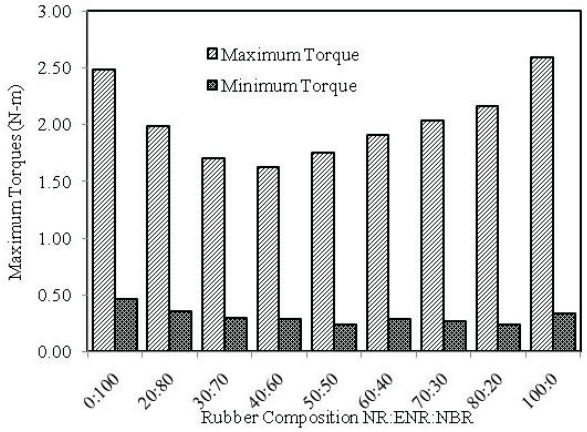

Figure 2 Min and Max torques of NR/NBR blends

For minimum and maximum torques shown in **Figure 2**, rubber blends appeared to show lower maximum torques than the neat rubber. This could be due to the phase separation between these two rubbers.

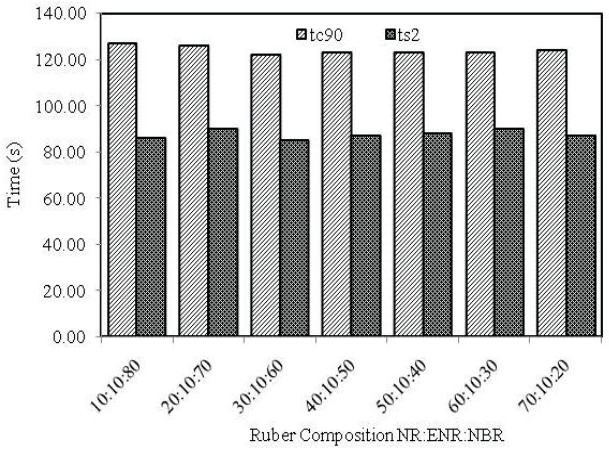

Figure 3 Scorch time and cure time of NR/ENR/NBR blends

With the addition of ENR 50, the scorch and cure time, shown in **Figure 3**, appeared to be lower than those of the previous systems. This could be explained by the compatibility between NBR and NR and hence the reaction could carry on in both NR and NBR phases.

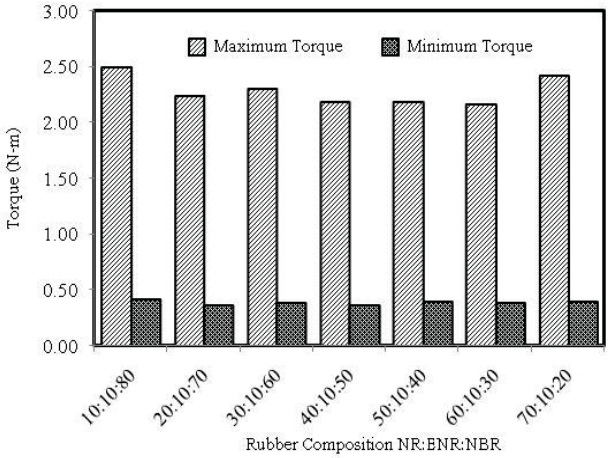

Figure 4 Minimum and maximum torques of NR/ENR/NBR blends

It was also found from **Figure 4** that minimum and maximum torque values were increased with the addition of ENR 50 as a compatibilizer. This could be due to phase compatibilization between these two rubbers. This also resulted in the mechanical performance of the rubber blends that will be shown in the next section.

Tensile Properties of the Rubber Blends:
Tables 1 and 2 exhibit tensile properties of NR/NBR and NR/ENR/NBR blends. It was shown that the addition of ENR in to the NR/NBR blends can enhance elongation of the rubber vulcanizates. The secant modulus of the vulcanizates appeared to be the same in every formulation. Tensile strength of the rubber blends system containing high NBR content

appeared to be improved by the NR which possess higher strength that NBR.

Table 1 Tensile Properties of NR/NBR blends

Material NR-NBR	Tensile Strength at Break (MPa)	% Elongation at Break (%)	Secant Modulus at 100 % (MPa)	Secant Modulus at 200 % (MPa)
0-100	1.70	346	0.92	0.64
20-80	2.24	531	0.75	0.55
30-70	3.49	758	0.70	0.51
40-60	3.91	836	0.62	0.46
50-50	4.74	927	0.61	0.45
60-40	7.92	1220	0.62	0.47
70-30	9.52	1390	0.58	0.44
80-20	8.99	1300	0.58	0.45
100-0	6.07	932	0.65	0.50

Table 2 Tensile Properties of NR/ENR/NBR blends

Material Formulation NR/ENR/NBR	Tensile Strength at Break (MPa)	% Elongation at Break (%)	Secant Modulus at 100 % (MPa)	Secant Modulus at 200 % (MPa)
10-10-80	2.11	476	0.81	0.58
20-10-70	2.91	654	0.74	0.54
30-10-60	4.44	875	0.67	0.49
40-10-50	6.10	1032	0.64	0.48
50-10-40	6.08	1030	0.63	0.47
60-10-30	6.91	1100	0.60	0.46
70-10-20	6.35	1045	0.59	0.46

4. Conclusions

From this work, it could be concluded that with the addition of ENR into NR/NBR blends, cure characteristic properties of the blends could be improved. Moreover the tensile property of the blend was also improved. The vulcanizates can possess high tensile strength as well as NR vulcanizate.

Acknowledgements

The authors would like to express their sincere thanks to the department of Materials Science and Engineering, Faculty of Engineering and Industrial Technology, Silpakorn University, for their support.

References

[1] S. Kohjya; Rubber Chem. and Technol.,73(3), 534 (2000).

[2] S. Thanawan, S. Radabutra, P. Thamasirianunt, T. Amornsakchai, K. Suchiva, Origin of phase shift in atomic force microscopic investigation of the surface morphology of NR/NBR blend film, Ultramicroscopy, Volume 109, Issue 2, January (2009), pp. 189-192

[3] G. N. Onyeagoro, Effect of zinc oxide level and blend ratio on vulcanizate properties of blend of natural rubber and acylonitrile-butadiene rubber in the presence of epoxidized natural rubber, Academic Research International, Vol. 3, No. 1, July (2012)

EFFECT OF MOLECULAR WEIGHT OF PEG ON STRUCTURAL AND MORPHOLOGICAL CHANGE IN PLA/PEG BLEND

Phuwadon Bunlengsuwan[1], Saran Srisuk[1], Sunanta Wachirahuttapong[1], and Chanchai Thongpin[1,*]

[1] Materials Science and Engineering Department, Faculty of Engineering and Industrial Technology, Silpakorn University, Sanamchandra Palace Campus, Nakornpathom, 73000, Thailand
[*] E-Mail: chanchai@su.ac.th, cmaterials@hotmail.com

Abstract: It has been widely known that brittleness is one of the many problems of using poly(lactic acid) in packaging application. One of the main reason is by main chain constrain hence molecular chain is difficult to rotate or re-orientation. To overcome the brittleness of the polymer, many toughening materials or polymer has been blended and studied, both as melt blending, solution blending and reactive blending. Low molecular weight polyethylene glycol (PEG) has been widely used as plasticizing agent in PLA in which the content is usually maintain at maximum 20% by weight of PLA. Grafting of anhydride onto PLA was also studied and used as ductility improvement in PLA. In this work, the effect of molecular weight of PEG used in PLA was studied via melt blending. The result shows that PLA chain breaking could occur during melt blending via trans-esterification. Melt flow index (MFI) of the polymer blend tended to be increased to a certain point. This also leads to structural change which was confirmed by ^{1}H NMR. Thermo-gravimetric analysis also confirmed the molecular change of PLA. The cross-linking in the blend is was also performed using peroxide. It is was found that the melted polymer was more viscous, confirming by their MFI.

1. Introduction

Poly (lactic acid) (PLA), a biodegradable polymer which can also be produced from renewable resources, is rigid and brittle below the glass transition temperature (T_g) which is in the range of 50-60 °C [1]. Its brittleness limited their uses in many applications. The degradation of PLA is also another limitation of PLA usage. To overcome this limitation various plasticizers can be added to improve its brittleness.

Polyethylene glycol (PEG) is one of the polymers that have been widely used to mix with PLA for its brittleness improvement. As PEG is polymer containing ethylene oxide as a repeating unit [2]. The addition of PLA could lead to trans-esterification between ester linkage of PLA and –OH of PEG during mixing [3, 4].

The in situ reactive grafting of hydroxyl terminated polyethylene glycol (PEG) onto the maleic anhydride modified PLA in PLA/PEG blends lowered significantly the glass transition temperature compared to the blends where no grafting could occur (neat PLA + PEG) and had a positive impact on the mechanical properties [2].

In this research, two types of PEG with different molecular weight were melted mixing in PLA and were compared.

2. Materials and Methods

2.1 Materials

Poly(lactic acid) was provided by NatureWorks LLC under the reference 3052D.

Two PEGs with nominal Mw equal to 1000 g/mol (PEG) and 35000 g/mol (PEG35k) were purchased form Merck.

Dicumyl peroxide (DCP), maleic anhydride (MA) was purchased from Sigma-Aldrich.

2.2 Preparation of polymer blend

Prior to blending, the PLA was dried at 60°C for 6h. Melt-blends containing 5, 10, 15 and 20 wt% of PEG were prepared using an Internal mixer operating at 180°C for 30 min at 60 rpm. Neat PLA was also processed in the same way in order to obtain a reference.

After the processing step, sample was pre-melted for 2 min and then compressed for 3 min, between two PET sheets, and pressed at 170 °C under pressure of 800 psi.

2.3 Investigation methods

2.3.1 Fourier transforms infrared spectroscopy

Chemical structure modification of PLA was evaluated by Fourier transforms infrared spectroscopy (FTIR) using the Attenuated Total Reflectance (ATR) mode. The signal was recorded from 400 to 4000 cm^{-1}.

2.3.2 Nuclear magnetic resonance spectroscopy

Nuclear magnetic resonance ^{1}H NMR spectra were recorded on a Bruker AVANCE300 apparatus at room temperature in D-Chloroform ($CDCl_3$).

2.3.3 Differential scanning calorimetry

Differential scanning calorimetry was performed on a Mettle Toledo. Heating and cooling scans were performed at 5 °C/min. The sample (6-10 mg) were subjected to the following temperature program: (i) a first heating step from 0 to 220 °C, (ii) a cooling step from 220 to 0 °C and (iii) a second heating step from 0-220 °C.

2.3.4 Thermogravimetric analysis

Thermogravimetric analysis was carried out under constant nitrogen flow at a heating rate of 5 °C/min from 50 to 600 °C, with PERKIN ELMER.

2.3.5 Melt flow index

Melt flow index measurements were carried out at an Intro enterprise Co., LTD with standard weight of 2.16 kg. The measurements were performed at 155±2 °C.

3. Results and Discussion

3.1 Characterization of Polymer Blends

From FTIR spectra shown in Figure 1 (a) compared to (b), the change at 1360-1384 cm^{-1} was noticed and this shows the change in C-H bending of the molecule. PLA blended with PEG with the addition of 1 phr of maleic anhydride (MA) and dicumyl peroxide (DCP), in Figure 1 (c) is considered. It could be seen that C-H stretching band is intensely shown and also C-H bending are shifted. These indicated the molecular change in the polymer during melt blending.

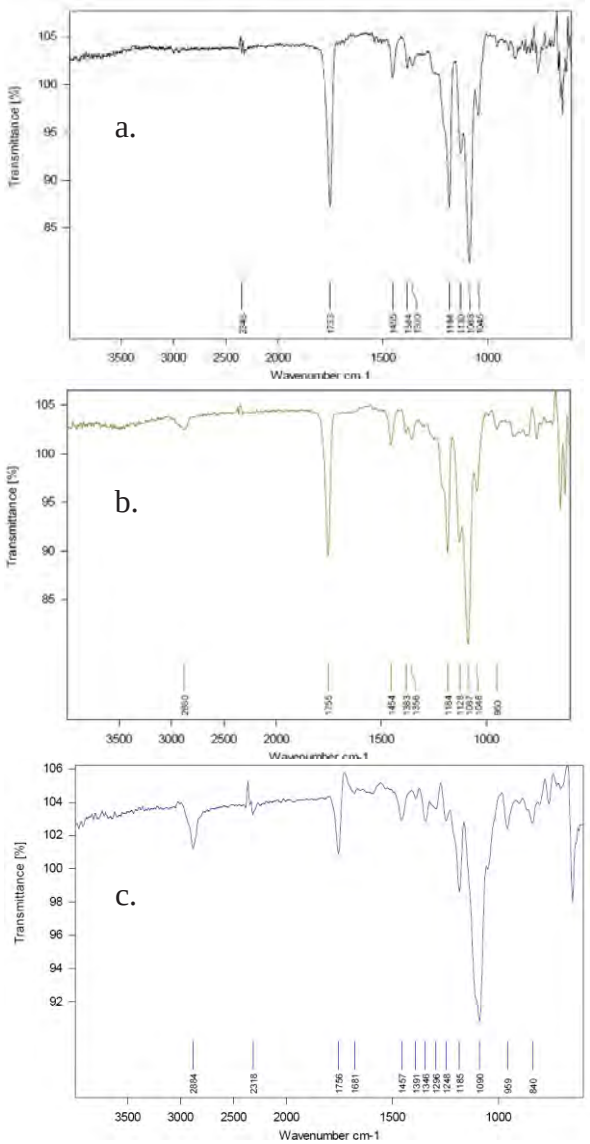

Figure 1 FTIR spectra of (a) PLA, (b) PLA: PEG at composition of 85:15 blend ratio and (c) PLA: PEG at composition of 85:15 blend ratio with the addition of MA and DCP

Figure 2 shows ^{1}H NMR of PLA, PLA: PEG and PLA: PEG with the addition of MA and DCP. It was shown in Figure 2 (a) that the chemical shift at 5.23-5.12 ppm was attributed to methylene proton in PLA molecule. Whereas the chemical shift at 1.5-1.6 ppm was attributed to CH_3 proton.

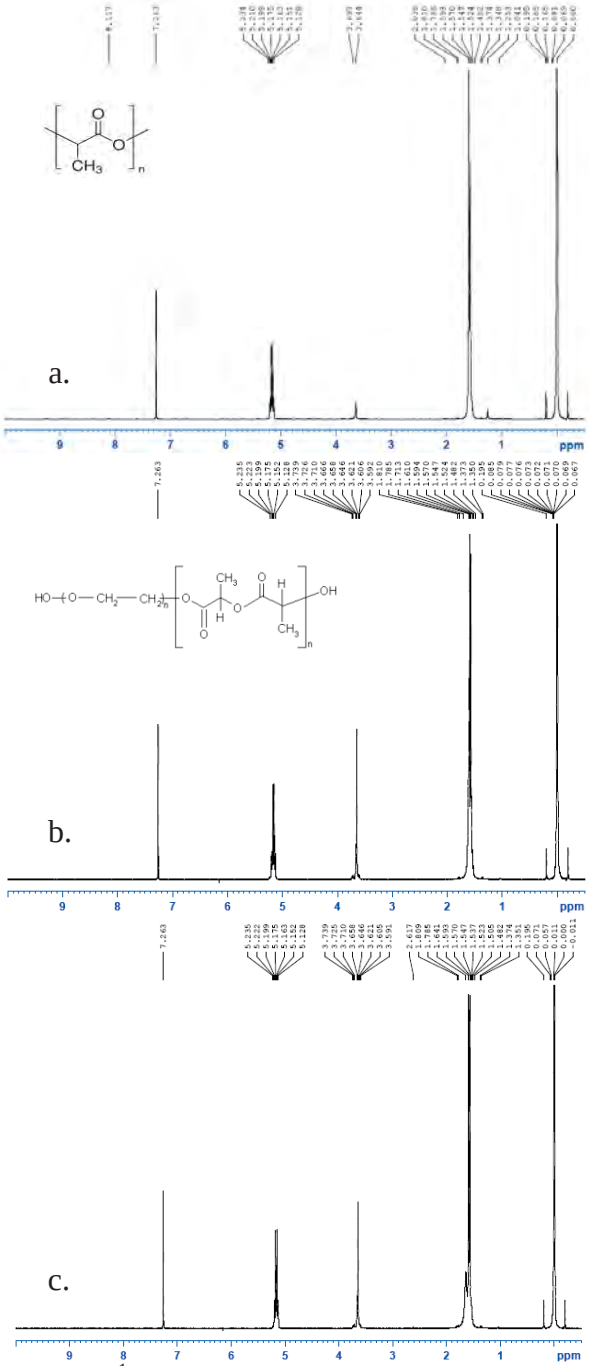

Figure 2 ^{1}H NMR of (a) PLA, (b) PLA: PEG at composition of 85:15 blend ratio and (c) PLA: PEG at composition of 85:15 blend ratio with the addition of MA and DCP

The chemical shift values at 1.253ppm and 3.69 ppm were attributed to CH_3 and CH at the chain ends, respectively. As the PEG was incorporated, chemical shift at 3.59-3.74 ppm become splitting and the integration become larger. This could be because of the trans-esterification between PLA and PEG leading to structural change designated in the figure. After

addition of MA and DCP the structure of the blend was found slightly changed. In terms of PEG 35k, it was found that there was no split signal appeared at the chemical shift of 3.59-3.74 ppm.

3.2 Thermal Properties of the Blends

3.2.1 Differential Scanning Calorimetry (DSC)

The results obtained from DSC are shown in Table 1. It was revealed that glass transition temperature (T_g) of PLA is higher than that of PEG and PLA due to the difference in their molecular weight and molecular structure. For the polymer blends, the Tg was decreased when the content of PEG was increased. It is important be aware that the melting temperature of PEG was not clearly found on the thermograms. It can also be noticed that the higher the molecular weight of PEG added, the higher of the T_g of the polymer are obtained. In the case of melting temperature, T_m was found to be decreased with the present of PEG nonetheless the T_m did not depend upon the content of PEG added. It is useful to notify that the melting temperature of PEG 1000 and PEG 35k are around 37-40 °C and 64-66 °C. We did not find the melting peak of PEG at both temperatures. With the addition of MA and DCP, the T_m was found to be lower than those without MA and DCP. This finding can be explained that the MA added could induce the PLA molecule to brake at ester linkage by the de-esterified as MA is very reactive for the reaction. This lead to the shorten of PLA molecule and hence lower in T_m

Table 1: T_g and T_m of PLA: PEG blends obtained from DSC second heating scan.

Composition	T_g, (°C)	T_m, (°C)
PLA95 PEG5	39.77	147.99
PLA90 PEG10	34.68	149.78
PLA85 PEG15	30.97	146.84
PLA80 PEG20	27.78	146.6
PLA95 PEG(35k)5	42.92	149.79
PLA90 PEG(35k)10	37.75	149.49
PLA85 PEG(35k)15	35.92	149.23
PLA80 PEG(35k)20	32.91	148.16
PLA95/PEG5/DCP/MA	36.94	147.11
PLA90/PEG10/DCP/MA	33.25	147.42
PLA85/PEG15/DCP/MA	30.28	145.13
PLA80/PEG20/DCP/MA	26.25	143.95
PLA95/PEG(35k)5/DCP/MA	38.94	148.42
PLA90/PEG(35k)10/DCP/MA	33.24	145.57
PLA85/PEG(35k)15/DCP/MA	36.44	143.86
PLA80/PEG(35K)20/DCP/MA	33.50	143.88

3.2.2 Thermogravimetric Analysis (TGA)

It could be seen from the data obtained from TGA that, in the case of adding PEG 1000 into the blends, Td was found to be lower than that of PLA. This could be explained by the low molecular weight of PEG added and also the molecular chain of PLA that has been shorten by the trans-esterification during melt mixing. After trans-esterification, PEG that incorporated onto PLA molecule is more flexible hence lower the T_{d1} of the polymer change. However, at high content of PEG 1000, the excess PEG was responsible for appeared T_{d2}. As it was mentioned earlier that the addition of MA could induce the degradation of PLA leading to shorten PLA molecular chain hence lower the T_{d1} of PLA as well.

Table 2 Degradation temperature of polymer blends.

Blend Composition	T_{d1}, (°C)	T_{d2}, (°C)
Neat PLA	319.765	-
PEG 1000	373.000	-
PEG 35K	384.221	-
PLA95 PEG5	264.263	-
PLA90 PEG10	241.799	-
PLA85 PEG15	240.424	321.943
PLA80 PEG20	231.856	329.007
PLA95 PEG(35k)5	325.623	-
PLA90 PEG(35k)10	305.448	364.099
PLA85 PEG(35k)15	334.036	375.809
PLA80 PEG(35k)20	329.297	383.292
PLA95/PEG5/DCP/MA	292.430	-
PLA90/PEG10/DCP/MA	259.135	-
PLA85/PEG15/DCP/MA	261.403	335.136
PLA80/PEG20/DCP/MA	245.042	335.105
PLA95/PEG(35k)5/DCP/MA	308.678	-
PLA90/PEG(35k)10/DCP/MA	306.800	381.073
PLA85/PEG(35k)15/DCP/MA	301.492	385.031
PLA80/PEG(35k)20/DCP/MA	295.970	377.989

3.3 Rheological property measurement

3.3.1Melt Flow Index (MFI) of the Blends

Table 3: Melt flow index (MFI) of PLA: PEG blends.

Composition	MFI (g/10 min)
Neat PLA	0.324
PLA95 PEG5	1.190
PLA90 PEG10	2.448
PLA85 PEG15	3.033
PLA80 PEG20	3.720
PLA95 PEG(35K)5	0.864
PLA90 PEG(35K)10	1.100
PLA85 PEG(35K)15	1.824
PLA80 PEG(35K)20	4.520
PLA95/PEG5/DCP/MA	1.183
PLA90/PEG10/DCP/MA	3.840
PLA85/PEG15/DCP/MA	4.388
PLA80/PEG20/DCP/MA	8.460
PLA95/PEG(35K)5/DCP/MA	1.280
PLA90/PEG(35K)10/DCP/MA	1.380
PLA85/PEG(35K)15/DCP/MA	1.480
PLA80/PEG(35K)20/DCP/MA	6.080

The viscosity of polymer blends decreases with increasing the amount of PEG. For PLA: PEG with the addition of MA and DCP, the viscosity decreases much more because the added MA could induce the scission of PLA molecule at ester linkage corresponding to DSC results.

4. Conclusions

From this work, it could be revealed that the addition of PEG1000 could lead to the molecular change of PLA. The molecular change could be observed even though it was very slightly. The thermal stability of PLA was found to be increased with the addition of PEG 35K both with and without MA and DCP. The PEG could induce crystallization indicated by the cold crystallization found in both first and second heating of DSC thermograms. It was also shown that the blends were easily flow when PEG content was increased.

Acknowledgements

The authors would like to express their sincere thanks to the Department of Materials Science and Engineering, Faculty of Engineering and Industrial Technology for their truly supported.

References

[1] E. Piorkowska, Z. Kulinski, A. Galeski, R. Masirek, Plasticization of semicrystalline poly(L-lactide) with poly(propylene glycol), (2006), Polymer 47: 7178-7188.

[2] Fatima Hassouna, Jean-Marie Raquez, Frédéric Addiego, Valérie Toniazzo, Philippe Dubois, David Ruch, New development on plasticized poly (lactide): Chemical grafting of citrate on PLA by reactive extrusion, (2012), European Polymer Journal 48: 404–415.

[3] Chunyan Wang, Sowndharya Ravi, Gary V. Martinez, Vignesh Chinnasamy, Payal Raulji, Mark Howell, Yvonne Davis, Jaya Mallela, Mohindar S. Seehra, Subhra Mohapatra, Dual-purpose magnetic micelles for MRI and gene delivery, (2012), Journal of Controlled Release 163: 82-92

[4] Bishwabhusan Sahoo, Anupam Bhattacharya, Hongyoug Fu, Wei Gao, and Richard A Gross, Influence of PEG Endgroup and Molecular Weight on Its Reactivity for Lipase-Catalyzed Polyester Synthesis, (2006), Biomacromolecules 7: 1042-1048.

SULFONIC ACID-CONTAINING RUBBER PREPARED FROM WASTE TIRE

Natdanai Charoensuk[1], Sirilux Poompradub[2], Chawalit Ngamcharussrivichai[2]*

[1] Program in Petrochemistry and Polymer Science, Faculty of Science, Chulalongkorn University, Patumwan,Bangkok, 10330 Thailand
[2] Fuel Research Center, Department of Chemical Technology, Faculty of Science, Chulalongkorn University, Patumwan,Bangkok, 10330 Thailand

* Author for correspondence; E-mail: Chawalit.Ng@chula.ac.th, Tel. +66 2187528, Fax. +66 22555831

Abstract: The environmental problems related to an increasing amount of waste tires drive the research on their reuse/recycle to valuable products. In this work, waste tire as crumb rubber was chemically modified to sulfonic acid-containing rubber (CR-SO_3H) via a control oxidation with hydrogen peroxide or nitric acid at ambient pressure. The influences of oxidation conditions, including type and concentration of oxidizing agent were studied. Fourier-transform infrared spectroscopy (FTIR) was used to characterize the surface functional groups. The cation-exchange capacity of oxidized rubber was determined by acid-base titration. Thermogravimetric-/differential thermal analysis (TG/DTA) was applied to study degradation behavior of the rubbers before and after the oxidation. The swelling degree of samples was measured by swelling test according to ASTM D471. The FTIR results indicated the presence of -SO_3^- in the oxidized rubber as evidenced by the stretching vibration of S=O at around 1360, 1160 and 1030 cm^{-1}. The crumb rubber oxidized with nitric acid had the ion-exchange capacity higher than that oxidized with hydrogen peroxide.

1. Introduction

The increasing amount of waste tires has become a serious environmental concern because the waste tires need a very long time for natural degradation due to the crosslinked structure of rubbers and the presence of stabilizers and other additives. Recycling or reusing is the way to eliminate or reduce amount of waste tires, for example, retreading to reduce spending of tires, combustion to produce energy and material recycling (devulcanization) to regenerate new rubber for applications [1]. The chemical devulcanization is a decomposing process of crosslink structure that affect on the poly-, di- and monosulfur bonds in the vulcanized rubber. Unfortunately, devulcanization also degrades the main chain of rubber, which causes the rubber product to have lower molecular weight and shorter chain. Moreover, most of devulcanizing agent is expensive and devulcanizing process requires a complex system and method. So, it was used by limitation.

Oxidation is an effiective route to devulcanize the crosslinked rubber due to process simplicity, low cost and high reactivity. The manner, in which the different types of sulfidic bonds are reacted and the structure of devulcanizate is formed, depends on types of oxidizing agent and reaction conditions [2,3,4]. The general oxidizing agents are hydrogen peroxide (H_2O_2) and nitric acid (HNO_3). It is well known that concentrated nitric acid is a strong oxidizing agent and can oxidize disulfide, as displayed in Equation 1.

$$\text{R-S-S-R} \xrightarrow[2HNO_3]{\text{Oxidation}} 2\text{R-SO}_3\text{H} + 2NO_2 \quad (1)$$

Oxidation of thiol (R-SH) and disulfides (R-S-S-R) will generate sulfonic acid group (R-SO_3H) which has high ion-exchange capacity. Also, oxidation of waste tires that has various type of sulfur bond with H_2O_2, HNO_3 is likely to generate sulfonic acid group in the structure. However, the oxidation of waste tires also generates oxygen-containings functional group, such as epoxide ring and hydroxy group [5]. Under severe conditions, the main rubber chain is oxidized, giving lower molecular weight devulcanizate as the product [6].

Due to their high ion-exchange capacity and high acidity, polymers with sulfonic acid groups were applied to many researches, for example, adsorptive removal of heavy metals from aqeous solution [7], cation exchange membranes for separation of sodium ions and alkaline earth cations [8] and conversion of fatty acids to biodiesel via heterogeneous catalysis [9]. Amberlyst® series are ion exchange resins composed of copolymer polystyrene crosslinked with divinyl benzene and sulfonation with oleum sulfuric acid. In the area of catalysts, Amberlyst-15 is a promising heterogeneous acid catalyst for reducing amount of free fatty acids in vegetable oils which are used as feedstock for biodiesel production [10]. However, its high cost limits the practical use in an industrial scale.

In this research, waste tire as crumb rubber was converted to polymer containing sulfonic acid groups via a controlled oxidation by using HNO_3 or H_2O_2 as the oxidizing agent. The influences of oxidation conditions, including type and concentration of oxidizing agent were studied. The ion-exchange capacity of oxidized crumb rubber was evaluated by an acid-base titration.

2. Materials and Methods

2.1 Oxidation of Crumb Rubber

Crumb rubber (CR) with particle size of 2.5-5.0 mm was obtained from the Thai Union Commercial

Development Company Limited. Composition and physical properties of the rubber as reported by the company are shown down in Table 1. The oxidation of CR was carried out in an 100-mL three-necked round bottom flask equipped with a reflux condenser and a magnetic stirrer. Different concentrations of HNO_3 (2 M and 8 M) or H_2O_2 (10, 20 and 30 wt.%) were used as oxidizing agents. Typically, 10 g of CR was mixed with a solution of oxidizing agent (100 mL) in the flask. Oxidation temperature was controlled by an oil bath at 50 °C in case of using H_2O_2 and at 80 °C for HNO_3. After 5 h of the reaction course, the oxidized CR was separated from the reaction mixture by filtration and washed thoroughly with deionized water until the filtrate became neutral. Then, the oxidized CR was dried in a vacuum oven at 80 °C for 2 h. The resulting rubber product was designed as CR-SO_3H-X(Y) where X rerepresents to the type of oxidizing agent, and Y indicates the concentration of oxidizing agent.

Table 1: Properties of crumb rubber (CR) from the Thai Union Commercial Development Co. Ltd.

Chemical analytical composition	
Acetone extract (%)	15±3
Ash (%)	6±3
Carbon black (%)	25±3
Moisture : less than (%)	1
Rubber hydrocarbon (%)	50±3
Physical properties of the vulcanized reclaim	
Specific gravity (at 25°C)	1.14±0.02
Mooney viscosity (ML 1' +4' at 100 °C)	60±15
Hardness (shore A)	55±3
Minimum tensile strength (psi)	920
Minimum elongation (%)	250

2.2 Rubber Characterization

Functional groups of the oxidized rubber were characterized using a Perkin Elmer (Spectrum One) infrared spectrometer and KBr method. Thermogravimetric/differential thermal analysis (TG/DTA) was applied to study degradation behavior of CR before and after the oxidation using a Perkin Elmer Pyris Diamond thermogravimetry with a heating rate of 10 °C/min and nitrogen flow (50 mL/min). Ion-exchange capacity (IEC) of the oxidized CR was measured by an acid-base titration method. In this section, CR and CR-SO_3H-X(Y) were immersed in 1M NaCl solution for ion exchanging process which continuous stirred. After 18 h of process, the solution was titrated with 0.1M NaOH.

The swelling degree of samples was measured by swelling test following ASTM D471. Initially 0.2 g of rubber were immersed in 5 mL of toluene at ambient temperature for 24 h. Then, the rubber was separated from the solvent by filtration. The solvent remaining on the rubber surface was carefully absorbed by tissue paper, and the weight of swollen rubber was measured. The swelling ratio (Q) was calculated according to the equation below;

$$Q = \frac{(M - M_0)}{M_0} \qquad (2)$$

where Q is the swelling ratio, M is the mass of swollen rubber and M_0 is the dry mass of initial rubber. The swelling degree and the solubility of polymer in organic solvents of polymer and other components in polymer were important for application in ion-exchange.

3. Results and Discussion

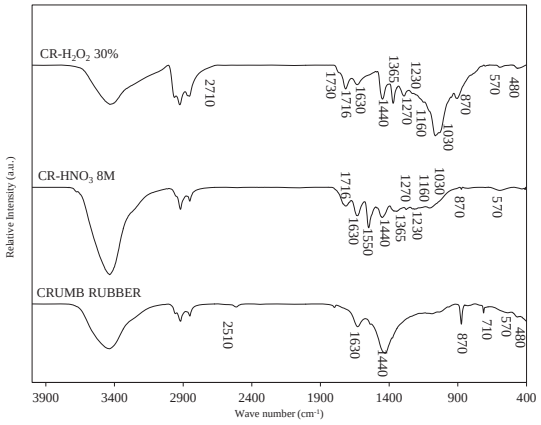

Figure 1. FTIR analyses of samples: (A) CR, (B) CR-SO_3H-HNO_3(8M) and (C) CR-SO_3H-H_2O_2(30 wt.%)

Figure 1 shows the FTIR spectra of CR and CR oxidized by different oxidizing agents, 8M HNO_3 and 30 wt.% H_2O_2. The starting CR had the IR bands at 870 and 570 cm^{-1} which attributed to =C-H bending and C-S stretching, respectively. The bands related to -C=CH_2 of the rubber backbone were observed at 1630 and 1440 cm^{-1}. The bands at 2510 and 710 cm^{-1}, found only in the spectrum of CR were assigned to S-H stretching of thiol group and =C-H stretching of the main rubber, respectively. The presence of sulfidic bonds in CR was confirmed by S-S stretching locating at 480 cm^{-1}. After the oxidation, the characteristic bands of natural rubber were decreased in the intensity concomitantly with a disappearance of the bands related to the thiol group. When HNO_3 was used as the oxidant, the sulfidic band was not observed anymore (CR-SO_3H-HNO_3(8M)), but it still remained in the case of CR-SO_3H-H_2O_2(30 wt.%). The sulfonic acid group in the oxidized CR was evidenced by the bands at 1360 cm^{-1} corresponding to S=O asymmetric stretching, at 1160 and 1030 cm^{-1}, related to S=O symmetric stretching, and at 3420 cm^{-1} can be ascribed to -OH bond [6,11,12]. Moreover, the oxidation resulted in the formation of carboxylic group (-COOH) since the bands owing to O-H, C=O and C-O stretching appeared at 3400, 1716, 1270 and 1230 cm^{-1} respectively. In the case of H_2O_2 as the oxidizing agent, the bands at 1730 and 2735 cm^{-1} were attributed respectively to C=O and C-H stretching of aldehyde (R-CHO). The strong adsorption band at

1550 cm^{-1} clearly observed in CR-SO_3H-HNO_3(8M) was related to nitro group (-NO_2).

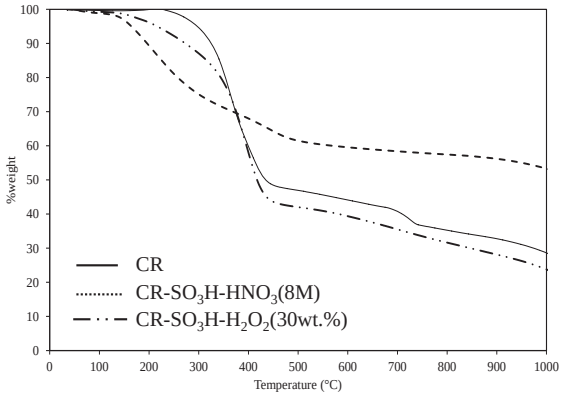

Figure 2. Thermal degradation behavior of CR, CR-SO_3H-HNO_3(8M) and CR-SO_3H-H_2O_2(30 wt.%)

The thermal degradation behavior of CR and oxidized CR was studied in N_2 atmospheres between 50 and 1000 °C (Figure 2). The decomposition pattern of original CR showed three step weight loss. The first and second steps occurred at around 250-390 °C and 390-480°C, which were assigned to the decomposition of natural rubber and styrene-butadiene rubber, respectively. Then the degradation of carbon black was found at 695-750 °C [13]. Apparently, the oxidation with 30 wt.% H_2O_2 and 8 M HNO_3 totally changed decomposition behavior of CR. CR-SO_3H-HNO_3(8M) lost weight in two steps. The first step was in the range of 180-350 °C, attributed to decomposition of functional groups, such as -COOH and -NO_2 groups [14]. The final step was related to the polymer backbone that was decomposed at 390-480 °C. This results indicated that 8 M HNO_3 was a strong oxidizing agent by which the main rubber chain was sucessively oxidized, giving less thermally stable products. The presence of acidic moieties might promote the carbonization of rubber molecules to form carbon residue, resulting in the smaller total weight loss. In the case of CR-SO_3H-H_2O_2(30 wt.%), the thermal decomposition was changed to weight loss at 200-480 °C due to the formation of new functional groups in the rubber chains. In addition, the weight loss ascribed to carbon black disappered after the oxidation using either H_2O_2 or HNO_3. This results indicated that carbon black in CR was leached into the solution during the oxidation.

Table 2: The swelling ratio of CR and CR-SO_3H-X(Y)

Samples	Swelling ratio after 24 h (Q)
CR	4.69
CR-SO_3H-H_2O_2(10 wt.%)	3.52
CR-SO_3H-H_2O_2(20 wt.%)	3.41
CR-SO_3H-H_2O_2(30 wt.%)	2.20
CR-SO_3H-HNO_3(2M)	2.33
CR-SO_3H-HNO_3(8M)	1.70

A B C

Figure 3. Swollen rubbers after 24 h: (A) CR, (B) CR-SO_3H-H_2O_2(30 wt.%) and (C) CR-SO_3H-HNO_3(8M)

The swelling degree and the solubility of the oxidized CR and other components were important for application in ion exchange. Table 2 summarizes the swelling ratio of CR before and after the oxidation with H_2O_2 and HNO_3. It can be seen that the swelling ratios of the oxidized rubber were significantly lower than that of initial CR. The concentration of oxidizing agents also affected the swelling ratio. When the concentration of the oxidants increased, the swelling ratio of rubber was decreased. It should be due to the presence of polar functional groups in CR-SO_3H-H_2O_2 and CR-SO_3H-HNO_3(8M). The swollen samples are representatively shown in Figure 3. Change of toluene color during the swelling test is indicative for solubility of the oxidized rubber in non-polar solvent. The swollen CR gave pale yellow solution (Figure 3A), while the toluene containing CR oxidized with H_2O_2 was clearer (Figure 3B). In the presence of CR-SO_3H-HNO_3(8M), the color of toluene became dark yellow. The shorter polymer chains cleaved from the rubber backbone should result in the higher toluene solubility of the CR oxidized with HNO_3.

Table 3: Ion exchange capacity (IEC) of CR and CR-SO_3H-X(Y)

Samples	Ion exchange capacity (mmol/g sample)
CR	0.000
CR-SO_3H-H_2O_2(10 wt.%)	0.150
CR-SO_3H-H_2O_2(20 wt.%)	0.150
CR-SO_3H-H_2O_2(30 wt.%)	0.150
CR-SO_3H-HNO_3(2M)	0.250
CR-SO_3H-HNO_3(8M)	1.100

The ion-exchange capacity (IEC) of the initial CR and CR-SO_3H-X(Y) is compared in table 3. It can be seen that CR-SO_3H-X(Y) possessed an ion exchange capacity because the oxidation generated the acid groups, such as sulfonic and carboxylic acids, all of which were able to give acidic proton during the ion exchange process. Although the FTIR results suggested that CR-SO_3H-H_2O_2 had a high amount of functional groups containing S=O bonds, its IEC was lower than that of CR-SO_3H-HNO_3 was lower than that of CR-SO_3H-HNO_3. This controversy could be explained by the fact that other sulfur oxides, e.g. sulfone, sulfoxide, are possibly formed by the oxidation of CR with H_2O_2 [16]. The assignments of IR bands derived from their S=O bonds are very close. These sulfur oxide groups are non-acidic and not active in the ion exchange. Other explanation was related to the TGA results and the swelling test, which

indicated the retention of rubber backbone in CR-SO_3H-H_2O_2, resulting in higher hydrophobicity property than CR-SO_3H-HNO_3. Since water is the liquid media for ion transfer, the ion exchange over CR-SO_3H-H_2O_2 might experience some limitations. On the other hand, the oxidation of CR with HNO_3 increased IEC to 1.1 mmol/g sample.

4. Conclusions

The oxidation process with H_2O_2 and HNO_3 showed an effective route to devulcanize crumb rubber. The reaction generated important functional group which has ion-exchange capacity, -SO_3H and -COOH. The weight loss of rubber in themal degradation behavior was changed. Weight loss was started at lower temperature than the initial of CR. Moreover, the swelling ratio was decreased after the oxidation, especially in case of CR-SO_3H-HNO_3(8M). However, the oxidation was able to increase the ion-exchange capacity of CR which creating functional groups having high acidity, especially sulfonic acid groups.

References

[1] S. Maciej, K.L. Justyna, J. Helenaand and B. Adolf, *Waste Manage.* **32** (2012) 1742–1751.
[2] K. Masayuki, N. Sayuri, I. Yuki, H. Honoka and N. Takuya, *Tetrahedron Lett.* **52** (2011) 3086–3089.
[3] K. Piotr, M. Katarzyna, O. Katarzyna and K. Zofia, *Tetrahedron* **61** (2005) 1933–1953.
[4] A. Miek, S. Chiyoshi and Y. Masahiko, *Tetrahedron Lett.* **46** (2005) 6097–6099.
[5] Z. Jing, Z. Qian, J. Xian-Hong, D. An-Ke, Z. Tao, V.K. Johannes and W. Yu-Zhong, *Polym. Degrad. Stabil.* **95** (2010) 1077-1082.
[6] R.V.A.R. Rachel, G. Manuela, P.F. Vany, M.L. Rochel and H.A. Maria, *J. Braz. Chem. Soc.* **17** (2006) 603-608.
[7] Q. Qishu, G. Qian, W. Chengyin, and H. Xiaoya, *Colloid Surface A* **415** (2012) 41– 46.
[8] S. Toshikatsu, Y. Takahiroand and M.I. Koji, *J. Membrane Sci.* **120** (1996) 101-110.
[9] C.S. Caetano, L. Guerreiro, I.M. Fonseca, A.M. Ramos, J. Vital and J.E. Castanheiro, *Appl. Catal. A-Gen*. **359** (2009) 41-46.
[10] J.Y. Park, D.K. Kim, and J.S. Lee, *Bioresource Technol.* **101** (2010) S62–S65.
[11] X. Tian, L.L. Zhang, P. Bai and X.S. Zhao, *Catal. Today* **166** (2011) 53-59.
[12] F. Shirini and O.G. Jolodar, *J. Mol. Catal. A-Chem.*, **356** (2012) 61-69.
[13] Q. Yang, L. Wang, W. Xiang, J. Zhou and J. Li, *Polymer* **48** (2007), pp. 2866-2873.
[14] D.D. Jiang, Q. Yao, M.A. McKinney and C.A. Wilkie, *Polym. Degrad. Stabil.* **63** (1999) 423-434.
[15] V.J. Inglezakis, *J. Colloid Interf. Sci.* **281** (2005) 68-79.
[16] L.H. Chou, C.K. Yang, M.T. Lee and C.C. Shu, *Compos. Part B* **41** (2010) 613–616.

EFFECT OF NR-g-PMMA AND ENR ON MECHANICAL PROPERTIES AND FUEL OIL SWELLING OF SILANE TREATED SURFACE-RICE HUSK ASH FILLED NATURAL RUBBER COMPOSITE

Kwanruethai Boonsong[1*] Diew Saijan[1] and Jutatip Artchomphoo[1]

[1] Department of Rubber and Polymer Technology, Faculty of Science and Technology, Rajamangala university of Technology Srivijaya, Nakhon Sri Thammarat 10880, Thailand

[*] Author for correspondence; E-Mail: : kwan_005@hotmail.com, Tel. +66 75773336, Fax. +66 75773338

Abstract: In this research, graft copolymer of natural rubber and polymethyl methacrylate (NR-g-PMMA) and epoxidized natural rubber (ENR) were used as coupling agent to improve the properties of silane treated-surface rice husk ash (SiRHA) filled natural rubber composite. The SiRHA filled NR was prepared in an internal mixer at kept contents of SiRHA (40 phr) and coupling agents (9 phr). The mechanical properties i.e. 300%modulus, tensile strength, tear strength, and hardness were examined. It was found that the incorporation of coupling agents could improve the composite properties. The SiRHA filled NR prepared with ENR coupling agent showed higher 300%modulus, tensile strength and tear strength than those compounded with NR-g-PMMA. Furthermore, fuel oil swelling (gasoline, gasohol91, gasohol95, diesel and biodiesel) at room temperature of composite was improved when NR-g-PMMA and ENR were used as coupling agent.

1. Introduction

Rice husk ash (RHA) was obtained by fuel efficiency from burning rice husk, that contained SiO_2 or silica main products about 33-91%. RHA or silica from natural rubber source was attracted to investigate as filler in a variety of rubbers [1-6]. The mechanical properties of RHA filled rubber composites were unsatisfied when compared with composites prepared from commercial fillers (silica and carbon black), which was attributed to the relatively large size of the RHA particle and the lack of silanol group (SiOH) are interferer to that only favors a moderate reinforcement. The additonal of silane as coupling agent into RHA filled-rubber system that little effect on the properties due to the lack of silanol groups on the ash surface [5]. Sombatsompop *et al*. [6] reported the properties of the fly ash filled 50/50 NR/SBR blends were improved when filled the silane treated surface of silica from fly ash in blends.

Epoxidized natural rubber (ENR) and Graft copolymer of natural rubber and polymethyl methacrylate (NR-g-PMMA) are a modified natural rubber having properties resembling those of synthetic rubbers rather than natural rubber such as good oil resistance, improved wet grip and rolling resistance, coupled with high strength. Pattamaprom *et al*. [1] found that the incorporation of rice husk ash in ENR composite showed higher tensile strength than that of natural rubber (NR). Therefore, it is also of intereste to study the effect of silane treated surface of RHA and rubber modification on the properties of rice husk ash composite.

2. Materials and Methods

2.1 Material

Natural rubber (rubber smoked sheet, RSS#3, obtained from the rubber replanting aid found, Krabe province Thailand). The NR-g-PMMA used was in-house synthesized as details described elsewhere [7]. The graft copolymer was prepared using a 80:20 molar percentage ratio of NR/MMA with a level of the grafted PMMA of 15% weight and percentage grafting efficiency of 80.35%. ENR, with 25 mol% epoxidation (Muang Mai Guthrie PCL, Thailand). Rice husk ash (RHA, obtained from Yala province, Thailand) contained of silicon dioxide (SiO_2) is 72%. Table 1 showed the chemical composition of the rice husk ash used in this study. Zinc oxide (Imperial Co., Ltd., Thailand) and stearic acid (Imperial Co., Ltd., Thailand) were used as activator. N-(1,3-dimethylbutyl) N-phenyl-p-phenylendiamine, 6PPD (supplied by K.S.P OCTATECH Co., Ltd., Thailand). N-tert-butyl-2-benzothiazole sulphenamide, TBBS (Flexsys, USA) and tetramethyl thiuram disulphide, TMTD (Flexsys, USA) were used as accelerator. Sulfur (Petch Thai Chemical Co., Ltd., Thailand) was used as vulcanizing agent. TESPT, bis (3-triethysilylpropyl) tetrasulphane (received form Cs Unitel technology, Co., Ltd., Thailand

Table 1 : Chemical composition of RHA (using X-ray Fluorescence Spectrometer)

Component	wt (%)	Component	wt (%)
SiO_2	72.100	MgO	1.016
K_2O	9.532	MnO	0.996
CO_2	4.188	Cl	0.986
P_2O_5	3.910	Fe_2O_3	0.293
CaO	2.085	Al_2O_3	0.269
H_2O	1.934	Rb_2O	0.260
CHNO	1.186	ZnO	0.064
SO_3	1.182		

2.2 Silane surface treatment of RHA

We used TESPT to modify the surface of RHA wi. Firstly, TESPT was hydrolyzed in 95% ethanol solution for 1 hour. Then a fixed amount of RHA with 95% ethanol as solvent was treated with ultrasonic vibrator for 1 hour. Finally, RHA dispersion was dropped into hydrolyzed TESPT with mechanical stir at 25 ^{o}C for 2 hours. The RHA/TESPT dispersion was centrifuged followed by rinsing with ethanol for 3 times and then with distilled with water for 2 times. The resultant product was designated as SiRHA.

2.3 Compounding SiRHA filled-NR composite

The SiRHA filled-NR was prepared in an internal mixer with a fill factor 0.65, at chamber temperature of 40 ^{o}C and a rotor speed of 40 rpm. NR was initially masticated in the mixing for 5 min and mixed with the coupling agent (NR-g-PMMA or ENR), followed by the other ingredients in this order: activators (stearic acid and ZnO) antioxidant (6PPD), filler (RHA or SiRHA), accelerators (TBBS and TMTD) and sulfur. After that the composite compound was sheeted at a laboratory sized two roll mill at room temperature. The required quantities of ingredients are given Table 2. The composite compounds were then compression molded at 150 ^{o}C at their respective optimal cure time obtained by using ODR (oscillating disk rheometer, model TECH OD+)

Table 2: Formulation of rubber compound

ingredients	Parts per hundred parts of rubber		
	SiRHA	ENR+SiRHA	NR-g-PMMA+SiRHA
RSS#3	100	100	100
SiRHA	40	40	40
ZnO	5	5	5
Stearic acid	2	2	2
6PPD	1	1	1
TBBS	1.2	1.2	1.2
TMTD	0.8	0.8	0.8
Sulfur	1.5	1.5	1.5
ENR	-	9	-
NR-g-PMMA	-	-	9

2.4 Mechanical testing

Dumbbell and angle shaped specimens were cut from the molded slabs for tensile and tear tests. Tensile strength was determined according to ASTM D412 and tear strength was determined according to ASTM D624. The experiments were carried out in a tensometer, Testometric M350-10AT model, operated at an extension speed of 500 mm/min. The hardness of the composites properties was performed using a shore type A durometer according to ASTM D2240. All tests were conducted at room temperature (25^{o}C).

2.5 Fuel oil swelling test

Fuel oil swelling test was determined by mass change of cure composite sample after immersion in fuel oil such as gasoline gasohol 91, gasohol 95, diesel and biodiesel at room temperature for 70 hours. The fuel oil swelling was calculated using the Eq. (1) as follows:

$$\text{Fuel oil swelling}(\%) = \frac{(M_1 - M_0)}{M_0} \times 100$$

Where, Mo is the initial mass of composite sample and M_1 is the mass of composite after immersed in fuel oil, respectively.

3. Results and Discussion

The cure characteristics at 150 ^{o}C of the SiRHA filled NR composites containing ENR and NR-g-PMMA as coupling agent compared with neat composite showed in Table 3. As can be seen that, the ENR+SiRHA composite shows highest maximum torque and shortest scorch time, followed by NR-g-PMMA+SiRHA composite and SiRHA composite, respectively. This is because the epoxy group in ENR tends to activate the adjacent double bonds in the rubber molecules yielding free radicals [8]. The radicals created from the reaction can quickly react and form crosslinks with sulfur. For NR-g-PMMA has a methyl methacrylate groups in NR-g-PMMA. Since the methyl methacrylate groups are polar, they can serve as a ligand of zinc complexes. The zinc complexes activated by the methyl methacrylate groups can react fast so that crosslinking reaction will also proceed fast. The molecular structure of ENR and NR-g-PMMA showed in Figure 1.

Table 3: scorch time, cure time and maximum torque of composites.

Sample	Cure characteristic at 150 °C		
	Scorch time (min)	Cure time (min)	Maximum torque (dN.m)
SiRHA	1.42	2.19	33.26
ENR+SiRHA	1.05	1.76	42.52
NR-g-PMMA+SiRHA	1.02	1.889	40.28

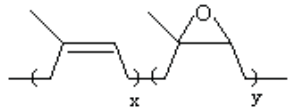

(a) x / y = 1

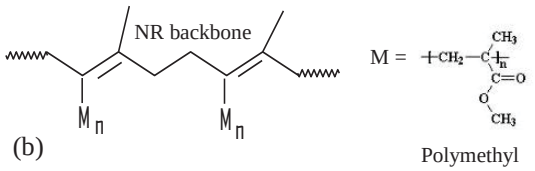

(b) Polymethyl methacrylate

Figure 1. Molecular structure of (a) ENR and (b) NR-g-PMMA

Figure 2–4 showed 300% modulus or tensile modulus at 300% elongation, tensile strength, tear strength and hardness of the SiRHA filled NR composites with and without ENR and NR-g-PMMA. The SiRHA+ENR and SiRHA+NR-g-PMMA composites, the tensile strength and tear strength showed a progressive increase. This may be due to increase crosslink density in composites. The crosslink density could investigate by maximum torque of cure curve obtained ODR instrument that shown in Table 3. However , there was no significant effect of coupling agent addition on the 300% modulus and hardness properties.

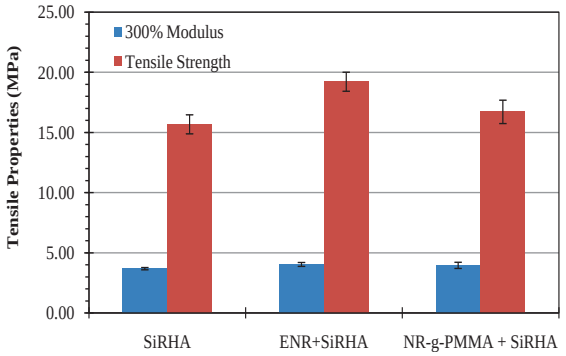

Figure 2. Tensile properties (300% modulus and tensile strength) of SiRHA, ENR+SiRHA and NR-g-PMMA+SiRHA composites.

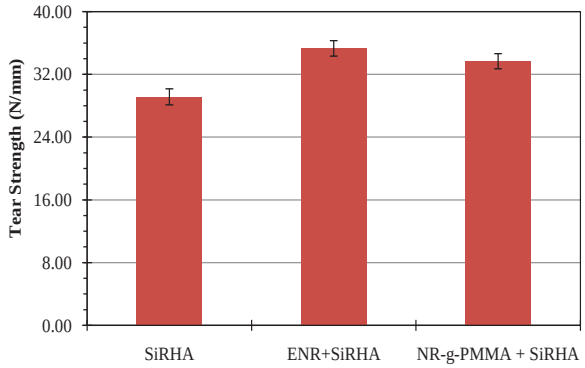

Figure 3. Tear strength of SiRHA, ENR+SiRHA and NR-g-PMMA+SiRHA composites.

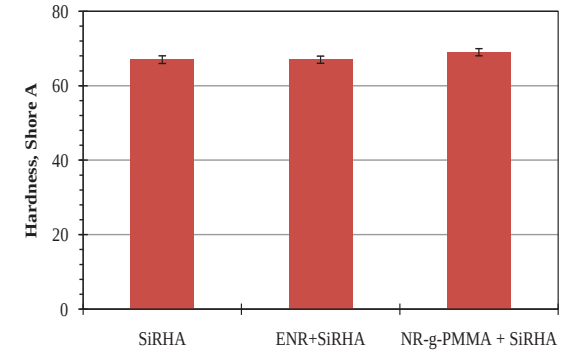

Figure 4. Hardness property of SiRHA, ENR+SiRHA and NR-g-PMMA+SiRHA composites.

Figure 5-9 show percentage of fuel oil swelling at room temperature, corresponding to degree of fuel oil resistance of SiRHA, ENR+SiRHA and NR-g-PMMA+SiRHA composites. The fuel oil swelling of composites with NR-g-PMMA and ENR are decreased, indicating a relatively high level of fuel oil resistance. This tendency was prove to be increase crosslink density of composites system.

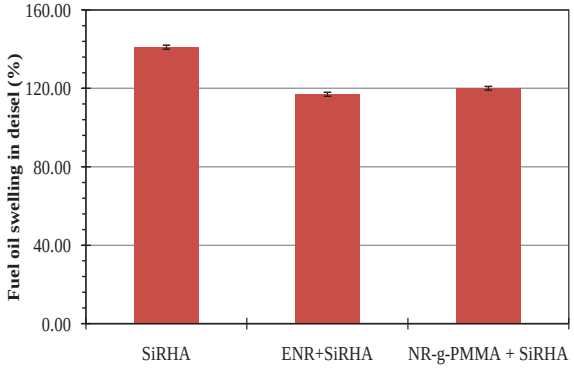

Figure 5. Fuel oil swelling in diesel of SiRHA, ENR+SiRHA and NR-g-PMMA+SiRHA composites.

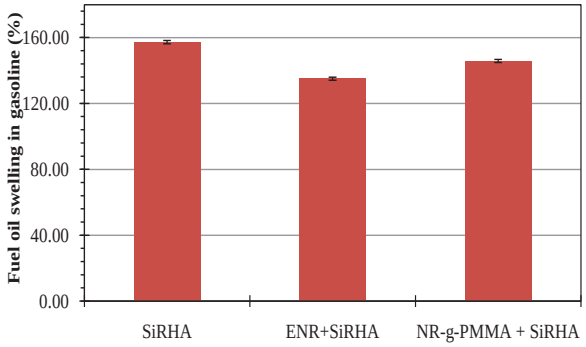

Figure 6. Fuel oil swelling in gasoline of SiRHA, ENR+SiRHA and NR-g-PMMA+SiRHA composites.

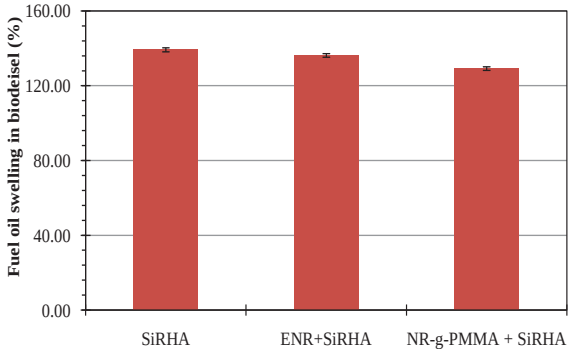

Figure 7. Fuel oil swelling in biodiesel of SiRHA, ENR+SiRHA and NR-g-PMMA+SiRHA composites.

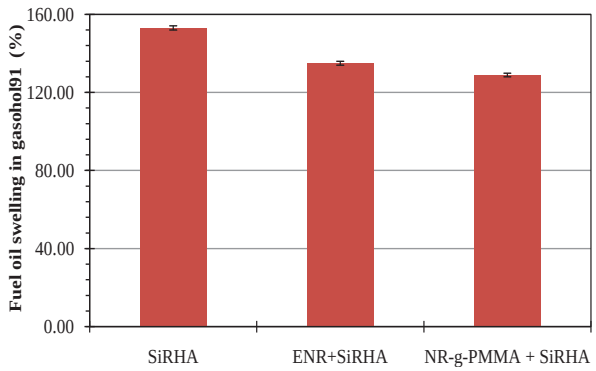

Figure 8. Fuel oil swelling in gasohol91 of SiRHA, ENR+SiRHA and NR-g-PMMA+SiRHA composites.

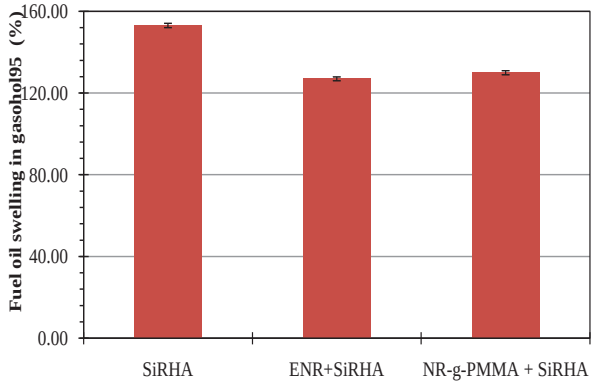

Figure 9. Fuel oil swelling in gasohol95 of SiRHA, ENR+SiRHA and NR-g-PMMA+SiRHA composites.

4. Conclusions

This purpose of this study was to use ENR and NR-g-PMMA as coupling agent for SiRHA filled natural rubber composite. The incorporation of coupling agents in SiRHA filled natural rubber composite improved 300% modulus, tensile strength, tear strength, hardness and fuel oil swelling. This may be due to increase crosslink density in composites via ENR and NR-g-PMMA.

Acknowledgements

The authors are grateful for financial support provided by Faculty of Science and Technology, Rajamangala University of Technology Srivijaya, Nakhon Sri Thammarat, Thailand.

References

[1] C. Pattamaprom, K. Bandidchutikun, S. Sotananan and S. Pharommedetch. Thammasat Int. J. Sci. Tech., Vol.**13** (2008) 38-42.

[2] H. M. Da Costa, L.L.Y. Visconte, R.C.R. Nunes and C.R.G. Furtado, J. Appl. Polym. Sci. **76** (1999) 1019-1027.

[3] H. M. Da Costa, L.L.Y. Visconte, R.C.R. Nunes and C.R.G. Furtado. J. Appl. Polym. Sci. **83** (2002) 2331-2346.

[4] W. Arayapranee, N. Na-Ranong and G.R. Rempel, J. Appl. Polym. Sci. **98** (2005) 34-41.

[5] P. Sae-oui, C. Rakdee and P. Thanmathorn, J. Appl. Polym. Sci. **83** (2002) 2485-2493.

[6] N. Sombatsompop, E. Wimolmala and T. Markpin, J. Appl. Polym. Sci. **104** (2007) 3369-3405.

[7] E.Kalkornsurapranee, K. Sahakaro, A. Kaesaman and C. Nakason, J. Appl. Polym. Sci. **114** (2009) 587-597.

[8] H. Ismail and S. Suzaimah, Polym. Testing **19** (2007) 879-888.

Petroleum Chemistry and Catalysis

HYDROGEN PRODUCTION FROM METHANE VIA CHEMICAL LOOPING REFORMING ON NiO/CeO_2

Apichaya Yahom[1], Varong Pavarajarn[2], Patiwat Onbhuddha[3], Sumittra Charojrochkul[3], Suttichai Assabumrungrat[1] *

[1] Center of Excellence in Catalysis and Catalytic Reaction Engineering, Department of Chemical Engineering, Faculty of Engineering, Chulalongkorn University, Pathumwan, Bangkok, 10330 Thailand
[2] Center of Excellence in Particle Technology (CEPT), Department of Chemical Engineering, Faculty of Engineering, Chulalongkorn University, Pathumwan, Bangkok, 10330 Thailand
[3] National Metal and Materials Technology Center (MTEC), 114 Paholyothin Road, Klong 1, Klongluang, Pathumthani, 12120 Thailand

*E-mail: Suttichai.A@chula.ac.th

Abstract: This work focused on the study of hydrogen production from methane via chemical looping reforming over NiO loaded on two types of supports i.e. CeO_2 and Al_2O_3. Experiments were conducted in a fixed-bed reactor operated at 1 bar and 600°C. NiO acts as a solid oxygen carrier which is reduced by methane and subsequently oxidized by air. NiO was selected due to its high catalytic activity for hydrogen production, cost and availability. The results show that a higher amount of H_2 was produced from NiO/CeO_2 than from NiO/Al_2O_3. This is because CeO_2 has high oxygen storage capacity to help promoting the reaction. In addition, the effect of CaO which was physically mixed with the oxygen carrier on the reaction performance was investigated. Higher H_2 purity and methane conversion were observed with the presence of CaO as CO_2 generated from the reaction was removed from the reaction mixture by reacting with CaO to form $CaCO_3$, thus enhancing the reaction and purifying the hydrogen product.

1. Introduction

Hydrogen can be produced by several reactions from methane such as partial oxidation, steam reforming, and autothermal reforming. Chemical looping reforming is a new technology developed from autothermal reforming in which methane does not contact directly with air but reacts with an oxygen-transporting solid. The oxygen carrier can be later reclaimed simply by oxidation with air. This technology requires less investment for a gas separation process.

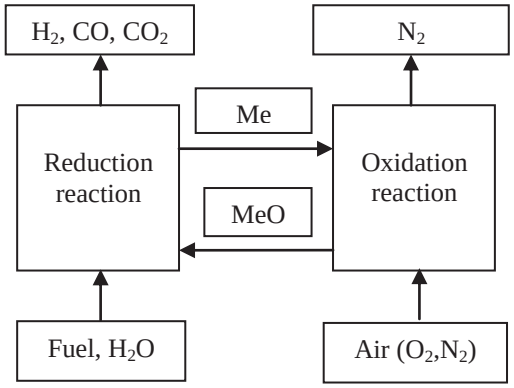

Figure 1. Chemical looping reforming

Among variety of oxygen carriers used in chemical looping reforming, NiO is the most popular one because of its high reactivity [1] and oxygen transport capacity [2]. A support for the oxygen carrier is also an important factor to boost the reactivity. Alumina support (Al_2O_3) is often used because of its low cost and low tendency for agglomeration. However, one major problem associated with alumina is carbon formation after repeated uses, which deactivates the oxygen carriers [3]. Ceria support (CeO_2) is famous for its high oxygen storage as well as the ability to release carbon from the oxygen carrier [4-8].

In addition, a use of CaO as CO_2 sorbent [9] can increase a hydrogen purity and a hydrogen production from the conversion of CO_2 to $CaCO_3$ [10].

2. Materials and Methods

2.1 Materials

Chemicals used in our experiments were 13wt%NiO/Al_2O_3, 13wt%NiO/CeO_2, silicon carbide (SiC), and CaO as CO_2 sorbent. Nickel-based oxygen carriers were prepared by wet impregnation of nickel nitrate aqueous solution on supports. After impregnation, the sample was calcined at 800°C for 4 hrs.

2.2 Reactions

Possible reactions during the processes are:

R1 $CH_4 + 4NiO \rightarrow CO_2 + 2H_2O + 4Ni$

$\Delta H_{298K} = 174.9$ kJ/mol

R2 $CH_4 + NiO \rightarrow CO + 2H_2 + Ni$

$\Delta H_{298K} = 208.6$ kJ/mol

R3 $CH_4 + 2NiO \rightarrow CO_2 + 2H_2 + 2Ni$

$\Delta H_{298K} = 169.9$ kJ/mol

R4 $CH_4 + H_2O \leftrightarrow CO + 3H_2$

$\Delta H_{298K} = 206.1$ kJ/mol

R5 $CH_4 + CO_2 \leftrightarrow 2CO + 2H_2$

$\Delta H_{298K} = 357.8$ kJ/mol

R6 $H_2O + CO \leftrightarrow CO_2 + H_2$

$\Delta H_{298K} = -41.2$ kJ/mol

R7 $Ni + \frac{1}{2}O_2 \rightarrow NiO$

$\Delta H_{298K} = -244.3$ kJ/mol

In addition, when CaO is used, one more reaction takes place:

R8 $CaO + CO_2 \leftrightarrow CaCO_3$

$\Delta H_{298K} = -178.8$ kJ/mol

2.3 Experimental

The experiments were conducted in a 500 mm long quartz fixed bed reactor, of which an inner diameter was 10 mm. The specimens used in our experiments composed of 1 g Ni-based oxygen carrier on support and 1 g of CaO in case of the sorption enhanced hydrogen production. For a reference case, 1 g of SiC was used instead of CaO.

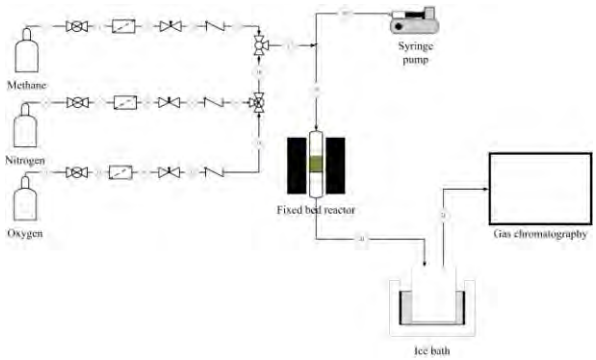

Figure.1 Process diagram of experimental set-up.

Total flow of gas in each experiment was fixed at 50 ml/min, and nitrogen was used as a carrier gas., A mixture of 3 vol% methane, 6 vol% steam was used in reduction reaction, while and 21 vol% oxygen was used for an oxidation reaction. Both reactions were conducted at 600°C and 1 bar.

3. Results and Discussion

At the beginning of chemical looping reforming process, a complete combustion occurred because there were plenty of oxygen in the solid. As the reaction progressed and the oxygen content in the metal oxide was decreased, an incomplete combustion occurred while part of methane reacted with steam via catalytic steam reforming in which metal was produced. Finally, in the depletion of oxygen in the solid, there was only metal or catalyst without any metal oxide. Ni metal in this experiment, led to a production of hydrogen via catalytic steam reforming.

From the reference experiments whereas NiO/Al_2O_3 was physically mixed with SiC without any CO_2 sorbent, the maximum hydrogen purity produced was 60.8%.

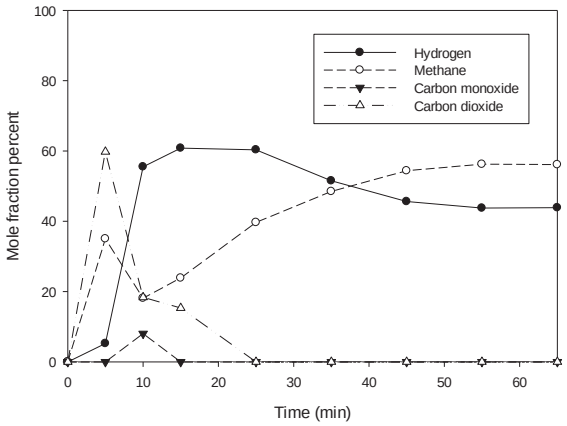

Figure 2. Reduction of 1 g NiO/Al_2O_3 physically mixed with 1 g SiC.

When CaO was physically mixed with NiO/Al_2O_3 , the hydrogen purity and methane conversion were increased as shown in Figure 3. The highest hydrogen purity produced was increased to 65.45%. This was because CaO adsorbed CO_2 from the product stream, thus shifting the reaction so that the methane conversion was increased.

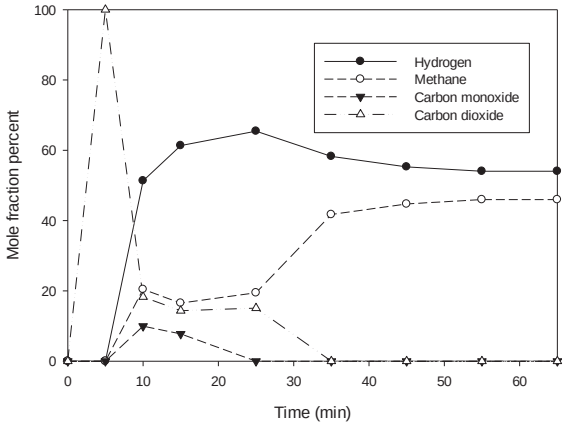

Figure 3. Reduction of 1 g NiO/Al_2O_3 physically mixed with 1 g CaO.

A comparison between NiO/Al_2O_3 and NiO/CeO_2, showed that NiO with ceria support produced greater amount of hydrogen than that from alumina support. Ceria support is famous for its high oxygen storage capacity [11] which can be released to react with methane in addition to oxygen from NiO. According to the experimental result, the chemical looping reforming using NiO/CeO_2 as an oxygen carrier without the use of CaO produced hydrogen at the highest purity of 65.7%, which is even higher than that achieved from the case of NiO/Al_2O_3 physically mixed with CaO.

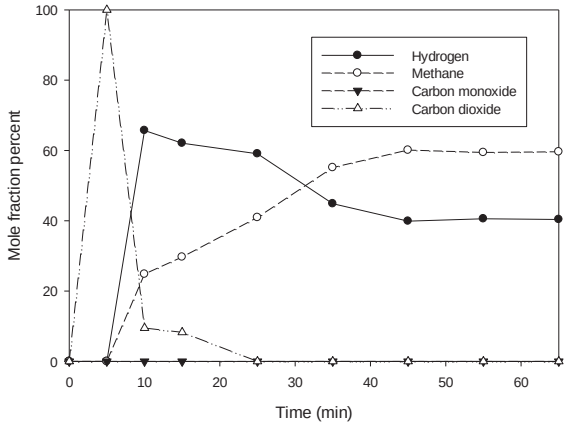

Figure 4. Reduction of 1 g NiO/CeO_2 physically mixed with 1 g SiC.

When CaO was physically mixed in NiO/CeO_2 , the result was shown in Figure 5 indicating similarity with the result from the alumina support. However, in this case, the maximum hydrogen purity was 72.36%.

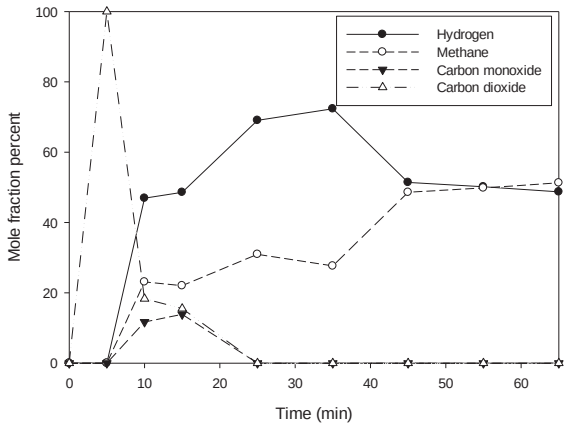

Figure 5. Reduction of 1 g NiO/CeO_2 physically mixed with 1 g CaO.

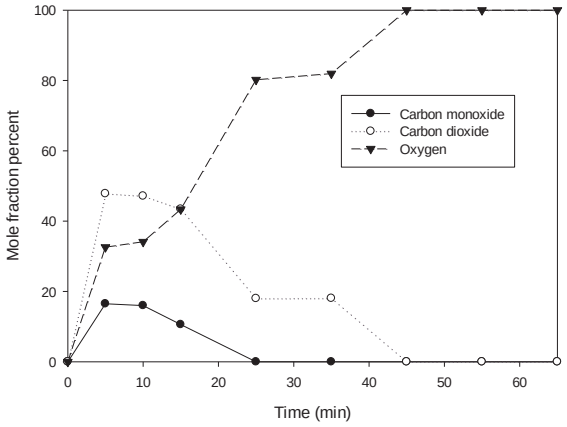

Figure 6. Oxidation of 1 g NiO/Al_2O_3 physically mixed with 1 g SiC.

To complete the chemical looping cycle, the Ni metal was oxidized by air to form NiO. Carbon deposited on metal was also oxidized to carbon monoxide and carbon dioxide (Figs.6-9).

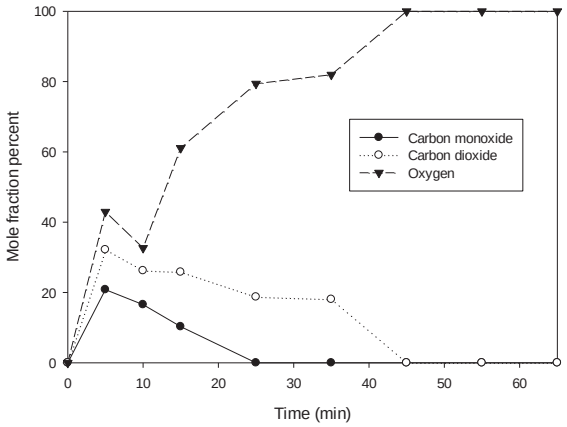

Figure 7. Oxidation of 1 g NiO/Al_2O_3 physically mixed with 1 g CaO.

In cases of NiO/Al_2O_3 and NiO/CeO_2 physically mixed with CaO (Figs.7 and 9), when metals were oxidized by air, the results were similar to those of the ones physically mixed with SiC (Figs.6 and 8) but with less carbon dioxide because CaO adsorbed carbon dioxide, forming $CaCO_3$, therefore, before starting a new loop, the solids must be calcined at a higher temperature to release carbon dioxide.

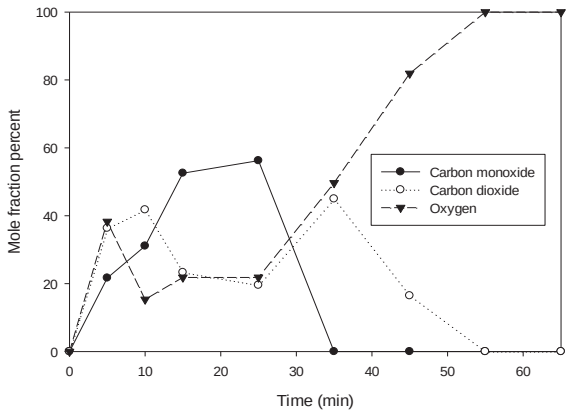

Figure 8. Oxidation of 1 g NiO/CeO_2 physically mixed with 1 g SiC.

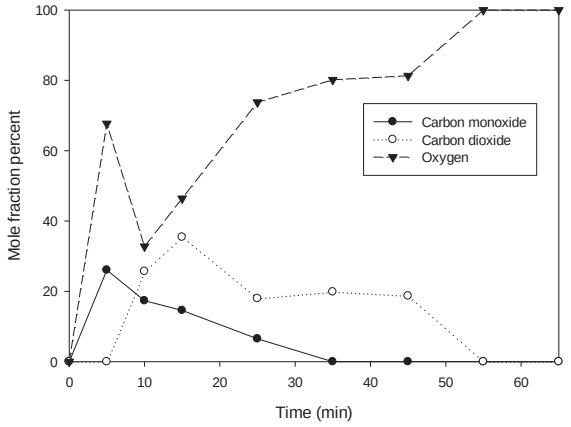

Figure 9. Oxidation of 1 g NiO/CeO_2 physically mixed with 1 g CaO

After oxidation, not all of carbon formed on solid was oxidized. Energy-dispersive X-ray spectroscopy (EDX) was used for analyzing the solid after experiments. The results were shown in Table 1, NiO/CeO_2 after oxidation had carbon less than NiO/Al_2O_3 after oxidation. According to the results, the advantage of ceria support is not only for its high oxygen storage which helps producing more hydrogen but also suppresses carbon formation on the oxygen carriers.

Table 1: Carbon formation on oxygen carrier after the first loop of chemical looping reforming

Oxygen carrier	% Weight carbon
NiO/Al_2O_3	2.83
NiO/CeO_2	1.79

4. Conclusions

Chemical looping reforming using Ni-based oxygen carrier on ceria support can produce greater amount of hydrogen than those on alumina support because the ceria support can release oxygen by itself to react with methane together with oxygen on the metal oxide. Moreover, after a regeneration of Ni by oxidation, NiO/CeO_2 has less carbon than NiO/Al_2O_3 . In addition, to produce higher purity of hydrogen, CaO as CO_2 sorbent is proposed. CaO does not only adsorb CO_2 from the product stream but also enhance the shift reaction, resulting in higher methane conversion and hence the hydrogen purity.

Acknowledgements

The authors would like to thank the support from The Thailand resarch fund (TRF).

References

[1] M. Rydén, A. Lyngfelt, T. Mattisson, De Chen, A. Holmen and E. BjØrgum, *Int. J. Greenh. Gas Con*. **2** (2008) 21-36.

[2] A. Abad, J. Adánez, F. García-Labiano, Luis F. de Diego, P. Gayán and J. Celaya, *Chem. Eng. Sci*. **62** (2007) 533-549.

[3] M. Ni, D.Y.C. Leung and M.K.H. Leung, *Int. J. Hydrogen Energ*. **32** (2007) 3238-3247.

[4] A.L. Alberton, M.M.V.M. Souza and M. Schmal, *Catal. Today*. **123** (2007) 257-264.

[5] D.K. Liguras, D.I. Kondarides and X.E. Verykios, *Appl. Catal. B-Environ*. **43** (2003) 345-354.

[6] S.M. De Lima, A.M. Silva, I.O. da Cruz, G. Jacobs, B.H. Davis and L.V. Mattos, *Catal. Today*. **138** (2008) 162-168.

[7] C. Diagne, H. Idriss, K. Pearson, M.A. Gómez-García and A. Kiennemann, *C. R. Chim*. **7** (2004) 617-622.

[8] A. Iriondo, V.L. Barrio, J.F. Cambra, P.L. Arias, M.B. Guemez, M.C. Sanchez-Sanchez, R.M. Navarro and J.L.G. Fierro, *Int. J. Hydrogen Energ*. **35** (2010) 11622-11633.

[9] S. Chen, D. Wang, Z. Xue, X. Sun and W. Xiang, *Int. J. Hydrogen Energ*. **36** (2011) 4887-4899.

[10]M. Rydén and P. Ramos, *Fuel Process Technol*. **96** (2012) 27–36.

[11] S. Huang, L. Li , O. Van der Biest and J. Vleugels, *Solid State Sci*. **7** (2005) 539–544.

EFFECT OF Au LOADING OVER ACTIVATED CARBON SUPPORT FOR VINYL CHLORIDE MONOMER PRODUCTION VIA ACETYLENE HYDROCHLORINATION

Boonvara Ngamlertkul[1], Wiboon Wittanadecha[1], Navadol Laosiripojana[2], Piyasan Praserthdam[1], Anawat Ketcong[3], Suttichai Assabumrungrat[1,*]

[1] *Center of Excellence in Catalysis and Catalytic Reaction Engineering, Department of Chemical Engineering, Faculty of Engineering, Chulalongkorn University, Bangkok 10330, Thailand*
[2] *The Joint Graduate School of Energy and Environment, King Mongkut's University of Technology Thonburi, Bangkok 10140, Thailand*
[3] *Thai Plastic And Chemicals Public CO., LTD., Maptaput Industrial Estate, Muang District, Rayong 21150, Thailand*

[*] E-Mail: Suttichai.a@chula.ac.th

Abstract: At present, the manufacture of vinyl chloride monomer (VCM) via acetylene hydrochlorination is based on mercuric chloride supported on activated carbon. However, loss of volatile mercury during reaction is harmful to human and environment. For reasons of toxicity, there is current interest to develop non mercury-based catalysts for the reaction, and gold catalyst is a promising candidate for this reaction. This paper studies the effect of gold loading of gold catalyst supported on activated carbon (Au/AC) for acetylene hydrochlorination. The Au/AC catalysts were prepared by impregnation method using $HAuCl_3.xH_2O$ as a precursor and characterized using X-ray diffraction (XRD) analysis. The catalyst test was carried out in a fixed bed reactor. The operating conditions for the experiments of acetylene hydrochlorination were the feed volumetric ratio of acetylene: hydrogen chloride: nitrogen of 1:1.1:1, gas hourly space velocity (GHSV) of 1467 h^{-1}, temperature of 180°C and atmospheric pressure. The results indicated that the Au/AC catalysts with high Au loading (1wt%, 1.5wt% and 2wt%) offered nearly the same acetylene conversion of about 75% after reaction time of 3 hr. For the catalysts with lower Au loading lower than 1wt%, the acetylene conversion below 10% was achieved. The XRD results indicate the presence of the Au^0 peak for the used catalysts with Au loading higher than 1wt%. The addition of an excess of Au probably resulted in poor dispersion of active site. Thus, 1wt% of Au loading is an optimum value of Au loading.

1. Introduction

Nowadays, polyvinyl chloride (PVC) has become the third of most production plastics. PVC is proper for a diversity of applications for instance door frame, pipe clothing and electronic accessories. Production of PVC is anticipated to be more than 40 million tons at 2016 [1]. PVC is produced from vinyl chloride monomer (VCM), which is currently synthesized from two main processes; i.e. 1) acetylene hydrochlorination and 2) oxychlorination of ethane.

In China, acetylene hydrochlorination is an important process to produce VCM owing to abundant and cheaper sources of coal. In acetylene hydrochlorination reaction, acetylene is produced from reaction of calcium oxide and coal to calcium carbide (Eq.1), which further reacts with water to manufacture acetylene and calcium hydroxide (Eq.2). VCM is produced by reacting acetylene with hydrogen chloride (Eq.3).

$$CaO + 3C \longrightarrow CaC_2 + CO \quad (1)$$
$$CaC_2 + 2H_2O \longrightarrow C_2H_2 + Ca(OH)_2 \quad (2)$$
$$C_2H_2 + HCl \longrightarrow C_2H_3Cl \quad (3)$$

For an industrial process, currently a commercial catalyst is mercuric chloride ($HgCl_2$) on activated carbon support. This reaction is carried out in a temperature range of 130-180°C. $HgCl_2$ catalyst has short life time and cannot reuse due to loss of mercuric chloride during reaction [2]. The volatile mercuric chloride is highly toxic and harmful to human and environment. To produce 1 ton of PVC requires 1.02-1.41 kg of catalyst ($HgCl_2$ loading containing from 10 wt% to 15wt%), which occurs 25% mass loss of $HgCl_2$ and cannot be reprocessed into reaction [3]. Therefore, development of green catalyst is a hot topic for PVC industries and alternative metals have been studied from many researchers to replace the mercuric chloride catalyst.

Vapor phase acetylene hydrochlorination has been studied. It was proposed a correlation between catalytic activity of metal chloride on activated carbon support and standard electrode potential ($M^{n+} + ne^- \rightarrow M$), which is a preferred parameter rather than the electron affinity [4]. Because the electron affinity is based on one electron transfer however interaction between acetylene and active site of metal chloride are transferred more than one electron. They described this correlation in two sections. First, at standard electrode potential below -0.7 E^0/V, increase of standard electrode potential shows decrease of catalytic activity. Second, at standard electrode potential higher than -0.7 V, catalytic activity increases with increasing standard electrode potential [4]. Gold (III) chloride having high

standard electrode potential was predicted to give high acetylene conversion to vinyl chloride monomer.

This research attempts to determine an optimum Au loading on activation support and to compare catalytic activity of Au with commercial mercuric chloride on activated carbon support.

2. Materials and Methods

2.1 Materials

$HAuCl_3.xH_2O$ (The content of Au essay 50%), commercial activated carbon (Carbokarn), $HgCl_2$ (Commercial catalyst).

2.2 Catalyst preparation and characterization

The activated carbon support was washed by stirring and dipping in solution of 1M hydrochloric acid for 6 hr at 70°C to eliminate any poison impurities such as Cu, Na and Fe, adjusted pH to 7 by deionized water and then dried at temperature 110°C overnight.The catalyst composing of 0.3-2wt%Au on activated carbon support was prepared by incipient wetness impregnation method using aqua regia as solvent. Then the catalyst after impregnation was dried at a temperature of 110°C overnight.

X-ray diffraction (XRD) was used for characterizing the bulk phase of catalyst by D8 Advance of Bruker AXS. The equipment was carried out with the use of long fine focus ceramic as X-ray source (using Cu K_α source). The pattern shows in range of $20° < 2\theta < 80°$ with an increasing step of 0.04°, wavelength 1.54056 nm and scan speed of 0.5. It should be noted that other techniques such as BET, XPS and TGA were not employed for catalyst characterization as a corrosive gas could be generated during characterization and become harmful to the equipments.

2.3 Reaction test

The acetylene hydrochlorination test was carried out in a fixed bed reactor (i.d. ¼ inch). Hydrogen chloride (99.999%) and acetylene (99.99%) were used as reactants. The schematic diagram of acetylene hydrochlorination is shown in Figure 1.

To perform experiment, the reactor containing 0.4 g catalyst was dried by nitrogen at 120°C for 30 min to eliminate moisture on catalyst. The catalyst was activated using mixed gases of hydrogen chloride and nitrogen at 160°C for 1 hr. After that acetylene was fed into the reactor at an acetylene: hydrogen chloride: nitrogen ratio of 1:1.1:1, reaction temperature of 180°C and reaction time of 3 hr. Then, remaining hydrogen chloride in outlet gases was eliminated by sodium chloride solution and then the gas product was analyzed by GC 2014. The reaction procedure is shown in Figure 2.

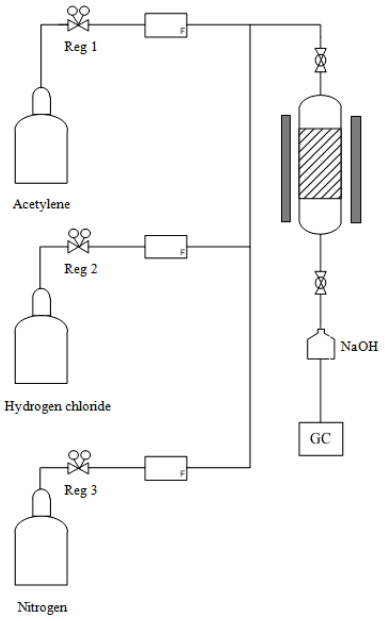

Figure 1. Schematic diagram of acetylene hydrochlorination.

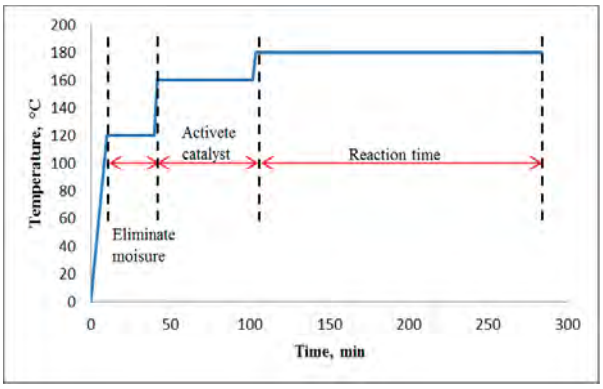

Figure 2. Reaction procedure for acetylene hydrochlorination [5].

3. Results and Discussion

3.1 Catalytic activity

The catalytic activity of catalyst for acetylene hydrochlorination was tested under the following conditions: temperature of 180°C, atmospheric pressure, feed volumetric ratio of acetylene: hydrogen chloride: nitrogen of 1:1.1:1, GHSV of 1456 h^{-1} and catalyst 0.4 g. This condition followed those reported by the previous work [5]. The experimental results are shown in Figure 3. Acetylene conversions with the higher percentage of Au loading (1wt%, 1.5wt% and 2wt%Au) on activated carbon support offer nearly the same acetylene conversion of about 75%. In addition, the lower percentages of Au loading (0.3wt%Au and 0.5wt%Au) showed the low acetylene conversion about 5%. Thus, the optimum percentage of Au loading was 1wt%.

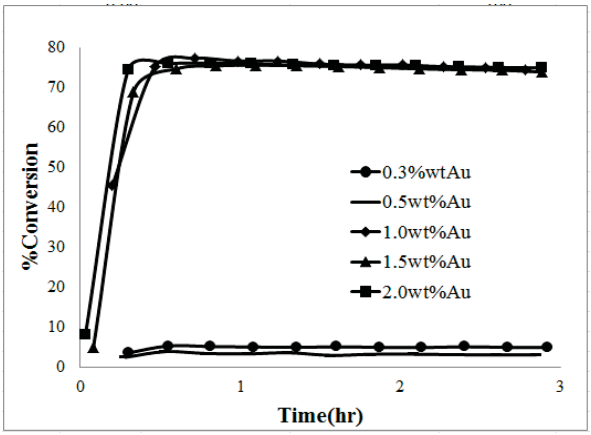

Figure 3. Acetylene conversion of 0.3wt%Au, 0.5wt%Au, 1wt%Au, 1.5wt%Au and 2wt%Au on activated carbon support.

Catalytic activity of Au on activated carbon support was compared with that of commercial catalyst ($HgCl_2$) as shown in Figure 4. The results indicated that the Au catalyst on activated carbon support has higher acetylene conversion than the commercial catalyst ($HgCl_2$). It was in good agreement with the previous work [4] that the catalytic activity of acetylene hydrochlorination was dependent on standard electrode potential. The standard electrode potential of Au^{3+} (1.401 E^0/V) is higher than that of Hg^{2+} (0.851 E^0/V).

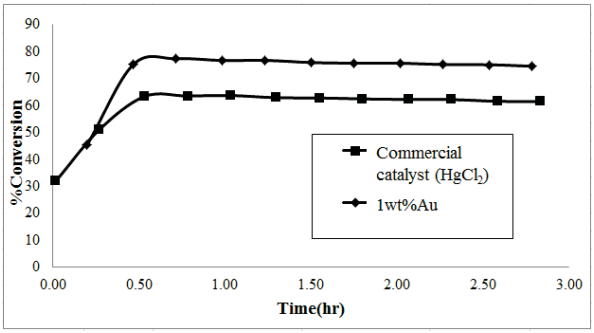

Figure 4. Comparison of catalytic activity of 1wt%Au on activated carbon support and commercial catalyst ($HgCl_2$).

3.2 X-ray diffraction characterization (XRD)

Figure 5 shows the XRD patterns of the fresh and used Au catalysts at different values of Au loading. It was observed that only for the 1.5wt% and 2wt%Au loading, the used catalysts show peaks of Au^0 (peaks at 38.36, 44.56, 64, 83, 77.90 degree (2θ) [6]). It was reported that the active form of Au for this reaction is Au^{3+} [5]. The results indicate that the state of Au was changed from Au^{3+} to Au^0 during the reaction for the high Au loading. This might be a reason for the insignificant improvement of acetylene conversion at Au loading of 1.5 and 2wt%. It should be noted that another possibility may be from the poor Au dispersion at high Au loading. This phenomena has been observed in a number of supported catalysts reported in literatures [7,8].

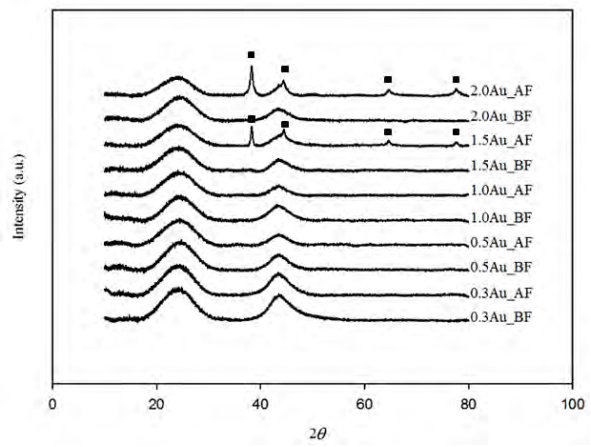

Figure 5. Shows XRD patterns of fresh(BF) and used(AF) Au catalyst (■ ; Au^0).

4. Conclusions

Gold (III) chloride catalyst shows higher catalytic activity than the commercial catalyst ($HgCl_2$) because of the higher standard electrode potential. The optimum of Au loading was 1wt%Au. At the higher percentage of Au loading, the reduction of Au^{3+} to Au^0) was observed.

Acknowledgements

This work was supported by Thai Plastic and Chemicals Public Company Limited (TPC).

References

[1] J. Zhang, N. Liu, W. Li and B. Dai, *Front. Chem. Sci. Eng*. **5** (2011) 514-520.
[2] M. Conte, A.F. Charley, C. Heirene, D.J. Willock, P. Johnson, A. A. Herzing, C.J. Kiely and G.J. Hutchings, *J. Catal.* **250** (2007) 231-139.
[3] K. Zhou, J. Jia, X. Li, X. Pang, C. Li, J. Zhuo, G. Luo and F. Wei, *Fuel Process. Technol.* xxx (2012) xxx-xxx.
[4] G. J. Hutchings, *J. Catal.* **96** (1985) 292-295.
[5] B. Nkosi, N.J. Covillie and G.J. Hutchings, M.D. Adams, J. Friedl and F.E. Wagner, *J. Catal.* **128** (1991) 366-377.
[6] H. Zhang, B. Dai, X. Wang, L. Xu and M. Zhu, *J. Ind. Eng. Chem.* **18** (2012) 49-54.
[7] V. Idakiev, T. Tabakova, Z.-Y Yuan and B.-L. Su, *Appl. Catal., A*. **270** (2004) 135-141.
[8] L. Delannoy, N. E. Hassan, A. Musi, N.N.L To, J.-M. Krafft and C. Louis, *J. Phys. Chem. B.* **110** (2006) 22471-22478.

CATALYTIC ACTIVITIES OF ALKALINE METAL HYDROXIDES ON BIODIESEL PRODUCTION

Manchulee Matchika[1], Kaokanya Sudaprasert[1], Kornkanok Aryusuk[2], Kanit Krisnangkura[2*]

[1] Division of Energy Technology, School of Energy, Environment and Materials, King Mongkut's University of Technology Thonburi, Bangkok, 10140, Thailand
[2] Division of Biochemical Technology, School of Bioresources and Technology, King Mongkut's University of Technology Thonburi (Bangkhuntien Campus), Bangkok, 10150,

[*] E-Mail: kanit.kri@kmutt.ac.th

Abstract: Commercial biodiesels are generally prepared by alkaline catalyzed trans-esterification. The catalytic activities between NaOH and KOH are still in doubt, ie: which catalyst has the greater catalytic activity, KOH or NaOH? In this study, a multi-ports continuous reactor was designed for accurate sampling the reaction products. Four alkaline metal hydroxides (LiOH, NaOH, KOH and CsOH) were investigated for catalytic activities at different temperatures but the molar ratio of methanol to palm oil was fixed at 6:1. Based on molarity of catalyst in methanol (0.125M), the order of catalytic activities are CsOH > KOH > NaOH > LiOH. On the other hand, the order of catalytic activities are LiOH > NaOH > KOH > CsOH, on the weight% of catalyst (0.7 wt%) in methanol.

1. Introduction

Now a day, biodiesel becomes a renewable fuel for diesel engine in Thailand. It can be produced from triglycerides, naturally occurring fats and oils, by trans-esterification with alcohol, usually methanol [1], in the presence of an alkaline catalyst (e.g. sodium hydroxide or potassium hydroxide etc.). Trans-esterifications by using alkaline metal hydroxides are still unclear about catalytic activities. According to Dorado et al.[2], KOH-catalyzed trans-esterification proceeded quicker than NaOH-catalyzed reaction. On the other hand, Vincent et al [3], also reported that NaOH was better than KOH. Also, Ofori-Boateng et al. [4] showed that NaOH performed better than KOH in term of product yield at the same operating conditions. In our previous work [5], both NaOH and KOH were very effective catalysts for trans-esterification. Theoretically, KOH should be more active trans-esterification catalyst than NaOH [6]. The reaction is fast and requires low temperature [4].

Thus, in this study, experiments were designed to clarify the catalytic activities of these two alkaline metal hydroxides on trans-methylation of palm oil. In addition, LiOH and CsOH were included in this study.

2. Materials and Methods

2.1 Materials

Refined palm olein oil was obtained from T S Oil Industry Co., Ltd. (Samutprakan, Thailand). Methanol, lithium hydroxide ($LiOH.H_2O$), sodium hydroxide pellets (NaOH), potassium hydroxide pellets (KOH), cesium hydroxide monohydrate ($CsOH.H_2O$), acetic acid 98% and sodium sulfate anhydrous crystals (Na_2SO_4) respectively were used for the experiment.

2.2 Reaction Conditions

All the experiments were carried out under the same reaction conditions: molar ratio of methanol to palm oil, 6:1; catalysts concentrations, 0.125M or 0.7 wt% (based on methanol); temperatures, 30, 40, 50 °C.

2.3 Methods

Trans-methylation of palm oil was carried out in multi-ports continuous reactor (15.5 m × 0.8 mm ID) with the volumetric flow of o.5 mL/min. as shown in Figure 1. Total flow and percent of methanolic alkaline metal hydroxide (A) and oil (B) (molar ratio of methanol/palm oil) were controlled by the HPLC pump (Shimadzu LC-20 AD). The reactor was immersed in a constant-temperature water bath. Two parameters were varied in this study, temperatures and types of catalysts.

Aliquots were taken (0.5 mL each, by dropping into 1 mL of 0.1M HCl) at 15.5, 10.5, 5.5, 3.5, 1 and 0.5 meters long of a continuous stainless steel reactor. The upper phase was dried over anhydrous $Na_2SO_4$and analyzed by HPLC according to Kittirattanaiboon and Krisnangkura [7].

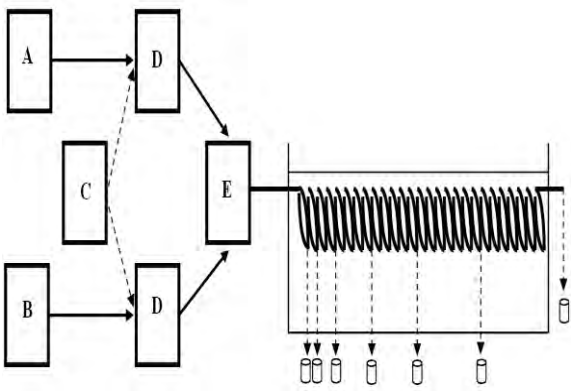

Figure 1. Schematic diagram of the reaction system for trans-methylation. A, reservoir containing methanolic alkaline metal hydroxides; B, reservoir containing palm oil; C, pump controller; D, HPLC pump; E, tee

connector; and F, reactor coil.The manuscript must contain topic and style according to this template.

3. Results and Discussion

3.1 The effect of catalyst concentration

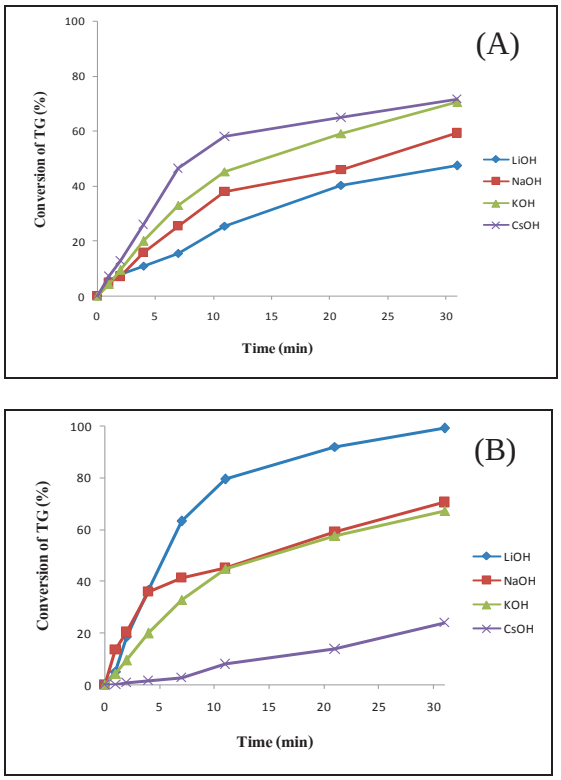

Figure 2. Comparison of trans-methylation of palm oil at 40°C by using different catalysts which based on (A) 0.125 M and (B) 0.7wt%.

The conversion of triglyceride to biodiesel by using LiOH, NaOH, KOH and CsOH as the catalysts are shown in Figure 2. On the same molarity of the catalysts (0.125M in methanol), the order of catalytic activities are CsOH > KOH > NaOH > LiOH. The experimental results agreed well with those of Dorado et al [2], ie. KOH is more active than NaOH for trans-methylation.

On the other hand, when the same weight percent of the catalysts (0.7%) in methanol are compared, the order of catalytic activities are LiOH > NaOH ≅ KOH > CsOH. These results are in good agreement with those reported by Vincent et al [3], Ofori-Boateng [4] and Kaewkool et al [5].

For trans-methylation of triglyceride (TG) with alkaline metal hydroxide, the hydroxide ion reacts with methanol to form methoxide anion, which is the true catalyst for trans-methylation. The methoxide anion then attacks the TG to form biodiesel and glyceryl anion. Methoxide anion is regenerated from the reaction between glyceryl anion and methanol as described below;

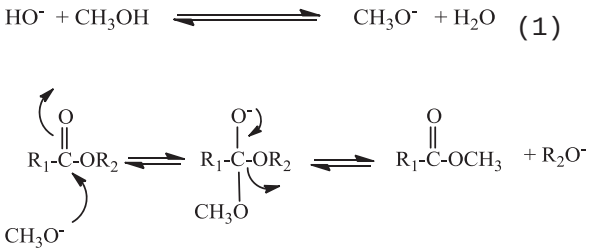

Thus, the amount or concentration of the methoxide anion in the reactor is critical to the rate of trans-methylation and its formation dictates by Eq.1. The higher basicity of the metal hydroxide, the equilibrium of Eq.1 will lie further to the right hand side. Consequently, higher amount of the methoxide anion will be formed from the same concentration of the metal hydroxide and greater catalytic activity is observed.

Results in Fig.2A are in accordance with the basicity of the alkaline metal hydroxide; CsOH is more basic than KOH, NaOH and LiOH, respectively. Therefore, at the same concentration of the hydroxide ion, higher methoxide ion will be formed from the more basicity metal hydroxide.

However, in the trans-methylation of fats and oils to biodiesel, the catalyst concentrations are general prepared on the weight percent. Therefore, comparison of catalytic activities of the alkaline metal hydroxides is difficult to correlate to theoretical basis. At 0.7 weight %, the molarities of LiOH, NaOH, KOH and CsOH are 0.292, 0.175, 0.125 and 0.047, respectively. Results in Fig.2B show that the catalytic activities of NaOH and KOH are approximately the same. Other concentration of catalyst can be used for comparison, if the product can be accurately quantitated.

3.2 The effect of temperature

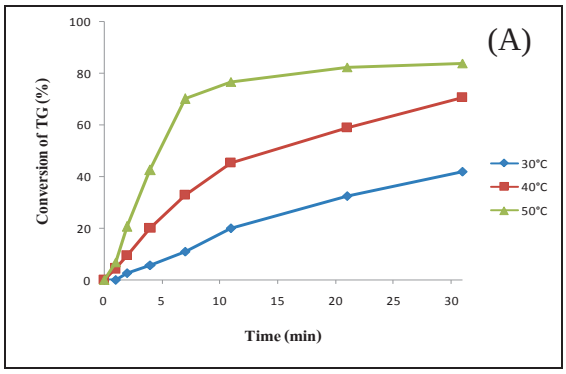

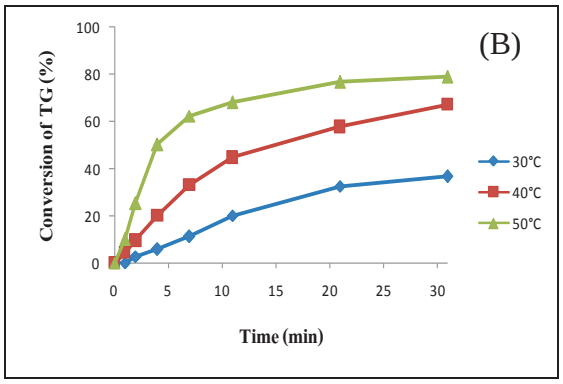

Figure 3. shows that the rate of trans-methylation of palm oil catalyzed by KOH follows the Arrhenius's equation. Temperature tends to accererlate the rate of trans-methylation.

The effect of temperature on palm oil trans-methylation was studied at a catalyst (KOH) concentration of 0.125 M (Fig.3A) and 0.7 wt% (Fig.3B) and a methanol/oil molar ratio of 6:1. The temperatures studied were 30, 40 and 50° C. As expected, increases in temperature would accelerate the reaction.

4. Conclusions

This study suggests that the base-catalyzed trans-methylation of palm oil depends on the basicity of the alkaline metal hydroxide used as the catalyst. Among the four catalysts (CsOH, KOH, NaOH and LiOH) CsOH is the most effective catalyst at the same molarity, while LiOH is the best catalyst at the same weight%.

Acknowledgements

This work was supported by Energy Policy and Planning Office.

References

[1] Muniyappa, P.R., Brammer, S.C, Berg, R.H., Noureddini, H. Biores. Technol. 1996;56:19-24.
[2] Dorado, M.P., Ballesteros, E., Mittelbach, M. and Lopez, F.J., Energy and Fuels 2004; 18, 1457-1462.
[3] Vicente, G., Martinez, M. and Aracil, J., Biores. Technol. 2004;92:297-305.
[4] Ofori-Boateng, C., Kwofie, E.M. and Mensah, M.Y. World App. Sci. J. 2012;16:1445-1449.
[5] Kaewkool, P., Kittiratanapiboon, K., Aryusuk, K. and Krisnangkura, K., Euro. J. Lipid Sci. Technol. 2009; 111, 474 - 480.
[6] Gryglewicz, S., Biores. Technol. 1999;70:249-253.
[7] Kittirattanaoiboon, K., and Krisnangkura, K. Eur. J. Lipid Sci. Technol. 2008; 110: 422–427.

BIO-OIL FROM PYROLYSIS OF JATROPHA STEM AND SOYBEAN CAKE

Supissara Suwapiromchote[1], Pongsakorn Vichayasiri[1], Pipat Pichestapong[2], Uthaiwan Injareon[2]
Boonnak Sukhummek[1*]

[1] Department of Chemistry / Faculty of Science, King Mongkut's University of Technology Thonburi, Bangkok, Thailand
[2]Research and Development Division, Thailand Institute of Nuclear Technology, Chatuchak, Bangkok, Thailand

[*] Author for correspondence; E-Mail: boonnak.suk@kmutt.ac.th, Tel. +66 24 709557, Fax. +66 24 708843

Abstract: This work aimed to investigate the effects of temperature, particle size and ratio of jatropha stem and soybean cake on bio-oil produced by means of conventional pyrolysis. The biomass sample was pyrolysed in a batch reactor at 400, 450 and 500 °C with N_2 as carrier gas at a flow rate of 0.25 L/min for 60 min reaction time. The maximum yield of bio-oil from the soybean cake (20.9 wt%) and jatropha stem (23.4 wt%, in pyrolysis liquid) were obtained at 450 °C. Copyrolysis of soybean cake and jatropha stem showed the bio-oil yield increased with the increasing of soybean cake ratio. Effect of gamma irradiation on soybean cake was also studied. At 200 kGy of gamma radiation dose, the bio-oil yield obtained from the pyrolysis at 450 °C was found to increase up to 20%. The bio-oil characteristic was characterized by Fourier Transform Infra-red (FT-IR) spectroscopy and gas chromatography/mass spectrometry (GC-MS) techniques.

1. Introduction

Fossil fuel, the primary energy resource of the world, is presently limited, while the energy demand is growing steadily every year. It is one of the main causes of global warming due to an increase in the amount of carbon dioxide resulting from the burning of fossil fuels. Therefore, it is necessary to invest in new energy resources which do not cause any damage to the environment. Energy from biomass is a renewable energy and has received a high attention as a kind of alternative energy resources. Due to burning of biomass fuels does not cause an increase in carbon dioxide gas since the increment of carbon dioxide gas produced is used in the growth cycle of the biomass plant itself. Besides, Thailand is an agricultural country so there has a lot of agricultural waste such as rice husk, bagasse, straw, corn cob and palm tree debris. All these matters can be used to produce biomass energy.

Oils from biomass is known as pyrolysis oil, pyrolysis liquid, bio-crude-oil and bio-fuel oil [1-2]. It is usually dark brown color with an acrid smell [2-4]. The bio-oil normally composes of some organic compounds such as acids, esters, alcohols, ketones, aldehydes, phenols and nitrogen compounds [5-8]. Pyrolysis process is made by thermal decomposition in an absence of oxygen at a high temperature range of 500-800 °C of biomass to convert it into gas, liquid and solid. Pyrolysis has two main types. The first one is conventional pyrolysis or slow pyrolysis to pyrolyse by a heat rate of less than 10 °C/s and a temperature less than 500 °C with a main product of tar and charcoal [9]. The second one is flash pyrolysis or fast pyrolysis to pyrolyse by a heating rate in the range of 10-10,000 °C/s with a temperature range of 400-1,000 °C, consequently produces main products of gases and liquid [10].

This work attempted to investigate the effects of temperature, particle size and ratio of jatropha stem and soybean cake on bio-oil produced by means of conventional pyrolysis. To increase bio-oil yield, copyrolysis of jatropha stem and soybean cake at various ratios was examined. The bio-oil characteristic was characterized by Fourier Transform Infra-red (FT-IR) spectroscopy, gas chromatography/mass spectrometry (GC-MS) techniques and heating value was involved. Moreover, bio-oil produced from the soybean cake exposed to gamma irradiation was also investigated.

2. Materials and Methods

2.1 Materials

Jatropha stem were dried under the Sun. It was ground and graded based on sizes e.g. smaller than 0.5, 0.5-1.0, 1.0-2.0 and larger than 2.0 mm, whereas soybean cake was completely dried in an oven, ground and screened with two sizes of smaller than 2.0 and larger than 2.0 mm. After that both jatropha stem and soybean samples were analysed to receive their proximate and ultimate properties. The proximate analysis including contents of moisture, ash, fixed carbon and volatile matter were analysed by Parr equipments (WI-EEE-EY-01 for moisture analysis, WI-EEE-EY-01-03 and WI-EEE-EY-01-05 for ash analysis, carbolite/VMF 10/15 for volatile analysis). The ultimate analysis was used to examine the content of elements; carbon, hydrogen, oxygen and sulfur by Parr equipments (TruSpec S for sulphate analysis, TruSpec CHN for CHN analysis). The results of the proximate and ultimate analysis of jatropha stem and soybean cake received were shown in Tables 1 and 2, respectively.

2.2 Bio-oil production

The pyrolysis experiment was firstly performed by charging 100.0 g of samples, jatropha stem or soybean cake, into a stainless tube reactor with 5 cm in diameter and 50 cm in length. Five condensers with a length of 12 inches and 0.5 inches in diameter were equipped to the tube reactor. Jatropha stem and

soybean sample with the particle size of 1.0-2.0 mm and larger than 2.0 mm were selected, respectively. The reactor was heated by a furnace at a fixed temperature with a nitrogen flow rate of 0.25 L/min for 60 min. The temperature was controlled by using a thermocouple. Cooled water kept constant at 20 °C was circulated inside the condenser to condense some gases. At the end of each experiment, the liquid product collected and solid char inside the reactor removed were weighed. Gas product was calculated by material balance and pH of liquid part produced was examined.

Table 1: Proximate and ultimate analysis of jatropha stem.

Proximate Analysis	
Parameter	**Value (wt%)**
Moisture	9.13
Volatile matter	73.45
Fixed carbon	14.62
Ash	2.80
Ultimate Analysis	
Parameter	**Value (wt%)**
Hydrogen	7.91
Carbon	52.29
Nitrogen	5.07
Oxygen	31.70
Sulfur	0.23

Table 2: Proximate and ultimate analysis of soybean cake.

Proximate Analysis	
Parameter	**Value (wt%)**
Moisture	9.63
Volatile matter	64.37
Fixed carbon	20.60
Ash	5.40
Ultimate Analysis	
Parameter	**Value (wt%)**
Hydrogen	6.35
Carbon	45.75
Nitrogen	0.23
Oxygen	42.24
Sulfur	0.02

Effect of reaction temperature: Jatropha stem with a particle size range of 1.0-2.0 mm and soybean cake with a particle size range of more than 2.0 mm were used in pyrolysis process. The experiment was carried out by maintaining the temperatures at 400, 450 and 500 °C. The pyrolysis was then processed as mentioned above.

Effect of jatropha stem and soybean cake ratio: To increase the amount of bio-oil produced, copyrolysis was carried out by mixing jatropha stem with the particle size of 1.0-2.0 mm. and soybean cake with the particle size of more than 2.0 mm. before loading the sample into the tube reactor. The pyrolysis process was then processed as mentioned above.

Effect of gamma irradiation: The soybean cake with the particle size of smaller than 2.0 mm was exposed to gamma irradiation of 100 and 200 kGy. After that, the treated soybean particle was processed by the pyrolysis process.

The chemical compositions of the bio-oils produced were determined by FT-IR spectroscopy and GC-MS analysis. HP-5 capillary GC column with a length of 30 m, ID 0.25 mm and film thickness of 0.25 μm was used. The heating value of the bio-oil was also examined by using Parr equipments.

3. Results and Discussion

3.1 Bio-oil synthesis from jatropha stem and soybean cake

Effect of particle size: The effect of particle size on bio-oil yield for jatropha stem and soybean cake pylolysed at 400 °C was shown in Figures 1 and 2.

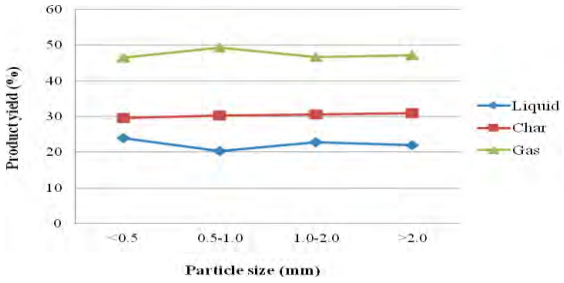

Figure 1. Effect of various particle sizes of jatropha stem on bio-oil yield produced at 400 °C.

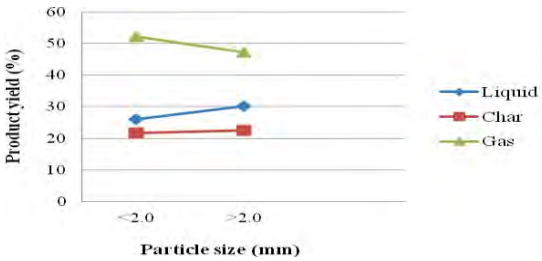

Figure 2. Effect of various particle sizes of soybean cake on bio-oil yield produced at 400 °C.

The results indicated that as the particle size increased the liquid yield production was slightly increased for jatropha stem and a significant increase for soybean cake was observed. This might be caused the heat and mass transfer was restricted at a larger particle size, consequently, a higher liquid yield was produced. The char parts of each sample revealed the same trend. Increasing the particle size used in pyrolysis process, they revealed an increment of char

content. However, pyrolysis of jatropha stem performed only one liquid part which mixed oil and water phase together. Liquid parts received from jatropha stem were acidic with pH values of 3.0-3.7, while those obtained from soybean cake was slightly basic with pH values of 7.0-7.5 (data were not shown here).

Effect of reaction temperature: The effect of temperatures on the product yields obtained from jatropha stem and soybean cake revealed the same trend as seen in Figures 3 and 4. Increasing the temperature of the pyrolysis process, the bio-oil content was increased. The maximum yield content was found at 450 °C. They were 23 wt% and 37 wt% for jatropha stem and soybean cake, respectively. The reason why at 400 and 500 °C produced less bio-oil content, this might be caused the organic compounds in the samples was not completely pyrolysed at 400 °C. In the case of at 500 °C, the heat might be too high, consequently cracking of volatile liquids was initiated, resulting in an increase gas phase while a reduction in the liquid phase.

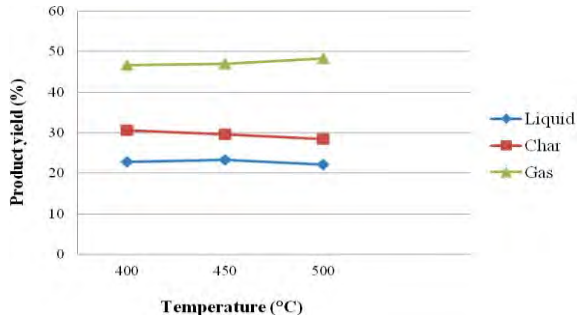

Figure 3. Effect of reaction temperatures on bio-oil yield produced from jatropha stem.

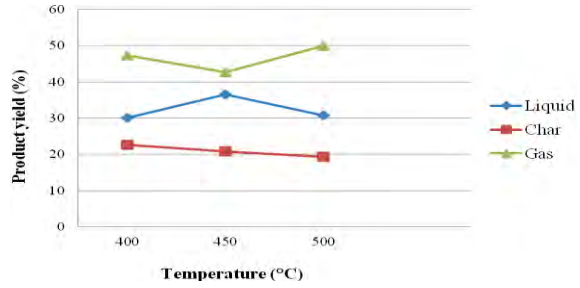

Figure 4. Effect of reaction temperatures on bio-oil yield produced from soybean cake.

Effect of jatropha stem and soybean cake ratio: Figure 5 shows the effect of the weight ratio between jatropha stem and soybean cake on bio-oil yield. The amount of bio-oil increased as increasing the soybean cake content. The maximum content of 32 wt% bio-oil was revealed at the ratio of 50:50.

Effect of gamma irradiation: Figure 6 shows the effect of gamma irradiation dose on bio-oil produced from soybean cake. The result showed that at 200 kGy, the maximum bio-oil produced was 18.89 wt%, which was found to increase up to 20% as compared to that of conventional one. This might be caused the irradiation could convert some big organic molecules to be smaller ones, consequently the cracking process initiated easily and bio-oil production was increased.

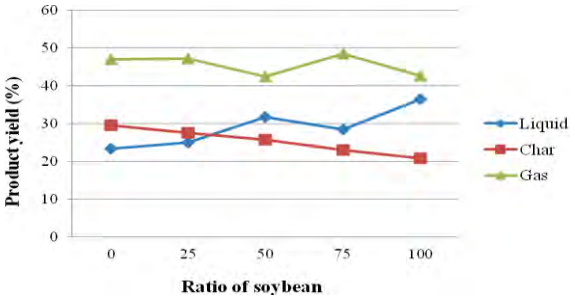

Figure 5. Effect of ratios between soybean cake and jatropha stem on bio-oil product.

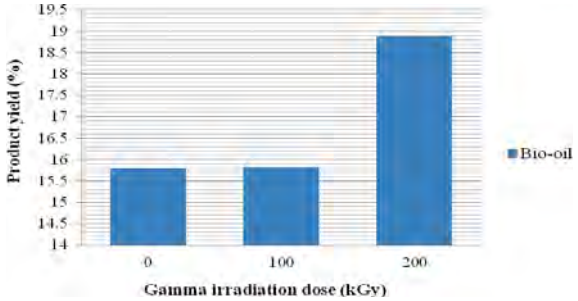

Figure 6. Effect of gamma irradiation on bio-oil product.

3.2 Chemical characterization of bio-oil

The FT-IR spectra, representing chemical functional groups, of all types of bio-oil produced were the same feature as shown in Figure 7. The C-O stretching vibration at 1700 cm^{-1} indicated the presence of aldehyde group. The C-H stretching vibration at 2900 cm^{-1} indicated the presence of alkanes and the absorption peaks between 690-900 cm^{-1} and 1350-1450 cm^{-1} were compatible with the presence of mono and polycyclic and substituted aromatic groups. The O-H stretching vibrations between 3200-3400 cm^{-1} indicated the presence of phenols and alcohols. The FT-IR spectra of bio-oil derived from palm shell also revealed very much similar to the FT-IR spectra characterized from the bio-oil received in this study [11].

Mass spectrum of GC-MS analysis of the bio-oil obtained from soybean cake pyrolysed at 450 °C was shown in Figure 8. The main component fragments identified were carbonyl, carboxyl and phenolic. The main components of the bio-oils from jatropha stem and the mixture of jatropha stem and soybean cake in this study exhibited many similar components with those in Table 3. The presence of the oxygenated compounds generally responded to a low heating value of bio-oil product. In this study, the heating value of bio-oil produced from copyrolysis of jatropha stem and soybean cake at the ratio of 50:50 exhibited the

highest value of 8,530 kcal/kg as seen in Table 4. However, this bio-oil is less efficient to be used as a fuel. It is needed to upgrade further to increase its heating value before being used. Generally, the heating value of the fuel is 10,881 kcal/kg [11].

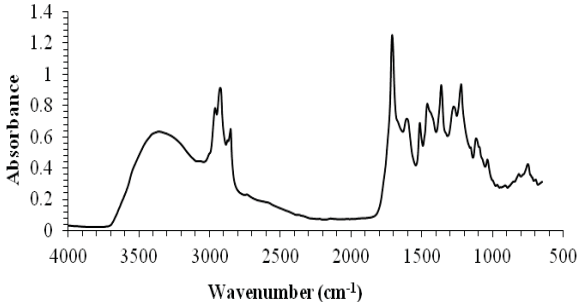

Figure 7. FT-IR spectra of bio-oil produced from soybean cake.

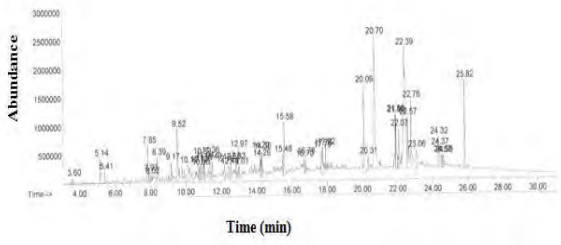

Figure 8. Mass spectrum of GC-MS analysis of the bio-oil obtained from soybean cake pyrolysed at 450 °C.

Table 3: Chemical components in bio-oil produced from soybean cake analysed by GC-MS analysis.

Chemical component	Peak area (%)
Acid	38.039
Phenol	10.201
Nitrile	7.432
Ketone	2.641
Alkene	10.652
Amide	8.111
Others	22.942

Table 4: Heating values of various matters.

Sample	Heating value (kcal/kg)
Soybean cake (2 mm)	5,100
Jatropha stem (1-2 mm)	4,020
Char of soybean cake*	6,440
Char of jatropha stem*	5,470
Bio-oil from soybean cake*	7,890
Bio-oil from mixed samples*	8,530

Remark * Pyrolysed at 450 °C

4. Conclusions

In this work, biomass samples were pyrolysed in a batch reactor under a nitrogen atmosphere. The maximum yield of bio-oil obtained from both soybean cake and jatropha stem was found at 450 °C. Pyrolysis of jatropha stem and soybean cake produced the maximum bio-oil content of 20.9 wt% and 23.4 wt%, respectively. Copyrolysis of soybean cake and jatropha stem at the ratio of 50:50 produced the highest content of bio-oil of 32%. Increasing gamma irradiation dose revealed an increase in bio-oil content. At 200 kGy, the bio-oil content was increased up to 20% as compared to that of the conventional one. The main chemical components of the bio-oil characterized by GC-MS were phenol, carboxylic acid, aldehyde. Since low heating value, the bio-oil produced was needed to be upgraded for using as fuel.

References

[1] A.V. Bridgwater, *Therm. Sci.* **8** (2004) 21–49.
[2] S. Czernik and A.V. Bridgwater, *Energ. Fuel* **18** (2004) 590–598.
[3] N. Ozbay, E. Apaydln-Varol, B. Burcu Uzun and A. Eren Putun, *Energy* **33** (2008) 1233–1240.
[4] M.R. Islam, M.S.H.K Tushar and H. Haniu, *J. Anal. Appl. Pyrol.* **82** (2008) 96–109.
[5] W.N. Peng and Q.Y. Wu, *New Energy Sour.* **22** (2000) 39-44.
[6] M. Garcia-Perez, A. Chaale, H. Pakdel, D. Hretscgner and C. Roy, *J. Anal. Appl. Pyrol.*. **78** (2007) 104–116.
[7] H.B. Goyal, D. Seal and R.C. Saxena, *Renew Sust. Energy Rev.* **12** (2008) 504–517.
[8] A. Aho, N. Kumar, K. Eranen, T. Salmi, M. Hupa and D.Y. Murzin, *Fuel* **87** (2008) 2493–2501.
[9] Asadullah, M., M.A. Rahman, M.M. Ali, M.S. Rahman, M.A. Motin, M.B. Sultan and M.R. Alam, *Fuel* **86** (2007) 2514-2520.
[10] Horne, P.A. and P.T. Williams, *Fuel* **75** (1996) 1051-1059.
[11] Heating value [online], available, http://www.ngvshop.com/board/index.php?topic=6.0 [2012, October 16].

PATIAL OXIDATION FOR HYDROGEN PRODUCTION OVER CuO/TiO_2 CATALYST IN ETHANOL SOLUTION

Kukkong Pornsatitpong[1], Sangobtip Pongstabodee[1, 2]

[1] Department of Chemical Technology, Faculty of Science, Chulalongkorn University, Bangkok 10330, Thailand
[2] Center for Petroleum, Petrochemicals, and Advance Materials, Chulalongkorn University, Bangkok 10330, Thailand

[*] Author for correspondence; E-Mail: sangobthip.p@chula.ac.th,

To study hydrogen production performance by photo catalytic oxidation in ethanol solution, copper (Cu) doped TiO_2 was used as catalysts. The photo catalysts were prepared by wet impregnation method. The photo catalysts were characterized by means of X-ray diffraction, UV-vis diffuse reflectance, X-ray fluorescence. The glass cylinder reactor was placed in a water bath to control the reactor temperature at 313 K. The effects of loading of Cu, pH of solution, concentration of ethanol on the catalytic activities were investigated. Additional, influences of intensity of UV light and visible light were considered. The experimental results showed that hydrogen production performance of the photo catalysts increased with loading of Cu and ethanol concentration from 0% to 3% and 0% to 30%, respectively. The maximum hydrogen production was obtained when using 10% loading of Cu on TiO_2 at pH = 7 under 33 W UV light of irradiation.

1. Introduction

Hydrogen, which has potential as a clean fuel, can be extracted from water, biomass, natural gas and other carbonaceous [1]. Currently, approximately 95% of hydrogen needs are sourced from the steam reforming of natural gas. However, these processes consume fossil fuel and can be representative as greenhouse gas production. Photocatalytic production of hydrogen using sunlight as the energy input is a valuable sustainable-energy technology. In this case, solar energy is stored by driving chemical reactions [2].

Titanium dioxide (TiO_2) is considered as a good photocatalyst for hydrogen generation because of its excellent resistance to chemical and photochemical corrosion in aggressive aqueous environments and due to its activity towards both light and aqueous solutions such as water and methanol. Noble metal loading onto TiO_2 has been widely investigated for hydrogen generation, and has been presented to be very effective to enhance TiO_2 photocatalytic activity because it can contribute to efficient electron hole separation [3].

The present work deals mainly with the photocatalytic hydrogen production from aqueous ethanol solution with CuO/TiO_2. Furthermore, the photocatalytic activities of NiO/TiO_2, La_2O_3/TiO_2, Ag_2OTiO_2 and Pt/TiO_2 nanocomposites were evaluated for the comparison

2. Materials and Methods

2.1 Catalyst preparation

The TiO_2 photocatalysts was synthesized by hydrolysis and calcination method. Titanium isopropoxide ($Ti(OCH(CH_3)_2)_4$) was added into propanol for hydrolysis . Subsequently, the solution was dispersed into 500 mL of deionized water. After agitation of 400 RPM for 24 hr, the suspension was filtrated and dried in air for 4 h at 623 K.

CuO/TiO_2 photocatalyst was prepared by the impregnation method. The TiO_2 powder was added into copper nitrate solution with minimum deionised water, followed by ultrasonic process and thorough mixing on a magnetic stirrer to get homogeneous slurry. After wet impregnation, the sample was dried at 378 K overnight and finally calcined in air for 4 h at 623 K. The NiO/TiO_2, La_2O_3/TiO_2 was also prepared by impregnation method with nickel nitrate solution and lanthanum chloride solution as precursor, respectively. Ag_2O/TiO_2 and Pt/TiO_2 was also prepared by impregnation method with silver nitrate and platinum chloride solution as precursor, respectively. The condition was same as CuO/TiO_2 with 10% loaded of metal.

2.2 Photocatalytic production

The photocatalytic reactions for hydrogen production were carried out by using Pyrex glass cylinder reactor. During a typical run, the entire reactor was enclosed inside a UV-light lamp. the reactor was filled with an ethanol solution in various quantity, in which prepared catalyst were constantly dispersed by a magnetic stirrer for 370 rpm. The temperature was constantly maintained at 313 K by circulated water bath . The irradiation time was 4 h. Hydrogen concentration was measured intermittently by extracting a small volume of the gas-phase product for gas chromatography analysis. The accumulative hydrogen production data were then calculated from the concentration data, assuming ideal-gas behaviour

2.3 Characterization of catalyst

The catalyst were characterised by X-ray diffraction (XRD) to determine the crystalline phase and grain size of the TiO_2 powders. The surface areas of nanocomposite photocatalysts were determined by the three-point BET method with di-nitrogen at 77 K. UV visible spectrophotometer was used to determine

UV-vis diffuse reflectance and amount of produced hydrogen from photocatalytic reaction was detemined by TCD-type gas chromatography with Polapack Q column using nitrogen as carrier gas.

3. Results and Discussion

3.1 Photocatalytic H_2-production activity

3.1.1 Effect of metal content on hydrogen production activity

Fig.1 shows time courses of hydrogen production over metal doped content over TiO_2 photocatalysts with variation of metal content type from 10%vol ethanol/water. As can be seen from this figure, the CuO content has a significant influence on the photocatalytic activity of TiO_2. With CuO content in TiO_2 photocatalyst, reaction gives amount of hydrogen production to 73.7 μmol. In contrast, non-doped TiO_2 gives lowest hydrogen production to 28.7 μmol.

TiO_2 alone barely generated hydrogen in reaction, which suggests that the co-catalylst of TiO_2 and CuO is necessary for high catalytic activity. Since the conduction band of CuO is lower than that of TiO_2, the excited electrons in the conduction band of TiO_2 could easily transfer to the conduction band of CuO[4]. This phenomenon prevents electron combination of electron/hole pairs which cause low activity in TiO_2 due to its low band gap energy. In other noble metal, excessive metal loading will result in the growth and agglomeration of nanoparticles on the semiconductor surface. This would absorb and scatter the ultraviolet irradiation.

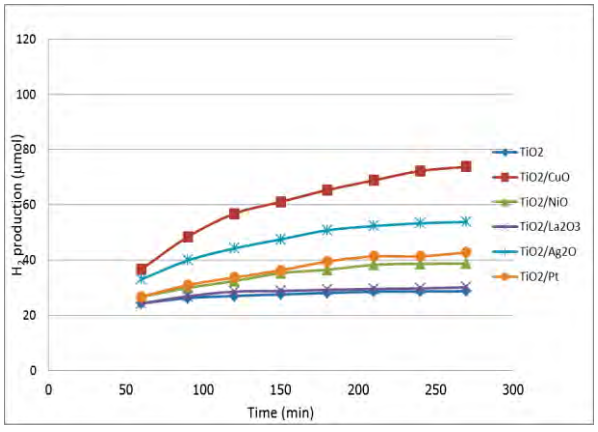

Fig.1 Effect of type of catalyst on H_2 production

3.1.2 Effect of Cu content on hydrogen generation activity

Fig.2 shows time courses of hydrogen evolution over CuO-TiO_2 photocatalysts with variation of Cu content from 10%vol ethanol/water. According to Fig.2, 10% of Cu contained catalyst has more activity than 5% of Cu contained catalyst. Above that, the hydrogen generation rate is declined to zero (pure CuO). Reason for the drop of activity at a higher content of copper was the light sensitization of TiO_2 was blocked by the surrounding CuO, which led to a lower density of excited electron accumulation in the Conduction band of CuO, and thus weakened the photocatalytic hydrogen production[1-2].

Furthermore, CuO distinguished to semiconductor as same as TiO_2 cannot be used in photocatalytic activity. Because of small band gap energy of CuO compared with TiO_2. Ultraviolet light source which has wave length between 350 to 400 nm has unsuitable energy to excite the electron from valence band to conduction band. For result, photocatalytic oxidation cannot be occurred [1, 3-4].

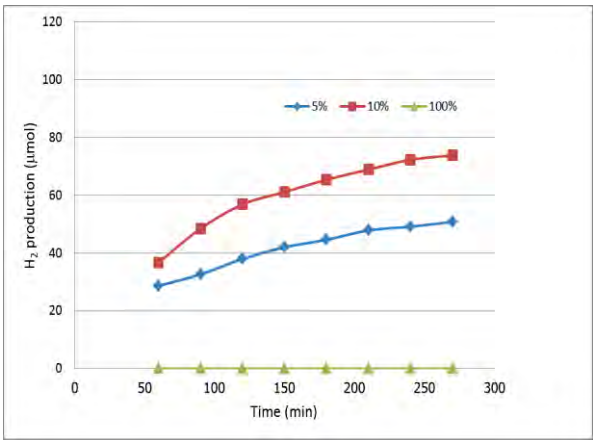

Fig.2 Effect of Cu loading on H_2 production

3.1.3 Effect of ethanol concentration on hydrogen production

Fig.3 shows time courses of hydrogen production over 10 mol% CuO/TiO_2 from aqueous solutions which contain various volume percentages of ethanol. Increasing the ethanol concentration promote hydrogen production to 84 μmol with 30%vol ethanol solution. Compared with pure water, hydrogen production is slightly increased to 20.1 μmol. From the outcome, ethanol can induce a substantial hydrogen evolution rate, which resulted from ethanol behaving as a sacrificial electron donor and preventing electron–hole recombination [5].

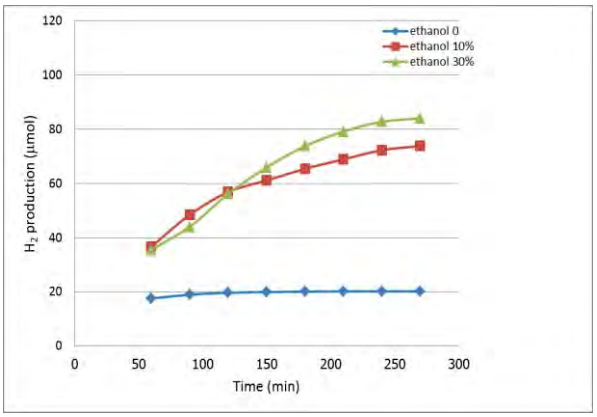

Fig.3 Effect of concentration of ethanol on H_2 production

3.1.3 Effect of initial pH of ethanol solution produced H_2 production

Fig. 4 shows time courses of hydrogen production over CuO-TiO_2 photocatalysts with initial pH of ethanol solution. The result shows that when the pH values are varied from 5 to 9. The photocatalytic activity reaches a maximum at about pH 5. With acidity, positive ion in solution acts as electron donor which can prevent electron recombination. On the other hand, Negative ion in solution causes blocking area between surface active sites and ethanol due to similar polarity [6].

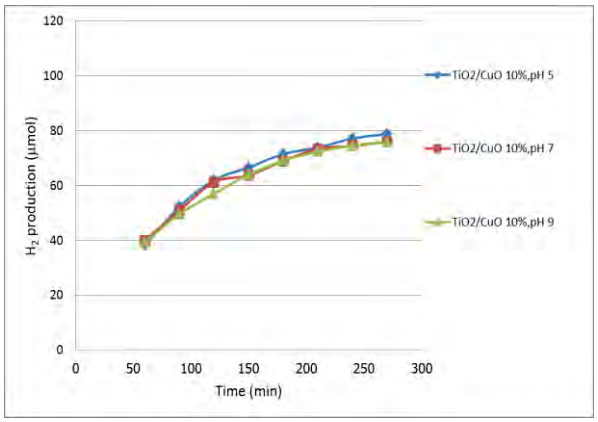

Fig.3 Effect of initial pH of ethanol solution on H_2 production

3.1.4 Effect of regeneration of catalyst

To study the stability of hydrogen generation over the CuO-TiO_2 photocatalyst, the used photocatalyst was brought out to calcination process in air for 4 h at 623 K and applied to reaction for 2 sessions. From the results of Fig. 4, the hydrogen production has decreased progressively with first and second cycle of regeneration, respectively. The reason for the decline of the hydrogen generation could be copper leaching from the photocatalyst[7]. Copper ion in solution weakened the ability to accept excited electrons from TiO_2, causing deactivation of hydrogen generation.

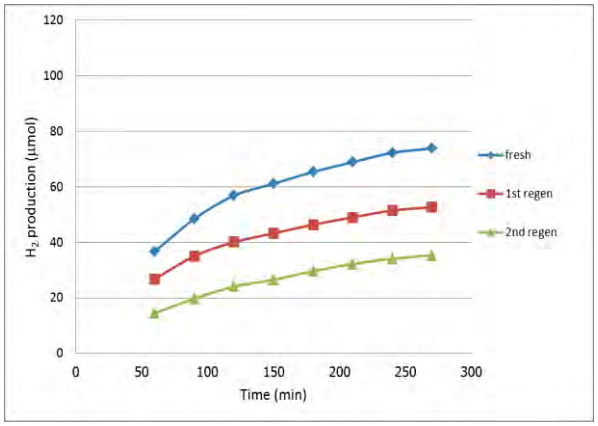

Fig.4 Effect of regeneration of catalyst on H_2 production

3.2 Catalyst characterization

3.2.1 XRD results

Fig.5 and Fig.6 show the XRD patterns for pure TiO_2 and 5% CuO/TiO_2 photocatalyst, respectively. As can be seen from this figure only anatase and bruklie phases of TiO_2 were observed in pure TiO_2 and 5% CuO/TiO_2. No characteristic peak of metallic copper or copper oxide was detected. This result indicate that photocatalyst synthesized by incipient wetness impregnation method, was highly dispersed Cu ion into TiO_2 crystalization[8].

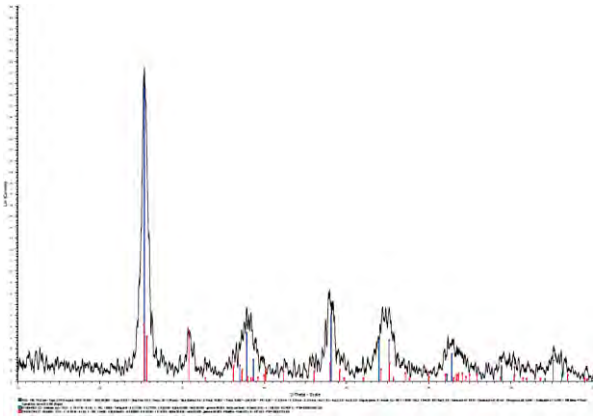

Fig.5 XRD pattern of pure TiO_2

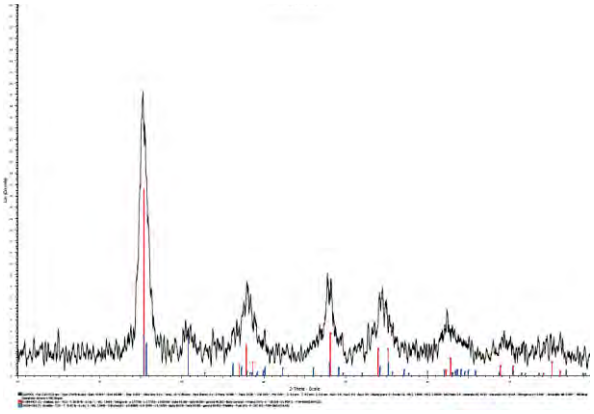

Fig.6 XRD pattern of 10% CuO/TiO_2

3.2.2 X-ray fluorescence results

To confirm the existence of CuO loading in TiO_2 photocatalyst, x-ray fluorescence was led to define each element. Table 1 shows that amount of Cu from XRF result is approximate to Cu from preparing in experimental which is 10 to 12 and 5 to 3.5 mol, respectively since wet impregnation method is effective to conserve particle and precursor solution from catalyst preparation.

Table 1: XRF results of CuO/TiO_2

Catalyst	***%mole***	
	TiO_2	Cu
5% of CuO/TiO_2	96.5	3.5
10% of CuO/TiO_2	88.0	12.0

3.2.2 BET results

From table 2, the result shows that CuO/TiO_2 has surface area more than pure TiO_2 since CuO particle penetrates into TiO_2. Despite of CuO accumulation, it seems that both inner and outer surfaces of TiO_2 were occupied by copper species which led to smaller pore size in CuO/TiO_2

Table 2: BET results of TiO_2 and CuO/TiO_2

Catalyst	*Surface Area (m^2/g)*	Pore size (Å)
TiO_2	104.96	92.2611
CuO/TiO_2	130.43	73.3828

3.2.3 UV-vis diffuse reflectance results

Fig. 7 shows the UV–vis diffuse absorbance spectra of the CuO/TiO_2 and TiO_2 catalyst. CuO/TiO_2 increases the absorption at wavelengths longer than 400 nm. According to the result, CuO/TiO_2 catalyst shows an enhanced absorption in the visible-light region

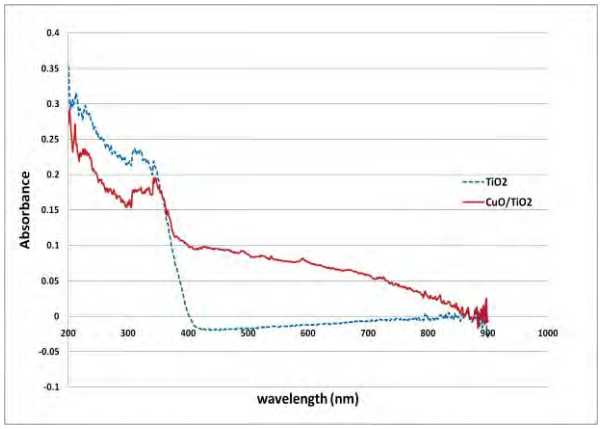

Fig.7 UV-vis diffuse reflectance CuO/TiO_2 and TiO UV-vis diffuse reflectance

4. Conclusions

$CuO\text{-}TiO_2$ with 10%mol of CuO prepared by the impregnation method can enhance the photocatalytic H_2-production activity in ethanol solution. Photocatalytic hydrogen evolution can take place efficiently on higher concentration of ethanol solution with higher concentration of ethanol solution. According to UV-vis diffuse reflectance result, Cu-doped-TiO_2 showed greater response to UV-visible light region than non-doped-TiO_2 due to lower band gap energy. In X-ray diffraction result, there is no Cu identification peak because of excellent penetration of Cu in TiO_2 crystallization.

Acknowledgements

This work is supported by Department of Chemical Technology Faculty Of Science Chulalongkorn University, Center of Excellence on Petrochemical and Materials Technology and Cu Graduate School Thesis Grant for financial support.

References

[1] Xu S, Delai D, *Significant improvement of photocatalytic hydrogen generation rate over TiO_2 with deposited CuO*, international journal of hydrogen energy 34 (2009) 6096 – 6104.
[2] A. Fujishima, K. Honda, Nature **238** (1972) 37.
[3] M.R. Hoffmann, S.T. Martin, W. Choi, D.W. Bahnemann, Chem. Rev. **95** (1995) 69.
[4] Miwa T, Kanecoa S, Katsumataa H, Suzukib T, Ohtaa T, Vermac T and Sugiharac K , *Photocatalytic hydrogen production from aqueous methanol solution with $CuO/Al_2O_3/TiO_2$ nanocomposite*, International Journal of Hydrogen Energy 35 (2010) 654-6560
[5] Wu N, Lee M, *Enhanced TiO_2 photocatalysis by Cu in hydrogen production from aqueous methanol solution*, International Journal of Hydrogen Energy 29 (2004) 1601 – 1605.
[6] Liu J, An T, Li G, Bao N, Sheng G, *Preparation and characterization of highly active mesoporous TiO_2 photocatalysts by hydrothermal synthesis under weak acid conditions*, Microporous and Mesoporous Materials 124 (2009) 197–203
[7] Xu S, Du A, Liu J, Ng J, Sun D, *Highly efficient CuO incorporated TiO_2 nanotube photocatalyst for hydrogen production from water*, international journal of hydrogen energy 36 (2011) 6560-6568
[8] Yu J, Hai Y, Jaroniec M, *Photocatalytic hydrogen production over CuO-modified titania*, Journal of Colloid and Interface Science 357 (2011) 223–228

HYDRODESULFURIZATION AND HYDRODENITROGENATION OF DIBENZOTHIOPHENE MIXED WITH PYRIDINE OVER HDS CATALYSTS SUPPORTED ON Al_2O_3-TiO_2 MIXED OXIDES

Teraporn Leungon, Akawat Sirisuk*

Center of Excellent on Catalysis and Catalytic Reaction Engineering, Department of Chemical Engineering, Faculty of Engineering, Chulalongkorn University, Bangkok, 10330, Thailand

* Author for correspondence; E-Mail: akawat.s@chula.ac.th, Tel. +662 218 6863, Fax. +662 2681877

Abstract: Two catalysts (A and B) were supported on two different Al_2O_3-TiO_2 binary mixed oxides, which were prepared by sol-gel methods. The supported catalysts were employed in hydrodesulfurization (HDS) and hydrodenitrogenation (HDN) of dibenzothiophene (DBT) mixed with pyridine in diesel oil. The TiO_2 content in the support for catalyst A was higher than in catalyst B. The catalysts were characterized by XRD, N_2-physisorption, NH_3-TPD, and H_2-TPR techniques. HDS and HDN reactions were carried out in a packed bed microreactor at 350°C and 80 bar. Five different nitrogen concentrations from pyridine were employed to investigate its effect on the catalytic activity. Prior to each run, the catalyst was sulfided using dimethyldisulfide (DMDS) at 350°C and 60 bar under hydrogen atmosphere to activate the catalysts. The catalytic activity was determined using total sulfur and nitrogen analyzer to measure the remaining sulfur and nitrogen contents in the samples after hydrotreatment. Catalyst A exhibited higher HDS and HDN activities than catalyst B as a result of higher surface acidity on catalyst A. Addition of pyridine to the feed lowered the HDS activity of the catalysts. Higher concentration of nitrogen in the feed led to further reduction in HDS activity.

1. Introduction

Petroleum or crude oil consist of primarily hydrocarbon. The hydrocarbons are mostly aliphatic and aromatic hydrocarbons. However, fossil fuel also contains some impurities such as sulfur compounds, nitrogen compounds, oxygen compounds, and metallic compounds. These impurities are harmful to the environment and human. Automobile emissions from such fuels are the major causes of increased pollution. The exhaust gases from automobile contain nitrogen oxides (NO_x) and sulfur oxides (SO_x). When these oxides are exposed to the atmospheric water, they are transformed into HNO_3 and H_2SO_4, which give rise to the acid rain phenomenon. Moreover, sulfur is a well-known poison for catalytic converter in automobile.

Nowadays, environmental regulations demand a reduction in sulfur, nitrogen, and aromatic contents in fuels for motor vehicles, particularly, the removal of alkylated dibenzothiophenes (DBT) and pyridine - the most refractory compounds in gas oil. Therefore, it is necessary to develop the more efficient catalysts Typically, $CoMo/A1_2O_3$ and $NiMo/A1_2O_3$ catalysts are employed for hydrodesulfurization (HDS) [1]. Several researchers attempt to develop new supports for HDS catalysts. J. Ramirez et al. [2] found that the catalytic activities of HDS catalysts supported on Al_2O_3 are lower than those supported on other supports such as anatase TiO_2 and ZrO_2. Among these new supports, binary oxides such as TiO_2-$A1_2O_3$ and TiO_2-ZrO_2 are promising.

The catalyst support has been modified to improve catalyst activity and selectivity. TiO_2 has attracted attention because of good HDS activity displayed by molybdenum sulfide supported on this oxide [3,4]. However, due to the low surface area and the poor thermal stability of the anatase structure at high temperature, this support is not suitable for industrial hydrotreatment. To solve this problem, much attention has been paid to the application of mixed oxides containing TiO_2 such as TiO_2-$A1_2O_3$ or TiO_2-ZrO_2. [5,6]

In this study, two different Al_2O_3-TiO_2 binary oxides were used as supports for CoMo catalysts. Then the supported CoMo catalysts were tested for hydrodesulfurization of dibenzothiophene (DBT) in the present of pyridine. The effect of nitrogen compound concentrations were also investigated.

2. Materials and Methods

2.1 Catalysts preparation

2.1.1 Preparation of Al_2O_3-TiO_2 supports by sol-gel method

Al_2O_3 and TiO_2 were prepared by sol-gel methods using aluminum isopropoxide and titanium (IV) isopropoxide as precursors, respectively. Al_2O_3 sol was added to TiO_2 sols at two different concentrations, the so-called Catalyst A and Catalyst B. The Al_2O_3 content in the support for catalyst A was lower than that in catalyst B. Then the binary mixtures were dried at 110 °C overnight and were calcined at 450 °C for 4 hours.

2.2.2 Impregnation of cobalt and molybdenum

Cobalt and molybdenum were co-impregnated on the supports, using cobalt (II) nitrate hexahydrate and ammonium heptamolybdate tetrahydrate as precursors, respectively. After impregnation, the CoMo catalysts

were dried at 110 °C for 12 hours and were calcined at 450 °C for 3 hours.

2.2 Catalyst characterization

The CoMo catalysts were analyzed by X-ray diffraction (XRD) at room temperature using Siemens D-5000 powder diffractometer with nickel-filtered Cu Kα radiation (α = 1.5404 Å) over the range of 2θ from 20° to 80° with step size of 0.04°. The BET specific surface area, pore volume, and pore size distribution of the catalysts were determined by N_2-physisorption. The metal content was determined using inductively coupled plasma-optical emission spectroscopy (ICP-OES).

The surface acidity of the catalyst was determined by temperature-programmed desorption with ammonia (NH_3-TPD). And the reducibility of the catalysts was assessed using temperature-programmed reduction with hydrogen (H_2-TPR).

2.3 HDS activity test

The simplified schematic diagram for HDS testing apparatus is shown in Figure 1.

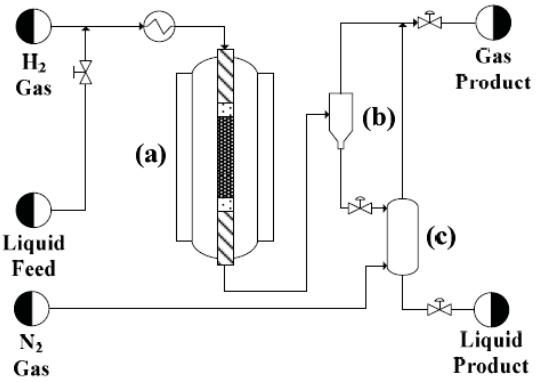

Figure 1. Schematic diagram of HDS reactor system: (a) packed bed microreactor, (b) liquid-gas separator, and (c) stripper.

Prior to each activity test, the catalyst was sulfided using dimethyl disulfide (DMDS) at sulfur content of 2.35 %(w/v) in diesel oil and hydrogen feeds. The reaction temperature was increased stepwise until the temperature reached 350 °C (see Figure 2.).

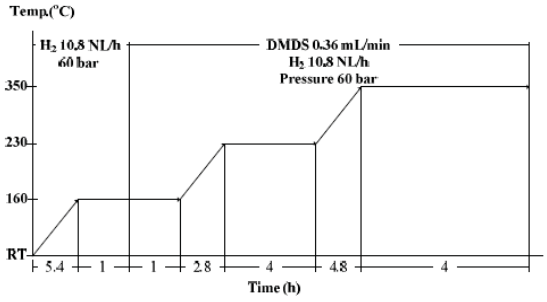

Figure 2. Temperature diagram for sulfiding step.

For HDS activity test, the feed consisted of dibenzothiophene with sulfur content of 2000 ppm and pyridine with various nitrogen content in diesel oil. Five different nitrogen concentrations (100, 200, 300, 400, and 500 ppm) were employed to investigate the effect of nitrogen content on HDS activity. The operating conditions for the microreactor system are listed in Table 1.

Table 1: Operating conditions for HDS reaction test

Parameter	Value
Liquid feed flow rate (mL/min)	0.36
H_2 Gas flow rate (nL/h)	10.8
N_2 Gas flow rate (nL/h)	5.0
Catalyst weight (g)	0.5
Temperature (°C)	350
Pressure (bar)	80

During the HDS test, the first sample was collected after 12 hours of time on stream and the sampling continued every 6 hours after that. These samples were analyzed using Analytik Jena Multi EA5000 for total sulfur and nitrogen contents, which were then used to calculate HDS and HDN activity as followed.

$$HDS\ activity=[(S_{In} - S_{Out})/S_{In}]\times 100$$

$$HDN\ activity=[(N_{In} - N_{Out})/N_{In}]\times 100$$

3. Results and Discussion

Figure 3 shows the XRD patterns of two Al_2O_3-TiO_2 supports. The peaks corresponding to the anatase structure were observed, particularly at the 2θ of 25.3º [7]. Therefore, the primary phase of TiO_2 was anatase with small amount of brookite.

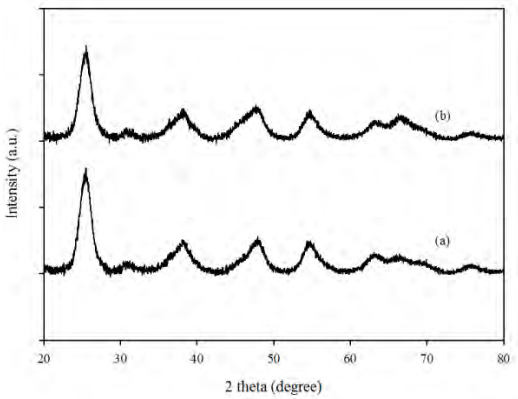

Figure 3. XRD patterns of (a) Catalyst A support, (b) Catalyst B support.

From the Table 2, the addition of Al_2O_3 in the mixed support led to increases in the specific surface area, pore volume, and pore diameter of the supports [8].

Table 2: Physical properties of the supports

Sample	Surface area (m^2/g)	Pore volume (cm^3/g)	Pore diameter (nm)
Catalyst A	267.0	0.285	4.27
Catalyst B	272.9	0.299	4.38

H_2-TPR results are presented in Figure 4. The first reduction peak was observed at ca.480 ^oC for Catalyst B, which was slightly lower than that for Catalyst A. The H_2 consumption in the reduction of the CoMo catalysts, as determined from area under the curve, are shown in Table 3.

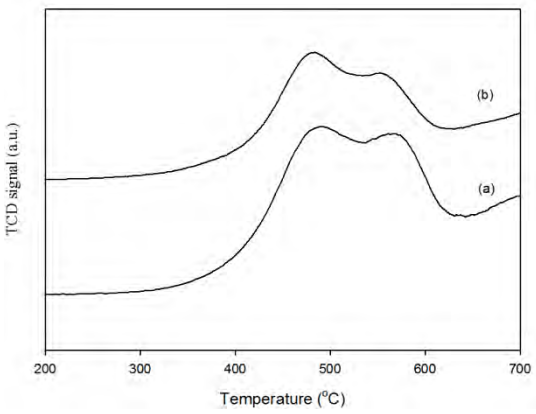

Figure 4. H_2-TPR results of (a) Catalyst A and (b) Catalyst B.

H_2 consumption in the reduction of catalyst A was higher than that of catalyst B as a result of higher TiO_2 content in the support of Catalyst A. An increase in TiO_2 gave rise to larger amount of reducible Mo by reducing the metal-support interaction [9].

The results from NH_3-TPD experiments are presented in Figure 5 and Table 3. The data in Table 3 was calculated from integrating both peaks of TCD signal versus time using a computer program, Chem Master™. The surface acidity of Catalyst A was higher than that of Catalyst B, which can be attributed to the higher content of TiO_2 in catalyst support.

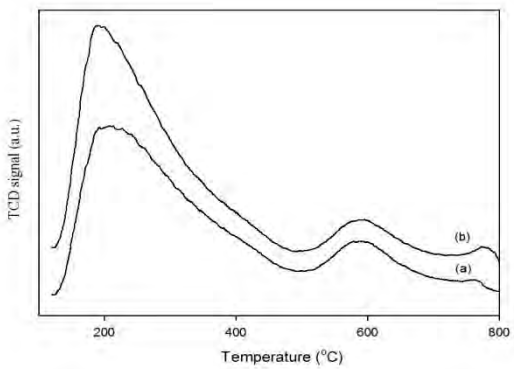

Figure 5. NH_3-TPD results of (a) Catalyst A and (b) Catalyst B.

The acidity of TiO_2 could increase the catalytic activity by facilitating hydrogenolysis of C-S bond [10].

Table 3: Chemical properties of the catalysts

Sample	Acid amount ($\mu mol\ NH_3/g$)	H_2 consumption ($mmol\ H_2/g$)
Catalyst A	4.403	2.974
Catalyst B	3.978	2.760

The HDS and HDN results for the feed containing DBT mixed with five different pyridine concentrations were shown in Figures 6 and 7, respectively.

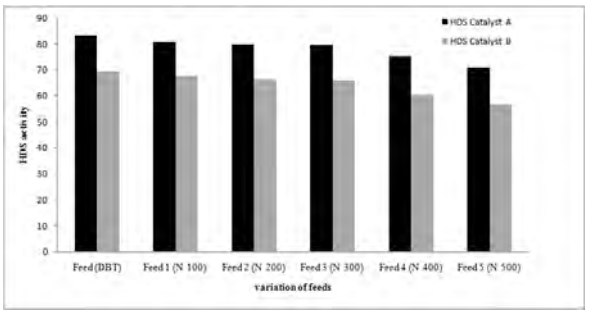

Figure 6. HDS activity of CoMo catalyst.

As seen in Figures 6 and 7, HDS activity and HDN activity of both Catalysts A and B were decreased when the concentration of pyridine became higher probably because nitrogen compounds are strong inhibitors for both HDS and HDN reactions. So the active site for hydrotreatment was hindered by the presence of nitrogen in pyridine [11].

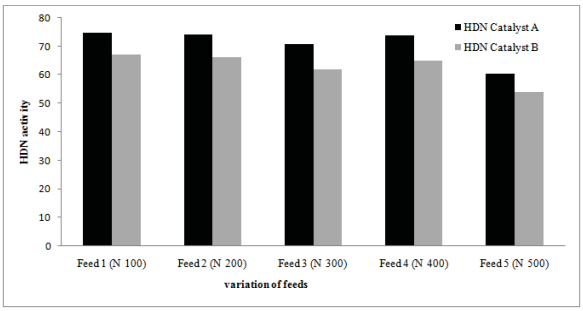

Figure 7. HDN activity of CoMo catalyst.

From this study, both HDS and HDN activities for Catalyst A were higher than those for Catalyst B due to larger TiO_2 content in Catalyst A. TiO_2 could facilitate the reduction of metal, as seen from H_2- TPR results (see Table 3). Moreover, TiO_2 in the support also increased the surface acidity of the catalyst, leading to higher catalytic activity.

4. Conclusions

The investigation of HDS and HDN activities that were obtained from two catalysts with different TiO_2 contents, namely, Catalyst A and Catalyst B,

suggested that the higher TiO_2 content in the catalyst support increased the HDS and HDN activities of the catalyst due to greater surface acidity and larger amount of H_2 consumption.

Acknowledgements

The financial support from the PTT Research and Technology Institute, PTT Public Co.,Ltd., is gratefully acknowledged.

References

[1] T.G. Parkham, R.E Merill, *J. Catal*. **85** (1984) 295.
[2] J. Ramirez, S. Fuentes, G. Diaz, M. Vrinat, M. Breysse, M. Lacroix, *Appl. Catal*. **52** (1989) 211.
[3] M. Breysse, J.L. Portefaix, M. Vrinat, *Catal. Today* **10** (1991) 489.
[4] F. Luck, Bull. Soc. *Chim. Belg*. **100** (1991) 781.
[5] E. Rodenas, T. Yamaguchi, H. Hattori, K. Tanabe, *J. Catal*. **85** (1984) 44.
[6] G.B. Mac Vicker, J.J. Ziemiak, *J. Catal*. **95** (1985) 473.
[7] Guofu Wan et al., *Energy and fuels* **23** (2009) 83.
[8] E. Olguin et al., *Appl. Catal*. **165** (1997) 3.
[9] G.M. Dhar et al., *Catal. Today*. **86** (2003) 48.
[10] M.S. Rana et al., *Fuel*. **86** (2007) 1259.
[11] F. Rota et al., *J. Catal*. **202** (2002) 195.

EFFECTS OF TRANSESTERIFICATION CONDITIONS ON SYNTHESIS OF TRIMETHYLOLPROPANE ESTERS

Surapoj Katekong[1], Suchada Butnark[2], Chawalit Ngamcharussrivichai[3]*

[1] *Program in Petrochemistry and Polymer Science, Faculty of Science, Chulalongkorn University, Patumwan, Bangkok 10330, Thailand*
[2]*PTT Research and Technology Institute, PTT Public Company Limited, Wangnoi, Ayutthaya 13170, Thailand*
[3]*Fuels Research Center, Department of Chemical Technology, Faculty of Science, Chulalongkorn University, Patumwan, Bangkok 10330, Thailand*
**E-mail: Chawalit.Ng@chula.ac.th*

Abstract: Trimethylolpropane (TMP) esters can be synthesized via catalytic transesterification of TMP with fatty acid methyl esters (FAME) in the base catalyst. This work investigated the catalytic performance of heterogeneous base catalysts, such as $Ca(OH)_2$ and CaO in the transesterification of TMP with mixed C_8-C_{10} FAME. The effects of the main operating variables, including temperature, molar ratio of FAME:TMP, and catalyst amount, on the FAME conversion and the product of TMP esters were investigated. The reaction products were analyzed to determine the distribution of TMP esters by gas chromatography (GC). The results showed that the heterogeneous catalysts produced no soap and were separated easily from the reaction products. An increase in the temperature and the molar ratio of FAME:TMP promoted the transesterification, while the catalyst amount had much smaller effect. The highest conversion of FAME (> 70 %) and the distribution of TMP triesters 97 % were achieved from the transesterification over $Ca(OH)_2$ at the molar ratio of FAME:TMP of 9:1, catalyst amount of 1 wt.%, temperature of 170 °C and reaction time of 8 h.

1. Introduction

Lubricants based on vegetable oils are rapidly and completely biodegradable, and they have low ecotoxicity compared to mineral oil based lubricants [1]. However, there are some performance limitations associated with them, e.g., thermal, oxidative, and hydrolytic stability, and inadequate low temperature fluidity due to high pour points. These limitations can be minimized by means of chemical modification through transesterification of vegetable oils with polyols such as neopentylglycol (NPG), trimethylolpropane (TMP) [2-4]. The structure of polyols causes the elimination of a hydrogen atom from the β-carbon of the triglyceride structure and provides esters with a high degree of oxidative and thermal stability [5].

The transesterification reaction is a reversible reaction which involves three consecutive mechanisms with the presence of catalyst. TMP monoesters (TMPME) and TMP diesters (TMPDE) are formed as the intermediate products toward the completion of the reaction producing TMP triesters (TMPTE). The overall reaction stoichiometry requires 1 mol of TMP and 3 mol of fatty acid methyl esters (FAME) [5]. The equations are shown below:

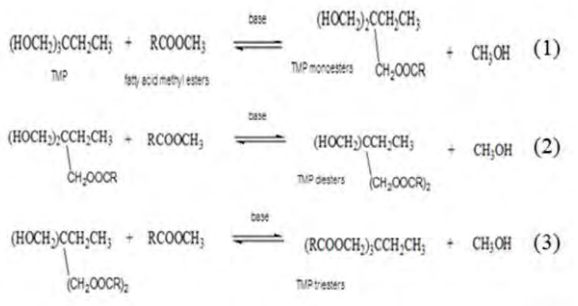

The reversible reaction can be modified to obtain the highest TMPTE yield by adjusting operating conditions, e.g., temperature, molar ratio of TMP: FAME, and catalyst amount. Generally, the homogeneous base catalysts are used but they contribute to soap formation via saponification in the presence of moisture. The fatty soaps formed are in colloidal form partially soluble in the reaction products, and hence are required to be separated from the final product [5]. The heterogeneous base catalysts are interesting because they produce no soap in the reaction. Moreover, they are gaining attention for green production of bio-based products due to less toxic nature, ease of separation and reusability [4]. Searching for a solid base with suitable physic-chemical and catalytic properties for the transesterification of highly branched polyols with large esters is a big challenge.

This work studied the catalytic performance of $Ca(OH)_2$ and CaO as heterogeneous base catalysts in the transesterification of TMP with mixed C_8-C_{10} FAME. The effects of reaction conditions were, i.e., temperature, molar ratio of FAME:TMP, and catalyst amount, on the FAME conversion and the distribution of TMP esters produced were studied.

2. Materials and Methods

2.1 Materials

Mixed methyl esters of C_8-C_{10} fatty acids were obtained from the Thai Oleochemicals (TOL) Co., Ltd. The composition of C_8-C_{10} FAME analyzed by gas chromatography (GC) is showed in Table 1. Trimethylolpropane (TMP) (assay > 98%) purum grade was

purchased from Fluka. Calcium hydroxide (AR grade, 98 %) was purchased from Fisher Scientific. Calcium oxide (AR grade, 98 %) was purchased from Qrec. For GC analysis, 1,4-dioxane (GC grade, 99.8%) as a solvent was purchased from Fisher Scientific. *N*-methyl-*N*-(trimethylsilyl)trifluoroacetamide (MSTFA) as a derivatizing agent was purchased from Sigma Aldrich. Methyl undecanoate (GC grade, 99.5%) as internal standard was purchased from Fluka. All reagents were used without prior purification.

Table 1: Composition of C_8-C_{10} FAME analyzed by GC

Component	Wt.%
Methyl hexanoate ($C_7H_{14}O_2$)	3.17
Methyl octanoate ($C_9H_{18}O_2$)	60.63
Methyl decanoate ($C_{11}H_{22}O_2$)	36.20

2.2 Synthesis of trimethylolpropane triesters (TMPTE)

A batch transesterification of TMP with C_8-C_{10} FAME was carried out in a 50-mL three-necked round bottom flask equipped with a water-cooled reflux condenser, a thermometer, a N_2 line and a magnetic stirrer. The reaction temperature was controlled by an oil bath. Typically, a predetermined amount of TMP was added to the flask and then melted by heating to 110 °C with continuous stirring at 1000 rpm under N_2 flow. The temperature was maintained at 110 °C for 15 min to remove moisture from the TMP due to its hygroscopic nature. Subsequently, a calculated amount of FAME according to the respective molar ratio of TMP: FAME was introduced into the flask, and the resulting mixture was heated to the desired temperature. A required amount of catalyst was then mixed with the reaction mixture for which 8 h of the catalytic transesterification was performed. After the reaction course, the product mixture was cooled down to room temperature by an ice bath. Then, the solid catalyst was separated from the product mixture by filtration.

2.3 Analysis of transesterification product

The FAME conversion and the distribution of esters produced were determined by gas chromatography (GC) [6]. Approximately, 0.1±0.05 g of the liquid sample was taken into a 3-mL vial and diluted with 1.5 times of 1,4-dioxane. Then, 0.1±0.05 mL of the diluted sample was taken in a 2-mL vial. For this solution, 0.1 mL of MSTFA was added in order to convert hydroxyl-containing molecules into more volatile species. The vial was well shaked and the derivatization was allowed for 30 min. Methyl undecanoate as the internal standard was added to the vial to which 1,4-dioxane was used to adjust the sample volume to 2 mL. The GC analysis was performed on an Agilent Technologies equipped with a capillary column (DB5-HT) and a flame ionization detector (FID) using He as a carrier gas. The oven temperature was heated initially at 45 °C for 2 min, and then elevated to 270 °C at a ramp rate of 10 °C min $^{-1}$. The temperatures of injector and detector were set at 270 and 300 °C, respectively.

3. **Results and Discussion**

3.1 Effects of catalyst type

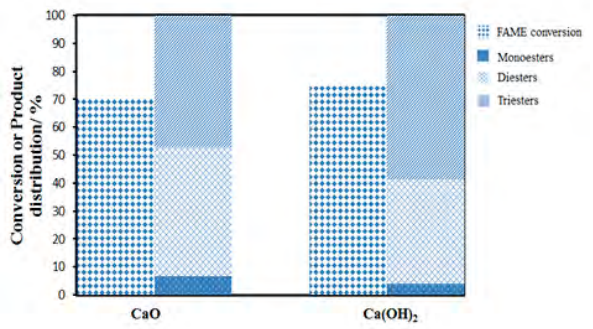

Figure 1. FmAME conversion and product distribution of TMP esters amount obtained from the transesterification of TMP with FAME. Reaction conditions: catalyst amount, 1 wt.%; molar ratio of FAME:TMP, 3.5:1; temp., 170 °C; time, 8 h.

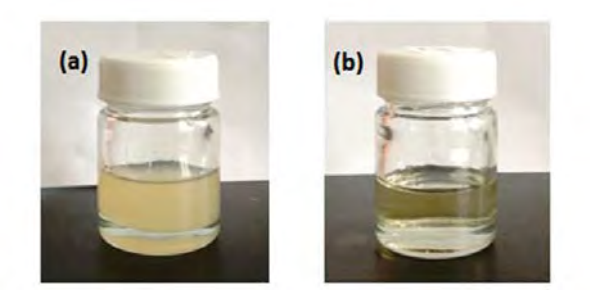

Figure 2. Comparison of the ester products obtained from (a) homogeneous and (b) heterogeneous catalyst.

Figure 1 compares the results attained from the transesterification of TMP with FAME over heterogeneous base catalysts. When compared with product attained from the homogeneously catalyzed reaction (Figure 2a), both CaO and $Ca(OH)_2$ did not produce fatty acid as soap (Figure 2b) and they were separated easily from the product mixture. Transesterification occurred on the surface of heterogeneous catalysts. Heterogeneous catalysts have less solubility in water so they did not give cation (i.e., Ca^{2+}) to catch with anion of carboxylate groups, resulting in rather less conversion into soap due to saponification. They gave the FAME conversion about 70%. The highest distribution of triesters (59%) was attained over $Ca(OH)_2$ at which the amounts of diesters and monoesters were small. From this result, $Ca(OH)_2$ gave a good result so we selected to study other effects.

3.2 Effects of temperature

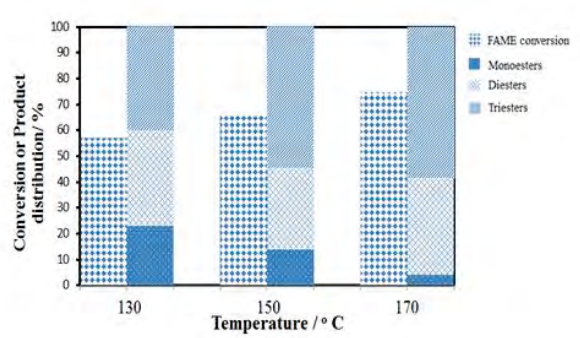

Figure 3. FAME conversion and product distribution of TMP esters amount obtained from the transesterification of TMP with FAME. Reaction conditions: catalyst amount, 1 wt.% of $Ca(OH)_2$; molar ratio of FAME:TMP, 3.5:1; time, 8 h.

To determine the effect of temperature as demonstrated in Figure 3, experiments were performed at fixed conditions of molar ratio of FAME:TMP of 3.5:1, reaction time of 8 h and 1 wt.% of $Ca(OH)_2$. The reactions were conducted at 130, 150 and 170 °C. It is evident that the FAME conversion was increased with increasing the temperature. The highest of FAME conversion was at 75 % since an increase in the temperature can stimulate reaction by increasing kinetic energy of the reactants. The distribution of triesters were low at 130 °C and kept on increasing with an increase in temperature. The highest distribution of triesters was at 170 °C giving 59 %. The distributions of monoesters were gradually decreased with an increase in the temperature which the equilibrium was shifted toward the esters product. The results showed that an increase in the temperature can stimulate reaction which monoesters reacted easily with FAME. In the case of diesters, they were intermediate agents [7] which can change to monoesters or triesters. However, diesters did not easy to react with FAME due to steric effect while monoester were changed easily to diesters. So they still appeared in the final product mixture. From this result, the suitable temperature was at 170 °C.

3.3 Effects of molar ratio

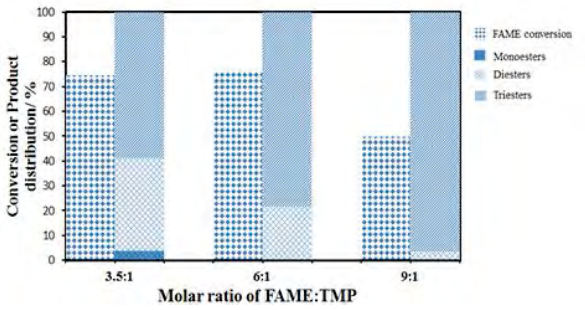

Figure 4. FAME conversion and product distribution of TMP esters amount obtained from the transesterification of TMP with FAME over $Ca(OH)_2$. Reaction conditions: catalyst amount, 1 wt; temp., 170 °C; time, 8 h.

Since the transesterification is a reversible reaction, it can be driven to achieve the hightest amount of triesters by an excess amount of FAME. The molar ratio of FAME:TMP was varied at 3.5:1, 6:1 and 9:1. Under fixed conditions at temperature of 170°C, reaction time of 8 h and 1 wt.% of $Ca(OH)_2$. As demonstrated in Figure 4, the result showed that when molar ratio of FAME:TMP was increased, the FAME conversion increased. Generally, a better product yield is obtained by keeping the molar ratio of reactants higher than the stoichiometric values since the reaction was driven more toward completion. However, the FAME conversion was decreased at 9:1 due to too much excess of FAME. From this result, the highest FAME conversion achieved at 76 % from molar ratio of FAME:TMP of 6:1. The highest distribution of triesters achieved at 97 % from molar ratio of FAME:TMP of 9:1 which did not appear monoesters. In addition, the FAME remaining in the final product affects physical properties of lube so it should be eliminated from the product mixture [2]. For the suitable molar ratio, 9:1 can be considered to produce the highest triestes.

3.4 Effects of catalysts loading

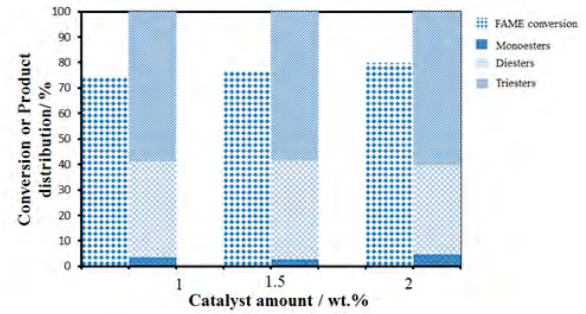

Figure 5. FAME conversion and product distribution of TMP esters amount obtained from the transesterification of TMP with FAME. Reaction conditions: molar ratio of FAME:TMP, 3.5:1; temp., 170 °C; time, 8 h.

In this study, the amount of $Ca(OH)_2$ was varied in the range of 1-2 wt.%. Other parameters were the molar ratio of FAME:TMP of 3.5:1, temperature of 170 °C, reaction time of 8 h and 1 wt.% of $Ca(OH)_2$. The result showed that an increase in the amount of $Ca(OH)_2$ affected a slight increase in the FAME conversion while the distribution of triesters was not sinificantly affected (Figure 5). An increase in amount of catalyst increased active sites for transesterification of FAME but mechanism of reaction was remained. The effects of catalyst amount were less noticeable than thoes of other parameters. So,the amount of suitable catalyst was at 1 wt.%.

4. Conclusions

This study demonstrated that heterogeneous catalysts produced no soap in transesterification of

TMP with FAME and were separated easily from the product mixture. $Ca(OH)_2$ served as an effective catalyst for transesterification of TMP with FAME to attain the highest conversion of FAME (>70 %). The highest distribution of TMP triesters was at 97 % which did not present monoesters. Moreover, the transesterification of TMP with FAME was adjusted to give the highest conversion of FAME and the highest TMP triesters by increasing temperature and molar ration of FAME:TMP. An increase in the temperature and the molar ratio of FAME:TMP can stimulate equilibrium to produce triesters. However, catalysts loading did not show any significant affect.

References

[1] S.Z. Sulaiman, A.L. Chuah, and R.A. Fakhrul, *J. Am. Chem. Soc.* **15** (2007) 2002-2005.

[2] S. Gryglewicz, W. Piechocki and G. Gryglewicz, *Bioresource Technology*. **87** (2003) 35–39.

[3] R. Yunus, R.A. Fakhrul, and S.E. Lyuke, *J. Am. Chem. Soc*. **81** (2004) 497-503.

[4] R. Yunus, H. Masood, S.Y. Thomas and U. Rashidb, *Applied Catalysis A: General*. **425–426** (2012): 184– 190.

[5] H. Masood, S.C. Teck, and R. Yunus, *Ind. Eng. Chem.* **51** (2012) 5438-5442.

[6] R. Yunus, S. Basri, *JAOCS*. **79** (2002) 1075-1080.

[7] R. Yunus, A.F. Razi, T.L. Ooi, R. Omar and A. Idris, *Ind. Eng. Chem. Res*. **44** (2005) 22.

BIODIESEL PRODUCTION FROM TUNG SEED OIL BY MICROWAVE COUPLING WITH ULTRASONIC TECHNIQUES

Achara Kleawkla[1*], Yonlada Juntaboon[1], Nutthawud Dussadee[2], Kittikorn Sasujit[2], Robert Molloy[3,4]

[1] Department of Chemistry, Faculty of Science, Maejo University, Chiang Mai, 50290 Thailand
[2] Energy Research Center, Maejo University, Chiang Mai, 50290 Thailand
[3] Polymer Research Group, Department of Chemistry, Faculty of Science, Chiang Mai University, Chiang Mai 50200, Thailand
[4] Materials Science Research Center, Faculty of Science, Chiang Mai University, Chiang Mai 50200, Thailand

[*] Author for correspondence; E-Mail: achara_kleawkla@yahoo.co.uk, Tel. +66 53873530, Fax. +66 53873548

Abstract: Biodiesel is an attractive alternative fuel for Thailand because Thailand is an agricultural country with an abundance of feedstocks for biodiesel production. Tung seed oil is another natural material that can be used in biodiesel production. This research project has been concerned with the production of biodiesel fuel from tung seed oil by transesterification using microwave coupling with ultrasonic techniques. The effects of catalyst, temperature, time, and mole ratio of tung seed oil to methanol were studied. It was found that the percentage of biodiesel produced was 84.41 % using 1.00 wt% calcium oxide (CaO) as catalyst, a reaction temperature of 338 K, and an oil / methanol molar ratio of 1:8. Fourier-transform infrared spectroscopy (FT-IR) was used to characterise the biodiesel and gas chromatography-mass spectrometry was used to separate and identify the methyl esters.

1. Introduction

The demand for energy has increased rapidly with the growing world population. The reserves of fossil fuels are being depleted, while the environmental problems caused by their use have become serious. Thus, renewable energies are being urgently developed [1-2]. Among the applicable renewable energies, biodiesel has attracted much attention [3]. Biodiesel is an eco-friendly and alternative energy source for diesel engines that can be synthesized by transesterification of vegetable oil or animal fat with alcohols. The reaction can be catalyzed by alkalis, acids, or enzymes [4-6]. Base catalysts can be either homogeneous or heterogeneous catalysts. The commonly used homogeneous base catalysts are NaOH, KOH and their alkoxides.

Homogeneous alkali-catalyzed transesterification is much faster than acid-catalyzed transesterification [7]. However, a large amount of water is required to transfer the catalysts from the organic phase to a water phase after the reaction. Therefore, it is considerably more costly to separate the catalyst from the product solution. Heterogeneous base catalysts have many advantages: they are non-corrosive, environmentally benign and present fewer disposal problems. Furthermore, they are much more easily separated from the liquid products and can be designed to give higher activity, selectivity and longer catalyst lifetimes.

Nowadays, many types of heterogeneous catalysts have been explored for transesterification of vegetable oils to biodiesel, such as alkaline earth metal oxides and various alkali metal compounds supported on alumina or zeolite [8-12].

Calcium oxide (CaO) is one of the most commonly used heterogeneous base catalysts for the transesterification of vegetable oil. Producing biodiesel using CaO as a solid base catalyst has many advantages such as higher activity, mild reaction conditions, reusable, low cost and so on [12-14].

As oil and methanol are not completely miscible, the mixing efficiency can affect the cause of the transesterification reaction [15-16]. The mixing process generally increases energy input for biodiesel production process, yet the biodiesel yield is generally lower than that in the homogeneous process [17]. Ultrasonic mixing can produce smaller droplets of the reacting phases than conventional agitation, leading to a drastic increase in the interfacial area and improved mass transfer. As a result, the mixing requirement during the process is also significantly lowered, translating in reduced energy consumption. Ultrasonic can also 'grind' the catalyst into smaller particles to create new active sites for the subsequent reaction, thereby resulting in the solid catalyst lasting longer in the ultrasonic-assisted process [6].

Microwave irradiation has been an alternative heating system in transesterification over the past few years. As a result, a drastic reduction in the quantity of by-products and a short separation time have been obtained [18]. Today, microwave irradiation is widely used in many areas including assisting transesterification of vegetable oils to produce biodiesel [14].

The main objective of this present study was to investigate the biodiesel transesterification reaction using a closed microwave irradiation technique and ultrasonic mixing to obtain the optimal procedure for achieving the highest possible percent yield of biodiesel. The optimal reaction conditions of amount of catalyst used, reaction temperature, reaction time and oil/methanol ratio were also investigated.

2. Materials and Methods

2.1 Materials

Tung seed oil was purchased from Gemon China. Methanol was purchased from Merck KGaA Co.Ltd., Germany. Calcium oxide (CaO) was purchased from RCI Labscan Co.Ltd., Ireland, and calcined in a muffle furnace at 500 °C for 10 h.

2.2 Equipment

The ultrasonic equipment used in the experiments had a working frequency of 28 kHz (CT-406) and an output power of 50 W.

The reactions were also performed using a commercially available domestic microwave oven (Samsung R-267) which comprised a continuous microwave power delivery system with a working frequency of 2.45 GHz, power output from 0 to 500 W, and temperature and time settings (Figure 1).

2.3 Experimental Procedure

Triglycerides were converted into esters with methanol using a heterogeneous CaO alkali catalyst. The transesterification comprises two discrete steps. In the first step, the catalyst was dispersed in methanol under magnetic stirring at room temperature for 30 min. The tung seed oil was then added with additional ultrasonic mixing 15 min [19].

Figure 1. Microwave irradiation-assisted transesterification of tung seed oil.

In the second step, the transesterification reaction was assisted by closed microwave irradiation 5 min [20]. The reaction temperature was set in this step. The molar ratios of oil to methanol were varied between 1:8, 1:10, 1:12, 1:14 and 1:16 while the catalyst loadings were varied in the range of 1.00 –5.00 wt %.

At the end of the reaction, the products were centrifuged forming two phases, the upper layer of which was biodiesel while the lower layer was a mixture containing the solid CaO.

2.4 Analytical Methods

The biodiesel products were characterized according to their chemical composition by Fourier-transform infrared spectroscopy (FT-IR) and by gas chromatography-mass spectrometry to separate and identify the methyl esters.

3. Results and Discussion

3.1 Effects of Mass Ratio of Catalyst to oil on Biodiesel Yield

The effects of the mass ratio of CaO to oil for percent yield of tung seed oil to biodiesel were studied under the reaction conditions of: oil/methanol molar ratio, 1:10; reaction temperature, 338 K; ultrasonic mixing, 15 min; and closed microwave irradiation, 5 min. Percent yield was calculated using equation (1).

$$\%\text{Yield} = \frac{\text{Actual Mass of Product}}{\text{Theoretical Mass of Product}} \times 100 \qquad (1)$$

The results shown in Figure 2 that as the weight% of CaO to oil is increased from 1.00-5.00 wt %, the amount of biodiesel yield decreased continuously. The reason may be offered to explain why 2.00-5.00 wt % of catalyst used resulted in lower percent yield. More catalyst used might initiate the saponification reaction. This might explain why 2.00-5.00 wt % of catalyst used resulted in lower percent yield than 1.00 wt % [21].

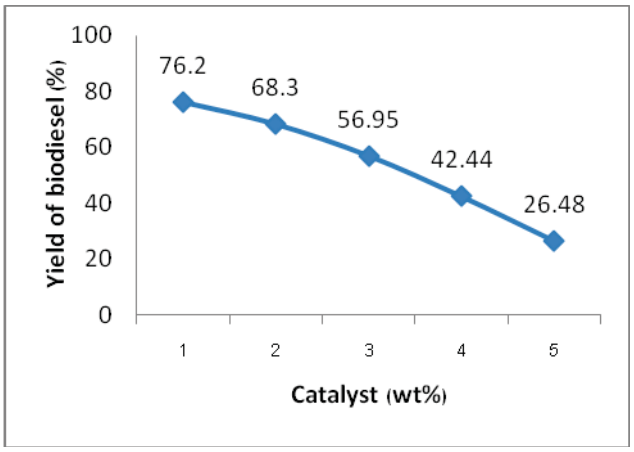

Figure 2. Effects of mass ratio of catalyst to oil on biodiesel yield. Reaction conditions: oil/methanol molar ratio, 1:10; reaction temperature, 338 K; ultrasonic mixing, 15 min; and closed microwave irradiation, 5 min.

3.2 Effects of Molar Ratio of Oil to Methanol on Biodiesel Yield

The effects of the molar ratio of oil to methanol on the production of biodiesel were studied under the reaction conditions of: CaO to oil, 1.00 wt %; reaction temperature, 338 K; ultrasonic mixing, 15 min; and closed microwave irradiation, 5 min. The results shown in Figure 3 that, the percent yield at these

oil/methanol molar ratios were 84.41%, 79.63%, 80.12%, 78.71% and 79.80%, respectively. The percent yield decreased when increased the oil/methanol molar ratio. The reason may be offered to explain why increased oil/methanol molar ratio resulted in lower percent yield. Excess methanol will increase the solubility of by-product (glycerol), which might initiate the reverse reaction to reduce the percent yield [21].

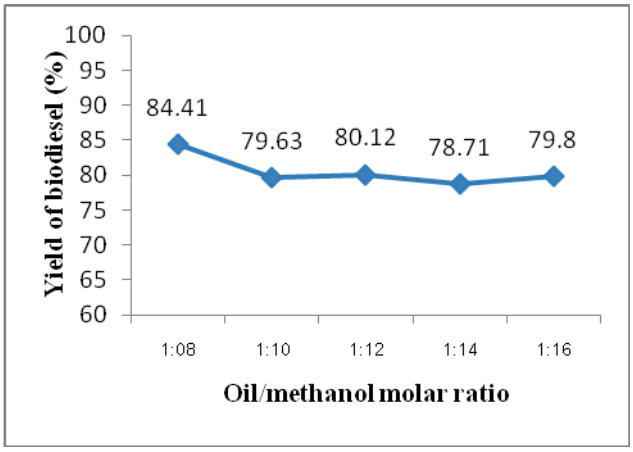

Figure 3. Effects of molar ratio of oil to methanol on biodiesel yield. Reaction conditions: Catalyst amount, 1.00 wt%: reaction temperature, 338 K: ultrasonic mixing, 15 min; and closed microwave irradiation, 5 min.

3.3 Characterization of Biodiesel from Tung Seed Oil by FT-IR

The FT-IR spectrum of the biodiesel from tung seed oil and *Thespesia populnea* oil are shown in Figure 4-5 and the most prominent peaks assigned in Table 1.

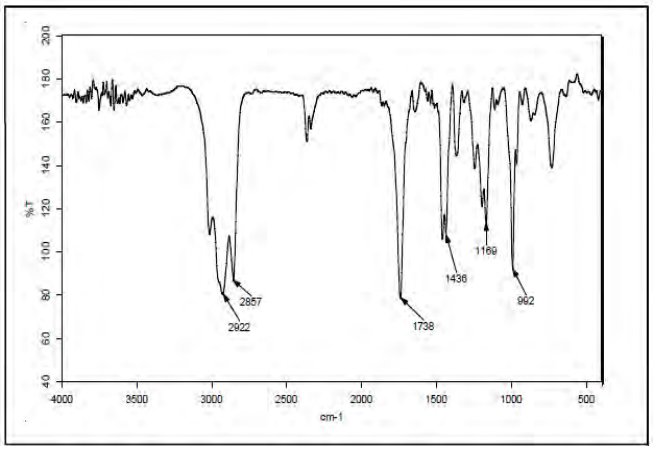

Figure 4. FT-IR spectrum of biodiesel produced from tung seed oil.

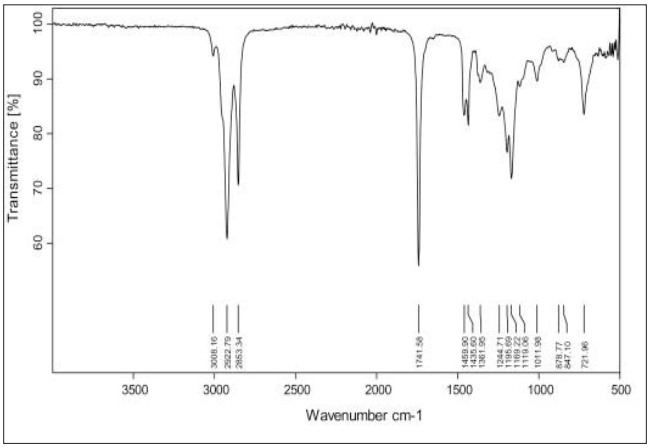

Figure 5. FT-IR spectrum of biodiesel produced from *Thespesia populnea* oil [22].

Table 1: Analysis of the functional groups of biodiesel in the FT-IR spectrum.

Wave number (cm^{-1})		**Functional groups**
Biodiesel from tung seed oil	**Biodiesel from *Thespesia populnea* oil** [22]	
2857-2922	2853-2922	CH_2-CH_3 stretching
1738	1741	C=O stretching
1436	1435	C-H bending
1169	1169	C-O stretching

3.4 Chemical Composition of Biodiesel by GC-MS

The chemical composition of the biodiesel from tung seed oil from GC-MS is shown in Figure 6. It was found that the retention times of the methyl esters of fatty acids were in the range of 13.974 to 19.205 min with a purity of 99.69 %.

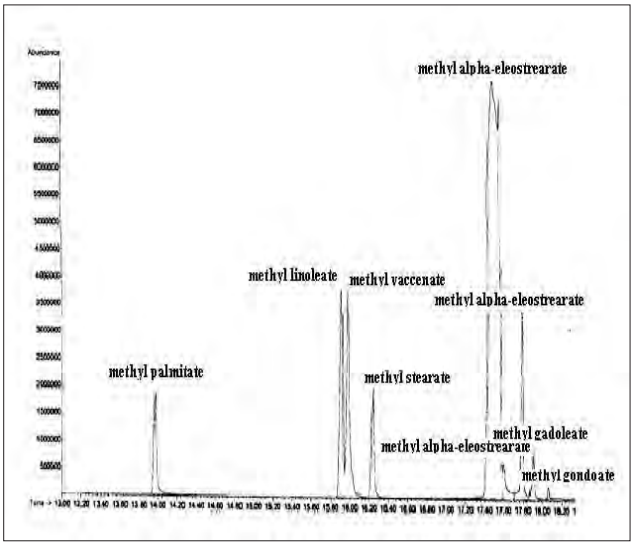

Figure 6. GC-MS chromatogram of biodiesel from tung seed oil.

4. Conclusions

In conclusion, biodiesel production from tung seed oil by microwave coupling with ultrasonic is a new technique. Results showed that under 15 min ultrasonic mixing and 5 min microwave irradiation the optimal reaction conditions of catalyst amount, 1.00 wt%; reaction temperature, 338 K; and oil/methanol molar ratio, 1:8, the percent yield of biodiesel achieved was 84.41 %. Microwave coupling with ultrasonic techniques reduce reaction time in biodiesel production.

Acknowledgement

The authors would like to thank the Department of Chemistry, Faculty of Science, Maejo University and Energy Research Center, Maejo University, for providing the laboratory facilities which made this study possible.

References

[1] S. Mori, *J. Environ. Eng. Manage.* **19** (2009) 167.
[2] J. Werther, *J. Environ. Eng. Manage.* **19** (2009) 135.
[3] D.V. Manh, Y.H. Chen, C.C. Chang, M.C. Chang and C.Y. Chang, *Journal of the Taiwan Institute of Chemical Engineers*. **42** (2011) 640-644.
[4] Y.C. Sharma, B. Singh and S.N. Upadhyay, *Fuel*. **87** (2008) 2355-2373.
[5] L.C. Meher, S.D. Vidya and S.N. Naik, *Renew Sust Energy Rev*. **10** (2006) 248–268.
[6] H. Mootabadi, B. Salamatinia, S. Bhatia and A.Z. Abdullah, *Fuel*. **89** (2010) 1818-1825.
[7] G. Vicente, M. Martinez and J. Aracil, *Bioresour Technol*. **92** (2004) 297-305.
[8] W.L. Xie, H. Peng and L.G. Chen, *Appl Catal A*. **300** (2006) 67-74.
[9] G.J. Suppes, M.A. Dasari and E.J. Doskocil, *Appl Catal A*. **257** (2004) 213-223.
[10] H. Tsuji, F. Yagi, H. Hattori and H. Kita, *J Catal*. **148** (1994) 750-759.
[11] D.G. Cantrell, L.J. Gillie, A.F. Lee and K. Wilson, *Appl Catal A*. **287** (2005) 183-190.
[12] X. Liu, H. He, Y. Wang, S. Zhu and X. Piao, *Fuel*. **87** (2008) 216-221.
[13] M.L. Grandos,M.D. Zafra Proves, D. Martin Alonso, R. Mariscl, F. Cabelo Galisteo and R. Moreno-Tost, *Appl Catal B*. **73** (2007) 327-336.
[14] M.C. Hsiao, C.C. Lin and Y.H. Chang, *Fuel.* **90** (2011) 1963-1967.
[15] J.P. Mikkola and T. Salmi, *Catal Today*. **64** (2001) 271-277.
[16] C. Stavarache, M. Vinatoru and Y. Maeda, *Ultrason Sonochem.* **13** (2006) 401-407.
[17] A. Kawashima, K. Matsubara and K. Honda, *Biores Technol*. **100** (2009) 696-700.
[18] J. Hernando, P. Leton, M.P. Matia, J.L. Novella and J. Alvarez-Builla, *Fuel*. **86** (2006) 1641-1644.
[19] D. Kumar, G. Kumar, Poonam and C.P. Singh, *Ultrasonics Sonochemistry.* **17** (2010) 839-844.
[20] N. Azcan and A. Danisman, *Fuel.***87** (2008) 1781-1788.
[21] M.C. Hsiao, C.C. Lin, Y.H. Chang and L.C. Chen, *Fuel.* **89** (2010) 3618-3622.
[22] U. Rashid, F. Anwar and G. Knothe, *Biomass and Bioenergy.* **35** (2011) 4034-4039.

EVALUATION OF PARTIALLY HYDROGENATED METHYL ESTERS OF JATROPHA OIL AS BIODIESEL

Kiatkong Suwannakij[1], Teerapong Baitiang[1], Somsak Supasitmongkol[1*]

[1] National Metal and Materials Technology Center, 114 Thailand Science Park Paholyothin Rd., Klong 1, Klong Luang, Pathumthani, 12120, Thailand

[*] Author for correspondence; E-Mail: somsaks@mtec.or.th, Tel. +66 2654 6500 ext. 74700, Fax. +66 2564 6403

Abstract: The low oxidative stability of biodiesel, derived from polyunsaturated fatty acids, is one of the great challenges to be overcome in biodiesel technology. This limitation results in corrosion of a metal component and the blockage of a filter by formation of sludge due to the product formed by oxidative degradation in biodiesel. The partially hydrogenated biodiesel is known as a technology to improve the oxidative stability. In this study, partially hydrogenated jatropha oil methyl esters (PHJME) were evaluated as biodiesel by measuring some fuel properties (e.g., density, viscosity, lubricity, oxidative stability and total acid number). Compared to conventional jatropha oil methyl esters (JME), the PHJME were found to have superior oxidative stability, acid number and lubricity, similar viscosity, but inferior density. However, both JME and PHJME are within the American standards for all properties measured in this study.

1. Introduction

Nowadays, researches and development of renewable energy for automobile have been increasingly interested. Among the proposed alternative fuels, biodiesel has been received much attention for diesel engines due to their advantages as the renewable and domestic energy sources. However, the disadvantage of biodiesel is mainly its low oxidation stability because biodiesel contains a large amount of polyunsaturated fatty acid methyl esters (FAME) [1]. The polyunsaturated FAME such as methyl linoleate and methyl linolenate can easily be oxidized by autooxidation and as a result form a series of byproducts like acids, esters, aldehyde, ketones, among others [2]. The products formed by oxidative degradation cause corrosion of a metal component and the blockage of a filter by formation of sludge.

To prevent these troubles, improvement of oxidation stability of biodiesel is desired. Partial hydrogenation, a method to improve the oxidation stability, is designed to convert the poly-unsaturated FAME into mono-unsaturated FAME. The oxidation stability of unsaturated FAME generally increases with decreasing the number of carbon-carbon double bond [3].

This research aimed to evaluate the potential of partially hydrogenated jatropha oil methyl esters (PHJME) as biodiesel. The fuel properties (e.g., density, viscosity, lubricity, oxidative stability and total acid number) of the PHJME were studied in comparison with conventional jatropha oil methyl esters (JME).

2. Materials and Methods

2.1 Chemicals

The partially hydrogenated jatropha oil methyl esters (PHJME) and jatropha oil methyl esters (JME) were obtained from Thailand Institute of Scientific and Technological Research (TISTR).

2.2 Experimental Procedures

To prepare and investigate fuel properties of the diesel-biodiesel blends, regular diesel was obtained from PTT Public Co., Ltd. (Bangkok, Thailand). Biodiesel was derived from jatropha oils. Biodiesel was mixed with diesel to obtain homogeneous phase of the solution. The concentration of biodiesel and diesel were 100:0 and 5:95 %v/v, where 'biodiesel' is denoted as 'B' and 'diesel' is denoted as 'DS'.

3. Results and Discussions

3.1 Density and viscosity

To study the potentials of PHJME as biodiesel, the properties of all test samples were conducted according to American Society for Testing Materials (ASTM) standard. The fuel properties of biodiesel at 100% by volume are presented in Table 1.

Table 1: Fuel properties of biodiesel

Properties	Thailand Biodiesel Standard [4]	JME	PHJME	Testing Method
Density (g/cm^3)	0.860-0.900	0.881	0.880	ASTM D1298
Viscosity @ 40 ^oC (cSt)	3.50-5.00	4.55	5.00	ASTM D445

Viscosity is an important fuel property because it affects the atomization of a fuel upon injection into the diesel engine combustion chamber and, ultimately, the formation of engine deposits. Fuels with higher viscosities are more likely to cause such problems. In the current study, the viscosity of the PHJME as shown in Table 1 is slightly higher than the JME. This is attributed to the fact that the partial hydrogenation leads to an increase in mono-saturated FAME (*trans*) content of the fuel, resulting in higher viscosity [4].

Both PHJME and JME have kinematic viscosities that fall within Thai commercial biodiesel specification ranges. Density of PHJME and JME (Table 1) was nearly identical and located in a standard limit for biodiesel fuel in Thailand.

3.2 Oxidation stability and acid number of biodiesel

To investigate the oxidative stability and acid number of biodiesel in Table 2, both JME and PHJME were kept in storage and left for 2 months at room temperature. The oxidative stabilities of fuels were tested by Metrohm 743 Rancimat to provide induction period, while their acid numbers were analyzed by Potentiometric Titration (KEM AT-610).

Table 2: Oxidation stability and acid number of biodiesel

Fuel properties	JME		PHJME		Testing method
	Before	After	Before	After	
Oxidation stability (hrs)	0.47	0.14	11.24	0.56	EN 14112
Total acid number (mg KOH/g)	0.107	1.05	0.227	0.398	ASTM D664-07

As can be seen in Table 2, before the partial hydrogenation, the JME is highly susceptible to oxidation and shows and induction time of less than 1 hr. This low value is a consequence of the high amount of double bonds. After the partial hydrogenation, the induction period increases to about 11 hr. The oxidative stability of fuel corresponds with the presence of acids in the fuel. Both oxidative stability and acid number of the PHJME are located in a standard limit for biodiesel fuel in Thailand. It is noted that the oxidative stability of biodiesel standard is more than 10 hr at 110 ^{o}C while the acid number is less than 0.50 mg KOH/g [5]. However, after stored 2 months (Table 2), only partial hydrogenation process may not sufficient to meet the biodiesel standard. It is likely that the PHJME may be treated with the addition of antioxidant or further hydrogenation.

3.3 Lubricity of biodiesel

The lubricity of biodiesel and biodiesel-diesel blends was measured by means of high frequency reciprocating rig (HFRR) method. The testing parameters and conditions are followed CEC-F-06-A-96 standard. After the test was completed, the wear scar on the ball was measured manually by means of an optical microscope. Then, wear scar diameter was corrected with the ambient temperature and humidity and reported as WS1.4 (Figure 1).

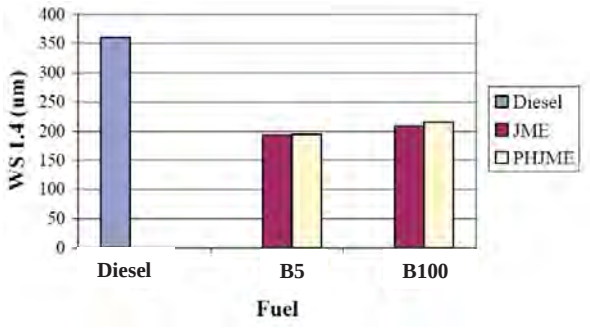

Figure 1. Effect of pure diesel and biodiesel blends on WS1.4

B5 which indicates a 5% by volume biodiesel blend has a lower WS1.4 when compared with base diesel (Figure 1). Adding a small quantity of biodiesel could promote the lubricity of diesel. The PHJME slightly decreased lubricity relative to JME based on the same B100 due to a reduction in the total number of double bonds. It is known that increasing unsaturation imparts more favourable lubricity on a substance [4].

4. Conclusions

1. Viscosity and density of all biodiesel (JME and PHJME) are in Thailand's biodiesel standard.
2. Partial hydrogenation was able to increase the oxidative stability of the JME from 0.47 to 11 hr.
3. Lubricity of diesel can be improved by biodiesel addition which corresponds with the low average wear scar size (WS1.4).
4. Changing B100 from JME to PHJME made little difference in the lubricity of biodiesel.

Acknowledgements

The author thanks National Metal and Material Technology Center (MTEC) for funding this research.

References

[1] R. Fajar, P. and B. Sugiarto, *Kasetsart J. (Nat. Sci.)* **46** (2012) 629–637.
[2] Y.H. Chen, J.H. Chen, Y.M. Luo, N.C. Shang, C.H. Chang, C.Y. Chang, P.C. Chiang and J.L. Shie, *Energy* **36** (2011) 4415-4421.
[3] S. Goto, M. Oguma and N. Chollacoop, *EAS-ERIA Biodiesel Fuel Trade Handbook*, Economic Research Institute for Asean and East Asia., Jakarta, (2010), pp. 196.
[4] B.R. Moser, M.J. Hass, J.K. Winkler, M.A. Jackson, S.Z. Erhan and G.R. List, *Eur. J. Lipid Sci. Technol.*, **109** (2007) 17-24.
[5] http://elaw.doeb.go.th/document_doeb/319_0001.pdf (Retrieved December 30, 2012).

CHARACTERIZATION AND CATALYTIC APPLICATION FOR METHYL ORANGE WET OXIDATION OF IRON-CONTAINING CLAY

Artit Ausavasukhi[1]*, Janya Mordeewang[1], Sukanya Sae-ngoe[1], Tanyarat Pattanate[1]
Tawan Sooknoi[2]

[1] Program in Applied Chemistry, Faculty of Sciences and Liberal Arts, Rajamangala University of Technology Isan, Nakhon Ratchasima 30000, Thailand
[2] Department of Chemistry, Faculty of Science, King Mongkut's Institute of Technology Ladkrabang, Bangkok 10520, Thailand

* Author for correspondence; ausavasukhi@gmail.com, Tel. +66 44 233000 ext. 4102, Fax. +66 44 233072

Abstract: Methyl orange decolorization by hydrogen peroxide was performed on local clay catalyst, a composite material that naturally contains crystalline magnetite (Fe_3O_4) and montmorillonite characterized by XRD. Under thermal treatment at 500 ^oC, the iron-containing clay catalyst was completely transformed into hematite (Fe_2O_3) and illite. Moreover, intensity of the ESR line at g = 2.3 which was characteristic of the Fe^{3+} ion in the iron oxide phase (Fe_2O_3) increased significantly. The weak signals were also visible on the ESR spectra which were attributed to Fe^{3+} ions in different coordination environments. From the catalytic results, the iron-containing clay treated at 500 ^oC provided a good performance toward total methyl orange decolorization (~ 65% decolorization at 50 ^oC). It is suggested that the dehydroxylation at the clay surface, which occurs by thermal treatment, plays an important role on the catalytic activity. Upon heating, the TGA/DTG profile of the catalyst sample showed the weight-loss at 450-700 ^oC which denoted the dehydroxylation of iron hydroxide and/or clay layer. Consistently, the FTIR result showed the decrease in O-H vibration at 3600-3200 cm^{-1} and 1630 cm^{-1}. The activate sites, i.e. FeO(OH)-like species, may be generated by reaction of H_2O_2 with Fe species formed by dehydroxylation of Fe_3O_4 in the clay structure.

1. Introduction

In the last decade, several systems based on heterogeneous Fenton-like catalyst (Fe-supported solids), such as iron oxides, zeolites, pillared clays, and alumina, have been investigated for use in environmental remediation processes [1-4]. Using such heterogeneous catalyst avoids the significant disadvantages of homogeneous Fenton: (i) the need for the removal of remaining iron ions after the treatment and (ii) a limited yield of reaction process due to the formation of stable iron-complexes [5-7]. Moreover, the heterogeneous catalyst can also be easily recycled, and all operations in the effluent treatment are significantly simplified if the solid catalyst is easy to handle.

Natural clays locally found in Thailand already contain iron that is present in the form of exchangeable iron cation and/or iron oxide minerals. Such incorporated iron within the clay structure makes them possible as Fenton-type catalyst designed for oxidation process. We have recently shown that the iron-containing clay is an efficient catalyst in the Fenton oxidation for methyl orange (MO) decolorization [8]. However, the understanding of the altering of iron species and/or phase transformation influenced their catalytic behavior during the reaction and also preparation by thermal treatment is unclear.

Therefore, this research will be studied the nature of the active species in the iron-containing clay catalyst used in the MO decolorization. For that purpose, the characterization of catalysts with various hydrothermal treatment has been undertaken using X-ray diffraction (XRD), Fourier transformed infrared spectroscopy (FTIR), Raman spectroscopy (Raman), electronspin resonance (ESR), and diffused reflectance-ultraviolet visible spectroscopy (DR-UV).

2. Materials and Methods

2.1 Catalyst preparation

The iron-containing clay sample was obtained from the SCG Chemicals. The sample material was brown color and was used as received. The sample was calcined at 100-700 ^oC for 5 hours. Hereafter, the catalysts will be designated as FeClay-(Temperature) according to their treatment temperature.

2.2 Catalyst characterization

X-ray fluorescence (XRF) was carried out for determining the elemental composition of the iron-containing clay. Powder X-ray diffraction (XRD) was employed for determining phase formation and crystallographic state. For TGA/DTG, the sample (10-15 mg) was heated from 50 to 900 ^oC under a flow of N_2 with a heating rate of 10 ^oC/min. FTIR spectra was acquired in the transmission mode at room temperature over the wavenumber range of 4000-650 cm^{-1}. The FT-Raman spectra was recorded using 1064 nm excitation from a Nd:YAG laser. Two thousand scans were accumulated at 8 cm^{-1} resolution. The UV-vis-diffuse reflectance spectra of the clay samples in the form of self-supporting pellets were recorded with $BaSO_4$ coated integration sphere. The ESR spectra was taken in the X-band at 20 ^oC and registered at microwave power 1 mW in the field range of 10-810 mT (one scan with a sweep time of 4 min).

2.3 Decolorization of methyl orange

The activity of this catalyst to decolorize methyl orange was tested by varying the parameters such as solution pH, initial concentration of H_2O_2, reaction time, and temperature [8].

3. Results and Discussion

3.1 Characterization of the iron-containing clay

From XRF result, the parent clay possesses a relatively high wt.% of Fe (~ 10 %), which makes it ideal as Fenton catalyst. The XRD patterns of the parent and the thermally treated iron-containing clay are shown in Figure 1.

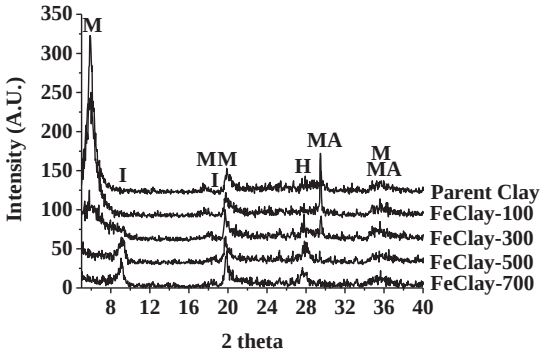

Figure 1. XRD patterns of the treated-clay (M = Montmorillonite, I = Illite, H = Hematite, MA = Magnetite).

The parent clay shows the strong diffraction peaks at 5.9°, 17.6°, 19.9° and 35.6° corresponding to montmorillonite phase [9]. While, the diffraction peaks at 29.5° and 35.6° are assigned to the magnetite (Fe_3O_4 or $FeO{\cdot}Fe_2O_3$) crystallite [10]. The presence of iron species may include; (i) iron species distributing onto the surface of montmorillonite and/or (ii) iron species present in the interlayer.

After thermal treatment (> 300 °C), the treated-clay shows the shift peak at 5.9° to 9.1° and peak at 17.6° to 18.3° (lower d-spacing). This is presumably due to a removal of interlayer water molecules as evidenced by TGA/DTG (Figure 2) and FTIR (Figure 3).

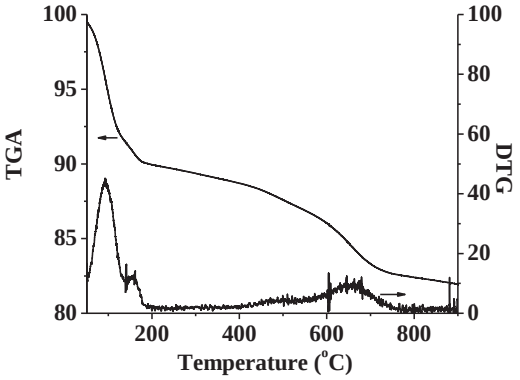

Figure 2. TGA/DTG thermogram of the parent clay.

The peaks at 9.1° and 18.3° indicate the formation of illite [11], as a result of thermal treatment. Moreover, the magnetite structure was altered after thermal treatment (> 300 °C). The new peak at 27.8° was appeared indicating the formation of hematite (Fe_2O_3) [12]. However, no significant change of XRD pattern can be observed after treating at temperature greater than 500 °C.

The oxidation of iron(II) to iron(III) (particularly iron present in the interlayer) may lead to a change in the total layer charge and consequently d-spacing layer. This result indicates that the oxidation may well promote a phase transformation of both iron species and clay.

From Figure 2, the weight-loss at 60-180 °C which corresponds to desorption of the physisorbed water can be observed [13]. While the weight-loss at 450-700 °C denotes the dehydroxylation of iron hydroxide and/or clay layer [13]. Consistent with the FTIR results (Figure 3) that a decrease in O-H vibration at 3600-3200 cm^{-1} and 1630 cm^{-1} can be observed after the thermal treatment.

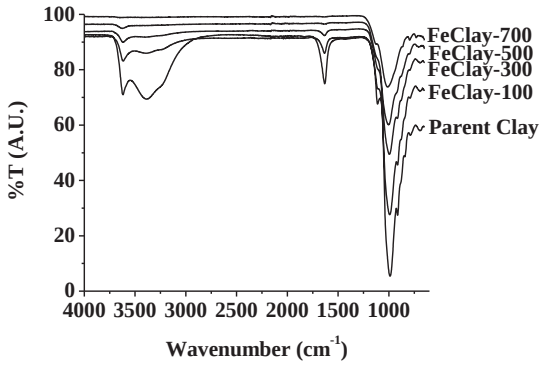

Figure 3. FTIR spectra of the treated-clay.

The formation of Fe_2O_3 after thermal treatment at 500 °C is further confirmed by the Raman results (Figure 4) showed that the characteristic features around 247, 293, 412, 503, 613, and 702 cm^{-1} [14].

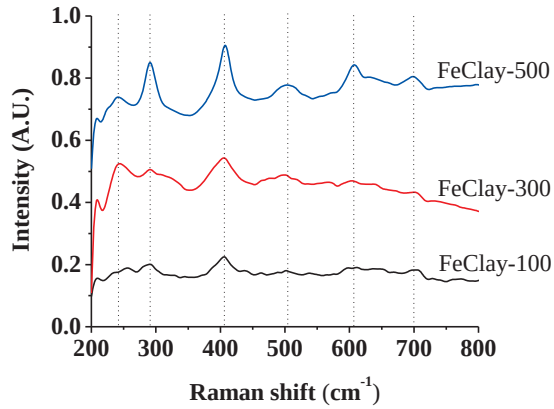

Figure 4. Raman spectra of the treated-clay.

The characteristic peaks at 298, 319, 540, and 668 cm^{-1} corresponding to Fe_3O_4 [14] cannot be observed over FeClay-100, although the XRD of FeClay-100

shows a strong diffraction peak assigned to the Fe_3O_4 (Figure 1). This is presumably because magnetite is easily prone to oxidation when exposed to heating or laser irradiation (from Raman analysis) [15].

In conclusion, the oxidation of iron species and the removal of water molecules by desorption of physisorbed water and dehydroxylation may lead to the phase transformation of the iron-containing clay.

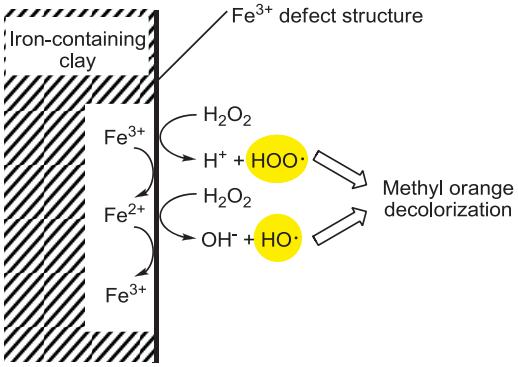

Scheme 1. Catalytic decolorization of the iron-containing clay.

3.2 Catalytic activity for MO decolorization

From Figure 5, it was observed that concentration of MO decreased after the additional of the iron-containing clay, particularly in the reaction with H_2O_2. This is due to the fact that loading H_2O_2 over the iron-containing catalyst can generate the hydroxyl (•OH) and perhydroxy (•OOH) radicals (Scheme 1). Such radicals can readily decompose the azo dye leading to decolorization of MO. This confirms that the iron-containing clay sample can readily provide the catalytic activity for Fenton-like reactions.

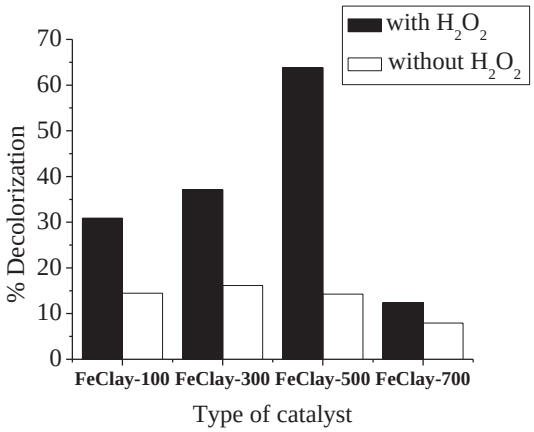

Figure 5. Effect of H_2O_2 on % MO decolorization catalyzed by various treated-clay.
Reaction condition: $[MO]_o$ = 60 mg/L, Catalyst = 50 mg, $[H_2O_2]_o$ = 0.5 mL, Temperature = 50 °C, pH = 3, Volume of MO = 250 mL, Reaction time = 30 min.

Moreover, it is found that FeClay-500 provides a relative higher % decolorization of MO (Figure 5). It is expected that the formation of active iron species by thermal treatment would play important role for MO decolorization. In the case of the FeClay-700, MO decolorization decreases with rise in treatment temperature. This is presumably due to the further dehydroxylation of clay under high thermal treatment at 700 °C leading to the lost of surface area of catalyst. This is consistent with the TGA/DTG (Figure 2) and FT-IR results (Figure 3) that show the dehydroxylation of clay layer.

In evaluating the activity of different iron minerals, the efficiency of the catalysts decreased in the sequence magnetite > hematite > goethite [16-17]. One can expect that if the iron species mostly present in iron oxide minerals it will be able to dramatically decolorize MO when using iron-containing clay treated with low temperature (FeClay-100 or FeClay-300). Conversely, the FeClay-500 provides a relative higher % decolorization of MO. It is suggested that the activate sites, i.e. FeO(OH)-like species, may be generated by reaction of H_2O_2 with Fe species formed by dehydroxylation of Fe_3O_4 in the clay structure. The formation of iron active site can be evidenced by ESR (Figure 6) and DR-UV (Figure 7).

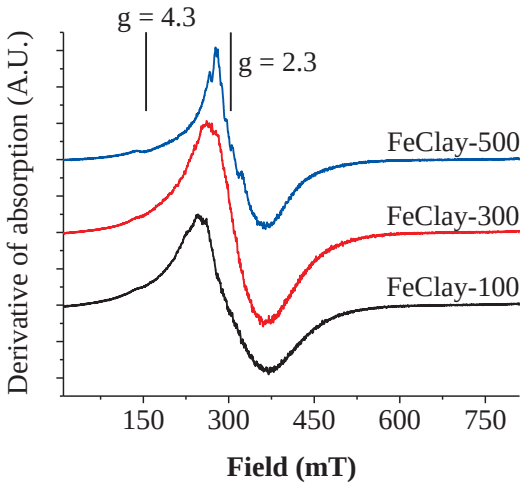

Figure 6. ESR signal of the treated-clay.

Figure 6 reveals the presence of two characteristic Fe^{3+} signals in iron-containing clay to values of g = 4.3 and 2.3. The signal at g = 4.3 is assigned to the presence of isolated Fe^{3+} [18-21] in tetrahedral or octahedral coordination, which in the case of the clay minerals corresponds to the iron located in the interior of the clay sheets (iron substituting aluminum in the octahedral layers). Therefore, we can suggest that the active iron species partially present in the interlayer of clay (due to the small signal at g = 4.3), while mostly present in iron oxide minerals generated by dehydroxylation.

Additionally, the signal at g = 2.3 is associated to the presence of clusters of iron [18-20]. Experimentally, the intensity of the ESR line at g = 2.3 increased significantly when the parent clay was thermal treatment due to the transformation of Fe_3O_4 to Fe_2O_3. It is interesting to note that the weak signals were also visible on the ESR spectra which were attributed to Fe^{3+} ions in different coordination

environments (FeClay-500) (Figure 6). This is consistent with the observed the DR-UV spectra recorded for the treated-clay (Figure 7).

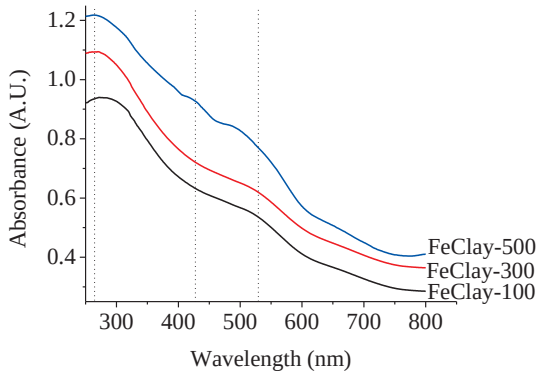

Figure 7. DR-UV spectra of the treated-clay.

In the spectrum of the FeClay-100 and FeClay-300 only two absorption bands are observed at about λ=263 nm, corresponding to octahedral Fe^{3+} substituting for Al^{3+} [22], and at about λ=525 nm, corresponding to larger particles of Fe_2O_3 aggregates [23]. Interestingly, the additional signal of the 425 nm band ascribed to the smaller and larger oligomeric octahedrally coordinated Fe^{3+} species [23], can be observed over the FeClay-500. This is the further evidenced supporting the formation of iron active site generated by the dehydroxylation under thermal treatment at 500 ^{o}C.

From the above results, it is suggested that the active iron species was successfully generated into surface of the iron-containing clay and was an amorphous after 500 ^{o}C treatment. This is consistent with the Zhang's report [24]. The structure of the activate iron species in the montmorillonite was an amorphous FeO(OH)-like species after calcining at 500 ◦C. Such iron active species generated by dehydroxylation reaction at high temperature are suggested to play a decisive role on the catalytic activity towards MO decolorization. Moreover, the catalytic behavior of the iron-containing clay is reproducible in consecutive experiments without a remarkable drop in the process efficiency, which indicates the absence of significant deactivation of the catalyst due to small loss of iron.

4. Conclusions

In this research, catalytic activity of the Fenton-like catalyst iron-containing clay towards successful decolorization of MO. Among the iron-containing catalyst, the sample treated at 500 ^{o}C was found to provide the highest activity. The formation of such iron active species by dehydroxylation reaction is suggested to play a decisive role on the catalytic activity.

Acknowledgements

This work was financially supported by the Thailand Research Fund (Grant No. MRG-5580065).

References

[1] J.H. Ramirez, F.J. Maldonado-Hodar, and A.F. Perez-Cadenas, *Appl. Catal. B: Environ.* **75** (2007) 312-323.
[2] G. Calleja, J.A. Melero, F. Martinez, and R. Molina, *Water Res.* **39** (2005) 1741-1750.
[3] M. Noorjaha, V.D. Kumari, M. Subrahmanyam, and L. Panda, *Appl. Catal. B: Environ.* **57** (2005) 291-298.
[4] J. Feng, X. Hu, and P.L. Yue, *Water Res.* **40** (2006) 641-646.
[5] J. Herney-Ramirez, M.A. Vicente, and L.M. Madeira, *Appl. Catal. B: Environ.* **98** (2010) 10-26.
[6] M. Neamtu, C. Zaharia, C. Catrinescu, A. Yedile, M. Macoveanu, and A. Kettrup, *Appl. Catal. Environ.* **48** (2004) 287-294.
[7] E.V. Kuznetsova, E.N. Savinov, L.A. Vostrikova, and V.N. Parmon, *Appl. Catal. B: Environ.* **51** (2004) 165-170.
[8] http://paccon2011.swu.ac.th/(Retrieved December 4, 2012). (J. Deepakwean, W. Kingkan, and A. Ausavasukhi, Decolorization of methyl orange using iron-containing Thai clay)
[9] M.N. Timofeeva, S.Ts. Khankhasaeva, S.V. Badmaeva, A.L. Chuvilin, E.B. Burgina, A.B. Ayupov, V.N. Panchenko, and A.V. Kulikova, *Appl. Catal. B: Environ.* **59** (2005) 243-248.
[10] K.C. Kim, E.K. Kim, J.W. Lee, S.L. Maeng, and Y.S. Kim. *Cur. Appl. Phys.* **8** (2008) 758-760.
[11] R.M. GARRELS, *Clay Clay Miner.* 32 (1984) 161-166.
[12] A.P. Roberts, Q. Liu, C.J. Rowan, L. Chang, C. Carvallo, J. Torrent, and C.S. Horng, *J. Geophys. Res.* 111 (2006) B12S35 1-16.
[13] P. Yuan, F.A.Bergaya, Q. Taoa, M. Fan, Z. Liu, J. Zhu, H. He, and T. Chen, *J. Coll. Int. Sci.* **324** (2008) 142-149.
[14] M.A. Legodi, and D. de Waal, *Dyes Pigments* **74** (2007) 161-168.
[15] C. Guo, Y. Hu, H. Qian, J. Ning, and S. Xu, *Mater. Charact.* **62** (2011) 148-151.
[16] R. Matta, K. Hanna, and S. Chiron, *Sci. Total Environ.* **385** (2007) 242-251.
[17] S. Lee, J. Oh, and Y. Park, *Bull. Korean Chem. Soc.* **27** (2006) 489-494.
[18] A. Montenero, K. Suzuki, T. Enoki, S. Vittorio, M. Dresselhaus, K. Koga, M. Endo, and N. Shindo, *Synthetic Met.* **55** (1993) 3736.
[19] A. Kucherov, and M. Shelef, *J. Catal.* **195** (2000) 106.
[20] D. Loveridge, and S. Parke, *Phys. Chem. Glasses.* **12** (1971) 19.
[21] E. Gue´lou, J. Barrault, J. Founier, and J.-M. Tatiboue¨t, *Appl. Catal. B:Environ.* **44** (2003) 1.
[22] M.N. Timofeeva, S.T. Khankhasaeva, Y.A. Chesalov, S.V. Tsybulya, V.N. Panchenko, and E.T. Dashinamzhilova, *Appl. Catal. B:Environ.* **88** (2009) 127-134
[23] S. Caudo, G. Centi, C. Genovese, and S. Perathoner, *Appl. Catal. B:Environ.* 70 (2007) 437-446.
[24] S. Zhang, S. Liang, X. Wang, J. Long, Z. Li, and L. Wu, *Catal. Today* **175** (2011) 362-369.

OPTIMIZATION OF ETHANOLYSIS OF *Jatropha curcas* OIL: A COMPARATIVE STUDY ON CATALYTIC ACTIVITY OF NaOH AND KOH

Sasiwimol Wootthikanokkhan[1*], Tapparath Leelasattarathkul[1], Auamporn Timabud[1]

[1] Rajamangala University of Technology Krungthep/Department of Chemistry, Sathorn, Bangkok, Thailand

[*] Author for correspondence; E-Mail: sasiwimol.w@rmutk.ac.th, Tel. +66 089 4563981, Fax. +66 22879600 ext 1204, 1205

Abstract: In the past few years, ethyl ester biodiesel has been increasingly attended because some agricultural crops can be used as raw materials. In several countries including Thailand, *Jatropha curcas* oil is one of the promising feed stocks for biodiesel production. The objective of this study was to determine the optimum condition (based on the highest ethyl ester yield) for ethanolysis of crude *Jatropha curcas* oil. The reaction variables used in the optimization were catalyst type (NaOH and KOH), catalyst concentration (0.5-1.5 wt.%), ethanol to oil molar ratio (6:1-15:1), reaction temperature (55-65°C) and reaction time (5-100 min). The results showed that the catalytic performance of NaOH was similar to KOH. Conversion of crude *Jatropha curcas* oil into ethyl ester improved when the molar ratio of ethanol to oil and catalyst concentration were increased. However, beyond the optimum values, ethyl ester yield was decreased. The highest ethyl ester yield was (97.8%) obtained by using 12:1 ethanol to oil molar ratio, 1 wt.% NaOH catalyst concentration, and the reaction temperature of 65°C. The reaction was completed within 1 h. Determination of the produced ethyl ester quality indicated that its properties met the Thai biodiesel (B100) standard and international standard ASTM D6751-07b.

1. Introduction

Due to positive economic changes in many countries, energy consumption has been largely raised and this leads to continued increase in petroleum-derived fuel price. Moreover, the subsequent exhaust emissions from fossil fuel burning have also been considered to be one factor contributing to the global climate change. For these reasons, several researches have attempted to explore various alternative renewable fuels. Compared to conventional diesel fuels, biodiesel has considerably properties including high cetane number, high flash point, no sulfur or carcinogenic polyaromatic compounds [1].

Biodiesel production is usually carried out by transesterification reaction or alcoholysis of triglyceride with alcohol under catalytic condition to form alkyl esters and a byproduct, glycerin. The transesterification performs well in the base catalytic system, where homogeneous alkaline catalysts such as NaOH or KOH are normally used in commercial due to fact that these chemicals are inexpensive and easy to handle. Types of alcohol also play i.e, reactivity of ethanol is relatively low as compared to that of methanol. Therefore, the former system requires longer times to complete the reaction [2]. Nevertheless, ethanol has several advantages such as superior dissolving power of vegetable oils, low toxicity, and a possibility of production from agricultural renewable resources.

Besides, trend in utilization of non-edible oils as raw materials in biodiesel production has been increased owing to the abundant feedstock availability. *Jatropha curcas*, non-edible oil, is considered to be a potential feedstock for biodiesel production by many researchers [3, 4]. The *Jatropha curcas* oil has valuable properties such as low acidity, good stability (compared with soybean oil), low viscosity (compared with castor oil) and better cold properties (compared with palm oil) [5].

The aim of this study was to investigate the effects of ethanolysis variables on properties and yields of the produced biodiesel. Optimum ethanolysis condition for producing biodiesel from crude *Jatropha curcas* oil is also of our interest.

2. Materials and Methods

2.1 Materials

The *Jatropha curcas* seeds were purchased from Thai Jatropha Co., Ltd., Pathum Thani Province. All chemicals were of analytical grade.

2.2 Extraction of oil

Extraction of crude *Jatropha curcas* oil was carried out using a screw press oil expeller. After filtering, the extracted oil was viscous, clear, and yellow. The chemical and physical properties of the oil are illustrated in Table 1.

2.3 Ethanolysis

Ethanolysis of crude *Jatropha curcas* oil was performed in a 250 ml round bottom flask equipped with condenser and heating system. The mixture was continuingly stirred at a constant rate of 600 rpm until the reaction completion. Before starting the reaction, 40 g of crude *Jatropha curcas* oil was preheated in the reaction flask to the desired temperature (± 2°C). The ethoxide solution, prepared freshly to maintain the catalytic activity and to prevent moisture absorbance, was slowly added to the crude oil. At this point, the

measurement of time was started. When the reaction completed, the mixture was stranded in a separatory funnel to allow it cooling down before adding 25% pure glycerin (based on the weight of oil) [6]. After two layer formation, an upper phase containing ethyl esters and a lower phase consisting of glycerin, the ester layer was then separated and washed with distilled water at 60°C several times until the draining water was neutralized. Finally, the remained water in the mixture was removed by evaporating at 110°C.

2.4 Determination of the ethyl ester content

The ethyl ester contents were determined by gas chromatography (Agilent 6890N) which was equipped with a flame ionization detector and a capillary column packed with crosslinked polyethylene glycol (HP-INNOWax, 25m x 0.20mm x 0.2µm). Determination was performed at the oven temperature of 200°C, a flow rate of carrier gas (He) at 0.2 ml/min, split ratio at 500:1, and the temperature of injector and detector was kept at 250°C. In this analysis, the n-heptane was used as solvent in preparation of sample solution and methyl heptadecanoate was used as the internal standard. The ethyl esters were identified by comparing their retention times to those of standard ethyl esters.

2.5 Properties of *Jatropha curcas* ethyl esters

The properties of *Jatropha curcas* ethyl esters were determined by standard methods.

3. Results and discussion

3.1 Properties of crude *Jatropha curcas* oil

Table 1 shows the chemical and physical properties of the extracted crude *Jatropha curcas* oil. The viscosity of the crude oil (at 40°C) was about 10 times higher than the diesel fuel viscosity (1.9-4.1 mm^2/s). For this reason, the oil is required chemical modification into smaller molecules such as esters before use as fuel. Analysis of the crude *Jatropha curcas* oil revealed that it composed of fatty acids containing 16-20 carbon atoms, which are in consistent with the previous reports on crude *Jatropha curcas* oil [3-5, 7]. The calculated molecular weight of triglyceride in crude *Jatropha curcas* oil was 871.48 g/mol. Determination of free fatty acid and water contents revealed that this crude *Jatropha curcas* oil could be used to produce biodiesel via alkaline catalytic reaction.

3.2 Effect of variables on the ethanolysis

3.2.1 Effect of catalyst type

Initially, type of catalyst for ethanolysis of crude *Jatropha curcas* oil was studied. According to the report of Rashid and Anwar [8], transesterification of crude oil under hydroxide catalytic condition yields more esters than the use of methoxide catalysts, so two commonly used catalysts, NaOH and KOH, were employed.

Table 1: Properties of crude *Jatropha curcas* oil

Property	**Method**	**Crude *Jatropha curcas* oil**
Kinematic viscosity at 40°C (mm^2/s)	ASTM D445-06	35.41
Water content (wt.%)	AOAC(1990), 984.20	0.0589
Free fatty acid content (as oleic acid) (wt.%)	AOAC(2000), 940.28	1.50
Fatty acid composition (%)[a]	AOAC (2005), 963.22, 969.33	
(i) Palmitic acid		13.10
(ii) Palmitoleic acid		0.82
(iii) Stearic acid		5.86
(iv) Oleic acid		36.19
(v) Linoleic acid		32.66

[a]Other fatty acids (linolenic and arachidic acids) were found to be < 0.30%

From the transesterification mechanism, alkaline catalyst involves formation of the ethoxide. Catalyst concentrations used for the reaction are generally calculated from the weight percentage on the oil weight basis. However, at the same given weight, the number of hydroxide moles between both catalysts is not equal since NaOH molecular weight is lower than that of KOH (40.0 g/mol and 56.1 g/mol, respectively). Therefore, in this study, both NaOH and KOH were used at equivalent hydroxide moles which were calculated based on 1 wt.% of NaOH.

Illustration in Figure 1 is a comparative study of ethanolysis of crude *Jatropha curcas* oil using NaOH and KOH. Considering the resulting ethyl esters conversed at various times during the reaction proceeding, ethanolysis reaction catalyzed by both catalysts rapidly proceeded within the first 5 min giving >90 wt.% of ethyl esters. After that, the ethyl ester content gradually increased with time and reached a plateau. With comparison between the ethyl ester contents obtained by using NaOH catalyst and those obtained by using KOH catalyst, it reveals no significant difference. This means that, in this study, type of basic catalyst has no effect on the ethanolysis. However, it is worth mentioning that cost of the NaOH is lower, and thus the above chemical was selected for further study.

3.2.2 Effect of catalyst concentration

At the catalyst concentration of 0.5 wt.%, less than 20 wt.% ethyl ester was obtained. This implied that the catalyst amount was insufficient for ethanolysis completion. When increasing the catalyst concentration into 1.0 wt.%, with the rising of the reaction rate, yielding was observed in increased amounts of ethyl esters. As seen in Figure 2, the maximum yield of ethyl esters was obtained when 1.0 wt.% NaOH was employed. The decrease in ethyl ester content occurred when 1.5 wt.% catalyst was used. One explanation is that the increased amount of catalyst enhanced saponification reaction where NaOH, a catalyst for transesterification, was a reactant.

Accordingly, the appropriate catalyst concentration was at 1 wt.% which was similar to the observation on ethanolysis of used frying oil [6]. The

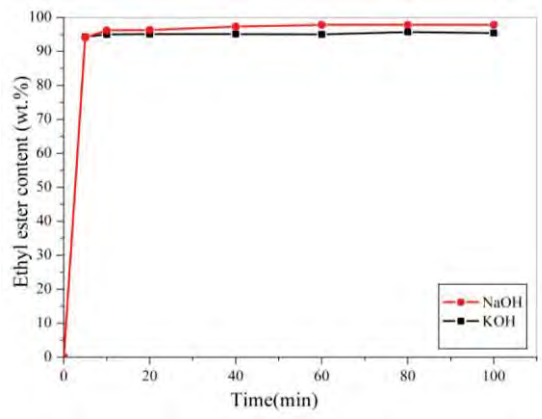

Figure 1. Effect of catalyst type on ethyl ester yield using ethanol to oil molar ratio of 12:1 and reaction temperature 65°C.

findings from this study and previous reports [6, 9] suggest that catalyst concentration as well as catalyst type is variables that are needed to be considered in each crude oil type for improvement of ethyl ester yields.

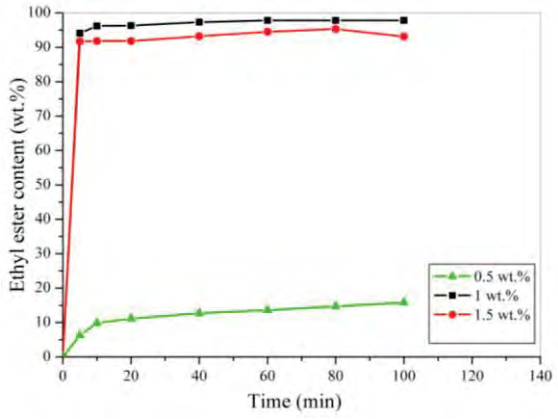

Figure 2. Effect of catalyst concentration on ethyl ester yield using ethanol to oil molar ratio of 12:1 and reaction temperature 65°C.

3.2.3 Effect of molar ratio

In this study, the molar ratio of ethanol to oil was varied between 6:1, 9:1, 12:1 and 15:1. Firstly, the ethanol to oil molar ratio at 6:1, which is a commonly used molar ratio in methanolysis for biodiesel production, was tested. As seen in Figure 3, at this molar ratio ethanolysis was not completed, only small amount of ethyl esters was obtained although the reaction time was expanded into 100 min. Conversion of crude oil into ethyl ester satisfactorily improved when the molar ratio of ethanol to oil was increased from 6:1 into 12:1. However, at ethanol to oil molar ratio of 15:1, excess ethanol in the reaction promoted dissolving of glycerin in the ethyl ester fraction leading to a more difficult phase separation of glycerin and ethyl esters, subsequently decrease of the ester content. From the results, it was found that the appropriate molar ratio of ethanol to oil was 12:1.

3.2.4 Effect of reaction temperature

From the previous report, at room temperature transesterification rate was slow and yielded only small amount of esters [6, 9]. In this study, the effect of reaction temperature between 55°C and 65°C on ester conversions was determined. The results showed that production of ethyl esters at temperature 65°C was higher than at 55°C and the equilibrium was reached within 5 min after the reaction was started. The result implied that ethanolysis proceeded very quickly at this reaction temperature (Figure 4). This indicated that reaction temperature has influenced on the reaction rate and ethyl ester yield. Theoretically, using high reaction temperature can facilitate reduction of crude oil viscosity which significantly improves the interaction between triglyceride molecule and ethanol. Therefore, the appropriate reaction temperature for ethyl ester production from crude *Jatropha curcas* oil was at 65°C.

From the results, the optimum condition for ethanolysis of crude *Jatropha curcas* oil was ethanol to oil molar ratio at 12:1, 1 wt.% NaOH, reaction temperature at 65°C, and reaction time at 60 min. At this condition, the ethyl ester content was achieved 97.8 wt.%.

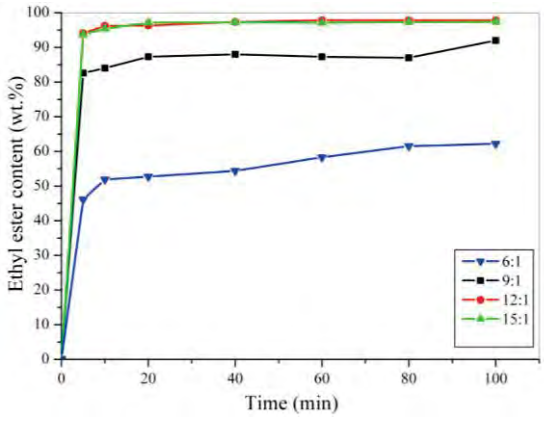

Figure 3. Effect of ethanol to oil molar ratio on ethyl ester yield using catalyst concentration 1 wt.% and reaction temperature 65°C.

3.3 Properties of *Jatropha curcas* ethyl esters

The properties of *Jatropha curcas* ethyl esters were comparable to those of the Thai biodiesel (B100) and ASTM D6751-07b (Table 2) confirming that the ethyl ester biodiesel can be practically used in standard diesel engines without consequent problems.

As expected, the viscosity of ethyl esters was lower than the viscosity of crude *Jatropha curcas* oil. Viscosity value is indicative of ethanolysis completion and high viscosity value implies for high contents of triglycerides in the mixture. Determination of

triglycerides content in the biodiesel revealed that at the optimum condition, triglycerides conversion into ethyl esters was completed. Interestingly, the viscosity value is lower than the maximum value of the

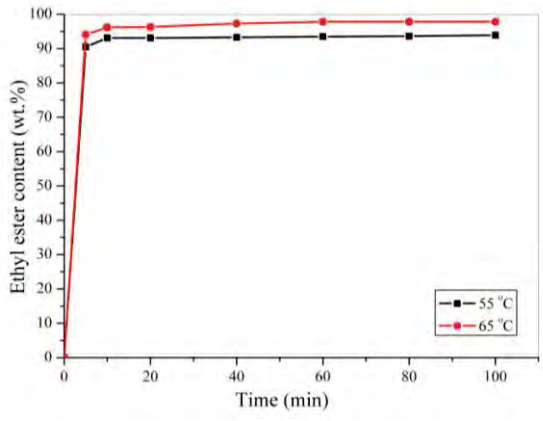

Figure 4. Effect of reaction temperature on ethyl ester yield using ethanol to oil molar ratio of 12:1 and catalyst concentration 1 wt.%.

biodiesel B-100 standard. This is most likely due to the nature of the raw material used. One possible explanation is that the seed oil obtained from *Jatropha curcas* cultivated in Thailand contains appropriate ranges of fatty acid contents for complete conversion into ethyl esters. This indicated that selection of raw materials for ethyl ester production also needs to be considered for fatty acid contents in vegetable oil.

Table 2: Properties of *Jatropha curcas* ethyl esters

Property	Limits		Ethyl esters
	ASTM D 6751-07b	Thai specification	
Kinematic viscosity at 40°C (mm^2/s)	1.9-6.0	3.5-5.0	4.811
Triglyceride (wt.%)	-	0.20 max	0.00
Flash point (°C)	130 min	120 min	> 120
Free glycerin (wt.%)	0.02 max	0.02 max	0.00
Acid number (mg KOH/g)	0.50 max	0.50 max	0.37
Cloud point (°C)	Report	-	8
Cold filter plug point (°C)	-	-	1
Pour point (°C)	-	-	0
Gross heat of combustion (MJ/kg)	-	-	37.9

Analysis of free glycerin and acid number is aimed to investigate completion of the separation step. It was found that free glycerin, a by-production from the transesterification reaction, could be completely removed by allowing the mixture stranded for layer separation before washing with water. In this study, biodiesel production was carried out by base catalyzed transesterification so the acid presented in the product would not result from the production method but instead from free fatty acids in the crude oil and partly from hydrolysis of triglyceride which was only at low amount. The cetane number is one of most commonly cited indicators of diesel fuel quality. In this work, ASTM D6890-10a was applied and the result of derived cetane number was at 70.3 min. In addition, the gross heat of combustion obtained in this study was consistent with that of *Jatropha curcas* methyl esters in the previous report [10]. For using as information when refers in different areas with different temperature, three tests were used to measure the cold flow properties of fuels for diesel engine including cloud point, cold filter plug point, and pour point. The results of cloud point, cold filter plug point, and pour point confirmed that ethyl ester biodiesel can be used as fuel for diesel engine in Thailand.

4. Conclusions

Crude *Jatropha curcas* oil can be effectively used to produce biodiesel by NaOH-catalyzed ethanolysis. The optimum condition at the ethanol to oil molar ratio of 12:1, 1 wt.% of NaOH, the reaction temperature of 65°C and the reaction time 60 min gave high purity of biodiesel where its properties were comparable to Thai biodiesel (B100) specifications and ASTM D6751-07b. Besides, this biodiesel exhibited characteristics that shed the light on replacement of fossil diesel fuel. However, further research is required for engine performance.

Acknowledgements

This research was financial supported by Rajamangala University of Technology Krungthep.

References

[1] A.K. Domingos, E.B. Saad, H.M. Wilhelm and L.P. Ramos, *Bioresour. Technol.* **99** (2008) 1837-1845.
[2] M. Černoch, M. Hájek and F. Skopal, *Bioresour. Technol.* **101** (2010) 1213-1219.
[3] N.C.O. Tapanes, D.A.G. Aranda, J.W. Carneiro de Mesquita and O.A.C Antunes, *Fuel* **87** (2008) 2286-2295.
[4] J.S.D. Oliveira, P.M. Leite, L.B.D. Souza,V.M. Mello, E.C. Silva, J.C. Rubim, S.M.P. Meneghetti and P.A.Z. Suarez, *Biomass Bioenergy* **33** (2009) 449-453.
[5] M.Y. Koh and T.I.M. Ghazi, *Renew Sustain Energy Rev.* **15** (2011) 2240-2251.
[6] J.M. Encinar, J.F. Gonzalez and A. Rodriguez-Reinares, *Fuel Process. Technol.* **88** (2007) 513-522.
[7] S. Jain and M.P. Sharma, *Renew Sustain Energy Rev.* **14** (2010) 3140-3147.
[8] U. Rashid and F. Anwar, *Fuel* **87** (2008) 265-273.
[9] L.C. Meher, V.D.D. Dharmagadda and S.N. Naik, *Bioresour Technol.* **97** (2006) 1392-1397.
[10] S.Y. No, *Renew Sustain Energy Rev.* **15** (2011) 131-149.

REMOVAL OF OLEIC ACID IN SOYBEAN OIL USING $KHSO_4$ SUPPORTED ON RICE HUSK SILICA

Pastraporn Kijsiri[1], Jintapa Tamseecram[1], Jatuporn Wittayakun[2], Nuttinee Supamathanon[1*]

[1]Department of Applied Chemistry, Faculty of Sciences and Liberal Arts, Rajamangala University of Technology Isan, Muang, Nakhon Ratchasima, 30000 Thailand
[2]School of Chemistry, Institute of Science, Suranaree University of Technology, Muang, Nakhon Ratchasima 30000 Thailand

[*] Nuttinee Supamathanon; E-Mail: nsupamathanon@gmail.com, Tel. +66 044-230000 ext.4313, Fax. +66 044-233072

Abstract: Oils with high content of free fatty acid (FFA) such as waste cooking oil or the other vegetable oils plays an important role as a feedstock for biodiesel production. Pre-treatment of these oils can be carried out by esterification with methanol in the presence of acid catalyst before alkaline catalyzed transesterification. In this work oleic acid as FFA present in soybean oil was investigated by esterification with methanol on $KHSO_4$ supported rice husk silica catalyst ($KHSO_4$/RH-SiO_2). The catalyst was characterized by XRD, FTIR and nitrogen adsorption analysis. The parameters for esterification including molar ratio of methanol to oil, amount of catalyst and reaction time were studied to obtain the optimum condition for maximum conversion of FFA. Conversion of FFA was determined by titration method. It was found that $KHSO_4$/RH-SiO_2 catalyst gave the maximal conversion of oleic acid about 98% in the reaction at 70 °C after 2 h, methanol to oil molar ratio of 10:1 and catalyst loading 3 w/w%.

1. Introduction There are various types of feedstock for biodiesel production [1]. Waste cooking oil and oils from seeds of non-edible plants such as Jatropha or rubber are interesting because they are cheaper than the edible vegetable oil. However, quality of those oils is low due to high content of free fatty acids (FFA) which are responsible for low biodiesel yield. The FFA favours saponification or hydrolysis reaction which are side reactions of transesterification in the presence of alkaline catalysts. Thus, it is necessary to reduce the amount of FFA in the biodiesel feedstock.

One of the methods to reduce FFA in the oils is esterification which converts FFA to esters. In general, homogeneous acid catalysts such as H_2SO_4 or HCl are used but they are difficult to remove from the reaction mixture or product and related to serious environment and corrosion problems [1-3]. Therefore, heterogeneous acid catalysts have been investigated to avoid those problems. The examples include various type of zeolites such as ZSM-5 (MFI), mordenite (MOR), faujisite (FAU) and beta (BEA) [4-6], mesoporous materials such as MCM-41, aluminium supported on MCM-41 (Al-MCM-41)[7], $Fe_2(SO_4)_3$ supported on silica [8] or active carbon [9].

Potassium bisulphate ($KHSO_4$), an acidic salt has been used in many organic reactions [10]. It can be used as solid catalyst under homogeneous and heterogeneous condition. Recently, it was loaded on microporous silica to generate Brönsted acid sites and enhanced the rate of transesterification of castor oil which has high content of Ricinolic acid (about 89.5%) [11, 12].

In this work $KHSO_4$ was supported on silica from rice husk and the obtained catalyst was characterized by X-ray diffraction (XRD), Fourier transform infrared spectroscopy (FTIR) and N_2 adsorption-desorption analysis. Finally, it was used as a catalyst in a batch reactor for esterification to reduce oleic acid, the main FFA in the soybean oil. Influence of reaction time, catalyst amount and molar ratio of methanol to oil on the conversion of FFA were investigated.

2. Materials and Methods

2.1 Materials

Rice husk silica (RH-SiO_2) was extracted from rice husk silica by a method in the literature [13] and used as a catalyst support for potassium bisulfate ($KHSO_4$). Oleic acid ($C_{18}H_{34}O_2$) as FFA was added in a soybean oil to prepare soybean oil with 5 wt.% oleic acid for esterification. Sodium hydroxide (NaOH), ethanol (C_2H_5OH) and phenolphthalein was used for determination of the acid number.

2.2 Catalyst preparation

The catalyst was prepared by a method by Goswami [12]. RH-SiO_2 (40 g) was impregnated with an aqueous solution containing 144 mmol $KHSO_4$. The mixture was dried in a hot air oven at 150 °C for 1 day.

2.3 Catalyst characterization

The catalyst was characterized by XRD (Bruker, D5005) using nickel-filtered Cu Kα radiation. Data were collected from 5 to 50° with a step size of 0.02. FTIR spectra were obtained from a Perkin Elmer Spectrum 100 connected with Universal ATR (UATR). Surface area of the catalyst and RH-SiO_2 by Brunauer-Emmet-Teller (BET) method were determined by N_2 adsorption-desorption analysis (Bel-Japan, Bel Sorp mini II). Prior to the adsorption measurement, the samples were degassed at 300 °C for 5 h.

2.4 Esterification of oleic acid with methanol

A reaction mixture contained 8 g of the sample oil, 0.4 g of catalyst and methanol in a 50-mL of round-bottom flask was fitted with a water-cooled condenser and heated by circulating water bath with controlled temperature at 70 °C (external) under magnetic stirring. The molar ratio of methanol to oil was varied in the range of 5:1 to 40:1. After the study period (1 to 5 h), the catalyst was removed from the reaction mixture by centrifugation and the excess methanol was removed by a rotary evaporator.

Acid value of the initial sample oil and the reaction mixture product was determined by titration method [14].The percentage conversion of oleic acid (FFA conversion, %) was calculated from difference between the acid value of the sample oil at the beginning (AV_0) and of the reaction mixture product at the final (AV_f) in the equation below:

$$\text{FFA Conversion, \%} = [(AV_0 - AV_f)]/AV_0] \times 100$$

3. Results and Discussion

3.1 Catalyst characterization

Figure 1 shows XRD pattern of $KHSO_4$, RH-SiO_2 and $KHSO_4$/RH-SiO_2 catalyst. The pattern of RH-SiO_2 indicated an amorphous phase. The pattern of $KHSO_4$/RH-SiO_2 catalyst did not show any peaks of $KHSO_4$. It indicated that the $KHSO_4$ had a good dispersion on RH-SiO_2.

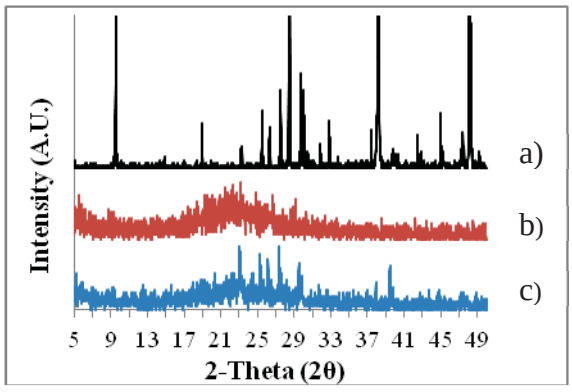

Figure 1. XRD patterns of $KHSO_4$ (a), RH-SiO_2 (b) and $KHSO_4$/RH-SiO_2 catalyst (c)

FTIR spectra of $KHSO_4$, RH-SiO_2 and $KHSO_4$/RH-SiO_2 catalyst are shown in Figure 2. $KHSO_4$ spectra showed the main peaks at 1283, 1165, 1069, 1001, 882 and 847 cm^{-1} similar to the values in the literature [12]. After loading $KHSO_4$ on RH-SiO_2, the peaks of $KHSO_4$ were not observed due to low loading.

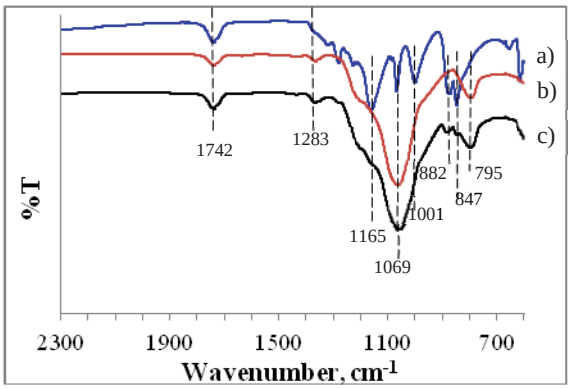

Figure 2. FTIR spectra of $KHSO_4$ (a), RH-SiO_2 (b) and $KHSO_4$/RH-SiO_2 catalyst (c).

The textural properties of the catalyst were summarized in Table 1. The surface area of RH-SiO_2 was 122 m^2/g and decreased to 19 m^2/g after loaded with $KHSO_4$. It is explained that $KHSO_4$ dispersed or occluded on surface of RH-SiO_2 effect to the decreasing of surface area of RH-SiO_2. The pore diameter was also reduced from 0.31 to 0.07 cm^2/g.

Table 1: The textural properties determined for RH-SiO_2 and $KHSO_4$/RH-SiO_2

Sample	Surface area (m^2/g)	Pore volume (cm^2/g)	Pore Diameter (Å)
RH-SiO_2	122	0.31	10.1
$KHSO_4$/RH-SiO_2	19	0.07	15.4

3.2 Esterification

Because $KHSO_4$/RH-SiO_2 catalyst does not catalyze transesterification of triglyceride in soybean oil, the acid value could be used for calculation of FFA conversion [8, 15]. The influence of reaction parameters on FFA conversion were studied as discussed below.

3.2.1 Effect of methanol to oil molar ratio

To increase the rate of methanolysis, excess methanol is necessary for the esterification of FFA. High molar ratio of methanol to oil is required for the reaction with heterogeneous catalyst to produce methyl ester to overcome limitation in mass transfer [16]. The results (Figure 3) show that the conversion of FFA gradually increased when the amount of methanol was increased. At 5:1 molar ratio of methanol to oil, the FFA conversion was 70.56 and then the conversion rapidly increased to 94.79 at 10:1 ratio, afterwards it gradually increased to 95.48, 97.80 at 20:1 and 30:1 ratio, respectively. The FFA conversion at 40:1 molar ratio of methanol to oil was similar value at 30:1. From this study, 10:1 methanol to oil molar ratio was used for further study due to less amount of methanol using.

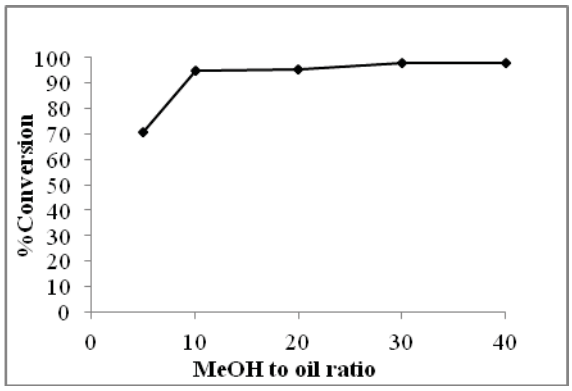

Figure 3. Effect of methanol to oil molar ratio for oleic acid conversion via esterification using $KHSO_4$/RH-SiO_2 catalyst under reaction time of 3 h, temperature of 70 °C and amount catalyst of 5 wt%.

3.2.2 Effect of reaction time

The effect of reaction time was investigated. The reaction time was varied in the range of 1-5 h. As shown in Figure 4, the conversion rapidly increased from 1 to 2 h and remained nearly constant thereafter suggesting an equilibrium. The maximum conversion of 97 % was obtained after 5 h. The optimum reaction time was 2 h in which the conversion of FFA was about 94 %.

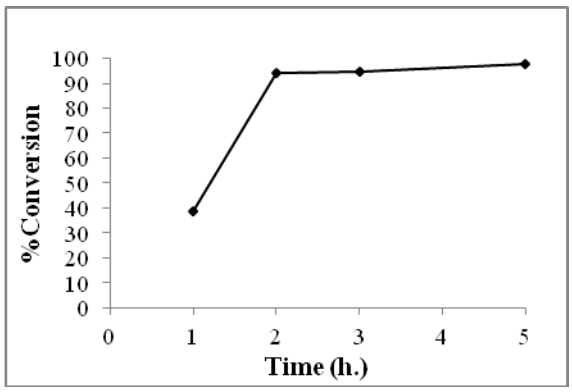

Figure 4. Effect of reaction time for oleic acid conversion via esterification using $KHSO_4$/RH-SiO_2 catalyst with methanol to oil molar ratio of 10:1, temperature of 70 °C and amount catalyst of 5 wt%.

3.2.3 Effect of amount of catalyst

The effect of the amount of $KHSO_4$/RH-SiO_2 catalyst on the FFA conversion was presented in Figure 5. The conversion increased with increasing of catalyst amount from 1 to 4 w/w%. However, the conversion decreased with the amount catalyst of 5 w/w%. It might be the effect of mass transfer of the solid acid catalyst, reactant and the product [17-18]. At higher amount of catalyst, the reacting mixture was viscous and leading to decrease the rate of mass transfer. Therefore, the resulting in a lower FFA conversion was obtained. The optimum amount of catalyst was 3 %w/w, and a 98% conversion of FFA was obtained.

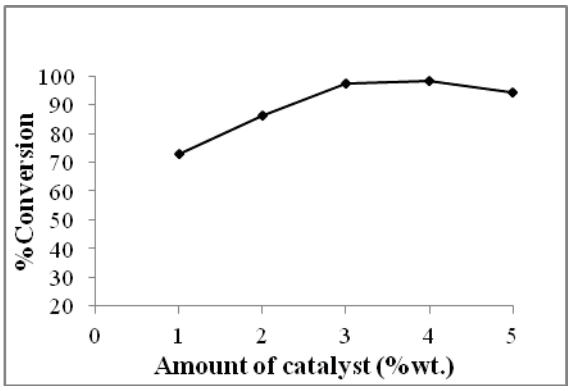

Figure 5. Effect of amount of catalyst for oleic acid conversion via esterification using $KHSO_4$/RH-SiO_2 catalyst with methanol to oil molar ratio of 10:1, reaction time of 2 h and temperature of 70 °C.

4. Conclusions

Esterification of oleic acid with methanol in the presence of soybean oil was analyzed using $KHSO_4$/RH-SiO_2 as an acid heterogeneous catalyst which was prepared by impregnation of RH-SiO_2 with a $KHSO_4$ solution to increase the acidity of RH-SiO_2. The optimum condition for $KHSO_4$/RH-SiO_2 catalyst included methanol to oil molar ratio of 10:1, a catalyst amount of 3 w/w%, reaction time of 2 h at 70 °C. FFA conversion of about 98 was obtained at the optimum conditions.

Acknowledgements

The authors thank the support from Rajamangala University of Technology Isan (RMUTI), Nakhon Ratchasima, Thailand.

References

[1] F. R. Ma and M. A. Hanna, *Bioresour. Technol*. **70** (1999) 1-15.
[2] E. Lotero, Y. Liu, D. E. Lopez, K. Suwannakarn, D. A. Bruce and Jr. J.G. Goodwin, *Ind. Eng. Chem. Res*. **44** (2005) 5353-5363.
[3] M. D. Serio, R. Tesser, L. Pengmei and E. Santacesaria, *Energy Fuels*. **22** (2008) 207–217.
[4] K.-H. Chung and B.-G. Park "Esterification of oleic acid in soybean oil on zeolite catalysts with different acidity", *J. Ind. Eng. Chem*. **15** (2009) 388–392.
[5] K.-H. Chung, D.-R. Changet and B.-G. Park, *Bioresour. Technol*. **99** (2008) 7438–7443.
[6] V. SathyaSelvabala, T. K. Varathachary, D. K. Selvaraj, V. Ponnusamy and S. Subramanian, *Bioresour. Technol*. **101** (2010) 5897–5902.
[7] B.R. Jermy and A. Pandurangan, *Appl. Catal., A*. **288** (2005) 25-33.
[8] M. Dokić, Z. Kesić, J. Krstić, D. Jovanović and D. Skala, *Fuel*. **97** (2012) 595-602.
[9] G. Mengyu, P. P. Deng, M. Li, Y. En and H. Jianbing, *Chin J Chem Eng*, **17** (2009) 83-87.
[10] B. Baghernejad, *Eurjchem*. **3** (2012) 125-128.
[11] A. Goswami, R. N. Das and N. Borthakur, *Indian J. Chem*. **46B** (2007) 1893-1895.

[12] A. Goswami, "An Alternative Eco-Friendly Avenue for Castor Oil Biodiesel: Use of Solid Supported Acidic Salt Catalyst", Biodiesel – Feedstocks and Processing Technologies. ISBN: 978-953-307-713-0, Publisher: InTech, November 09, 2011 (p. 379-396)
[13] J. Wittayakun, P. Khemthong and S. Prayoonpokharach, *Korean J. Chem. Eng*. **25** (2008) 861-864.
[14] AOAC (2000). Official Methods of Analysis. 17th edn. Association of Official Analytical Chemists, Washington DC, USA
[15] Y. Wange, S. Ou, P. Liu and Z. Zhang , *Energy Convers Manage*. **48** (2007) 184-188.
[16] S. Gan, H.K. Ng, C. W. Ooi, N. O. Motala and M. A. F. Ismail, *Bioresour. Technol*. **101** (2010) 7338–7343.
[17] H-J. Kim, B-S. Kang, M-J. Kim, Y-M. Park, D-K. Kim, J-S. Lee and K-Y. Lee, Catal. Today. **93-95** (2004) 315-320.
[18] L. C. Meher, S.D.Vidya and S. N. Naik, *Renewable Sustainable Energy Rev*. **10** (2006) 248–268.

ESTERIFICATION OF WATER SOLUBLE BIO-OIL MODEL COMPOUND OVER BASIC SOLID CATALYSTS

Natchalee Rattana, Sabaithip Tungkamani, Tanakorn Rattana,
Monrudee Phongaksorn, Samitthichai Seeyangnok*

Department of Industrial Chemistry, Faculty of Applied Science,
King Mongkut's University of Technology North Bangkok, Bangkok, 10800 Thailand

* Author for correspondence; E-mail: samitthichais@kmutnb.ac.th, Tel. +66 2 555 2000 Ext. 4806, Fax. +66 2 587 8251

Abstract: Crude bio-oil has a high content of carboxylic acids which can cause corrosion in combustion chamber, and the high oxygen content of these acids also reduce the oil's heating value. Therefore, bio-oil requires an upgrading step before it can be used as a transport fuel. As a model reaction in stabilization of bio-oil was used from esterification of acetic acid with methanol. The alumina supported is prepared by sol-gel process by using iso-propanol as template compound with high surface area ca. 378 m^2/g and various kind of metal oxides; Na_2O, K_2O, and CaO are prepared by impregnation. The catalytic activities are tested for esterification at 55 ºC with a 1:2 molar ratio of methanol to acetic acid with reaction time at 0.5 h, 1 h, 2 h, 4 h and 24 h. Three different kind of catalysts loading are investigated on 10%, 15% and 20% wt/v and the results are showed that the series of CaO/γ-Al_2O_3 catalyst is high activity for the acetic acid conversion, 10%-CaO/γ-Al_2O_3, 15%-CaO/γ-Al_2O_3, and 20% CaO/γ-Al_2O_3 with 36.6%, 39.3%, and 41.5% conversion respectively. These results indicate that it is possible to increase the conversion of acetic acids by increasing catalyst loading and increasing reaction time.

1. Introduction

The energy exerting from petroleum combustion has been widely used while such energy source is derived from a long life cycle source and must be imported from abroad cause instability of the price of energy [1]. At present, the government has supported to education, research and development in several of renewable energy. Thailand is an agricultural country with abundant and natural forests which can be used as starting materials of biomass for the production of bio-oil to be used as renewable energy of petroleum.

Pyrolysis is a technology to produce liquid fuels from biomass. However, bio-oil derived from this process is still a lot of oxygen compounds. Mostly in the form of carboxylic acid, alcohol, aldehyde, ketone and phenol derivative. The resulting bio-oil has low heating value, high acidity and viscous cause many effect on the engine such corrosion. From this reasons lead to improve the bio-oil that can be used in the engine and the industries [2].

This research is emphasized on improve the quality of bio-oil to be used as a fuel for internal combustion engines. The authors have selected some of the components contained in bio-oil to be a model compound for the reaction which acetic acid components is available on large amount in bio-oil. This research focuses on preparing solid base catalyst for the Esterification of acetic acid and methanol to obtain methyl ester. The prepared catalyst has to be an effective than homogeneous catalysts used in industries today.

2. Materials and Methods

2.1 Chemicals and materials

Alumina support (Al_2O_3) was synthesized from aluminium nitrate nonahydrate ($Al(NO_3)_3{\cdot}9H_2O$) and 2-propanol were used as template in sol-gel technique. After gel was dried in an oven at 45 °C for 48 h, then calcined at 550 °C for 4 h, and then crushed and screened to a size in the range 355-600 μm. The commercial Raschig rings and Al_2O_3 support were obtained loading of different metal ($NaNO_3$, KNO_3, $Ca(NO_3)_2$) and vary of %loading by impregnation and then calcined at 550 °C for 4 h.

2.2. Catalyst characterization

The surface area was characterized using the Brunauer-Emmett-Teller (BET) method and the pore size distribution using the BJH method based. Nitrogen adsorption–desorption isotherms were taken at 77 °K using an automatic gas adsorption apparatus (BELSORP, BEL, Japan).

2.3. Esterification

Acetic acid and methanol (2:1 molar ratio) was carried out in a two-necked round bottom flask 100 ml with a reflux condenser, which was placed in a thermostatic bath with a magnetic stirrer. In a typical experiment before the reaction, the solution mixtures (acetic acid 4M, methanol 2M) were heated to 55°C and using stirring speeds 400 rpm. Once the desired temperature was reached, the esterification reaction was started by introducing the catalyst into reaction solution. In all cases, a syringe was used for sampling at defined time intervals. A sample was taken prior to catalyst charging as the zero point for every run.

2.4 Acid titration

The resulting mixture from esterification of acetic acid and methanol at defined time intervals was titrated with potentiometrical by tiamo autotitrator

with drop wise addition of 0.1 M KOH in distilled water and the total acid content was calculated.

3. Results and Discussion

The textural properties of catalysts are shown in Table 1. The Al_2O_3 support has the highest of surface area at 379 m^2g^{-1} compared to CaO, K_2O, Na_2O loaded Al_2O_3 supports that the BET surface areas slightly lowered to 332 m^2g^{-1}, 239 m^2g^{-1} and 220 m^2g^{-1} respectively. The metal oxide was agglomerated on the surface of Al_2O_3 support resulting in decrease of the BET surface areas. The pore structures corresponding to Figure 1 are in the range of mesoporous meterials [3,4]. The N_2 adsorption–desorption isotherms of the synthesized samples had characteristic Type IV hysteresis loops as seen in Figure 1.

Table 1, Textural properties of catalyst.

Composition	Textural properties		
	S_{BET} (m^2g^{-1})	Mean pore diameter (nm)	V_P (cm^3/g)
Al_2O_3 support	379	3.07	0.29
10% CaO/ Al_2O_3	332	3.12	0.26
10% K_2O/ Al_2O_3	239	6.30	0.38
10% Na_2O/ Al_2O_3	220	4.09	0.22

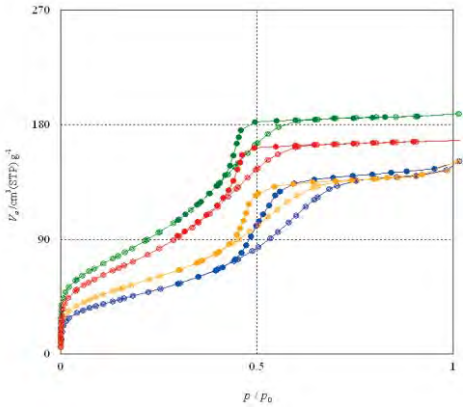

Fig. 1 N_2 adsorption–desorption isotherms of
: Al_2O_3 support :10%CaO/Al_2O_3
:10%Na_2O/Al_2O_3 :10%K_2O/Al_2O_3

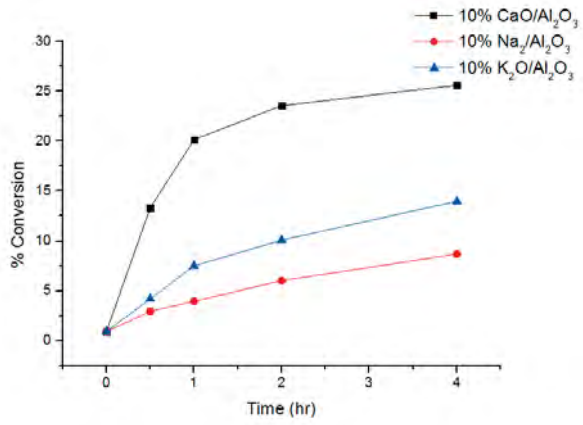

Fig. 2 The comparison of %acid conversion and reaction time of different metal oxides on Al_2O_3.

Figure 2, correlation of the %acid conversion with reaction times of esterification with various kinds of catalysts. The results show that 10% CaO/Al_2O_3 has the highest conversion compared with 10% Na_2O/Al_2O_3 and 10% K_2O/Al_2O_3. This is probably caused by the basicity of metal loading on the prepared catalysts.

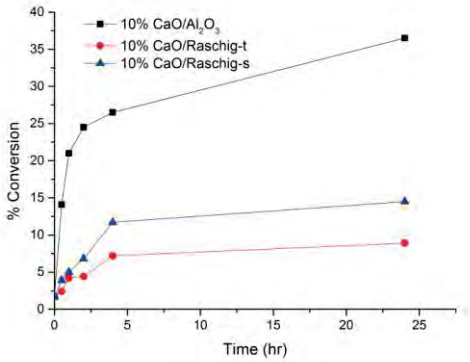

Fig. 3 The comparison of %acid conversion and reaction times on different support.

Figure 3, correlation of %acid conversion and reaction times compared with different support including Al_2O_3 (synthetic), raschig ring-t (tube) and raschig-s (355-600 Mic). The results show that the catalyst using Al_2O_3 support has the highest % acid conversion.

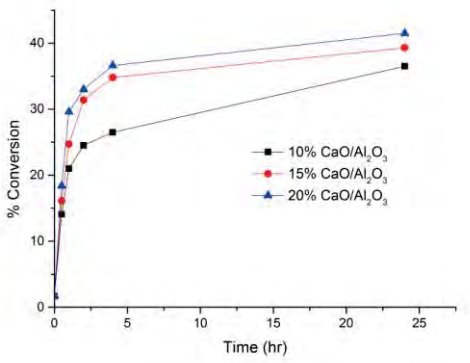

Fig. 4 Comparison of % acid conversion and reaction times on different % CaO.

From Figure 4, comparison of %acid conversion and reaction times for the series of CaO/γ-Al_2O_3 catalyst. The % acid conversion of 10%CaO/□-Al_2O_3 , 15% CaO/γ-Al_2O_3, and 20%CaO/γ-Al_2O_3 were 36.6, 39.3, and 41.5 %conversion respectively indicating that the yield of esterification is possibly increased by higher amount of CaO loading.

4. Conclusions

In this research intended to examine solid base catalyst for the esterification and prepared catalysts were successful synthesized with high surface area and all of these catalysts were mesoporous materials [3,4]. The catalyst loading with CaO was found to be highest catalytic activities for esterification.

Acknowledgements

All support of this research by Research and Development Chemical Engineering Unit Operation. (RCC). Department of Industrial Chemistry, Faculty of Applied Science, King Mongkut's University of Technology North Bangkok.

References

[1] L. Qiang, L. Wen-Zhi and Z. Xi-Fen, *Energ. Convers. Manage.*, **50** (2009) 1376-1383.
[2] K. Seon-Jin, J. Su-Hwa and K. Joo-Sik, *Bioresource Technol*., **101** (2010) 9294–9300.
[3] I.K. Mbaraka and B.H. Shanks, *J. Catal.,* **229** (2005) 365–373.
[4] I.K. Mbaraka, D.R. Radu, V.S.Y. Lin and B.H. Shanks, *J. Catal*., **219** (2003) 329–336.

PRODUCTION OF BIOESTER THROUGH SOLID-CATALYZED TRANSESTERIFICATION OF *STERCULIA FOETIDA* OIL USING AN OPTIMIZED PROTOCOL

Wichayasith Intakusol[1], Pongsakorn Hanpongpun[1], Poolsak Sahakitpichan[2], Anusorn Vorasingha[1,*]

[1] Department of Chemistry, Faculty of Science, Naresuan University, Phitsanulok 65000, Thailand
[2] Chulabhorn Research Institute, Kamphaengphet 6 Road, Bangkok 10210, Thailand

[*] Author for correspondence; E-Mail: anusornv@nu.ac.th, Tel. +66 55 963461, Fax. +66 55 963401

Abstract: The transesterification reaction of *Sterculia Foetida* oil with methanol using natural fiber catalyst was investigated. Various experimental variables, such as the natural oil and methanol molar ratio (1:3, 1:6, and 1:9), temperature (45, 65 and 80 ^{o}C), rate of stirring (200, 400 and 600 rpm), and solid-catalyst concentration (1.0, 3.0 and 5.0 %) were adopted. Natural oil and methanol molar ratio of 1:9 with solid-catalyst concentration 5.0 %, mixing intensity of 600 rpm, and reaction temperature 80 ^{o}C offered the best *Sterculia Foetida* oil fatty acid methyl esters (FAMEs) was accomplished by gas chromatography (GC). The bioester were characterized for their physical and main fuel properties including density, specific gravity, kinematic viscosity, high heating value, cetane number, flash point and cloud point. The chemical structure of bioester oil products were studied by nuclear magnetic spectroscopy (NMR) and Mass spectrometry (MS) techniques. The result showed our solid acid catalyst from sulfonate natural fiber could be used as transesterification catalyst.

1. Introduction

Biofuels are liquid or gaseous fuels made from biomass materials such as agricultural crops, municipal wastes, and agricultural and forestry by products via biochemical or thermo chemical processes. They can replace conventional fuels in vehicle engines, either totally or partially in a blend [1]. Vegetable oil methyl esters, commonly referred to as “biodiesel”, are prominent candidates as alternative diesel fuels. The name biodiesel has been given to transesterified vegetable oil to describe its use as a diesel fuel [2]. Vegetable-oil fuels have not been acceptable because they are more expensive than petroleum fuels. However, with recent increases in petroleum prices and uncertainties surrounding petroleum availability, vegetable oils have become more attractive recently because of their environmental benefits and the fact that they are made from renewable resources [3,4].

Studies with the oil from seeds of S. Foetida have reported high content of cyclopropenoids fatty acids (CPFA) [5-7]. Compounds containing cyclopropenoid ring are associated with several biological properties, such as: insecticide, antifungal, antibiotic, antiviral, hormonal, carcinogenic or antitumoral activities and enzyme inhibitor [8,9]. The effects of CPFA in animals have been the subject of several investigations, including cocarcinogenic and carcinogenic activities [10-12]. Sterculic acid is an inhibitor of Δ^{9}-desaturase which converts stearic acid into oleic acid and is potentially noxious to man, since it can alter the cellular membranes permeability and inhibit the cellular reproduction [13].

Transesterification is the reaction of vegetable oil or animal fat with an alcohol to form esters and glycerol. A catalyst is used to improve the reaction rate and yield. Since the reaction is reversible, excess alcohol is used to shift the equilibrium to the products side [14]. The liquid acid-catalyzed transesterification process does not enjoy the same popularity in commercial applications as its counterpart, the base-catalyzed process. The fact that the homogeneous acid-catalyzed reaction is about 4000 times slower than the homogeneous base-catalyzed reaction has been one of the main reasons. However, acid-catalyzed transesterifications hold an important advantage with respect to base catalyzed ones: the performance of the acid catalyst is not strongly affected by the presence of FFAs in the feedstock. In fact, acid catalysts can simultaneously catalyze both esterification and transesterification. Thus, a great advantage with acid catalysts is that they can directly produce biodiesel from low cost lipid feed-stocks, generally associated with high FFA concentrations (low-cost feed-stocks, such as used cooking oil and greases, commonly have FFAs levels of ≥6%) [15].

2. Materials and Methods

2.1 Materials

The seeds of *Sterculia foetida* ware collected on April 2011 at Naresuan University in Phitsanulok, Thailand and *Sterculia foetida* oil was purchased from department of Chemistry, Faculty of Science, Naresuan University. Analytical reagents using as standards for gas chromatograph (GC) were purchased from Sigma-Aldrich Chemical Corporation, USA. Other chemical were analytical reagents (AR) and purchased Wako Chemical Corporation, Japan.

2.2 Oil extraction methods

Sterculia foetida seeds (400 g) were ground, homogenized and oil was extracted with hexane by cold solvent and soxhlet extraction. The organic

extract was filtered and dried with anhydrous sodium sulfate. The hexane was removed under vacuum. The oil obtained was transesterified to determine fatty acids composition by gas chromatography mass spectrometry (GC/MS, Model Agilent 7890/5973). The oven temperature of GC was held at the initial temperature of 140 ^{o}C for 1 min and then heated at 8 ^{o}C min^{-1} to 210 ^{o}C, 2 ^{o}C min^{-1} to 260 ^{o}C, and then to a final temperature of 280 ^{o}C at a rate of 30 ^{o}C min^{-1}, held for 1 min. The total run time was 36.42 min. The injector temperature was 250 ^{o}C and that of the detector was 230 ^{o}C. Helium gas was used as the carrier at a flow rate of 1 ml min^{-1}. The analysis with mass detector was carried out at the following conditions: helium as carrier gas, electron energy of 70 eV and mass range from 40 to 500.

2.3 Preparation of solid catalyst

The carbon material with SO_3H groups was prepared from dried bamboo cellulose. The starting material (20 g) was heated for different temperatures (300-500 ^{o}C) and carbonize times (15 h) under N_2 flow to produce a black solid, which was then ground by ball mill for 6 h (particle size, <90 µm). The powder (5 g) was then boiled in 50 ml of sulfuric acid (H_2SO_4) at 150 ^{o}C under N_2. After heating time for 18 h and then cooling to room temperature, the suspension was filtered to yield a black precipitate, with was washed repeatedly with distilled water until impurities such as sulfate ions were no longer detected in the wash water (detect pH by universal indicator). Dry and determine all acids content by back titration.

2.4 Methylation procedure

The procedures of transesterification were designed to 1, 3 and 5 wt% catalyst concentration (Catalyst (%wt) is relative to the total weight of oils) at the reaction times 1, 3, 6, 12 and 24 h and 1:9 molar ratio of oil to methanol at temperature 80 ^{o}C. After cooling, the reaction mixture was filtrated for cleave solid catalyst then poured into a collecting tube and then was centrifuged at 2,000 g for 10 min, which resulted in the phase separation of the methyl esters and the glycerol. The glycerol phase (bottom layer) was removed, and the methyl esters biodiesel phase (top layer) was evaporated with a thermostatic bath at 65 ^{o}C to remove the methanol. Then the biodiesel product was analyzed % conversion with ^{1}H NMR spectrometer.

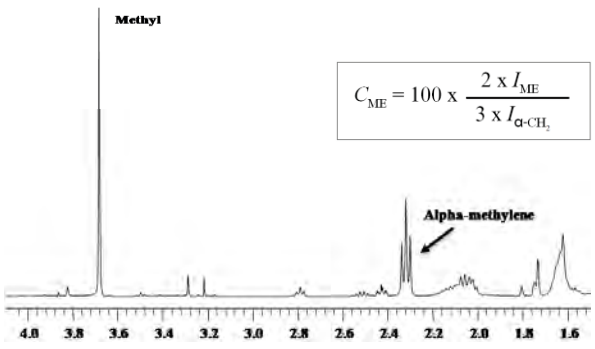

Figure 1. ^{1}H NMR spectra of 97.8% methyl ester from *Sterculia foetida*.

In the ^{1}H NMR spectrum of methyl esters is shown in Fig 1., methyl groups were observed singlet spectra at δ 3.678 and triplet spectra of alpha-methylene at δ 2.349. The conversion percentage of methyl ester were determined by ratio of intrigration value between methyl and alpha-methylene spectra.

3. Results and Discussion

3.1 Lipid content

The reference in several extration oils were found 70-15 percentage and *Sterculia foetida* was 26.15 percentage. The extracted oil (soxhlet extraction) was found among moderate yields, that show in table 1.

Table 1: Yield of vegetable oils [16].

Oil	Oil content (%)
Soybean	15-20
Sunflower	25-35
Rapeseed	38-46
Palm oil	30-60
Peanut oil	45-55
Olive oil	45-70
Corn (Germ)	48
Coconut	63-65
Castor	45-50
Jatropha	30-40
Tung	16-18
*Sterculia foetida**	26.15

*Soxhlet extraction from 25 g sample seed.

3.2 Methyl ester properties

The present study introduced a process for biodiesel production through high effective acidic transesterification catalyzed by cellulose sulfonic acid.

Table 2: Fatty acids composition from *Sterculia foetida* seed oil

Peak	Fatty acid	Sample	Ref [5]
		Mean (%)	Mean (%)
1	$C_{16:0}$	18.77	15
2	$C_{16:1}$	0.42	0.13
3	$C_{18:0}$	4.11	1.66
4	Mavalic acid	-	5.4
5	$C_{18:1}$ cis	10.93	5.6
6	Sterculic acid	-	54
7	$C_{18:2}$ cis/cis	10.85	7.7
8	$C_{18:3}$	-	0.20
9	$C_{20:0}$	0.95	0.15

Gas chromatography mass spectrometer showed the fatty acids composition in Table 2. The mass spectra of mavalic acid and sterculic acid were not shown up because their structures decompose in high

temperature reaction. The mass spectra of other fatty acid were as same as previous work.

^{1}H NMR analysis showed no artifact formation when acid catalyzed process was used. ^{1}H NMR spectra of the methyl esters obtained in basic catalyzed process showed no signals for triacylglycerols (δ 4.1–4.3) indicating that the transesterification was quantitative. These spectra showed an additional signal at δ 3.678, characteristic for methyl esters hydrogens and signal at δ 0.900, characteristic for cyclopropene hydrogens of methyl mavalate or methyl sterculate. Thus peaks at δ 3.678 (OCH_3) and at δ 0.910 (terminal CH_3 groups) showed the same area indicating a complete methylation.

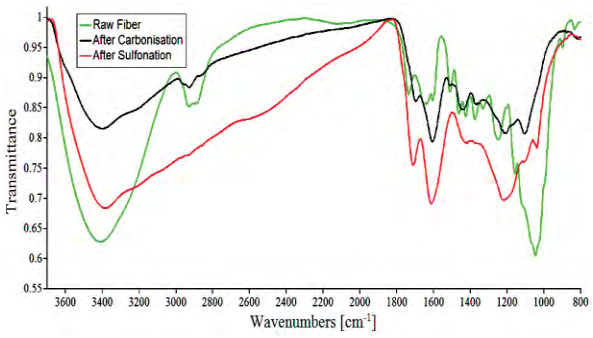

Figure 2. FTIR spectrum label : (Green) Raw material, (Black) Carbonized material, (Red) Sulfonated material.

The FTIR spectra of the carbon catalyst before and after sulfonation showed the vibration bands at 3400 cm^{-1} (-OH stretching), 1713 cm^{-1} (C=O bending), 1615 cm^{-1} (-OH stretching), 1040 cm^{-1} (SO_3- stretching) and 1365 cm^{-1} (O=S=O stretching in SO_3H) as showed in (Fig. 2). The material is carbonization at 300^{o}C, 5 h.

3.3. Solid acid catalyst properties

The sample carbonized at lower temperatures presented smaller carbon sheets and therefore have hight acids densities because the SO_3H groups are attached only to the edegs of the carbon sheets (Polycyclic Aromatic Hydrocarbon). The all acid value have shown in Table 3.

Table 3: Determination of acid value on solid catalyst

Carbonization Temperatures (^{o}C)	All acid content (mmol/g)
300	7.9970
400	5.8351
450	4.3719
500	3.7938
550	3.3267

3.4 Effect of catalyst concentration

The concentration of trifluoroacetic acid catalyst used in the process was varied as 1, 3 and 5 %wt based on the volume of the reaction solution. An appropriate concentration of solid acid catalyst was 5%wt as it gave the higher amount of the methyl ester content (98.4%) after 12 h of reaction time. Therefore, 5 %wt catalyst concentration was suggested in the acidic transesterification catalyzed by solid acid catalyst. The changes of the product specific gravity and the methyl ester content with reaction time under the conditions of 9:1 M ratio of methanol to oil and 80 ^{o}C with 5 %wt catalyst concentration were further investigated.

3.5 SEM analysis of prepared catalyst

Scanning electron microscopy images of the solid acid catalyst were shown in Fig. 3. The catalyst is comprised from the union of many crystals. There are many cracks with sizes of micrometers and relatively large pores among these agglomerates. Therefore, triglyceride and methanol may fully contact with the surface of the catalyst to synthesize biodiesel. This solid acid catalyst can be effectively and easily separated from the products by filtration and centrifugation after the reaction.

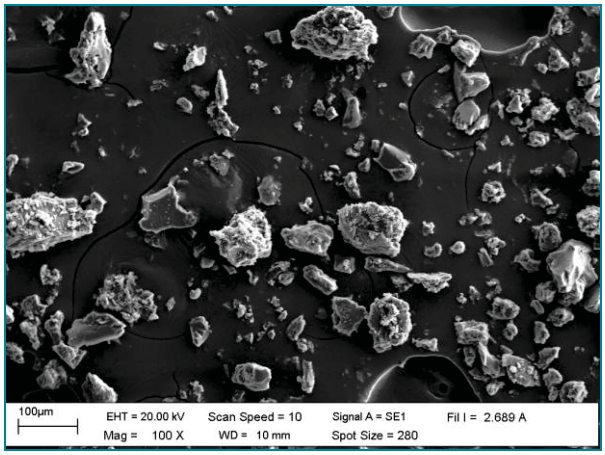

Fig. 3. SEM images of the new prepared solid acid catalyst.

4. Conclusions

The present study introduced a process for biodiesel production through high effective acidic transesterification catalyzed by cellulose sulfonic acid. A range of methanol to oil ratios, acid catalyst concentrations, reaction temperatures and reaction times were established. The research indicated that the oil could be converted to biodiesel directly by one-step cellulose sulfonic acid catalyze process without extreme temperature and pressure conditions. The best process combination was 5%wt catalyst content with 9:1 M ratio of methanol to oil at temperature of 80 ^{o}C. The methyl ester content reached as high as 98.5%. The present procedure represents a simpleand mild method for bioester production in short reaction time

and with high conversion rate, which would offer potential for an industrial process.

Acknowledgements

We are grateful for the financial support of the Naresuan University Research Grant, 2011. We thank to Assist. Prof. Dr. Pornsawan Amornsakchai from Faculty of Science, Naresuan University for her kind suggestion and discussions. Special thanks to Prof. Dr. Masahiko Iyoda from Tokyo Metropolitan University for his kind discussions. Thank to Assoc. Prof. Dr. Thaweechai Amornsakchai from Mahidol University for discussions. Thanks to Assist. Prof. Dr. Kittipong Chainok for his kind discussion.

References

[1] EC (European Commistion), **(**2004**)** Proting Biofuels in Europe, Directorate –General for Energy and Transport, B-1049 Brussels, Belgium.
[2] A. Demirbas, *Energy Convers Mgmt* **43 (**2002**)** 2349–2356.
[3] A. Demirbas, *Energy Convers Mgmt* **44 (**2003**)** 2093–2109.
[4] P.N. Giannelos, F. Zannikos, S. Stournas, E. Lois and G. Anastopoulos, *Ind Crop Prod* **16** (2002) 1–9.
[5] S. Aued-Pimentel, J.H.G. Lago, M.H. Chaves and E.E. Kumagai, *J. Chromatogr. A.* **1054** (2004) 235-239.
[6] N.E. Pawlowsky, J.E. Nixon, R.O. Sinnhuber, *J. Am. Oil Chem. Soc.* **49** (1972) 387.
[7] J. Miralles, E. Bassene, E.M. Gaydou, *J. Am. Oil Chem. Soc.* **70** (1993) 205.
[8] J. Salaun, M.S. Baird, *Curr. Med. Chem.* 2 (1995) 511.
[9] J. Salaun, *Top. Curr. Chem.* **207** (2000) 1.
[10] R.O. Feuge, L.P. Codifer, H.J. Zeringue, *J. Am. Oil Chem. Soc.* **58** (1981) 718.
[11] N.E. Pawlowski, J.D. Hendricks, M.L. Bailey, J.E. Nixon, G.S. Bailey, *J. Agric. Food Chem.* **33** (1985) 767.
[12] S.W. Park, K.C. Rhee, *J. Food Sci.* **53** (1988) 1497.
[13] P.M. Dewick, *Medicinal Natural Products*: A Biosynthetic Approach, second ed., John Wiley and Sons, New York (2001) 48–50.
[14] A. Demirbas, *Energy Conv. Manage.* **47** (2006) 2271-2282.
[15] L. Edgar, L. Yijun, E.L. Dora, S. Kaewta, A.B. David and G.G. James, *Ind. Eng. Chem. Res.* **44** (2005) 5353-5363.
[16] K. Aninidita, K. Subrata and M. Souti, *Bioresource Technology* **101** (2010) 7201-7210.
[6] C. Petrone, *Degradable calcium polyphosphate compaction strategies for the delivery of therapeutic agents*, Master's Thesis, Dalhousie University, (2005).
[7] S. Laksanacharoen, *Artificial muscle construction using natural rubber latex in Thailand*, 3rd Thailand Materials Science and Technology Conf. Proc., Bangkok, Thailand, (2004), pp. 14-18.
[8] http://www.paccon2012.com/ (Retrieved September 28, 2011).

CATALYTIC DRY METHANE REFORMING OVER Ni BASED FOAM CATALYST

Xishol Pinijchai[1], Sabaithip Tungkamani[1,3*], Monrudee Phongaksorn[1,3*], Phavanee Narataraksa[2,3], Thana Sornchamni[4], Tanakorn Ratana[1,3]

[1] Department of Industrial chemistry, Faculty of Applied Science , King Mongkut's University of Technology North Bangkok , Bangkok, 10800, Thailand
[2] Department of Chemical Engineering, Faculty of Engineering, King Mongkut's University of Technology North Bangkok , Bangkok,10800, Thailand
[3] Research and Development Center for Chemical Engineering Unit Operation and Catalyst Design (RCC), King Mongkut's University of Technology North Bangkok, Bangkok , 10800, Thailand
[4] PTT Public Company Limited, PTT Research and Technology Institute, Wangnoi, Ayutthaya, 13170, Thailand

[*]Author for correspondence; E-Mail: sabaithip.tungkamani@gmail.com, monrudee@gmail.com Tel. +66 2-555-2000 ext.4822

Abstract: This work focuses on developing supported Ni catalyst shaped as foam material for dry methane reforming. The foam catalyst provides high porosity in a form of megaporous structure. To prepare foam catalyst, polyurethane (PU) used as a template was soaked by the diluted and non-diluted catalyst slurry, namely 10NAM. The foam catalyst was dried and calcined. The properties of the catalyst were revealed by H_2-TPR, H_2-TPD and OM techniques. The activity of the catalyst on dry methane reforming was carried out in a fixed bed reactor at 620°C. The results show that foam-10NAM catalyst prepared from the diluted 10NAM catalyst provides higher dispersion of Ni components, greater activity of catalyst for dry methane reforming and higher reducibility compared to the foam-10NAM prepared from the non-diluted 10NAM.

1. Introduction

As a situation of non-renewable energy becomes more and more critical, hydrogen is considered as an alternative fuel while syngas (a mixture of H_2 and CO) plays a vital role for downstream processes [1]. In recent years, dry methane reforming process (DMR), equation (1), is being an interesting hydrogen and/or syngas production process [2]. During the process, methane (CH_4) reacts with carbon dioxide (CO_2) over the surface of solid catalyst to transfrom into equimolar syngas (a mixture of H_2 and CO).

$$CH_4 + CO_2 \rightarrow 2CO + 2H_2 \quad (1)$$

This process is generally performed at high temperatures over pellet Ni-based catalysts. A major problem of this catalyst type is the catalyst deactivation either by coke formation or by sintering of Ni. According to the thermodynamics of the operating condition, the carbon species formation can take place on the surface of catalyst along methane cracking and CO disproportionation as seen in equation (2) and equation (3), respectively [3].

$$CH_4 \rightarrow C + 2H_2 \quad (2)$$

$$2CO \rightarrow C + CO_2 \quad (3)$$

Another reaction involved in the process is the reverse water gas shift (RWGS) reaction (equation 4) since DRM has a source of CO_2 and also provides H_2 at the same time.

$$H_2 + CO_2 \rightarrow CO + H_2O \quad (4)$$

Although the pellet Ni-based catalysts have been being developed, the bottom neck of this type of catalysts is the limitation of the surface area. To overcome this limitation, on one hand, the micro channel reactor coated by catalyst has been developed. On the other hand, a different catalyst structure has been created [5, 6].

Ceramics foam (CF) is one of the high porosity materials, it provides pore size in the range of megapore[7]. The diameter of pore is about 0.04 – 1.5 mm. In the previous work, the ceramic foam was prepared and used as a substrate to be coated with the catalyst slurry.

This research works on the development of foamed catalyst. The Ni-based catalysts were made as a foam shape in an only one step using the method adapted from the CF preparation method. The properties of all catalyst prepared in this work were investigated by H_2-TPR, H_2-TPD and OM techniques and the DMR performance was carried out at 620°C.

2. Materials and methods

2.1 Catalyst preparation

The catalysts were prepared by sol–gel method [8,9]. The precursors were $Ni(NO_3)_2.6H_2O$, aluminium isopropoxide (98%), magnesium ethoxide (98%) and HNO_3 supplied by QREC and Aldrich. A suitable amount of alumina isopropoxide was mixed with de-ionized (DI) water before adding HNO_3. The mixture was refluxed at 85-90°C for 20h. After 20h, magnesium ethoxide was dropped into the

mixture following by addition of $Ni(NO_3).6H_2O$ solution. Then, the product was stirred for 1h to give homogeneous slurry called 10NAM. In order to prepare a foamed catalyst, polyurethane (PU) used as a template was dipped into diluted and non-diluted catalyst slurry. Open pores of PU were filled with an aqueous slurry. The product were dried at 45°C for 48h and calcined at 1150°C for 3h resulting in foamed catalysts.

The various percentages of dilutions were applied to find an optimum condition. The catalyst samples with different percentage of dilutions were coded as xCF-10NAM (x is 25, 50, 75, 100) according to the content of 10NAM summarized in Table 1.

Table 1: The diluted conditions of 10NAM slurry

No.	Catalyst	10NAM (%)	DI. water(%)
1	100CF-10NAM	100	0
2	75CF-10NAM	75	25
3	50CF-10NAM	50	50
4	25CF-10NAM	25	75

2.2 Catalyst characterization

In this work, temperature-programmed reduction (H_2-TPR) and temperature programmed-desorption (H_2-TPD) were used to determine the reduction conditions and the number of active sites, respectively. For TPR procedure, a catalyst sample packed in a down-flow reactor was pretreated with pure argon at 150°C for 40 min, following by bringing temperature of reactor down to room temperature. Then, the reactor was heated up at 10°C/min from room temperature to 800°C in a $5\%H_2/Ar$. The output gas was detected by TCD detector and reported as TPR profile.

Similarly, for TPD technique, the sample was firstly packed and reduced at the suitable temperature obtained from TPR technique for 3h. The reactor was cooled down to room temperature in inert gas before the H_2-adsorption step. Pure hydrogen gas was flowed into reactor for 30 min to allow hydrogen to adsorb on the active surface followed by flushing with inert gas. Finally, the temperature of the reactor was ramping at 10°C/min up to 800°C in inert gas. The amount of H_2 desorption was detected by TCD detector and presented as TPD profile.

Optical microscope (OM) was used to study the foam catalyst structure. PU foam and 50CF-10NAM (after dried step and calcined step) were demonstrated at 5x magnification in order to observe the structure of foam catalyst without catalyst and after soaking.

2.3. DMR performance

To perform DMR tests, the catalyst was reduced in-situ at 620°C under H_2 atmosphere overnight. After the reduction, the DMR activity was tested over the catalyst at the same temperature with 400 min time-on-steam in a mixture of CH_4, CO_2 and N_2 at 15 mL/min, 25 mL/min and 20 mL/min feed. The exit gas was analyzed by on line GC (model 7890N Agilent). Finally, the activity, %yield and stability were determined.

3. Results and Discussion

3.1 Reducibility of catalyst

Figure 1 represents TPR profiles of all catalyst samples. TPR profiles of all catalyst samples illustrate a broad peak and T_{max} of TPR profiles show in the temperature range of 580°C-620°C. After 750°C, the profile seems to rise up. The broad peak in the lower temperature region represents the reduction of NiO to metallic Ni, whereas, the peak exists at higher temperature represents the reduction of nickel aluminate species [10].

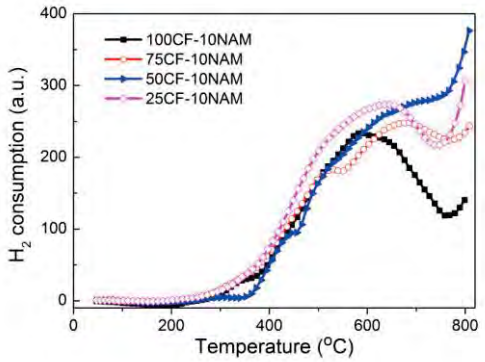

Figure 1. H_2-TPR profiles of xCF-10NAM (x=100, 75, 50, 25)

3.2 Number of active sites

Number of active sites adsorbing hydrogen can be qualitatively indicated using H_2-TPD. The more the amount of H_2 desorption, the more the number of active sites. From TPD profile (Figure 2), the results show that 25CF-10NAM and 50CF-10NAM present larger H_2 desorption, indicating higher number of active site.

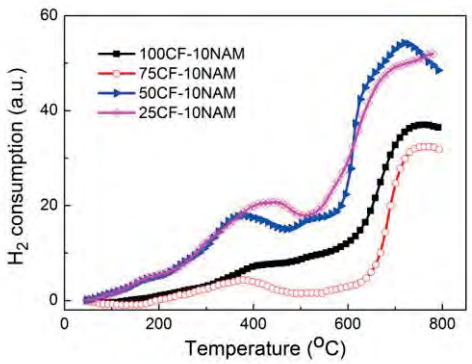

Figure 2. H_2-TPD profiles of xCF-10NAM (x=100, 75, 50, 25)

To calculate metal dispersion from H_2-TPD profiles, the adsorption stoichiometry of one hydrogen atom per nickel surface atom (H:Ni 1:1 at room temperature) was assumed to estimate Ni dispersion [11]. Ni dispersion of all foam catalysts are presented in Table 2.

Table 2 : Metal dispersion of xCF-10NAM

No.	Catalyst	Ni dispersion (%)
1	100CF-10NAM	3.8
2	75CF-10NAM	4.3
3	50CF-10NAM	14.2
4	25CF-10NAM	23.0

The results show that foam-10NAM catalyst prepared from the diluted 10NAM catalyst provides higher dispersion of Ni components.

3.3 The structure of the foam catalyst

Figure 3. shows the structure of the PU foam and 50CF-10NAM after dried and calcined step. In the Figure 3(a), it is shown that the PU foam structure depicts a boundary of the cell, opened cell without thin film layer (TFL) and closed cell with TFL. After dried step (the figure 3(b)), the structure was covered by 50CF-10NAM on the boundary of the cell and TFL. When the PU foam was removed after calcined step as presented in the figure 3(c), the result indicated that it remains only 50CF-10NAM although some part of the structure was damaged.

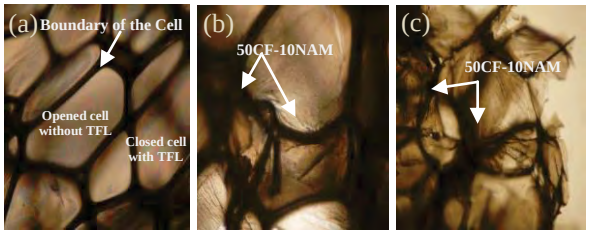

Figure 3. The foam structure of PU foam (a), after dried step (b) and calcined step (c).

3.4 Catalytic performance

The catalytic activity of all catalyst investigated was determined by CH_4 conversion. The results show that the dilution of 10NAM slurry for the preparation of foamed catalyst has an effect on the CH_4 conversion. All the catalysts prepared from diluted 10NAM provide higher conversion of CH_4 compared to the non-diluted catalyst. This could be explained that the diluted catalyst slurry could easily migrate into the inner pore of PU template, resulting in the high surface area of active sites. In contrast, non-diluted one has high viscosity, property; the diffusion of slurry is quite limited so only outer pore of PU template was coated with the slurry. Therefore, the surface area of this catalyst is lower than the first one.

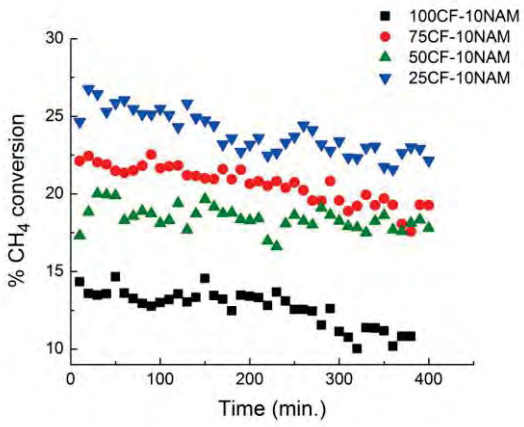

Figure 4. Methane conversion of xCF-10NAM (x = 25, 50, 75 and 100) for DMR (CH_4: 15 mL/min, CO_2: 25 mL/min, N_2: 20 mL/min) at 620°C, over 400 min time-on steam.

Although the diluted catalyst gives the better catalytic activity but the results are not presented as a trend. 25CF-10NAM was observed to give the highest conversion of methane when compared with other catalysts.

Figure 4 depicts the comparison of $\%H_2$ yield and %CO yield obtained from xCF-10NAM (x = 25, 50, 75 and 100) for DMR. The $\%H_2$ yield and %CO yield is in the order of 50CF-10NAM > 75CF-10NAM > 25CF-10NAM catalyst. The interesting results obtained could further indicate the stability of 50CF-10NAM catalyst. Accordingly, it has to be noted here that the dilution of catalyst slurry has an effect on the catalytic behaviour of foamed catalyst. The optimum conditions for preparation was observed for 50CF-10NAM catalyst due to the stability of CH_4 conversion and the highest yield of H_2 and CO.

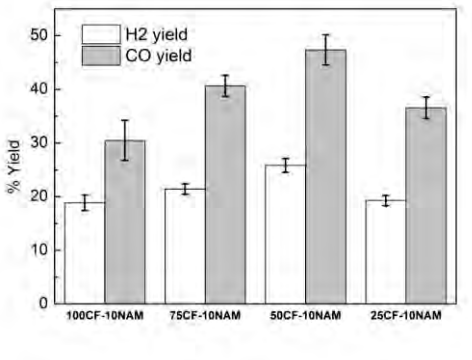

Figure 5. $\%H_2$ yield and %CO yield of xCF-10NAM (x = 25, 50, 75 and 100) for DMR (CH_4: 15 mL/min, CO_2: 25 mL/min, N_2: 20 mL/min) at 620°C, over 400 min time-on steam.

4. Conclusions

The dilution of catalyst slurry has an effect on the catalytic behaviour of foamed catalyst. Among the catalyst investigated, 50CF-10NAM catalyst shows the best performance due to the stability of CH_4 conversion and the highest yield of H_2 and CO.

Acknowledgements

The authors would like to acknowledge PTT Public Company Limited for the research funding.

References

[1] K. J. Puolakka and A. O. I. Krause, Cat. Lett. 116 (2007).
[2] H. Zhou, Y. Cao, H. Zhao, H. Liu, W. P. Pan, Energy and Fuels. 22 (2008) 2341-2345.
[3] Y. Cui, H. Zhang, H. Xu, W. Li, Appl. Catal. A 318 (2007) 79-88.
[4] T. Osaki, T. Horiuchi, K. Suzuki, T. Mori, Cat. Lett. 35 (1995) 39-43.
[5] P. Ciambelli, V. Palma, E. Palo, Cat. Today 155 (2010) 92-100.
[6] M. Nacken, L. Ma, S. Heidenreich, F. Verpoort, G. V. Baron, Appl. Catal. B 125 (2012) 111-119.
[7] M. V. TWIGG, J. T. Richardson, iChem 80 (2002)
[8] N. Gokon, Y. Osawa, D. Nakazawa, T. Kodama, Hydro. Energy 34 (2009) 1787-1800.
[9] H. Li, H. Xu, J. Wang, Nat. Gas Chem. 20 (2011) 1-8.
[10] N. F.P. Ribeiro, R. C.R. Neto, S. F. Moya, M. M.V.M. Souza, M. Schmal, Int J Hydrogen Energy 35(2010) 11725-11732.
[11] W. Gac, Appl. Surf. Sci. 257 (2011) 2875 – 2880

FISCHER-TROPSCH REACTION OVER COBALT SUPPORTED MESOPOROUS SILICA CATALYST

Saowaluk Intarasiri[1,3], Sabaithip Tungkamani[1,3*], Monrudee Phongaksorn[1,3], Phavanee Narataraksa[2,3], Hassanai Sukkathanyawat[1,3]

[1] Department of Industrial chemistry, Faculty of Applied Science , King Mongkut's University of Technology North Bangkok, Bangkok, 10800, Thailand
[2] Department of Chemical Engineering, Faculty of Engineering, King Mongkut's University of Technology North Bangkok, Bangkok, 10800, Thailand
[3] Research and Development Center for Chemical Engineering Unit Operation and Catalyst Design (RCC), STRI Building, Floor 1st and 7th (Room 702), King Mongkut's University of Technology North Bangkok, Bangkok , 10800, Thailand

*Author for correspondence; E-mail: sabaithip.tungkamani@gmail.com, Tel. +662-555-2000 ext. 4822

Abstract: Hexagonal mesoporous silica such as SBA-15 and MCM-41 was synthesized and used as a support for Fischer-Tropsch catalyst. 20%Co (w/w) and 1%Ru-20%Co (w/w) supported catalysts were prepared by incipient wetness impregnation method. Catalyst was characterized by BET, TPR, H_2-TPD and TPSR technique. Catalytic behaviors of these catalysts on Fischer-Tropsch synthesis were carried out in a continuous flow reactor. According to the results, Ru promoter increases reducibility of cobalt supported catalyst. A promoted catalyst gives higher metal dispersion compared to unpromoted catalyst. Activity of CO hydrogenation over both promoted and unpromoted 20%Co/SBA-15 catalysts are higher than 20%Co/MCM-41 catalyst. Fischer-Tropsch reactions over 1%Ru-20%Co/SBA-15 and 1%Ru-20%Co/MCM-41 are selective toward long chain hydrocarbons in the range of kerosene (C_9-C_{15}) product comparing to unpromoted 20%Co/SBA-15 and 20%Co/MCM-41 catalyst.

1. Introduction

Fischer–Tropsch synthesis (FTS) has been renewed interesting for alternative fuel, especially for the purpose of aviation and jet fuel. Synthesis gas (H_2 and CO) derived from biomass, coal and natural gas, is a feedstock for FT process known as biomass to liquid (BTL), gas to liquid (GTL) and coal to liquid (CTL), respectively. Valuable product obtained is synthetic liquid hydrocarbons such as gasoline, kerosene and diesel etc.

Desired product is dependent on selective metal supported catalyst. A catalyst based on Fe metal is selective towards olefin hydrocarbons, while Co based catalyst favors to produce saturated hydrocarbons. Kerosene used for aviation fuels mainly compose of paraffin [1],[2]. Thus, Co-based catalyst has normally selected for the production of paraffin via FTS [3].

High loading of Co metal supported on high surface area material (Al_2O_3 and SiO_2) is generally designed for FT catalyst preparation. Recently, the hexagonal mesoporous material such as SBA-15 and MCM-41 has been pointed to be an interesting catalyst support because of its high surface area. The dispersion of active cobalt on high surface area of support is therefore expected to increases. As a result, agglomeration of active cobalt and deactivation of catalyst under FTS condition is minimized. Moreover, the improvement of catalyst behavior is enhanced by the promoters. Thus, noble metal promoters such as Ru, Pt and Re have been sometime employed in cobalt catalysts in order to increase the reducibility and activity[4].

In a present work, Fischer Tropsch reaction over 20%(w/w) Co supported SBA-15 and MCM-41 has been investigated. The effect of Ru promoter on the catalytic behavior of Co based catalyst has been also included in this study.

2. Material and Methods

2.1 Catalyst Preparation

The SBA-15 and MCM-41 support were synthesized according to the methodology proposed by literature[5],[6] and [7]. The Co based catalysts were prepared by incipient wetness impregnation method. The solution of $Co(NO_3)_2.6H_2O$ was added dropwise to the support (both SBA-15 and MCM-41). Then it was saturated in room temperature for 4h, dried and calcined at 550^oC for 5h. The catalysts obtained were 20%Co/SBA-15(w/w) and 20%Co/MCM-41(w/w). These catalysts were named as 20%CP and 20%CT, respectively. Mixed solution of $Ru(NO)(NO_3)_3$ and $Co(NO_3)_2.6H_2O$ was added dropwise to the support (both SBA-15 and MCM-41) and the same preparation procedures were performed to obtained 1%Ru-20%Co/SBA-15(w/w) and 1%Ru-20%Co/MCM-41(w/w), which were denoted as 20%CP-1%Ru and 20%CT-1%Ru respectively.

2.2 Catalyst characterizations

- Total surface area, total pore volume and pore size diameter of calcined catalysts were measured by BET method. 0.2 g of sample was pretreated by degassing under N_2 flow at 350^{o}C for 4h. The BET measurements were carried out using N_2 as adsorbate at liquid N_2 temperature (-196^{o}C).
- Temperature programmed reduction (H_2-TPR) was used to examine the reducibility of synthesized catalyst. 0.2 g of calcined catalyst was pretreated at 220^{o}C by Ar gas. Then 5%H_2/Ar gas mixture was switched through the catalyst, while temperature was programmed from RT to 900^{o}C. TCD installed in GC 6820 Agilent was used to determine the amount of H_2 consumed for the reduction of catalyst.
- Temperature programmed surface reaction (TPSR) of pre-adsorbed CO by hydrogenation showed methanation on cobalt active site. 0.2 g of calcined catalyst was reduced in H_2 gas at 500^{o}C for 2h, then 10%CO/He was allowed through a catalyst bed at RT for 30 min. Physisorbed CO was purged by inert gas. The hydrogenation of pre-adsorbed CO was then performed by temperature programming from RT to 900^{o}C at a heating rate of 10^{o}C/min under H_2 flow. Products obtained were detected by FID. TPSR profile represents the methanation over catalyst investigated.
- Temperature programmed desorption (H_2-TPD) was used to determine a metal dispersion and average metal active site. 0.2 g of reduced catalyst was absorbed by H_2 at 100^{o}C for 30 min. Then, the catalyst was purged and cooled down under Ar. H_2-TPD was started by temperature programming from RT to 900^{o}C at a heating rate of 10^{o}C/min. Co dispersion and average site were calculated base on the total peak area obtained from TPD profile.

2.3 FT reaction

The Fischer–Tropsch reaction was carried out in a fixed bed reactor (1 g of catalyst) under a continuous flow of syngas (H_2:CO = 2:1). Before the reaction, catalyst was reduced under H_2 flow (40 ml/min) at 500^{o}C overnight. Subsequently, the catalyst bed was cooled down to the reaction temperature at 200^{o}C under inert gas. After that the FT reaction was performed under atmospheric pressure in a flow of syngas at GHSV 300h^{-1}for 24h. Liquid product was collected in a cold trap (-30^{o}C) and analyzed by gas chromatograph using FID (GC 430 Bruker). Effluent gas compositions were detected by on-line GC (GC 450-valve Bruker) using FID and TCD.

3. Results and Discussions

3.1 Catalyst characterizations

3.1.1 N_2 adsorption measurement

N_2 adsorption shows adsorption/desorption isotherm of type II and type IV indicating non-porous and meso-porous material, respectively. The hysteresis loop due to capillary condensation at higher partial pressures was reported. This observation is due to the mesoporosity of support [8],[9]. However, the total surface area, pore size diameter and pore volume were observed to decrease (Table 1.) due to site blocking of porous by cobalt particles.

3.1.2 Temperature programmed reduction , H_2-TPR

Figure 1 presents H_2-TPR of Co based catalyst. The reduction profile of bulk Co_3O_4 illustrates two-steps reduction [10]. The first peak is normally assigned to the reduction of Co_3O_4 to CoO, while the second peak shows a broad shoulder, which is assigned to the second step reduction. This presents main reduction of CoO to Co^0. However, the broad peak observed at higher temperature presents a reduction peak of cobalt silicate species [11].

The reduction profiles of the promoted catalysts (Co-Ru) are also included in Figure 1. The first step of reduction shifts to lower temperature when compared to unpromoted catalyst. The result indicates that promoted catalyst increases reducibility, Ru promoter enhances the reduction of cobalt oxides by spillover of hydrogen from Ru to the cobalt oxide [12].

Table 1: Physical properties of cobalt based catalysts

Sample	V_m [cm^3(STP) g^{-1}]	a_s BET [m^2g^{-1}]	Total pore volume [$cm^3.g^{-1}$]	Mean pore diameter [nm]	% Dispersion (from TPSR)
Support T	203.480	885.66	0.44	3.34	-
20% CT	152.180	662.35	0.41	3.38	0.15
20% CT-1%Ru	66.75	290.54	0.21	2.83	0.44
Support P	89.618	390.06	0.32	6.21	-
20% CP	81.372	354.17	0.33	6.36	0.27
20% CP-1%Ru	41.44	180.48	0.14	3.14	0.34

3.1.4 Temperature programmed surface reaction, TPSR

TPSR technique was used to determine the hydrogenation of pre-adsorbed CO at transient state. TPSR profiles present CH_4 formation. Peak area under TPSR profile represents amount of CH_4 produced from the hydrogenation of pre-adsorbed CO. The hydrogenation of CO can be written as below:

$$CO + 3H_2 \longrightarrow CH_4 + H_2O$$

The adsorption stoichiometry of one CO molecule per cobalt surface atom (CO/Co surface = 1 at room temperature) was assumed to estimate Co dispersion. Co dispersion of all catalysts is presented in Table 3.

Figure 2 displays methanation of unpromoted and promoted cobalt based catalyst. The comparison of 20%CT and 20%CP catalyst reports that T_{max} of TPSR profile obtained from 20%CP catalyst shifts to lower temperature, indicating a higher activity compared to 20%CT catalyst. The promoted catalyst of both supports presents a shift of T_{max} to higher temperature compared to the parent catalyst. The results also show that both promoted catalyst displays higher methane produced indicating that higher amount of active sites exist on the catalyst surface. The Ru promoter might assist the hydrogenation of pre-adsorbed CO by spillover of H_2 to Co active component.

3.1.5 Temperature programmed desorption (H_2-TPD)

The H_2-TPD profiles in Figure 3 show two regions of desorption temperature. The first peak appears in a lower temperature range (50-200^{o}C), indicating H_2 physisorption and weak chemisorption. T_{max} of H_2-TPD peaks at around 150^{o}C. The second peak locates in a higher temperature region (400-800^{o}C).

The unpromoted catalyst both 20%CT and 20%CP gives a higher H_2 uptake when compared with promoted catalyst. This result was found to correlate with the pore volume of the catalyst. The Larger pore volume, the higher amount of H_2 adsorbed.

3.2 FT reaction

The result from FT reaction carried out at 200^{o}C for 24h is presented in Figure 4. The 20%CP-1%Ru catalyst is the most active and selective toward C_9-C_{15} hydrocarbons. The chromatogram of commercial Jet fule, JET-A1 and JP-8 compared to synthetic liquid fuels obtained from 20%CP-1%Ru is presented in Figure 5. Chromatogram of FT product obtained from 20%CP-1%Ru catalyst could be comparable to the commercial jet fuel both JET-A1 and JP-8.

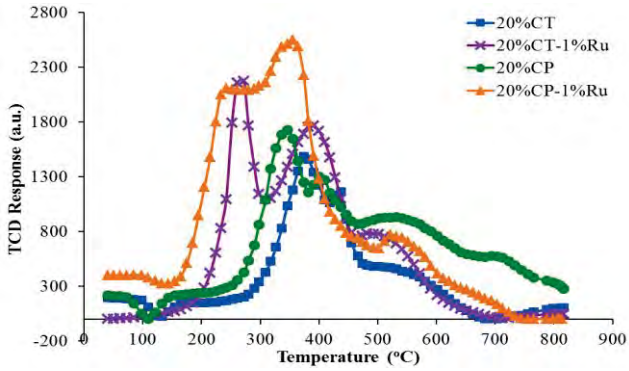

Figure 1. TPR profile of cobalt based catalyst

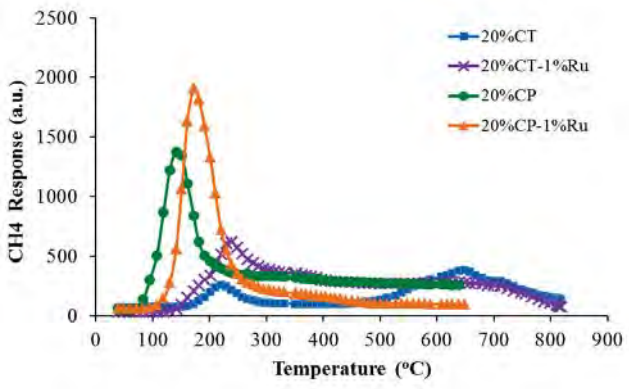

Figure 2. TPSR profile of cobalt based catalyst.

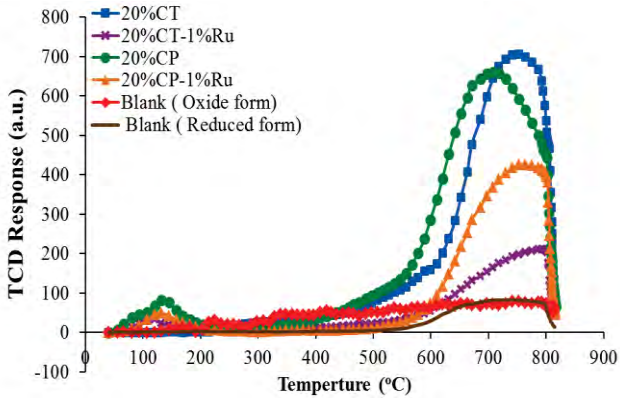

Figure 3. H_2-TPD profile of cobalt based catalyst.

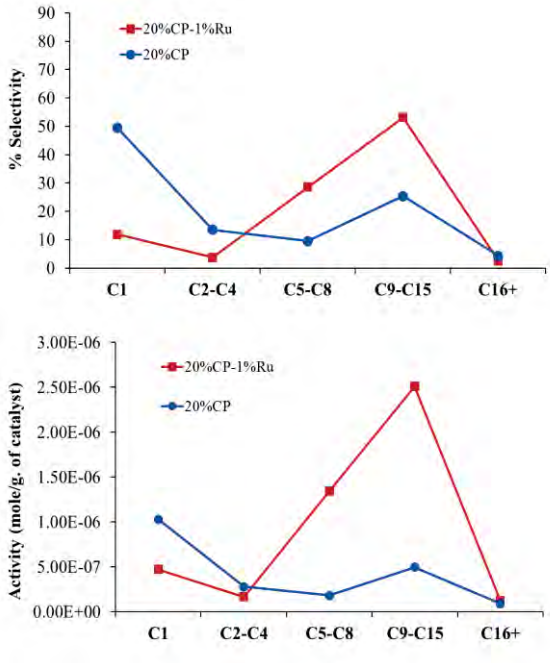

Figure 4. Activity and selectivity of cobalt based catalyst for FT reaction.

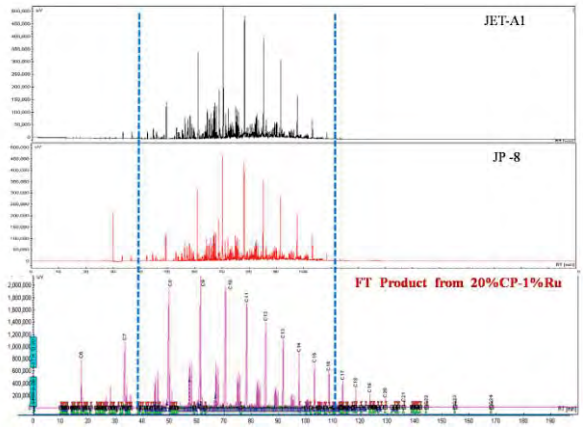

Figure 5. Comparison of kerosene chromatograms obtained from the FT product and commercial Jet fuels.

4. Conclusions

Fischer-Tropsch reactions over 1%Ru-20%Co/SBA-15 and 1%Ru-20%Co/MCM-41 are selective toward long chain hydrocarbons in the range of kerosene (C_9-C_{15}) product comparing to unpromoted 20%Co/SBA-15 and 20%Co/MCM-41 catalyst. FT products obtained from 1%Ru-20%Co/SBA-15 catalyst could be comparable to the commercial jet fuel both JET-A1 and JP-8.

Acknowledgements

The authors would like to acknowledge the Royal Thai Air Force for research funding. The authors also acknowledge MTEC (National Metal and Materials Technology Center), NSDTA (National Science and Technology Development Agency) and RCC (Research and Development Center for Chemical Engineering Unit Operation and Catalyst Design) for their supports in information and operations.

References

[1] Wikipedia 2009. Available from: en. wikipedia. org/ wiki/ Kerosene.

[2] Bian G, Koizumi N, Yamada M , J Jpn Inst Energ 2002;81:974–80

[3] Kazuhiro K, Takuya S, Kozo M, Yasuyuki I, Tatsuya H, Fuel 89 (2010) 2088–2095

[4] Wenping M, Gary J, Robert A. K, Dragomir B. B, Burtron H. D, Applied Catalysis A: General 437– 438 (2012) 1– 9

[5] Liang C, Michal K, Colloids and Surfaces A: Physicochem. Eng. Aspects 357 (2010) 91–96

[6] Shan W,Tao D,Yuping L,Ying Z,Xiaofeng L,Zichun Y, Journal of Solid State Chemistry 177 (2004) 4800–4805

[7] Bianca V.S, Meiry G.F R, Leonardo A,Maria V C, José F B, Sérgio G M, Gina P, Catalysis Today 172 (2011) 152– 157

[8] Haifeng X, Yuhua Z, Kongyong L, Jinlin Li, Journal of Molecular Catalysis A: Chemical 295 (2008) 68–76

[9] Andrei Y, Anne G-C, Rafeh B,Vladimir L. Z, Journal of Catalysis 206, 230–241 (2002)

[10] Reza M. M, Mariane T., Ajay K. D , Applied Catalysis A: General 345 (2008) 134–142

[11] Agustín M., Carlos L., Francisco M., Isabel D., Journal of Catalysis 220 (2003) 486–499

[12 Haifeng X, Yuhua Z, Kongyong L, Jinlin L , FUEL PROCESSING TECHNOLOGY 90 (2009)237–246

HYDRODEOXYGENATION OF m-CRESOL OVER MODIFIED COMO SULFIDE CATALYSTS

Suriyawech Boonthalarath[1,2], Sabaithip Tungkamani[1,2*], Tanakorn Ratana[1,2], Samitthichai Seeyangnok[1,2], Monrudee Phongaksorn[1,2]

[1] Department of Industrial chemistry, Faculty of Applied Science, King Mongkut's University of Technology North Bangkok, Bangkok, 10800, Thailand
[2] Research and Development Center for Chemical Engineering Unit Operation and Catalyst Design (RCC), STRI Building, Floor 1st and 7th (Room 702),King Mongkut's University of Technology North Bangkok, Bangkok , 10800, Thailand

*Author for correspondence; E-mail: sabaithip.tungkamani@gmail.com, Tel.+66 2555-2000 ext. 4822,

Abstract: Hydrodeoxygenation (HDO) of m-cresol used as model oxygenated compound containing in pyrolysis bio oil was investigated over a parent and a modified CoMo sulfide catalyst with different loading of 1%, 3% and 5%Co w/w. A series of catalysts was characterized by using BET, H_2-TPR and NH_3-TPD technique. Hydrodeoxygenation of m-cresol over sulfide catalyst was carried out in autoclave reactor at 300°C under pressure of hydrogen 50 bar for 2h. Aromatic, naphthene and oxygenated compounds are main products observed from GC-MS. The conversion of m-cresol using CoMo and modified CoMo sulfide catalyst increases with enhancement of cobalt loading. Hydrodeoxygenation of m-cresol over modified 3%CoMo sulfide catalyst presents the best catalytic behavior (92%HDO).

1. Introduction

Up to now, fossil fuels are unreliable source of energy because of the uncertainty of oil price and inadequacy. Therefore, the search for new sources of energy is essential and has been a great deal of attention today. Thailand is agricultural country and has potential to produce energy from biomass. Agricultural residues and wastes could be used as renewable feedstock for sustainable energy. Recently, biofuels derive from non-food biomass has become the most attractive issue. The conversion of lignocellulosic biomass via fast pyrolysis produces mainly bio oil. Pyrolysis bio-oil is unstable, low oxidation stability, low heating value, high viscosity and high acid value. These physical and chemical properties can be changed during the long period of storage. This could be due to the content of oxygenated compound containing in bio oil. Improvement of bio oil via hydrotreatment is a promising process to remove oxygenated compound from lignocellulosic bio oil. Currently, upgrading of bio oil is the interesting route to produce hydrocarbons for transportation fuels.

From the point of view, the investigation of hydrodeoxygenation of m-cresol used as model compound over modified CoMo sulfide catalyst was emphasized in this research.

2. Materials and methods

2.1 Catalyst preparation

The preparation of sulfide CoMo catalyst and modified catalyst was presented elsewhere [1-2]. A series of CoMo catalyst was prepared by incipient wetness impregnation of cobalt nitrate hexahydrate solution into Mo supported catalyst at 1, 3 and 5%loading of Co(w/w). After impregnation, wet powders were dried at 45°C for 48h. Finally, powders were calcined at 550°C for 4h. In this case CoMo catalyst was named CMAD and modified CoMo catalyst was denoted as CMAD1 catalyst. The number in front of each symbol presents the %loading of Co used as promoter.

2.2 Catalyst characterization

- BET measurement

0.2 g of catalyst prepared was purged under N_2 flow at 350°C for 4h. BET measurement was performed in N_2/He flow at -196°C. Total surface area, pore size diameter and pore volume were obtained from the analysis.

- H_2-TPR

Catalyst 0.2 g was packed in a reactor. Then it was pretreated under Ar flow at 200°C for 30 min. The catalyst was cooled down to room temperature. 5%H_2/Ar used as reducing gas was allowed to the reactor. Temperature programmed reduction was carried out from 40°C to 900°C. The hydrogen consumption was monitored by thermal conductivity detector and displayed as H_2-TPR profile.

- NH_3-TPD

Temperature programmed desorption of NH_3 was studied to determine the acidity of catalyst using chemisorptions analyzer (BELCAT B, BEL JAPAN). Catalyst 0.05 g was flushed under He flow at 500°C for 30min and cooled down to 100°C. Then, ammonia was adsorbed at 100°C for 30 min. Subsequently, the samples were purged by a flowing of He stream at

100°C for 1h to remove excessive and physically adsorbed NH_3. Finally, the samples were heated from 100°C to 900°C at the heating rate of 10°C/min in pure He. The desorption profile were recorded.

2.3 Catalytic reaction test and product analysis

Hydrodeoxygenation of m-cresol over CMAD and CMAD1 was performed in a high-pressure batch reactor (Parr autoclave reactor). 20g of liquid mixture (m-cresol, tetralin and n-hexadecane) was filled in a batch reactor. Prior to the activity test, 0.8 g of catalysts were sulfided at 400°C under 10%H_2S/H_2 atmosphere at a flow rate of 25 ml/min for 4 h. Then, sulfide catalyst was loaded into the reactor under N_2 atmosphere. Catalytic activities were undergone at 300°C under 50 bar of H_2 for 2h. The product was analyzed using GC-MS technique.

3. Results and Discussion

3.1 Catalyst characterization

- BET measurement

Total surface area, pore size diameter and pore volume of CoMo and modified CoMo catalyst are summarized in Table 1. Total surface area of both catalysts decreases with increasing Co loading. This could be due to the blocking effect of promoter addition [3].

- H_2-TPR

H_2-TPR profiles of all catalyst investigated illustrate in Figure 1. A series of CMAD and CMAD1 catalysts shows two reduction temperature regions. The lower temperature range between 400-500°C is assigned to the reduction of Mo^{6+} to Mo^{4+}. The higher temperature between 800-900°C is attributed to the reduction of Mo^{4+} to Mo. Considering the CMAD catalyst, temperature maximum (T_{max}) for the reduction of CMAD shifts to lower temperature when Co loading was increased. This is explained that some Mo species are easier to reduce with the presence of a Co species [3]. The reduction of CMAD1 catalyst show a similar behavior as a CMAD catalyst.

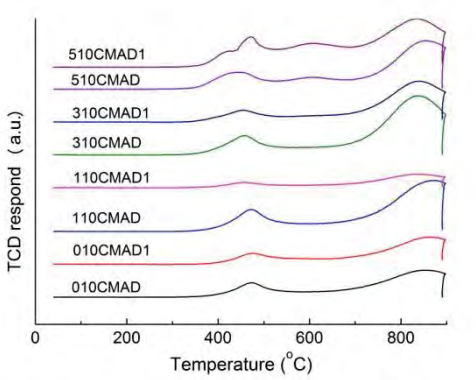

Figure 1. H_2-TPR profiles of CoMo and modified CoMo catalyst

- NH_3-TPD

Result of NH_3-TPD obtained from CMAD and CMAD1 catalyst are summarized in Table 1. In a series of CMAD catalyst, the total acidity of catalyst decreases with Co content. This decrease in the total acidity could be attributed to the pore blockage of large particle of active species located in the external surface[4-5]. This result is in agree with the result from BET measurement. On the other hand, the total acidity of CMAD1 catalysts increases with the cobalt content, except in the case of 510CMAD1. The additive effect observed from the modified CoMo catalyst might produce Co^{2+} ion, which is also active as Lewis acid sites. However, 510CMAD1 catalyst contains too much Co loading, which particles might hinder the access of ammonia molecules to the acid sites located in the inner surface, and hence leads to the lower acidity [4-5].

3.2 Catalytic reaction test and product analysis

Hydrodeoxygenation (HDO) of 10 wt% m-cresol in mixed of tetralin and n-hexadecane over CMAD and CMAD1catalyst reports in Table 2. The result shows that m-cresol conversion of CMAD catalysts and CMAD1 increases with Co loading.

From conversion values, the addition of additive increases the catalytic performance of CMAD1 catalyst. The presence of additive on the surface of catalysts has an influence on the acidic properties.

It indicates that m-cresol conversion for the CMAD1 catalysts are higher than CMAD catalyst. The highest m-cresol conversion for the CMAD1 catalyst with a loading of 3% is 94.32%.

Table 1: Results from characterization of CoMo and modified CoMo catalyst with cobalt loading

Catalyst	Total surface area (m^2/g)	Pore diameter (nm)	Pore volume (cm^3/g)	Total acidity (mmol/g)
010CMAD	273.22	4.30	62.77	0.119
110CMAD	260.39	4.35	59.83	0.096
310CMAD	254.00	4.36	58.36	0.092
510CMAD	250.82	4.24	57.63	0.082

CMAD is CoMo sulfide catalyst

Table 1: Results from characterization of CoMo and modified CoMo catalyst with cobalt loading (continue)

Catalyst	Total surface area (m^2/g)	Pore diameter (nm)	Pore volume (cm^3/g)	Total acidity (mmol/g)
010CMAD1	242.19	4.35	55.65	0.073
110CMAD1	221.17	4.70	50.82	0.080
310CMAD1	208.91	4.25	48.00	0.096
510CMAD1	207.09	4.36	47.58	0.083

CMAD1 is modified CoMo sulfide catalyst

The HDO of m-cresol over CMAD and CMAD1 catalysts with different cobalt loading are concluded in Figure 2. The optimum Co loading for HDO is 3% and it is more effective if it present on CMAD1 (310CMAD1), corresponding to the 92.44%HDO. Higher activity of CMAD1 catalyst is due to the increase in acidity of the catalysts. The addition of additive lead to the formation of new Lewis and Brönsted acid sites on the catalyst surface, resulting in the higher of HDO.

The mechanism for HDO of m-cresol was proposed in Figure 3. The first one is direct deoxygenation route (DDO), leading to the production of toluene. The second one is hydrogenation reaction pathway (HYD), in which aromatic ring of m-cresol is firstly pre-hydrogenated, to form 3-methylcyclohexanol and then deoxygenated to form methylcyclohexane. The HYD:DDO ratio presents the reaction pathway. The DDO products observed over promoted catalysts are the same compared with unpromoted catalyst, but their yields are dependent on amount of promoter. The HYD pathway is the main route for hydrodeoxygenation of m-cresol. The promoting effect of cobalt is essentially due to the enhancement of DDO pathway, while the additive might affect the strengthening between the interaction of the support and active species. This results in higher DDO products. It could be concluded that 310CMAD1 is the most efficient catalyst.

Table 2: Result of reaction for hydrodeoxygenation of m-cresol by CoMo and modified CoMo catalysts

Catalyst	%Conversion	%HDO	HYD:DDO
010CMAD	51.57	44.00	3.49
110CMAD	57.54	54.36	1.35
310CMAD	85.34	83.62	1.15
510CMAD	88.75	86.43	1.29
010CMAD1	45.97	35.45	3.24
110CMAD1	79.14	71.72	1.28
310CMAD1	94.32	92.44	1.13
510CMAD1	56.66	44.77	0.66

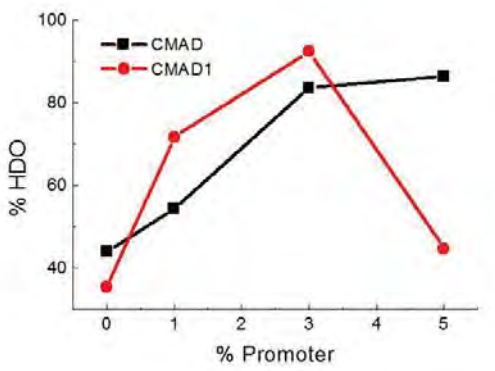

Figure 2. HDO activities of m-cresol over sulfide CoMo and modified CoMo catalyst

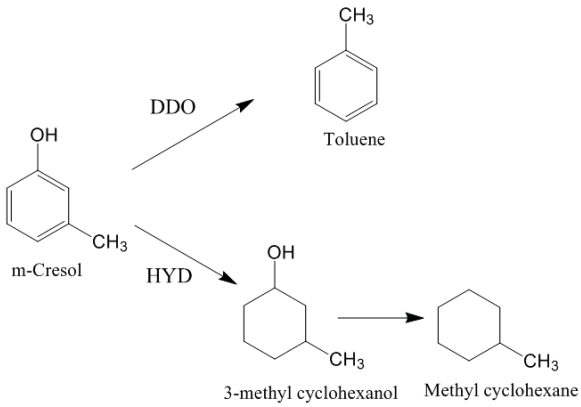

Figure 3. Reaction pathway for hydrodeoxygenation of m-cresol

4. Conclusions

The conversion of m-cresol using CMAD and CMAD1 sulfide catalyst increases with enhancement of cobalt loading. Hydrodeoxygenation of m-cresol over 310CMAD1 catalyst presents the best catalytic behavior (92%HDO).

Comparison of the CoMo catalyst (CMAD) with the modified CoMo catalyst (CMAD1) found that the addition of additives have an effect on the direct deoxygenation pathway.

Acknowledgements

The authors would like to acknowledge JICA and NSTDA for the financial support. The authors also sincerely thank all AIST researchers for their technical supports for this research collaboration project.

References

[1] Yaseen Muhammad , Chunxi Li, *Fuel Processing Technology.* **92**(2011) 624-630.

[2] Usma, Tomoya Yamamoto, Takeshi Kubota, Yasuaki Okamoto, *Applied Catalysis A: General.* **328**(2007) 219-225.

[3] E. Rodríguez-Castellón , A. Jiménez-López, D. Eliche-Quesada, *Fuel.* **87**(2008) 1195-1206.

[4] Anjie Wang, Yao Wang, Toshiaki Kabe, et al. *Journal of Catalysis.***210**(2002) 319-327.

[5] A.Infantes-Molina, J. Mérida-Robles, E. Rodríguez Castellón, et al. *Applied Catalysis A: General*. **286** (2005)239-248.

[6] Yu Fan, Gang Shi, Haiyan Liu, Xiaojun Bao, *Fuel.***90** (2001) 1717-1722

[7] Li Cuiqing, Sun Guida, Li Chengyue, et al. *Chinese J. Chem.Eng.***14(2)**(2006) 184-193

[8] Y.Romero, F.Richard, S.Brunet, *Applied Catalysis B : Environmental.***98**(2010)213-223.

[9] V. Sundaramurthy, A.K. Dalai, J. Adjaye, *Applied Catalysis A: General*.**311**(2006)155-163.

Analytical Chemistry (Additional)

DEVELOPMENT OF MICROMOLD MASTER TEMPLATE FOR PDMS MICROFLUIDIC DEVICE FABRICATION BY DEEP X-RAY LITHOGRAPHY

Umnoui Petprapai[1], Jatamane Rattana[1], Muanfuan Tongtem[1], Rungrueang Phatthanakun[2] and Waraporn Threeprom[1, 3*]

[1]*Department of Chemistry and Center of Excellence for Innovation in Chemistry, Faculty of Science, Mahidol University, Rajathewi, Bangkok, 10400, Thailand*
[2]*The Siam Photon Laboratory of the Synchrotron Light Research Institute (SLRI), Suranaree, Muang District, Nakhon Ratchasima, Thailand 30000*
[3*]*Mahidol University, Kanchanaburi Campus, Kanchanaburi, 71150, Thailand*
[*]*Email: wthreeprom@yahoo.com*

Abstract:

This work presents a method for fabrication of non-metallic and metallic micro mold masters for the manufacture of polymer microfluidic devices. The manufacturing method based on Deep X-ray Lithography (DXL) was used. It consists of three steps: (1) UV lithography for making X-ray mask, (2) X-ray synchrotron microbeam irradiation for transferring the desired structure of microchannels into substrate sheet and (3) the development of channel structure on substrate to form the mold master.

In this work, the two different materials, glass and stainless steel, were used as substrates for SU-8 photoresist binding in X-ray exposure step. The proposed manufacturing method enables manufacture of non-rectangular channels in microfluidic devices. The experimental results confirmed that high quality molds can be fabricated. Advantages and limitations of the fabrication methods will be compared and discussed.

1. Introduction

Microfluidic device is the miniature analysis system device that is interested in now a day. The system as so called “Lab-on-a-chip” includes micro valves and pumps, micro mixers, micro reactors and incubators, separation columns, and microfluidic modules within a variety of function [1-3]. Microfluidic chips can be fabricated from various kinds of material such as polydimethylsiloxane (PDMS) [4-6], poly (methyl methacrylate) (PMMA) [7] and glass [8]. However, the numerous microfluidic devices are made of PDMS due to its excellent properties in term of high flexibility, optical transparency, and easy release from a master and replica transfer via the molding technique, i.e., soft lithography [8, 9].

Soft lithography is the replica molding technique by transferring the pattern of microchannel from micro structure master mold to elastomeric materials [8]. Therefore the “master mold” is the key factor in transferring step that leads to accurate size and dimension of the device.

The master molds can also be fabricated from many kinds of material such as silicon [10], PDMS [11], SU-8 [12] and metallic [13-14]. Several procedures namely etching technique [10], lithography [12] and electroplating [13-14] are involved. Among of them, lithography is wildly used because it provides extremely high resolution of structures containing specific small sidewall roughness and high aspect ratios of fabrication product [12]. Nevertheless, electroplating is a best choice for metallic mold. Therefore, the method combined between lithography and electroplating might be emerged for the high aspect ratio of metallic mold. For this mold, the fabrication details included: (1) fabricate the X-ray mask which contained the microchannel pattern, (2) transfer the 2D pattern on X-ray mask to photoresist layer that coated on substrate by X-ray exposure, (3) remove of unexposed photoresist, the 3D micro channel of photoresist appeared on the surface of substrate, (4) fulfill the metal on the substrate by electroplating and (5) remove the remained photoresist, the 3D metallic micro channel appeared on the surface of substrate.

In this work, the alternative fabrications of non-metallic and metallic master mold based on deep X-ray lithography technique for PDMS molding were developed. Two different substrates, glass and stainless steel used in X-ray exposure process were investigated. The advantages and disadvantages in use of different substrates will be compared and discussed in term of cost, ruggedness, production time and stability.

2. Materials and Methods

2.1 Materials

The X-ray light source was provided from the Beamline 6a: Deep X-ray Lithography station at Synchrotron Light Research Institute (Public Organization), Thailand.

Liquid SU-8 as negative photoresist and PG removal were purchased from Micro. Chem. Corp., USA.

The SU-8 developer was in-house prepared by Beamline 6a : Deep X-ray Lithography station.

The AZ-4620 as positive photoresist was purchased from AZ electronic materials Limited.

The AZ-4620 developer was prepared by mixing of 4.0 g of potassium hydroxide (Merck, Germany) with

1.0 g of boric acid (Merck, Germany) in 200 mL of water.

Stainless steel plate (Grade 304) in dimension of 5.0×10.0×0.3 mm was obtained from S.T.K. Steel Co., Ltd., Thailand.

Nickel solution for electroplating was prepared in 1000 mL of water and composed of 500.0 g of nickel sulfamate, 6.0 g of nickel chloride and 30.0 g of boric acid (Merck, Germany) [14].

The in-house electroplating box was set by Beamline 6a: Deep X-ray Lithography station.

2.2 Methods

The X-ray mask contained microchannel pattern was fabricated based on referred method [12]. First, the pattern was designed by drawing software (Solid work and Adobe Illustrator) and printed in the transparency sheet with high- resolution printer. After that, the pattern was transferred by UV exposure onto the thin layer of AZ-4620 positive photoresist coated on X-ray transparent material (graphite). Subsequently, an unexposed photoresist was washed out by AZ-4620 developer solution. Then, Au-electroplating process was run in order to fill up the metallic layer on graphite sheet for shielding the X-ray. Finally, the exposed AZ-4620 was removed out and the metallic X-ray mask was obtained as illustrated in Fig. 1.

Second, the substrate for X-ray exposure was prepared. Two different substrates, glass and stainless steel, were used.

For glass substrate, high viscosity of SU-8 solution was gently poured on the cleaned surface of glass plate for over 300 µm thickness and then kept in the oven at 90 ºC for 12 hrs. The SU-8 was changed to solid state. Next, solid SU-8 surface was covered with 300 µm thickness frame as controlled guard before gently burnished by polishing machine (Struers Model Rotopol -25) with oxide polishing and diamond polishing. The glass substrate coated with SU-8 film was called as "Glass raw mold". Then SU-8 film was simultaneously pre-baked step by step at 60, 70 and 80 ºC, respectively for 5 min and subsequently soft-baked at 95 ºC for 30 min in order to minimize the stress of a thick SU-8 layer on a glass surface [15]. After that, the negative X-ray mask was placed on SU-8 surface. The X-ray synchrotron irradiation was subsequently run.

For stainless steel substrate, the plate was burnished until mirror like surface was appeared and then dried and cleaned. After that it was coated with the thin film of Al/Ti/Al by volatile deposition at a thickness of 500 Å layer by layer. Next, the thin film was coated with liquid SU-8 for over 300 µm thickness and then kept in the oven at 90 ºC for 12 hrs. The SU-8 was changed to solid state. The stainless steel substrate coated with Al/Ti/Al and SU-8 film was called as "S-T raw mold". After that, the positive X-ray mask was placed on SU-8 surface. The X-ray synchrotron irradiation was subsequently run.

Third, the unexposed area of SU-8 was then removed by SU-8 developer. For Glass raw mold, it was post-baked at 95 ºC for 30 min, slowly cooled down to room temperature before the removal. In contrast, for S-T raw mold, it was kept at 90 ºC for 45 min for annealing the irradiated and unirradiated area of SU-8 before the removal. After the removal of unexposed SU-8 from the two raw molds, the 3D microchannel structures of SU-8 were showed. The "SU-8 Glass mold" was finally obtained and ready to use from this step.

Fourth, the S-T raw mold contained positive channel of SU-8 was full filled with nickel by electroplating. Wood's Strike technique was applied to the raw mold [13, 14] in order to activate the surface of stainless steel before the running. The Ni-electroplating process was conducted by nickel solution in electroplating box. The S-T raw mold and Ni plate were set as cathode and anode, respectively. The electroplating process was run at constant current density of 1.00 mA/cm^2 for 7 days at room temperature for slow fulfilling. The surface of filled nickel in SU-8 channel was daily checked in order to achieve the flat and smooth surface. After the electroplating process was completed, the S-T raw mold was covered with 300 µm thickness frame as controlled guard before gently polished by polishing machine (Struers Model Rotopol -25) with oxide polishing and diamond polishing. It was polished in order to remove the overfilled Ni and polished until 300 µm filled-Ni thickness (desired mold thickness) was obtained.

Fifth, the remained SU-8 was removed by PG removal. Then O_2/CF_4 plasma was run for etching and cleaning the mold surface. At the end of this step, the 3D nickel microchannel structure was appeared. The "Ni-stainless steel mold" was achieved.

The scheme of fabrication process on two substrates is illustrated in Fig. 2.

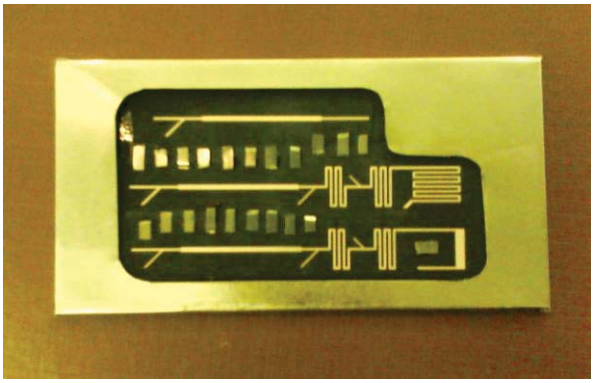

Figure 1. The X-ray mask with positive golden pattern on graphite sheet.

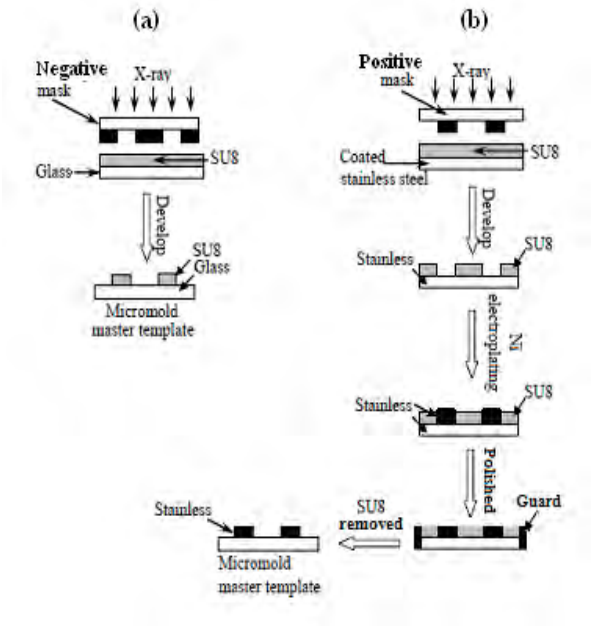

Figure 2. Deep X-ray lithography schematics: (a) SU-8 Glass mold and (b) Ni-Stainless steel mold.

3. Results and Discussion

3.1 SU-8 Glass mold

The SU-8-Glass mold was successfully fabricated in short step and short time. The fabricated mold can be shown in Fig. 3. The thickness of the microchannel was controlled in substrate preparation step by polishing (second step). Therefore, the polishing is the main key factor affecting the smoothness and the height of the microchannel. However, the vertical side walls of the microchannel were still smooth. The width of microchannel could be made down to 40 µm with an accurate dimension. This mold could be replicated by polydimethylsiloxane (PDMS) in soft lithography many times. However, over 50 castings, the SU-8 microchannel was detached from the glass substrate resulting in unusable mold. This might be come from the fact that the adhesion between SU-8 and glass was not strongly and permanently contacted. The baking condition (second step) of the Glass raw mold might be played an important role in attachment.

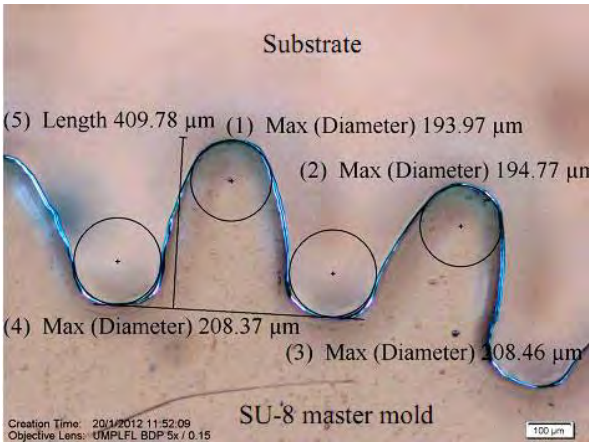

Figure 3. The SU-8 Glass mold [12].

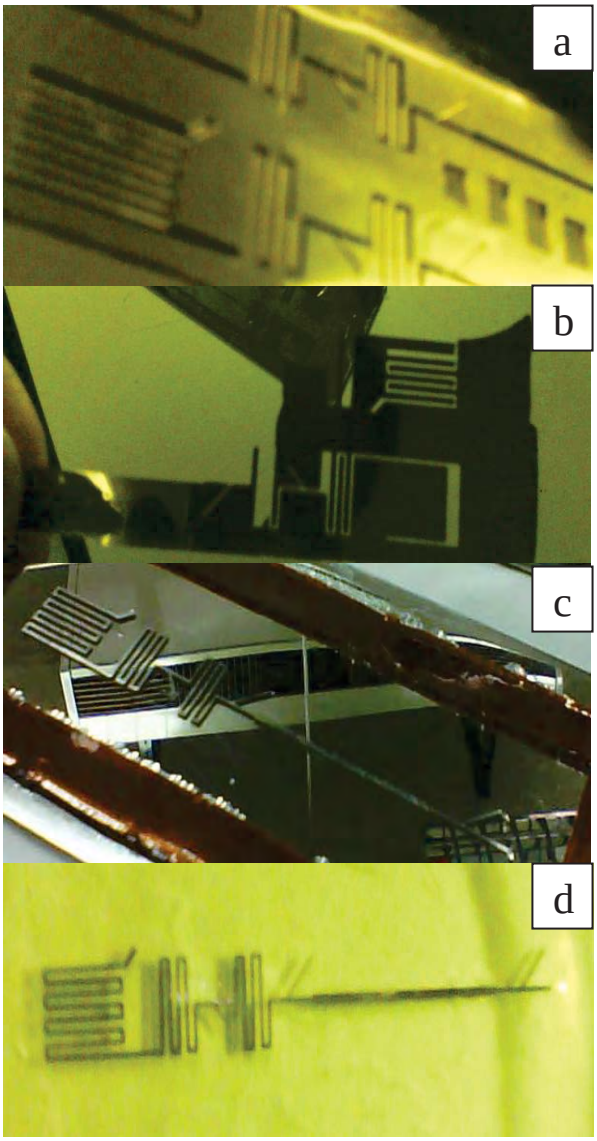

Figure 4. Ni-Stainless steel mold fabrication: (a) S-T raw mold, (b) detached S-T raw mold, (c) completed Ni-Stainless steel mold, and (d) detached Ni microchannels.

3.2 Ni-Stainless steel mold

The fabricated Ni-Stainless steel mold was effectively prepared as shown in Fig. 4(c) with longer time than the preparation of SU-8 Glass mold as a result of many steps. The smooth vertical side wall of microchannel was also achieved. The master mold obtained by this method showed the well attachment between the microchannel of SU-8 photoresist and stainless steel substrate as illustrated in Fig. 4(a). Nevertheless, the surface of stainless steel was needed to be clean before doing the volatile deposition of metallic thin film (second step) otherwise the SU-8 photoresist was possibly detached from the metallic surface as shown in Fig. 4(b).

The thickness of the metallic microchannel was directly controlled by electroplating and polishing process (fourth step). In this case, the condition set (time and current density) in electroplating process is

the key factor affecting the smoothness of filled nickel plane. The thickness of the microchannel was further controlled by polishing. The roughness of nickel surface could be occurred during nickel electroplating process if small bubbles appeared in microchannel template resulting in nickel holes. Thus, to avoid these bubbles, the S-T raw mold was vacuumed until all bubbles were removed before electroplating [14].

The Ni microchannels were finally achieved after remained SU-8 was completely removed (fifth step). The attachment between Ni and the stainless steel surface was strongly depended on the cleanliness of the steel surface. The Ni microchannels could be detached from the substrate surface if the insoluble SU-8 photoresist still remained on the substrate before electroplating as shown in Fig. 4(d). Thus, the thin film of insoluble SU-8 should be clearly removed by O_2 plasma prior to Ni electroplating [14]. Therefore, Ni-Stainless steel mold could be perfectly obtained if substrate surface and electroplating process were carefully controlled.

The completed Ni-stainless steel mold could be used in soft lithography of PDMS replica molding as well as SU-8 glass mold [13, 14]. More than 50 moldings could be run without detachment of Ni microchannels. The advantages and disadvantages in fabrication process and usage of SU-8 Glass mold and Ni-Stainless steel mold for PDMS molding were summarized in Table 1.

Table 1. Advantages and disadvantages of SU-8 Glass mold and Ni-Stainless steel mold.

Parameter	SU-8 Glass mold	Ni-Stainless steel mold
Cost	high	higher
Fabrication time	short (3 days)	long time (> 7 days)
Fabrication process	easy	more complicated
Stability	not suitable for some organic solvent and high temperature	not suitable for high concentrated acid or base
Robustness	glass might be cracked	high strength
Molding	< 50 replicates	>50 replicates

4. Conclusions

The fabrications of non-metallic (SU-8 photoresist) and metallic (Ni) microchannel mold template on glass and stainless steel substrates were successfully demonstrated using modified deep X-ray lithography, respectively. The finite vertical side walls of microchannel were clearly appeared on both fabricated molds. These molds can be used in soft lithography for PDMS casting very well. In addition, Ni-Stainless steel mold can be used in longer time as a result of its high strength. However, the fabrication process of Ni-Stainless steel mold is more complicated.

Acknowledgements

All supports from staffs and all facilities from Beamline 6a: Deep X-ray lithography (BL6a : DXL) of the Synchrotron Light Research Institute (Public Organization) are acknowledged. The authors would also like to thank the Center of Excellence for Innovation in Chemistry (PERCH-CIC) for the financial support. The International Foundation of Science (IFS) was also acknowledged for the partial financial support from the project No.AW/22073.

References

[1] C. H. Ahn, J. Kai, S-H Lee, N. Santiago, D. W. Sehy, R. Schultheis, J. Han and A. Puntambekar, *Procedia Engineering* **25** (2011) 651 – 656.

[2] C. Ericson, J. Holm, T. Ericson and S. Hjerten, *Anal. Chem.* **72** (2000) 81-87.

[3] M. Vazquez and B. Paull, *Anal. Chim. Acta* **668** (2010) 100–113.

[4] Y. Hongbin, Z. Guangya, C. F. Siong, W. Shouhua and L. Feiwen, *Sensors and Actuators B* **137** (2009) 754–761.

[5] Q-S Kang,Y. Li, J-Q Xu, L-J Su, Y-T Li, W-H Huang, *Electrophoresis* **31** (2010) 3028– 3034.

[6] S. Julich, M. Riedel, M. Kielpinski, M. Urban, R. Kretschmer, S. Wagner, W. Fritzsche, T. Henkel, R. Moller and S. Werres, *Biosensors and Bioelectronics* **26** (2011) 4070–4075.

[7] J-E Kim, J-H Cho and S-H Paek, *Anal. Chem*. **77** (2005) 7901-7907.

[8] G. S. Fiorini and D. T. Chiu, *BioTechniques* **38** (2005) 429-446.

[9] D. Lee, H. Mekaru, H. Hiroshima, S. Matsumoto, T. Itoh, M. Takahashi and R. Maeda, *Microelectronic Engineering* **86** (2009) 920–924.

[10] S-W Youn, T. Noguchi, M. Takahashi and R. Maeda, *Microelectronic Engineering* **85** (2008) 918–921.

[11] W-M Choi and O-O Park, *Microelectronic Engineering* **70** (2003) 131–136.

[12] R. Phatthanakun, C. Pantong, C. Sriphung, W. Pummara and N. Chomnawang, *Reproduction of Microparts based on Standard X-ray LIGA Processes for Mass Production*, 9th Electrical Engineering/Electronics, Computer, Telecommunications and Information Technology Conf. Proc., (2012).

[13] J. Ruenin, S. Sukprasong, R. Phatthanakun, N. Chomnawang, and P. Kuntanawat, *Fabrication of Microfluidic Device for Quantitative Monitoring of Algal Cell Behavior using X-ray LIGA Technology*, World Academy of Science, Engineering and Technology 69 (2012).

[14] C. Yunphuttha, R. Pattanakul, S. Porntheeraphat, A. Wongchaisuwat and P. Viravathana, *NSTI-Nanotech*. 2 (2012) 400-403.

Organized by **Faculty of Science, Burapha University**
& The Chemical Society of Thailand